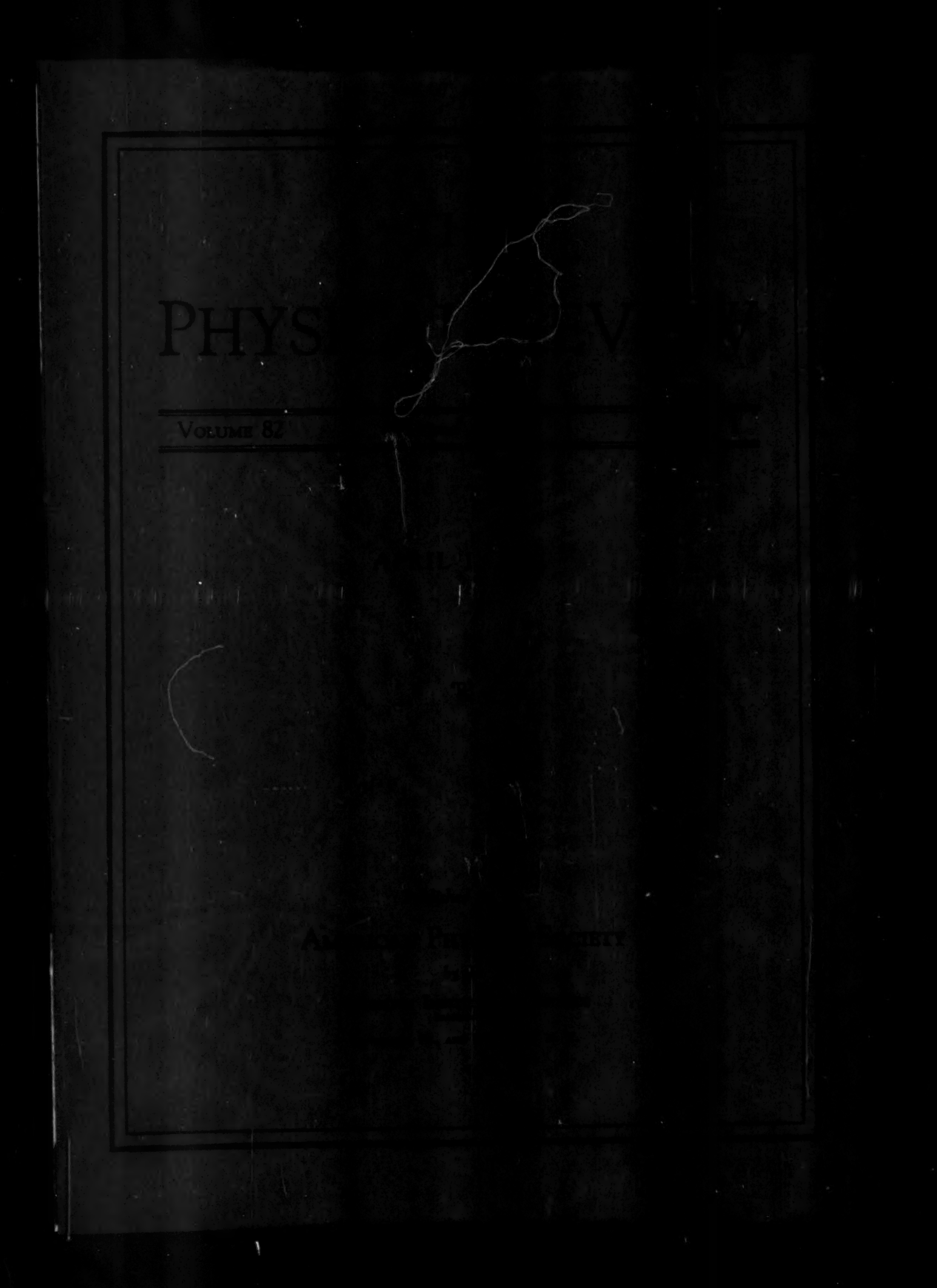
PHYS
VOLUME 82

Information for Contributors

Manuscripts

Send manuscripts [illegible] Brookhaven National Laboratory, Upton, Long Island, New York.

Each article submitted [illegible] in general consist of (a) textual material which is to be set in type, and (b) drawings or photographs from which zinc or copper halftones will be made. The textual material will consist of an abstract, the [illegible] material, references, [illegible] captions. All of this material must be [illegible] typewritten (except mathematical [illegible] double spaced with wide margins ([illegible] instructions to the printer) on a durable [illegible] paper, preferably letter size. The original, not the carbon, should be submitted.

For general style, [illegible] abbreviations, and form, recent issues [illegible] should be consulted.

The prime requisite [illegible] copy shall be clear to the typesetter, [illegible] either a physicist nor a mathematician.

Abstract

An abstract must [illegible] such article. It should be adequate [illegible] and as a summary. As an index, [illegible] all subjects, major and minor, [illegible] new information is presented. As a [illegible] it should give the conclusions of the [illegible] all numerical results of general interest.

Mathematical Expressions

All but the simplest [illegible] mathematical expressions should be carefully [illegible] hand. Be sure to distinguish between [illegible] and small letters. Indicate clearly, [illegible] and subscripts by inverted carets and [illegible] respectively. Avoid complicated superscripts. Avoid repetition of a complicated [illegible] expression by representing it by some [illegible] symbol. Identify in the margin Greek letters [illegible] unusual symbols. Use fractional exponents [illegible] of root signs. Use the solidus (/) [illegible] wherever it will save vertical space.

References

References should be [illegible] footnotes; numbered consecutively, and [illegible] thus:

[1] A. B. Smith, Phys. Rev. [illegible] (1932).
[2] H. Lamb, *Hydrodynamics* (Cambridge University Press, Cambridge, England, [illegible]), pp. 573, 643.

Tables

All but the simplest [illegible] material should be organized in [illegible] rather than as a part of the running text. Tables may be [illegible] written on sheets separate from the running [illegible] with indications in the margin of the running [illegible] where the table is to be inserted. Each table should have a caption which will make the data in the table intelligible without reference to the [illegible] Avoid complicated column headings; if necessary, use symbols which are explained in the table caption.

Figures

Wherever possible figures should be planned for the width of a column of the *Physical Review* (3 inches). A convenient reduction ratio is about 2:1 or 3:1. The original drawings or photographs should therefore be in general about 6 to 9 inches wide and the lettering and symbols should be large enough on the original that when reduced they shall not be less than about $\frac{1}{16}$ in. (1.5 mm). If the reduction is 3:1, the original lettering should be not less than $\frac{1}{8}$ in. high.

The process of making zinc etchings or copper halftones is a black and white photographic one. Therefore line drawings must be in sharp black and white on paper or tracing cloth. Coordinate paper is not desirable but if used must be blue lined and the coordinate lines which are to show must be inked over.

Photographs should have maximum black and white contrast.

Plan figures to use space efficiently. Avoid wasting space, particularly at the top or bottom.

Identify on the black or other suitable [illegible] each original drawing or photograph with the author's name and the figure number. Figures should be numbered consecutively and their approximate position indicated in the margin of the running text. Figure captions should be typed and included with the manuscript (not on the face of the figure).

Avoid round and oval photographs.

Alterations

Take great care that each manuscript is [illegible] graphically accurate. A limited number of alterations in proof are unavoidable, but the cost of making extensive alterations after the article has been set in type will be charged to the author.

Proof and all correspondence concerning [illegible] in the process of publication should be addressed to the Publication Manager, American Institute of Physics, 57 East 55 Street, New York 22, New York.

THE PHYSICAL REVIEW

A journal of experimental and theoretical physics established by E. L. Nichols in 1893

VOLUME 82

Second Series

APRIL 1–JUNE 15, 1951

Published for the

AMERICAN PHYSICAL SOCIETY

by the

AMERICAN INSTITUTE OF PHYSICS

Incorporated

THE PHYSICAL REVIEW

A journal of experimental and theoretical physics established by E. L. Nichols in 1893

Published by the American Institute of Physics for the

AMERICAN PHYSICAL SOCIETY

Officers

President

C. C. LAURITSEN
California Institute of Technology
Pasadena, California

Vice-President

J. H. VAN VLECK
Harvard University
Cambridge, Massachusetts

Secretary

K. K. DARROW
Bell Telephone Laboratories
Office:
Columbia University
New York 27, New York

Treasurer

G. B. PEGRAM
Columbia University
New York 27, New York

Local Secretary for the Pacific Coast

J. KAPLAN
University of California at Los Angeles
Los Angeles, California

Managing Editor

S. A. GOUDSMIT
Brookhaven National Laboratory
Upton, Long Island
New York

BOARD OF EDITORS

Editor

S. A. GOUDSMIT

Assistant Editor

S. PASTERNACK

Associate Editors

J. BARDEEN, T. BONNER, R. G. HERB, W. E. LAMB, JR., A. J. F. SIEGERT, W. E. STEPHENS, HARVEY BROOKS, R. F. CHRISTY, C. L. CRITCHFIELD, M. DEUTSCH, T. H. JOHNSON, BRUNO ROSSI, M. GOLDHABER, R. HOFSTADTER, A. W. LAWSON, A. PAIS, R. SERBER, C. H. TOWNES

Manuscripts for publication should be submitted to S. A. GOUDSMIT, Brookhaven National Laboratory, Upton, Long Island, New York. The authors' institutions are requested to pay a publication charge of $8 per page which, if honored, entitles them to 100 free reprints. Instructions will be sent with galley proofs.

Proof and all correspondence concerning papers in the process of publication should be addressed to the Publication Manager, American Institute of Physics, 57 East 55 Street, New York 22, New York.

Subscription Price

United States and Canada $25.00
Elsewhere $27.00

Back Numbers [1]

Yearly back number rate when complete year is available:
Prior to 1949: $20.00
Thereafter: $27.00
Single copies: $2.00 each, prior to July, 1929;
$1.00 each, July, 1929–December, 1941;
$2.00 each, January, 1942–December, 1946;
$1.00 each, January, 1947–December, 1948;
$1.25 each, thereafter.
General index, 1893–1920: $4.00.

Subscriptions, renewals, and orders for back numbers should be addressed to the American Institute of Physics, 57 East 55 Street, New York 22, New York.

Changes of address in the case of members of the American Physical Society should be addressed to the Treasurer; in the case of other subscribers to the American Institute of Physics.

[1] For Series 1 inquire of Physics Department, Cornell University, Ithaca, New York.

The Physical Review is published semi-monthly at Prince and Lemon Streets, Lancaster, Pennsylvania.

Entered as second-class matter March 6, 1947, at the Post Office at Lancaster, Pennsylvania, under the Act of March 3, 1879.

Acceptance for mailing at special rate of postage provided for in paragraph (d-2), section 34.40, P. L. & R. of 1948, authorized January 27, 1933.

THE
PHYSICAL REVIEW

A journal of experimental and theoretical physics established by E. L. Nichols in 1893

SECOND SERIES, VOL. 82, NO. 1 APRIL 1, 1951

Angular Distribution of $Li^7(p,\alpha)\alpha$

F. L. TALBOTT, A. BUSALA, AND G. C. WEIFFENBACH
Department of Physics, Catholic University of America, Washington, D. C.*
(Received December 11, 1950)

The angular distribution of the alpha-particles from the reaction $Li^7(p,\alpha)\alpha$ has been investigated from 0.5 to 1.4 Mev with a photographic emulsion technique. Values of the coefficients of the $\cos^2\theta$ and $\cos^4\theta$ terms are given and compared with the results of other observers.

I. INTRODUCTION

THE angular distribution of the two alpha-particles produced when lithium is bombarded with protons has been investigated a number of times; but there are still a number of questions to be settled, especially with regard to the existence of a $\cos^4\theta$ term at lower energies and its dependence on energy. Early experiments[1–3] showed no deviation from spherical symmetry. This is not surprising, as the work was all done at rather low energies where the yield is small and the symmetry is still uncertain. Subsequent observers[4,6] showed the presence of a $\cos^2\theta$ term, so that the yield at any angle θ compared to the yield at 90° is given by

$$Y(\theta)/Y(90°)=1+A\cos^2\theta,$$

where A is a function of the bombarding energy. Heydenburg, *et al.*,[7] have recently found evidence of a $\cos^4\theta$ term in the region from 1 to 3.5 Mev, so that the equation becomes

$$Y(\theta)/Y(90°)=1+A\cos^2\theta+B\cos^4\theta,$$

where A and B are both functions of the bombarding energy. Critchfield and Teller[8] considered the possibility of a $\cos^4\theta$ term as early as 1941, and Inglis[9,10] has explained the distribution in terms of entrant p- and f-protons. In the present paper we have measured the angular distribution in the region from 0.5 to 1.4 Mev and calculated the coefficients A and B.

II. EXPERIMENTAL METHOD

The present work was done with the pressurized van de graaff generator of the Department of Terrestrial Magnetism of the Carnegie Institution of Washington, through the courtesy of Dr. Merle A. Tuve and his staff. Some preliminary work was carried out with the atmospheric pressure generator, and it is hoped that further work at the lower energies can be done with it. Both of these generators have been described in publications of the Department of Terrestrial Magnetism. The smaller machine has a range from 0 to about 1.1 Mev, while the pressurized generator operates from about 0.5 to 3.6 Mev.

The photographic emulsion method of recording has been used. The bombardment chamber is shown in Fig. 1. The proton enters from a slit at the top of the diagram striking the target at the center of the chamber. The target holder is mounted on a sylphon toggle so that it can be rotated from outside the chamber. A stove for evaporating lithium onto the target is shown at the lower right. A protecting sleeve on the stove can also be run in and out by a sylphon toggle. The lithium on the target is renewed before each run, as it is oxidized every time the vacuum is broken. This can be done rather quickly without contaminating the rest of the chamber with lithium by simply turning the target around to face the stove and bringing the sleeve up tight against the target while distilling lithium onto it. To the left is shown the removable box containing the

* Assisted by the joint program of the ONR and AEC.
[1] F. Kirchner, Physik. Z. **34**, 785 (1933).
[2] J. Giarratanna and C. G. Brennecke, Phys. Rev. **49**, 35 (1936).
[3] H. Neuert, Ann. Physik **36**, 437 (1939).
[4] Young, Ellett, and Plain, Phys. Rev. **58**, 408 (1940).
[5] Schwartz, Rossi, Jennings, and Inglis, Phys. Rev. **65**, 80 (1944).
[6] Rubin, Fowler, and Lauritsen, Phys. Rev. **71**, 212 (1947).
[7] Heydenburg, Hudson, Inglis, and Whitehead, Phys. Rev. **73**, 241 (1948).
[8] C. L. Critchfield and E. Teller, Phys. Rev. **60**, 10 (1941).
[9] D. R. Inglis, Phys. Rev. **74**, 21 (1948).
[10] Heydenburg, Hudson, Inglis, and Whitehead, Phys. Rev. **74**, 405 (1948).

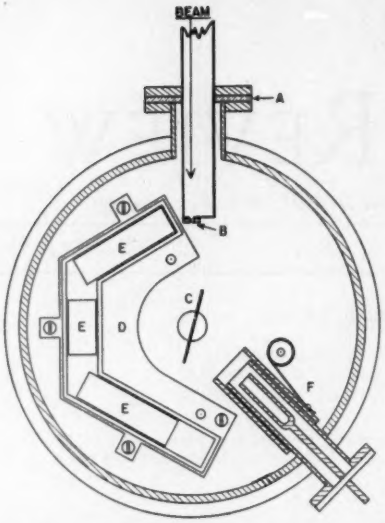

FIG. 1. Schematic diagram of bombardment chamber. The proton beam enters from above and is defined by the slit B, falling on the lithium target at C. The lithium targets are prepared by distilling metallic lithium from the stove F onto a beryllium plate C. C can be rotated from outside the chamber by a sylphon toggle. The alpha-particles are recorded in the photographic plates E (Eastman NTA 25-micron emulsions) which are mounted in the removable "camera" D at 45 degrees to the plane of the diagram. The insulator A permits the measurement of the beam current passing through B. A current integrator connected between the chamber and ground can then be used to indicate relative exposures. A Lucite cover, fitted with a neoprene gasket, is placed on the chamber to permit evacuation of the chamber during target preparation and bombardment.

photographic plates which we shall call the "camera." The three plates are mounted on 45° blocks. The alpha-particles enter the camera through aluminum foil windows. These windows not only keep the camera light-tight but can be so varied as to discriminate between alpha-particles and the scattered protons. The camera lid has breather-cap to allow the inside of the camera to be evacuated. The lid of the chamber is made of Lucite with a neoprene gasket.

Eastman NTA plates have proved very satisfactory for this work. The only difficulty is that they show a tendency to peel, apparently because of the placing of thick emulsions in high vacuum. A thin line of shellac around the edge of the plate seems to have ended this difficulty. A set of three plates are processed together, using stain racks and dishes such as are used for biological slides. Exposures ranging from a few minutes to an hour, depending on the voltage, with from about 0.1 to 0.8 μamp proton current have been made. The yield varies considerably, but we try for the best compromise between too few tracks for good statistics and too many overlapping tracks for accurate counting. We like to have about 1000 tracks per square mm at 90°, which makes the maximum density several thousand per square mm. At first, the tracks were counted directly with a binocular microscope under low power, using the area defined by a Whipple disk as an increment of angle. This was about one square mm of the emulsion. Fatigue and the possibility of large counting errors made us substitute a system of making enlargements. The one square mm of emulsion area is enlarged to about 10 in.$\times$10 in. Counting from these enlargements has proved to be much easier, and, we believe, has reduced errors considerably. It is possible to mark each track with a pencil, or stylus, to prevent missing or double counting. And it is also possible for several observers to check their counting techniques against each other. Using this method, we always checked each other within one or two counts per thousand.

Usually the tracks at 10 to 14 different angles are counted for each run, so that the calculation for any one run is based on the counting of 20,000 to 30,000 tracks. Several runs were made at each energy. A table has been prepared changing various positions on the plates into angles subtended at the target. Corrections must, of course, be made for oblique incidence and for the inverse square law to get the angular distribution in the laboratory coordinates. The angles and counts are then corrected to center-of-mass coordinates, according to the method described by Heydenburg and Inglis.[11]

III. NUMERICAL CALCULATIONS

The pairs of numbers (x, y), where $y=Y_\theta/Y_{90°}$ and $x=\cos^2\theta$, can be used in several ways to evaluate A and B. They can, firstly, be plotted on a graph and a curve drawn "by eye" giving A and B directly. Secondly, a least squares analysis can be employed.[12] Then, with either of the above methods there is the choice either of evaluating each run separately or of combining all points from runs taken at any given bombardment energy into a single graph or analysis. If each run is calculated separately, there arises the further problem of assigning weights to the A and B values of all runs at any one energy to obtain the "grand mean."

Since small changes in curvature can yield quite different values of A and B, the graphical method was rejected as entirely too subjective. Because there was no satisfactory criterion for the assignment of weights, the separate evaluation of each run was also rejected. The only method remaining, that of using all points from runs at a single bombardment energy in a least-squares analysis, was the one used in this paper. The coefficients a, b, and c in the equation

$$y_c=a+bx+cx^2, \tag{1}$$

which gave the best fit to the observed points were found in this way. When Eq. (1) is divided by a, the

[11] N. P. Heydenburg and D. R. Inglis, Phys. Rev. **73**, 230 (1948).

[12] E. T. Whittaker and G. Robinson, *The Calculus of Observations* (Blackie and Son, Ltd., London, 1944), fourth edition.

equation is reduced to

$$y'=1+(b/a)x+(c/a)x^2,$$

and A and B are given directly as b/a and c/a, respectively.

The residuals, d, having been defined as

$$d=y_e-y,$$

the probable errors in A and B were computed by using the formula[13]

$$p_A=0.6745[(A_{22}/D)\Sigma d^2/(n-3)]^{\frac{1}{2}},$$
$$p_B=0.6745[(A_{33}/D)\Sigma d^2/(n-3)]^{\frac{1}{2}},$$

where n is the number of points, D is the determinant of the three "normal" equations used in the least-squares analysis, and A_{ii} is the cofactor of the element D_{ii} in D.

It should be noted that the probable errors are defined above in terms of the internal consistency of the observed data. Following the suggestion of Birge[14] a separate least-squares calculation was made for each run. The values of A and B so obtained were used to evaluate probable errors based on external consistency by means of the formulas,

$$p_{A\ \mathrm{ext}}=0.6745[\Sigma(A-\bar{A})^2/N]^{\frac{1}{2}},$$
$$p_{B\ \mathrm{ext}}=0.6745[\Sigma(B-\bar{B})^2/N]^{\frac{1}{2}},$$

where $\bar{A}$ is the average of A's at any one energy, $\bar{B}$ is the average of B's at any one energy, and N is the number of runs at the energy under consideration. Birge states[15] that if the ratio $p_{\mathrm{ext}}/p_{\mathrm{int}}$ exceeds unity by several times, the results so compared are inconsistent; i.e., some experimental error has altered the conditions under which the different observations were made. The results obtained here indicate that there have been changes in the experimental conditions from run to run. One of the most serious sources of these changes is undoubtedly the variation in target thickness from one run to the next, a factor which is very difficult to evaluate.

IV. DISCUSSION OF RESULTS

Figure 2 shows a typical set of data for one energy showing the experimental points for several runs and also the curve obtained from them by the least-squares method. Table I and Fig. 3 show our values of A and B together with their probable errors for the energies 0.5 Mev through 1.4 Mev. Figure 4 compares our results with those of Heydenburg *et al.*, and with those recently reported by a group in Melbourne.[16,17]

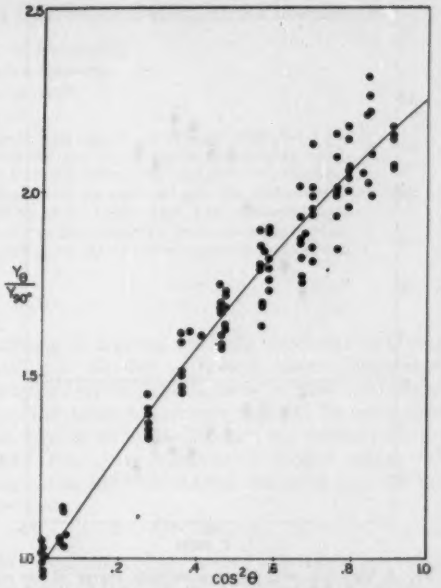

FIG. 2. Curve shows typical least-squares fit to the observed data. The points were obtained from several runs made at a bombardment energy of 0.7 Mev. θ is the angle in center-of-mass coordinates of the observed points to the incident beam. $Y_\theta/Y_{90°}$ is the relative yield.

Comparison of the probable errors using external and internal consistency (see above) gave ratios ranging from about three to six. Hence, the probable errors indicated in Table I and Fig. 3 may be somewhat optimistic. Nevertheless, since these estimates are derived from a single computation which includes all of the observations at any one energy, all discrepancies between individual runs have been incorporated into the probable errors as listed herein. For this reason it is felt that the results of this paper effectively define the limits within which the true values of A and B must lie. It is generally accepted that the region defined by twice

TABLE I. Angular distribution coefficients A and B, as defined by $Y_\theta/Y_{90°}=1+A\cos^2\theta+B\cos^4\theta$, for the reaction $Li^7(p,\alpha)\alpha$. E is the energy in Mev, and p and σ are the probable error and standard deviation, respectively.

E	A	p_A	σ_A	B	p_B	σ_B
0.5	0.95	0.11	0.16	0.15	0.12	0.17
0.6	1.22	0.08	0.12	0.34	0.09	0.14
0.7	1.58	0.09	0.14	0.31	0.10	0.15
0.8	1.85	0.08	0.12	0.31	0.09	0.13
0.9	2.38	0.12	0.17	0.54	0.12	0.18
1.0	2.43	0.09	0.14	0.53	0.10	0.15
1.1	2.71	0.12	0.18	0.76	0.13	0.19
1.2	2.78	0.14	0.20	0.75	0.15	0.22
1.3	2.32	0.11	0.16	0.63	0.12	0.17
1.4	2.46	0.10	0.14	0.92	0.11	0.16

[13] Reference 12. p_A and p_B as defined here are actually the errors in "b" and "c" of Eq. (1). However, the factor $1/a$ is used only to correct for having used an observed $Y_{\theta'}$ instead of a true $Y_{90°}$, and it can easily be demonstrated that the error in "a" does not appear in A or B

[14] R. T. Birge, Phys. Rev. **40**, 215 (1932).

[15] Reference 14, p. 219.

[16] Martin, Bower, Dunbar, and Hirst, Nature **164**, 310 (1949).

[17] Martin *et al.*, Australian J. Sci. Res. **A2**, 25 (1949).

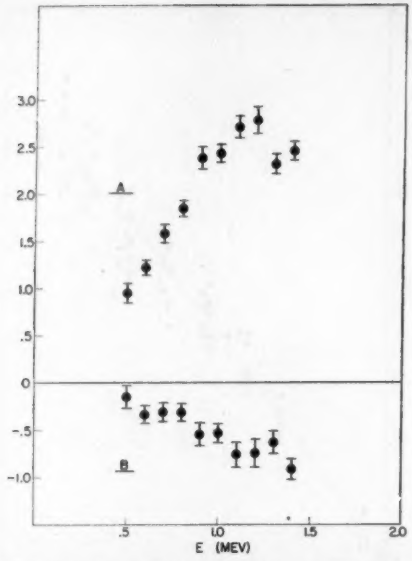

FIG. 3. Variation with the bombardment energy of the coefficients A and B in the equation $Y_\theta/Y_{90^\circ}=1+A\cos^2\theta+B\cos^4\theta$. The probable errors are indicated.

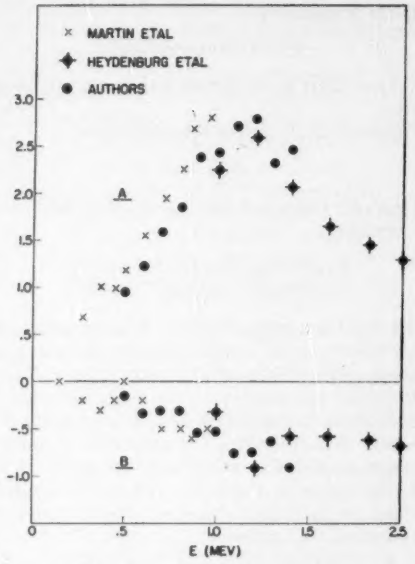

FIG. 4. Comparison with previous results.

the standard deviation[18] must encompass the true values.

It will be noted that our values are slightly displaced from those of the Melbourne group, probably indicating some systematic difference between measurements of the two laboratories. The displacement is in the direction which could be caused by our targets being thicker than theirs. All the targets used here were about 25 kev thick or less as indicated by the breadth of the 440 gamma-ray resonance. However, since they were placed at an angle of 15° to the incident proton beam, the effective thickness was of the order of 100 kev. This places all of our A and B values at an energy of approximately 50 kev higher than the correct energy. If this correction is applied, the values of A so obtained agree remarkably well with those obtained by Martin *et al.*, at Melbourne.

The position of our target has an additional deleterious effect in that the area defined by the beam on the target is also increased by a factor of about four over the actual cross section of the beam. If we pursue the problem further, we will probably put our lithium targets on thin beryllium[19] foils so mounted as to permit observation of α-particles that have passed through the beryllium as well as those coming off the front of the target. In this way the plane of the target can be kept nearly perpendicular to the proton beam, decreasing both the effective target thickness and bombarded area, while permitting observations at $\theta=0°$, instead of being limited to angles greater than 20° as at present.

We wish to express our appreciation of the hospitality and assistance of the staff of the Department of Terrestrial Magnetism, and particularly to Dr. Norman P. Heydenburg, without whose help we could not have pursued this investigation. We also wish to thank Dr. David Inglis for suggesting the problem and advising us along the way.

[18] 2σ defines a probability of 0.95. The results obtained here establish the existence of B beyond any reasonable doubt, since the possibility that a $\cos^4\theta$ term has been observed only because of a fortuitous combination of statistical fluctuations and experimental errors is considerably less than one in a thousand. This is consistent with Inglis's statement that f-protons enter into this reaction.

[19] Martin *et al.*, used aluminum leaf, which is satisfactory at lower energies; but at higher energies considerable difficulty is experienced with the emission of x-rays from the aluminum target backing. Beryllium is completely satisfactory in this respect, and also has the advantage of being very transparent to the product alphas.

Neutron Depolarization on Scattering from Carbon, Paraffin, and Phosphorus*

W. E. Meyerhof and D. B. Nicodemus†
Stanford University, Stanford, California
(Received December 15, 1950)

The depolarization of polarized thermal neutrons scattered from carbon, paraffin, and phosphorus has been measured. The results have been interpreted in terms of the spin flip probability on scattering, which for carbon was found to be equal to -0.09 ± 0.21 and for hydrogen 0.56 ± 0.10, consistent with the theoretically expected values 0 and 0.65, respectively. For phosphorus, the measured spin flip probability of 0.73 ± 0.15 yields an incoherent scattering cross section of 3.7 ± 0.8b, of the same order of magnitude as the total scattering cross section (3.4b). This would imply one or more s-neutron resonance levels in phosphorus above 400 ev, the present upper limit of the well investigated part of the total neutron cross section of phosphorus.

I. INTRODUCTION

It follows from the assumption of spin-dependent nuclear forces that a slow neutron can change its spin orientation in a scattering process. It seemed to us to be of interest to demonstrate this effect directly. Furthermore, it was our intention to measure the effect qualitatively and thereby to open the possibility of another method of investigating certain features of the compound system.

The probability Q of the spin flip depends on the spin I of the nucleus and on its interaction with the neutron. The effect of this interaction is usually expressed in terms of the spin dependent scattering lengths a_+ and a_- for the compound system of spin $I+\frac{1}{2}$ and $I-\frac{1}{2}$, respectively. In terms of these quantities, the total scattering cross section, σ, of a free nucleus for a slow neutron can be expressed as:[1]

$$\sigma=4\pi[(I+1)a_+^2+Ia_-^2]/(2I+1), \tag{1}$$

and the spin flip probability Q is found to be:[1]

$$Q=\frac{2I(I+1)}{3(2I+1)}\frac{(a_+-a_-)^2}{[(I+1)a_+^2+Ia_-^2]}. \tag{2}$$

It may be noted that the maximum value of Q is $\frac{2}{3}$, independent of I. If the scattering nucleus is strongly bound, the scattering cross section must be multiplied by $[(A+1)/A]^2$, where A is the atomic weight of the nucleus.[2] If more than one isotope is present in the scatterer, the formulas become more complicated.[1,2] In the present experiments only mono-isotopic scatterers were used.

The method which is described below is not the only one by means of which the change of neutron spin orientation can be observed. Indeed, in the crystalline scattering of neutrons one finds incoherent scattering[4] which may be due to isotope effects, temperature scattering, crystal imperfections, random distribution of nuclear spins, and neutron spin flip. In many cases it is possible to isolate the last two causes from the others[5] and, thus, to obtain Q; in fact calling this contribution to the incoherent scattering σ_{inc}, one can show that

$$Q=\tfrac{2}{3}(\sigma_{\text{inc}}/\sigma). \tag{3}$$

In a comparison of our method with crystal scattering, it may be noted that the two methods are fundamentally different as is shown, for example, by the fact that in the latter method crystalline material is essential for a determination of σ_{inc}, whereas this is not the case for a direct measurement of Q. As a matter of fact it will be argued later that appreciable crystalline interference is a disturbing factor for the direct determination of Q.

II. METHOD

The present experiment is a direct method for the determination of the spin flip probability Q. After having checked the results in two cases (C^{13} and H^1) where they were known from other experiments,[4] the method was also applied to the determination of the spin flip probability for an isotope not as yet investigated (P^{31}).

Instead of the depolarization of a beam of polarized slow neutrons as measured by Q it is convenient to introduce the ratio $R(-1\leqslant R\leqslant 1)$ of the polarization[6] of the scattered beam of neutrons to that of the incident beam. It can be shown[1] that for single scattering

$$R=1-2Q. \tag{4}$$

For multiple scattering the relation between R and Q is much more complicated[6] and depends on the solution of a diffusion equation.

* This research was supported by the joint program of the ONR and AEC. A preliminary report of some of the measurements given below has been presented by Meyerhof, Nicodemus, and Bloch, Phys. Rev. 80, 132 (1950).
† Now at Oregon State College, Corvallis, Oregon.
[1] O. Halpern and M. H. Johnson, Phys. Rev. 55, 898 (1939).
[2] E. Fermi, Ricerca Sci. 7, 13 (1936).
[3] For a review of the scattering theory and for references see E. O. Wollan and C. G. Shull, Phys. Rev. 73, 830 (1948).
[4] Reference 3; and for later work C. G. Shull and E. O. Wollan, Naturwiss. 36, 291 (1949); as well as data quoted in K. Way *et al.*, *Nuclear Data* (Nat. Bur. Standards Circ. No. 499, 1950).
[5] Polarization is defined as the ratio $(I_+-I_-)/(I_++I_-)$, where I_+ and I_- are the intensities of the neutrons with the two possible spin orientations respectively.
[6] S. Borowitz and M. Hamermesh, Phys. Rev. 74, 1285 (1948). Contrary to the opinion of these authors the depolarization-

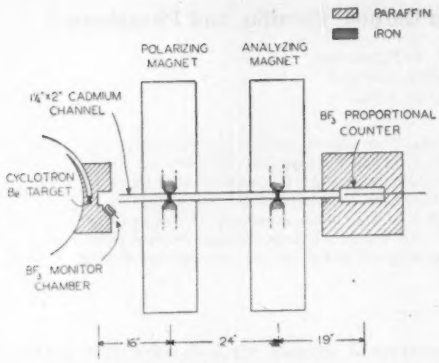

FIG. 1. The straight arrangement of polarizer and analyzer magnets.

Equation (4) shows that the single scattering experiment is very insensitive to small $Q(<0.05)$, and a diffusion type experiment is to be preferred in that case because the total spin flip probability increases with each collision of the neutron. However, for reasons of intensity and interpretation of results the width of the neutron beam should be greater than the thickness of the scatterer (5 to 10 mean free paths). Since such a wide neutron beam was not available to us, we performed a single scattering experiment.

It should be mentioned here that this type of depolarization experiment was first suggested by Schwinger and Rabi[7] who calculated R [Eq. (4)] for hydrogen and

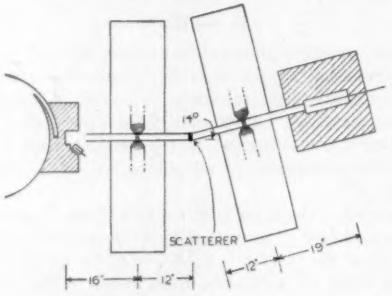

FIG. 2. The oblique arrangement of polarizer and analyzer magnets. The symbolism is the same as for Fig. 1.

pointed out that a measurement of R for neutron scattering by hydrogen atoms would easily demonstrate the nature of the excited state of the deuteron. The results of the present experiment are in agreement with their calculations for a virtual state.

Our experimental method follows rather closely that described in previous papers[8,9] and the reader is referred to these for details. Only such information is repeated here as is necessary for the understanding of the experiment.

The neutrons used in the experiment were produced by a Be(d,n) reaction in the Stanford cyclotron ($2\frac{1}{2}$-Mev deuterons) and thermalized in a paraffin moderator. The neutrons were partially polarized by passage through iron blocks[10] magnetized close to saturation. The detailed theory of the polarization has been studied by Halpern and Holstein[11] and has been adequately verified.[9,12] However, except for a correction factor discussed below, our experiment is independent of the theory of the polarizing effect. Our apparatus[13] consisted of a "polarizer" magnet and an "analyzer" magnet which provided magnetic fields of the order of 12,000 oersteds in two identical hot rolled steel blocks, $1\frac{1}{2}$ in. $\times 2$ in. in cross section and $\frac{1}{2}$ in. thick in the direction of the neutron beam. The neutron beam was channeled in rectangular cadmium channels, also $1\frac{1}{2}$ in. $\times 2$ in. in cross section. We made measurements both with the straight arrangement shown in Fig. 1, when no scatterer was used, and with the oblique arrangement shown in Fig. 2, when a scatterer was inserted. The reasons for these arrangements are discussed in Sec. IIIA.

We shall now analyze briefly the experiments necessary to determine the polarization ratio R [Eq. (4)], using the above arrangements. Considering the straight arrangement (Fig. 1) first, let $f(\tau)d\tau$ be the number of neutrons with inverse velocities (usually expressed in μsec/meter) between τ and $\tau+d\tau$, which are recorded in the detection chamber per unit time after having passed the polarizer and analyzer iron blocks, both unmagnetized. If either one or both of the iron blocks are magnetized, the number of neutrons recorded will increase by a factor $C(\tau)$, which we denote as follows:

(a) polarizer and analyzer both magnetized:

$$C(\tau)=C_D(\tau);$$

(b) polarizer magnetized, analyzer unmagnetized:

$$C(\tau)=C_P(\tau);$$

(c) analyzer magnetized, polarizer unmagnetized:

$$C(\tau)=C_A(\tau);$$

diffusion experiment seems to be quite feasible with the broad neutron beams available from piles. Indeed, for a nonabsorbing scatterer of 10 mean free path thickness the fractional transmitted intensity in the forward direction is approximately $0.3\omega_d/4\pi$, where ω_d is the solid angle intercepted by the detector. Similar conditions are encountered in the present experiment, but the available neutron beam was not broad enough to perform a diffusion type experiment. Figure 3 in the above paper is not labeled correctly and should be either $\Delta_0(10)$ *vs* α or $\sigma(10)$ *vs* β. This would bring the calculations into rather close agreement with those of Halpern. See O. Halpern, Phys. Rev. **75**, 1633 (1949); and O. Halpern and R. K. Luneberg, Phys. Rev. **76**, 811 (1949).

[7] J. Schwinger and I. Rabi, Phys. Rev. **51**, 1003 (1937).

[8] Bloch, Nicodemus, and Staub, Phys. Rev. **74**, 1025 (1948).

[9] Fleeman, Nicodemus, and Staub, Phys. Rev. **76**, 1774 (1949).

[10] F. Bloch, Phys. Rev. **50**, 259 (1936); **51**, 994 (1937).

[11] O. Halpern and T. Holstein, Phys. Rev. **59**, 960 (1941).

[12] Hughes, Wallace, and Hotzman, Phys. Rev. **73**, 1277 (1948).

[13] All the apparatus used in this experiment had been constructed previously under the direction of Professor H. H. Staub, now at the University of Zurich, Switzerland.

(d) polarizer and analyzer both unmagnetized:

$$C(\tau)=1.$$

The total recorded intensities corresponding to these four cases are:

$$I_D=\int C_D(\tau)f(\tau)d\tau, \tag{5a}$$

$$I_P=\int C_P(\tau)f(\tau)d\tau, \tag{5b}$$

$$I_A=\int C_A(\tau)f(\tau)d\tau, \tag{5c}$$

$$I_0=\int f(\tau)d\tau, \tag{5d}$$

where the integration is assumed to extend only over inverse velocities of neutrons absorbed in cadmium (C-neutrons) (Sec. IIIA and B). By means of these measured quantities one can conveniently define the "double transmission effect" η_D:

$$\eta_D=\frac{I_D-I_0}{I_0}=\frac{\int(C_D-1)fd\tau}{\int fd\tau}; \tag{6a}$$

the "single transmission effect, polarizer on," η_P:

$$\eta_P=\frac{I_P-I_0}{I_0}=\frac{\int(C_P-1)fd\tau}{\int fd\tau}; \tag{6b}$$

and the "single transmission effect, analyzer on," η_A:

$$\eta_A=\frac{I_A-I_0}{I_0}=\frac{\int(C_A-1)fd\tau}{\int fd\tau}. \tag{6c}$$

Considering next the oblique arrangement of Fig. 2, we note that the scattered intensity I_0^*, recorded when both the polarizer and the analyzer iron blocks are unmagnetized, is:

$$I_0^*=\int k(\tau)f(\tau)d\tau, \tag{7}$$

where $k(\tau)$ is a factor which depends on the solid angle ω_d, which the detector subtends at the scatterer on the absorption cross section σ_a and on the scattering cross section σ [Eq. (1)], of the scatterer. Although $k(\tau)$ can be determined completely experimentally by a velocity selection method (see Appendix), it is not difficult to show that for isotropic scattering in the forward direction from a thin scatterer:[14]

$$k(\tau)=[(A+1)/A]^2\sigma nd\exp(-\sigma_a nd)r\omega_d/4\pi. \tag{8}$$

Here n is the number of scattering atoms per unit volume, d is the thickness of the scatterer, and r is the ratio of the solid angle subtended by the scatterer to that subtended by the detector at the neutron source in the straight arrangement (Fig. 1). By thin scatterer is meant here that $n\sigma d\ll 1$.

In the presence of crystalline interference the form of $k(\tau)$ may be altered radically[14,15] and may depend not only on the previously mentioned quantities, but also on crystallite size and structure, angle of scattering, and temperature. For the present experiment it is imperative that crystalline interference be negligible if the formulas given below are used, because it is assumed implicitly in the derivation that the coherently and incoherently scattered neutron intensities are reduced by the same factor $k(\tau)$.

When both the polarizer and the analyzer iron blocks are magnetized in the oblique arrangement (Fig. 2), it can be shown[16] that the scattered neutron intensity I_D^* recorded is:

$$I_D^*=R\int C_D(\tau)k(\tau)f(\tau)d\tau + (1-R)\int C_P(\tau)C_A(\tau)k(\tau)f(\tau)d\tau. \tag{9}$$

R is the ratio of the polarization of the scattered neutrons to that of the incident neutrons and is the quantity which we wish to determine [see Eq. (4)].[17] It may be of interest to point out that the first term of the expression for I_D^* corresponds to those neutrons which have not changed their spin orientation on scattering, while the second term corresponds to those that have undergone spin flip. At this point it can be seen that the assumption of equal values of $k(\tau)$ for both terms implies the absence of crystalline interference.

Equation (9) can be rewritten in a more convenient form by using the fact[8] that C_P and C_A are close to unity (1.04 in our experiment), so that $C_PC_A\cong C_P+C_A-1$:

$$I_D^*=R\int C_Dkfd\tau+(1-R)\int C_Pkfd\tau+(1-R)\int C_Akfd\tau.$$

[14] Equation (8) does not take into account temperature scattering. See, for example, R. Weinstock, Phys. Rev. 65, 1 (1944).

[15] Halpern, Hamermesh, and Johnson, Phys. Rev. 59, 981 (1941).

[16] Equation (9) is analogous to Eq. (4) of reference 8. In order to derive this equation it is necessary to consider the neutrons with different spin orientations separately.

[17] It may be noted that in the single scattering experiment R is independent of the neutron velocity, whereas in the diffusion type experiment it will depend on the neutron velocity unless absorption is negligible.

Defining η_D^* as "double transmission effect on scattering" similar to Eq. (6a), we obtain with the help of Eq. (7):

$$\eta_D^* = \frac{I_D^* - I_0^*}{I_0^*} = R\frac{\int (C_D - 1) k f d\tau}{\int k f d\tau}$$

$$+ (1-R)\left\{\frac{\int (C_P - 1) k f d\tau}{\int k f d\tau} + \frac{\int (C_A - 1) k f d\tau}{\int k f d\tau}\right\}. \quad (10)$$

The fractions containing the integrals resemble the transmission effects defined in Eqs. (6a–6c), except for the factor k appearing in the integrals. It is shown in the Appendix that by defining a "hardening factor," H, in general not very different from unity,

$$H = \left(\int p^2 f d\tau \Big/ \int f d\tau\right) \Big/ \left(\int p^2 k f d\tau \Big/ \int k f d\tau\right), \quad (11)$$

where p is the polarization cross section of iron,[10,18] Eq. (10) can be rewritten as

$$\eta_D^* = (1/H)[R\eta_D + (1-R)(\eta_P + \eta_A)].$$

From this equation we obtain the polarization ratio R:

$$R = [H\eta_D^* - (\eta_P + \eta_A)]/[\eta_D - (\eta_P + \eta_A)] \quad (12)$$

and the spin flip probability, by inserting this value of R into Eq. (4):

$$Q = (\eta_D - H\eta_D^*)/2[\eta_D - (\eta_P + \eta_A)]. \quad (12a)$$

This determination of the spin flip probability rests, therefore, on the experimental determination of the quantities η_D, η_P, η_A, η_D^*, and the theory of neutron polarization by magnetized iron[11] is needed only to calculate the correction factor, H, usually not very different from unity.

III. MEASUREMENTS AND RESULTS

(A) Preliminary Considerations

In the production of polarized neutrons by passage through magnetized iron, a compromise must always be made between the increase in polarization and the decrease in intensity as the thickness of the iron blocks is increased. Taking account of these factors as well as of the expected background, consisting mostly of neutrons not captured by cadmium, we found ½ in. to be the best thickness for both the polarizer and the analyzer iron blocks.

Inspection of the expressions for the various intensities which have to be measured [Eqs. (5), (7), and (9)] shows that the critical measurement is that of the difference between the scattered intensities I_D^* and I_0^*. In fact the scattered intensities are severely reduced by the factor k which is proportional to the fractional solid angle $\omega_d/4\pi$ subtended by the detector at the scatterer [Eq. (8)]. ω_d cannot be made arbitrarily large because the dimensions of the polarizer and analyzer magnets, necessary to produce a saturation field, prescribe a minimum distance between the scatterer and the detector which was about 30 in. in our case (see Fig. 2). If it were not for this practical limitation, considerably larger solid angles could have been used, limited only by the distance necessary to avoid neutrons which are diffusely scattered in the iron blocks. These neutrons render the blocks less effective. By separate measurements we have shown that the full effectiveness is obtained at distances larger than 6 in. from the analyzer. While our actual distance certainly satisfied this requirement, it disadvantageously reduced the solid angle to $\omega_d/4\pi \cong 3\times10^{-4}$. Also, we measured for the solid angle ratio r, appearing in Eq. (8), $r \cong 4.1$.

Connected with these considerations is that of the angle of scattering in the oblique arrangement (Fig. 2). It is desirable to make this angle as small as possible, because a small scattering angle avoids crystalline interference (Sec. IIIC). But here again one is limited by the consideration that no direct neutrons from the polarizer must strike the analyzer iron block in order to insure that all neutrons passing through the analyzer indeed come from the scatterer. In view of these considerations, we have chosen a scattering angle of 14°.

Measurements of the slow neutron intensity scattered from paraffin (0.3 cm thick) yielded approximately 100 cpm with the cyclotron running at maximum beam current (20 μamp). The fast neutron intensity was about 4 times larger, convincing us that a rough velocity selection method was necessary in order to reduce the fast neutron background. Consideration of the neutron velocity spectrum[9] and actual measurements indicated that the following type of pulsing cycle, repeated at a rate of 500 cps, would be advantageous:

0–880 μsec: cyclotron on, detector off;
1180–1980 μsec: cyclotron off, detector on;
remaining time: cyclotron and detector off.

The pulsing equipment is described in reference 9. With an average cyclotron beam current of 10 μamp this pulsing yielded approximately 50 slow neutrons/min scattered from paraffin and recorded by the detector above an epithermal background of 15 cpm. These numbers were considered encouraging enough to warrant the attempt of the main experiment.

(B) Measurements with the Straight Arrangement

A determination of the spin flip probability [Eq. (12a)] requires, first, a knowledge of the "straight"

[18] J. Steinberger and G. C. Wick, Phys. Rev. 74, 1207 (1948).

single- and double-transmission effects η_P, η_A, and η_D, which are, of course, independent of the scatterer. These effects were measured as described in reference 9, leaving both polarizer and analyzer iron blocks in place during all measurements as in reference 8. The neutron intensity was monitored by an integrating boron trifluoride chamber[19] which caused the appropriate polarizing magnets to be alternately switched on and off.[9] Any transmission effect is then given by:

$$\eta=(N'-N)/(N-N_{Cd}), \tag{13}$$

where N', N, and N_{Cd} are the total number of counts for an equal number of monitor intervals with the appropriate magnets on, the magnets off, and with a cadmium shield in front of the cadmium channel (Fig. 1), respectively.

All measurements were checked for statistical consistency and were repeated several times throughout the course of the experiment. About 200 monitor intervals (each of approximately 2-min duration), totaled for each of the numbers in Eq. (13), yielded the following values:

$$\begin{aligned}\eta_A&=\ 4.20\pm0.19 \text{ percent},\\ \eta_P&=\ 4.24\pm0.15 \text{ percent},\\ \eta_D&=14.67\pm0.13 \text{ percent}.\end{aligned} \tag{14}$$

These transmission effects are larger than those found by Fleeman, Nicodemus, and Staub[9] for similar thicknesses of iron, because the pulsing used here accentuates the low energy part of the slow neutron spectrum (Fig. 3) with a resulting increase in the effective polarization cross section.[18]

(C) Measurements with the Oblique Arrangement—Carbon

According to Eq. (2) a scatterer with spin equal to zero should not depolarize the neutron beam [$Q=0$ and $R=1$, Eq. (4)]. To check this point we scattered polarized neutrons from graphite, since it has a very low absorption cross section and a reasonable scattering mean free path for thermal neutrons (2.7 cm for our graphite).

In order to obtain enough scattered intensity we used a scatterer of 2.5 cm thickness. Under these conditions double scattering takes place to some extent, but the disturbing effect on our results is negligible compared to our statistical error.

As was mentioned in Sec. II, crystalline interference is to be avoided in this experiment. This can be achieved by observing the scattering under small angles and by rejecting neutrons below the long wavelength Bragg cutoff through pulsing. Under these conditions one observes only incoherent scattering,[20] and, furthermore, the Bragg cutoff occurs at small neutron inverse velocities with the advantage that the major part of the available neutron spectrum can be used. Indeed, calling τ_B the neutron inverse velocity corresponding to the Bragg cutoff:

$$(h/m)\tau_B=2d_{max}\sin\theta, \tag{15}$$

where h is Planck's constant, m the mass of a neutron, d_{max} the maximum interplanar distance in the polycrystal, and θ the glancing angle between the neutron beam and the crystal plane with d_{max} (here, $\theta=7°$). For graphite[21] $d_{max}=6.69$A, so that $\tau_B=420$ μsec/m.

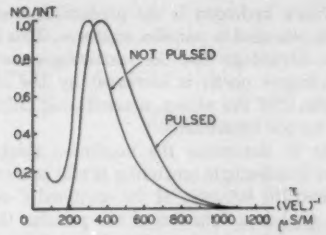

FIG. 3. The effect of cyclotron pulsing on the detected neutron spectrum. The maxima of both curves have been arbitrarily normalized to unity.

For reasons of intensity we were not able to use a system of pulsing which would have eliminated all coherent scattering. Inspection of Figs. 3 and 5 shows that roughly only one-half of the neutrons were scattered incoherently under our conditions. However, this does not invalidate our final conclusions for carbon below, because for $Q=0$ the distinction between coherent and incoherent scattering is immaterial in our experiment.

The final result of 300 monitor intervals each for the numbers in Eq. (13) yielded for the double-transmission effect on scattering from graphite:

$$\eta_D^*=13.6\pm2.2 \text{ percent}.$$

The error indicated is the standard deviation. Calculation of the hardening factor (see Appendix) gave $H=1.16$, so that Eqs. (12a) and (14) yield

$$Q=-0.09\pm0.21 \quad \textbf{(Carbon)}. \tag{16}$$

This result is consistent with the theoretical result $Q=0$ [Eq. (2)] expected for a scattering nucleus with zero spin. It is also in agreement with the fact that carbon has no measurable spin incoherent scattering.[3]

(D) Measurements with the Oblique Arrangement—Hydrogen

We measured the spin flip probability for hydrogen, because it had been investigated by other methods[22,23] and, thus, allowed us to establish a check for our

[19] E. M. Fryer and H. Staub, Rev. Sci. Instr. 13, 187 (1942).
[20] E. Fermi and L. Marshall, Phys. Rev. 72, 408 (1948).
[21] *Handbook of Chemistry and Physics* (Chemical Rubber Publishing Company, Cleveland, 1941).
[22] Sutton, Hull, Anderson, Bridge, De Wire, Lavatelli, Long, Snyder, and Williams, Phys. Rev. 72, 1147 (1947).
[23] Shull, Wollan, Morton, and Davidson, Phys. Rev. 73, 842 (1948).

method. Since hydrogen is the predominant scatterer in paraffin, we used a paraffin scatterer. This has the additional advantage that the scattering cross section of the hydrogen nuclei is increased by the chemical binding effect[2] of the atoms, necessitating only a thin scatterer for our experiment.

In order to determine the maximum thickness of paraffin at which single scattering is still predominant, we measured the intensity of the scattered C-neutrons [I_0^*, Eq. (7)] as a function of the paraffin thickness (Fig. 4). It can be seen from Fig. 4 that 0.3 cm is still a suitable thickness, since single scattering is predominant as long as a linear relation exists between the scattered intensity and the thickness.

Using a paraffin scatterer 0.31 cm thick, we obtained for the double-transmission effect on scattering:

$$\eta_D^* = 7.9 \pm 1.1 \text{ percent},$$

after measuring 200 monitor intervals for each of the numbers of Eq. (13). Consideration of the hardening factor for paraffin (see Appendix) shows that in our case $H \cong 1.00$, so that Eqs. (12) and (14) give for the the polarization ratio:

$$R = -0.08_8 \pm 0.18. \quad (17)$$

Since the carbon atoms contribute slightly to the scattering from paraffin, a small correction must be applied to Eq. (17) in order to obtain the polarization ratio for hydrogen, R_H. If R_C represents the polarization ratio for the carbon atoms and $\langle\sigma'_H\rangle_{Av}$ and $\langle\sigma'_C\rangle_{Av}$ are the average differential scattering cross sections in the forward direction for the hydrogen and carbon atoms respectively, it is easily seen that for single scattering:

$$R = (46\langle\sigma'_H\rangle_{Av} R_H + 22\langle\sigma'_C\rangle_{Av} R_C) / (46\langle\sigma'_H\rangle_{Av} + 22\langle\sigma'_C\rangle_{Av}), \quad (18)$$

where we have assumed the chemical formula of paraffin to be $C_{22}H_{46}$. Since $R_C = 1$ [Eq. (16)], $\langle\sigma'_H\rangle_{Av} = 81/(4\pi)$ b/sterad[24] and $\langle\sigma'_C\rangle_{Av} = 5.2/(4\pi)$ b/sterad[3] in the forward scattering direction, we obtain from Eqs. (17) and (18) $R_H = -0.11 \pm 0.19$ and, hence, from Eq. (4) for the spin flip probability:

$$Q = 0.56 \pm 0.10 \quad \textbf{(Hydrogen)}.$$

This result is consistent with the value $Q = 0.650 \pm 0.005$, obtained by substituting the free coherent and total scattering cross sections ($\sigma_{coh} = 0.50 \pm 0.075$b[4] and $\sigma = 20.36 \pm 0.10$b[24]) into Eq. (3) for Q. The agreement shows, together with the previously mentioned result on carbon, that our arrangement was equally capable of detecting the presence or absence of depolarization in the scattering of neutrons.

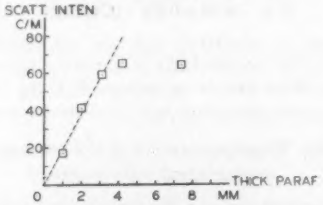

FIG. 4. Intensity of neutrons scattered from paraffin vs thickness of scatterer. The ordinate scale corresponds approximately to counts per minute.

(E) Measurements with the Oblique Arrangement—Phosphorus

Having, thus, demonstrated the applicability of our method, we have likewise applied it to the scattering of polarized neutrons from white phosphorus, the only one of the easily available mono-isotopic elements with nonzero spin which had not been investigated[25] by other methods.[4] Red phosphorus cannot be used for this experiment because it contains various amounts of adsorbed water depending on its age and method of preparation. Our phosphorus sample was melted into a brass box (0.010-in. wall thickness) approximately 5.4 cm long and fitting into the knee of the cadmium channel (see Fig. 2). The scattering mean free path in white phosphorus is 8.5 cm and, the scattered C-neutron intensity was only about 10 cpm. Seven hundred monitor intervals for each of the quantities entering into Eq. (15) yielded for the double-transmission effect on scattering:

$$\eta_D^* = 5.2 \pm 1.6 \text{ percent}.$$

The hardening factor was calculated to be $H = 1.13$ (see Appendix), and since the scattered neutrons showed no crystalline interference (Fig. 7), we can substitute into Eq. (12) to obtain the polarization ratio $R = -0.40 \pm 0.29$. Correction for the neutrons scattered from the brass container[26] (about 4 percent of the total scattered intensity) changes this number to -0.46 ± 0.30 and gives for the spin flip probability [Eq. (4)]:

$$Q = 0.73 \pm 0.15 \quad \textbf{(Phosphorus)}.$$

This result together with the value[27] 3.4b for the free

[24] Calculated from the free proton scattering cross section of 20.36b [E. Melkonian, Phys. Rev. **76**, 1744 (1949)]. The reason for using the bound scattering cross section comes from a consideration of center of mass effects. See, for example, L. I. Schiff, *Quantum Mechanics* (McGraw-Hill Book Company, Inc., New York, 1949), p. 105.

[25] We believe that this is due to a general reluctance to handle white phosphorus. Although due precautions must be taken not to touch the material, it can be melted under water at approximately 50°C and can then easily be poured (also under water) from one container to another. If copper sulfate is added to the water, the copper will plate out on the phosphorus and will protect it from oxidation when it is exposed to air. (We want to thank Professor Eric Hutchinson of the Chemistry Department, Stanford University, for having given us this valuable information.)

[26] Cu and Zn scatter predominantly coherently (reference 4) The correction follows from an expression similar to Eq. (18).

[27] "Columbia velocity selector," unpublished, quoted by R. K. Adair, Revs. Modern Phys. **22**, 249 (1950). Our own results would favor a value near 3.8b, while Hibdon and Muehlhause [Phys. Rev. **76**, 100 (1949)] give 4.1b.

TABLE I. Scattering data for isotopes with $I \neq 0$.[a]

Isotope	Spin I	Free total scattering cross section σ (barns)	Spin incoherent scattering cross section, σ_{inc} (barns)	Spin flip probability Q [Eq. (3)]	Prominent s-neutron scattering resonance[b]	Remarks
H^1	1/2	20.36	19.86	0.650		Virtual state of H^2.
H^2	1	3.3	1.1	0.22	?	
Li^7	3/2	~1.5	~0.9	~0.4	1.15 Mev[c]	
Be^9	3/2	6.1	0	0		No s-res. <1.5 Mev.
N^{14}	1	9.96[d]	6.0	0.4	?	2–150 kev not investigated; res. >500 kev.
F^{19}	1/2	~3.6	~0.5	~0.09		0.3–10 kev not investigated; res. >30 kev.
Na^{23}	3/2	3.2	1.8	0.37	3 kev	
Al^{27}	5/2	1.4	0	0		No res. <40 kev.
P^{31}	1/2	3.4	≥ 2.9[e]	≥ 0.58[f]	?	No res. <0.4 kev; not well investigated >0.4 kev.
V^{51}	7/2	5	>4.9	>0.65[f]	~2.7 kev	
Mn^{55}	5/2	2.2	0.9	0.27	0.345, 2.4 kev	
Co^{59}	7/2	~5	~3	~0.4	115 ev	
As^{75}	3/2	~7	~2	~0.2	10^3–10^5 ev	
Nb^{93}	9/2	6.2	~0.2	~0.02		No res. <0.4 kev; not investigated >0.4 kev.
I^{127}	5/2	3.8	0.4	0.07	20–40 ev	
Ta^{181}	7/2	7.0	0.9	0.09	4.0 ev	
Au^{197}	3/2	~9	~1.5	~0.1	4.8, >345 ev	
Bi^{209}	9/2	~10	~0	~0		No res. <1.5 Mev.

[a] Except where otherwise mentioned, the spin and cross section data are taken from K. Way *et al.*, *Nuclear Data* (Nat. Bur. Standards Circ. No. 499, 1950).
[b] Except where otherwise mentioned, the resonance scattering energies are taken from Harris, Muehlhause, and Thomas, Phys. Rev. **79**, 11 (1950); and from R. K. Adair, Revs. Modern Phys. **22**, 249 (1950).
[c] R. K. Adair, Phys. Rev. **79**, 1018 (1950).
[d] E. Melkonian, Phys. Rev. **76**, 1750 (1949).
[e] Present paper.
[f] Maximum value of Q is $\frac{1}{2}$.

total scattering cross section of phosphorus would yield a spin incoherent scattering cross section [Eq. (3)]:

$$\sigma_{inc} = 3.7 \pm 0.8\text{b},$$

or a coherent cross section of less than 0.5b.

IV. DISCUSSION

Other isotopes with non-zero spin for which σ and σ_{inc} are known[4] are listed in Table I. Calculations[28–32] using the Breit-Wigner formula[33] for resonance and potential scattering indicate that large spin incoherent scattering (or large spin flip probability) in these cases can be accounted for, at least in part, by one or more prominent s-neutron scattering resonances. These resonances are given in Table I.

Inspection of the available data on the total neutron cross section of phosphorus[27] shows no neutron resonances, but this is not too remarkable since the cross section has been measured with good energy resolution only between 0.02 and 400 ev. As in every well investigated light isotope, one might expect neutron resonances in the range of 0.05 to 3 Mev. Such resonances have been found recently[34] in the $P^{31}(n,p)$ cross section in the range of neutron energies from 1.9 to 3.8 Mev. However, in addition to these resonances our result of a large spin flip probability for phosphorus strongly suggests one or more prominent s-neutron scattering resonances even closer to the thermal region than 0.05 Mev. Indeed, we believe that the case of P^{31} may be similar to that of Na^{23}, which shows[35] a rather unsuspected scattering resonance at about 3000 ev, but our available means do not permit us to test this point.

The authors wish to thank Professor F. Bloch for the many stimulating discussions and encouragement during the course of this experiment. They also wish to thank Mr. H. Roderick for the preparation of the phosphorus scatterer and for the assistance in taking some of the data.

APPENDIX

We first wish to show that an expression in Eq. (10) of the form

$$\left[\int (C-1) k f d\tau\right] \Big/ \left[\int k f d\tau\right] \tag{19}$$

can be written as

$$\left[\int (C-1) f d\tau\right] \Big/ \left[H \int f d\tau\right], \tag{20}$$

where H is given by Eq. (11), independently of whether $C = C_A$, C_P, or C_D. Calling the thickness of the iron blocks magnetized in a particular experiment d_m, the theory of the polarizing effect[11] gives for $C-1$:

$$C-1 \cong \tfrac{1}{2} n^2 p^2 d_m^2 F. \tag{21}$$

n is the number of Fe atoms per cm^3, p is the polarization cross

[28] M. Hamermesh and C. O. Muehlhause, Phys. Rev. **78**, 175 (1950).
[29] C. T. Hibdon and C. O. Muehlhause, Phys. Rev. **79**, 44 (1950). This particular calculation may be somewhat inaccurate if the potential scattering of Cl^{35} or Cl^{37} is spin dependent.
[30] C. O. Muehlhause, Phys. Rev. **79**, 1002 (1950).
[31] R. K. Adair, Phys. Rev. **79**, 1018 (1950).
[32] W. Selove, Phys. Rev. **80**, 290 (1950).
[33] H. A. Bethe, Revs. Modern Phys. **9**, 69 (1937).
[34] E. Luescher *et al.*, Helv. Phys. Acta **23**, 561 (1950).
[35] Hibdon, Muelhause, Selove, and Woolf, Phys. Rev. **77**, 730 (1950).

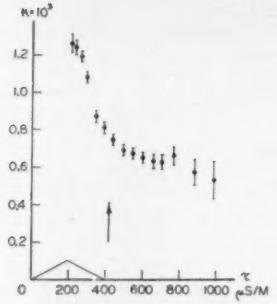

FIG. 5. The scattering factor $k(\tau)$ for the graphite scatterer. The arrow indicates the calculated position of the long wavelength Bragg cutoff. The resolution triangle is also shown.

section, and F is a function about which we need to know only that it depends on d_m and that it is velocity independent. Equation (21) assumes $n\rho d_m \ll 1$, which is fulfilled to a sufficient degree in our case. Substitution of Eq. (21) into Eq. (19) shows that the velocity-independent factor $\frac{1}{2}n^2 d_m{}^3 F$ cancels out, thus, establishing Eq. (20), independent of d_m.

In the calculation of the hardening factors [Eq. (11)] we have used plots of f and $p^3 f$ made by Professor Staub for reference 9. The scattering factor k was obtained for each scatterer by measuring the velocity spectrum of the scattered neutrons and comparing it to the direct spectrum from the howitzer. The iron blocks were removed for this measurement in order to gain intensity, and the inverse velocity resolution was made rather poor (200 μsec/m half-width) for the same reason.

Figure 5 shows k for the graphite scatterer. The drop around 300 to 400 μsec/m corresponds to the long wavelength Bragg cutoff expected at 420 μsec/m but broadened by the inverse velocity resolution.[36] In the calculation of H we have not corrected for this broadening, since it would not affect the accuracy of our results.

Figure 6 shows k for paraffin. Since the scattering cross section is proportional[3] to μ^2 and since the number of neutrons scattered

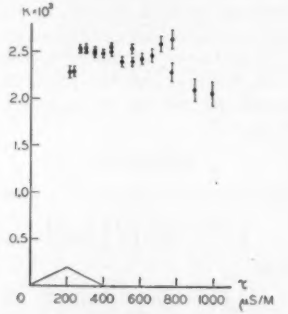

FIG. 6. The scattering factor $k(\tau)$ for the paraffin scatterer. At some neutron inverse velocities two independent measurements of the direct and scattered neutron spectra were made.

[36] The shape of this curve is quite similar to that taken for lead by R. Latham and J. M. Cassels, Nature **161**, 282 (1948).

in the *forward direction* into the detector is proportional[37] to $1/\mu^2$, where μ is the reduced mass of the neutron in terms of the neutron mass, k is expected to be practically velocity independent. At a scattering angle of 14° the calculated variation of k in our range of neutron velocities (Fig. 3) is only 2½ percent and, therefore, we have assumed $H=1.00$ in the calculation of Eq. (17).

Figure 7 shows k for the phosphorus scatterer. The absence of a noticeable Bragg cutoff, expected around 460 μsec/m corresponding to a lattice spacing[38] of 7.17A, shows the absence of any appreciable crystalline interference. This is consistent with the very diffuse scattering of x-rays at room temperature[39] and also with the large spin flip probability found in this experiment. If we assume that the decrease in scattered intensity with increasing inverse velocity is caused only by absorption in the phosphorus (the brass container contributes less than 6 percent to the absorption), the shape of the curve of Fig. 7 should follow Eq. (8). Comparison with this equation yields an absorption cross section many times larger than the values of[39] 0.15 to[40] 0.3b quoted in the literature.

Subsequent experiments have shown that the total *direct transmission* cross section of our phosphorus sample is consistent

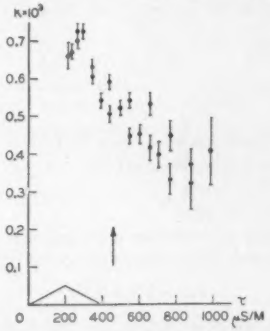

FIG. 7. The scattering factor $k(\tau)$ for the phosphorus scatterer. The arrow indicates the calculated position of the long wavelength Bragg cutoff. At some neutron inverse velocities two independent measurements of the direct and scattered neutron spectra were made.

with the literature values of the absorption cross section so that there are no absorbing impurities in our sample. Also, by using a thinner scatterer, we have shown that the apparent large absorption cross section for the *scattered* neutrons is not due to multiple scattering. Therefore, we are forced to assume that the decrease in k with increasing neutron wavelength is mostly due to temperature scattering effects[14] and that, hence, Eq. (8) is not applicable to Fig. 7. Although we have not compared the shape of our curve with the rather complicated[14] and by no means certain[41] calculations on temperature scattering, we feel that we were justified in calculating the hardening factor for phosphorus by using the experimentally determined k values (Fig. 7).

[37] L. I. Schiff, *Quantum Mechanics* (McGraw-Hill Book Company, Inc., New York, 1949), p. 105.

[38] G. Natta and L. Passerini, Nature **125**, 707 (1930).

[39] H. Pomerance, unpublished, quoted by K. Way *et al.*, *Nuclear Data* (Nat. Bur. Standards Circ. No. 499, 1950). See also F. C. W. Colmer and D. J. Little, Proc. Phys. Soc. (London) **A63**, 1175 (1950).

[40] M. Ross and J. S. Story, Progress Reports in Physics **12**, 291 (1949).

[41] J. M. Cassels and R. Latham, Phys. Rev. **74**, 103 (1948).

Radioactivity of Astatine Isotopes*

G. W. Barton, Jr.,† A. Ghiorso, and I. Perlman
Radiation Laboratory and Department of Chemistry, University of California, Berkeley, California
(Received December 18, 1950)

A number of new neutron deficient isotopes of astatine have been identified in the mass number range 200 to 209 following the irradiation of bismuth with high energy helium ions. Their alpha-decay properties fall in line with predictions for isotopes in this region with less than 126 neutrons; that is, the alpha-energies increase with decrease in mass number. Because of the complexity of the isotopic mixtures, half-lives and mass number assignments were made, in most cases, through the identification of decay products of lower atomic number. The decay properties as now known are summarized.

I. INTRODUCTION

As part of the program in this laboratory to determine and correlate radioactive properties of the heavy elements, a study was undertaken of the isotopes of astatine which can be prepared by the irradiation of bismuth with high energy helium ions. Of particular interest in the case of astatine isotopes is the characterization of those with less than 126 neutrons, since it has been shown[1] that there are abrupt changes in the trends of alpha-decay properties in crossing this region. The well-known isotope At^{211} is the one with 126 neutrons,[2] and the present study includes identification of new isotopes tentatively assigned to mass numbers as low as 201. All of the astatine isotopes discussed here are unstable toward electron capture, and the difficult problem of assigning partial half-lives for that mode of decay and for alpha-emission is still in an unsatisfactory state.

Some of the energies and half-lives found in the present study have been referred to briefly in another publication.[1] The present picture of all nuclei in this region is shown as a segment of an "isotope chart" (Fig. 1) in which are indicated half-lives, *observed* modes of decay, and alpha-energies for the new and previously reported isotopes of astatine. Some isotopes of polonium, bismuth, lead, and thallium are also entered because these will be referred to in the discussion of isotopic assignments of the astatine isotopes.

II. METHODS

The most feasible method for preparing astatine isotopes in the mass number region in question is the irradiation of bismuth (Bi^{209}) with helium ions of 60 Mev and greater. At these energies a complex mixture of activities is invariably encountered, and genetic relationships with previously known activities must be relied upon for the most part in making isotopic assignments. The variation of projectile energy is of some importance in these studies, since the order of appearance of new activities with successive increase in energy sets the order of mass numbers.

Most of the irradiations in the 184-in. cyclotron were made with the undeflected beam striking an internal probe target in which strips of bismuth metal were clamped to a water-cooled copper block. In some cases bismuth oxide in aluminum foil envelopes was similarly bombarded. For the short-lived activities, powdered bismuth metal or oxide was bombarded in a special stainless steel tube which was drawn out of irradiation position, through a pneumatic tube, directly into the chemistry laboratory. This pneumatic tube target allows one to begin chemical separations within about 20 sec after the beam is turned off.

For either type of target arrangement, energies were changed by radial displacement of the target permitting selection of helium ion energies up to the maximum of 380 Mev. In all irradiations, energies were such that the particular bismuth samples used could be considered to be "thin targets."

III. CHEMICAL PROCEDURES

Besides the mixture of astatine isotopes, each target contained, in high yield, isotopes of polonium, bismuth, lead, and thallium; and in lower yield, spallation products further removed from bismuth, and bismuth fission products. The methods of identifying the astatine isotopes varied for different species and will be discussed for the individual cases, but some general remarks can be made to give reason for the chemistry employed. The general procedure was to obtain a pure astatine fraction without carrier so that alpha-particles could be identified according to energy and half-life with the alpha-pulse analyzer,[3] and then to remove from this fraction, periodically, such polonium, bismuth, and lead isotopes as had grown through electron capture and alpha-particle decay. The identification of the growth of known daughter activities with particular astatine activities was the principal method employed for making mass number assignments. Since the astatine isotopes in question have half-lives of the order of an hour down to a few minutes, rapid chemical procedures were required.

* This work was performed under the auspices of the AEC.
† Now at the Argonne National Laboratory, Chicago, Illinois.
[1] Perlman, Ghiorso, and Seaborg, Phys. Rev. 77, 26 (1950).
[2] Corson, Mackenzie, and Segrè, Phys. Rev. 58, 672 (1940).
[3] Ghiorso, Jaffey, Robinson, and Weissbourd, *The Transuranium Elements: Research Papers* (McGraw-Hill Book Company, Inc., New York, 1949), paper No. 16.8, Vol. 14B. National Nuclear Energy Series, Plutonium Project Record.

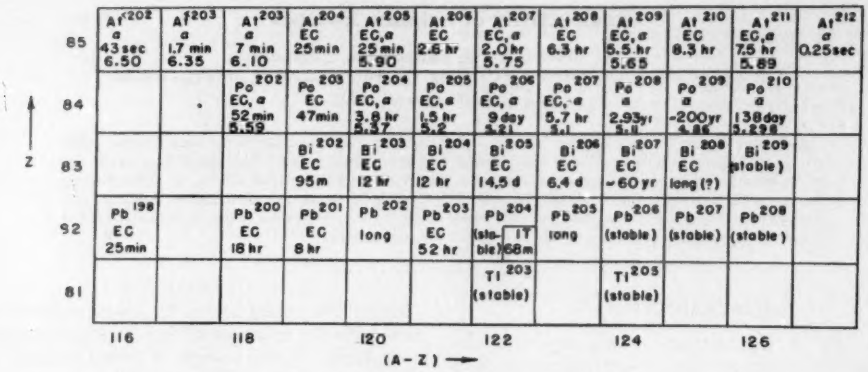

FIG. 1. Isotope chart of thallium-astatine region.

The method developed for removal of pure astatine consisted in its extraction, presumably while in the zero oxidation state, into diisopropyl ether (DIPE). The bismuth target was dissolved in such a manner as to end up with a solution in concentrated hydrochloric acid to which ferrous sulfate was added to make sure that the astatine was reduced to the zero state. This solution was contacted with DIPE. The DIPE solution was washed with dilute sulfuric acid, or hydrochloric acid, and so far as could be told by absence of polonium and bismuth alpha-activity, the astatine was pure. Samples of the DIPE solution could then be evaporated on platinum or stainless steel disks for radiation measurement.

A solution containing pure astatine isotopes in the mass number range in question begins to grow, successively, polonium and lower element daughters principally by electron capture decay. In an experiment to identify astatine isotopes through genetic relationships, the astatine is first purified, allowed to stand for an interval of the order of the half-life of the parent, the daughter elements removed and separated from each other, and the decay characteristics of each followed. This "milking" process is repeated on the parent solution at equal time intervals.

The polonium, bismuth, and lead may be removed periodically by adding one-tenth volume of 20 percent tributyl phosphate (TBP) in isobutyl ether to the DIPE solution and extracting into a $2M$ nitric acid $-4M$ hydrochloric acid aqueous solution. These elements leave the organic phase, quantitatively, in only about one minute contact time while the astatine remains quantitatively in the organic layer. The polonium can then be separated from bismuth and lead by extracting into TBP solution after destroying the nitrate ion and making the aqueous solution $6M$ HCl. (The behavior of polonium in TBP extraction from HCl and HNO_3 solutions has been investigated by others in this laboratory.)[4] The bismuth and lead are separated by precipitating the bismuth as BiOCl and the lead as $PbSO_4$.

For very rapid separation of astatine from the bismuth target, a different method was used which gives astatine of somewhat uncertain purity but which was considered adequate for determination of short-lived alpha-emitters. The basis for the method is the distillation of astatine from molten bismuth. The bismuth target is dropped into a stainless steel crucible fitted on top with a water-cooled steel finger to which a collecting platinum disk is clamped. When the bismuth is kept slightly above its melting point (as measured by a thermocouple fitted into a well in the crucible), within a few seconds astatine distills onto the collecting plate. Polonium does not distill in appreciable quantities until considerably higher temperatures are reached. Using the vacuum carrier system to deliver the target, this procedure permits samples to be in the alpha-pulse analyzer within 90 seconds after the cyclotron beam is shut off.

In some instances recoil methods were used to separate the alpha-decay daughters. The astatine, plated on a silver foil, was placed in a vacuum chamber with a collecting plate maintained at a few hundred volts negative potential. Some astatine volatilized across the gap and contaminated the bismuth daughters caught by alpha-particle recoil. To remove this, some sulfuric acid was placed on the platinum collecting plate which was heated until the H_2SO_4 was fumed off. This step converted the bismuth to its sulfate which remained on the plate when flaming it to remove the astatine.

IV. RESULTS

In all irradiations the previously known isotopes of astatine, 7.5-hr At^{211} and 8.3-hr At^{210}, could be observed. At^{211} is identified readily, using an alpha-pulse analyzer,

[4] D. G. Karraker and D. H. Templeton, Phys. Rev. 81, 510 (1951).

by the characteristic twin alpha-particle peaks,[5] that of the alpha-decay of At^{211} itself (5.89 Mev) in 40 percent of the events, and a high energy peak (7.43 Mev) which is the alpha-particle of Po^{211} (AcC') from the 60 percent electron capture branching at At^{211}. The other isotope, At^{210}, decays by electron capture with 8.3-hr half-life[6] and no observable alpha-branching. Its presence may be determined quantitatively by counting the alpha-particles of the daughter, Po^{210}, after decay of the parent.

The other astatine isotopes observed in these studies have not been reported previously aside from mention of two of them in the Table of Isotopes.[6] In discussing some of these, excitation functions will be of value and such curves, over a limited energy range (60–95 Mev), are shown in Fig. 2. As will be noted, no attempt has been made to define the curves accurately, but as they stand they are helpful in making mass number assignments and in visualizing the mixture of activities encountered in this energy range. The curve for At^{211}, as shown, is a segment of that obtained by Kelly.[7] At^{211} was used as a monitor to which the other isotopes were normalized; that is, all yields determined for a given sample were measured relative to the At^{211} in that sample.

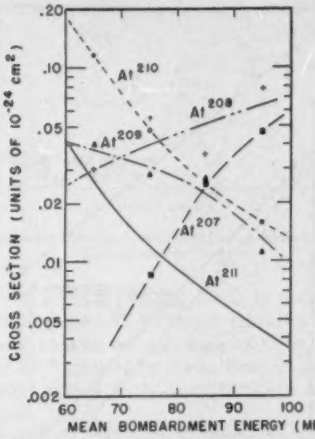

FIG. 2. Rough excitation functions of the astatine activities produced with 60–100-Mev helium ions on bismuth. (The points observed have been normalized to fit the excitation function of Kelly (see reference 2) for At^{211}.) ———— At^{211} (according to Kelly). ●– – – – – – ● At^{210}. ▲– – – – ▲ At^{209}. +——– – ——+ At^{208}. ■—— —— ■ At^{207}.

At^{209}

An activity assigned to At^{209} is characterized by a half-life of 5.5±0.3 hr and an alpha-particle of 5.65 Mev. It is estimated that it decays with about 5 percent alpha-branching and about 95 percent electron capture.

The assignment to At^{209} is based on several pieces of evidence. One point concerns its relationship, in Fig. 2, to At^{208} assigned with some confidence through its genetic relationship[8] with Po^{208}. As seen, the yield of the activity assigned to At^{209} falls off at energies at which At^{208} is still climbing. While attention is focused on the excitation curves, it may be mentioned that no At^{209} could be identified below 55 Mev, but this is not to be interpreted as the threshold. The reason the threshold cannot be determined is because of the rapidly climbing yield of At^{211} with decrease in energy and the tail of its 5.89-Mev alpha-group obscures the 5.65-Mev group of At^{209}. The pulse analysis of the astatine fraction from the irradiation of bismuth with 65-Mev helium ions is shown in Fig. 3. The energy band was spread out to cover only about ¾ Mev over the entire register bank; therefore, the high energy group accompanying At^{211} (7.43 Mev Po^{211}) was not registered. Only the two groups are seen because At^{210} and At^{208} decay almost entirely by electron capture and inappreciable quantities of At^{207} are formed at this energy (compare with Fig. 2). The At^{209} peak is smaller than that of At^{211}, while the cross section for formation is shown larger in Fig. 2 because At^{209} is assumed to have only 5 percent alpha-branching while that for At^{211} is 40 percent.

The half-lives of the alpha-particle groups cannot be resolved with any accuracy by gross alpha-counting, but with the pulse analyzer the decay of the two peaks may be followed separately. The decay observed in this manner is plotted in Fig. 4, from which the value 5.5±0.2 hr is obtained. The two limits shown denote the uncertainty in resolution of the two alpha-peaks of Fig. 3 and are felt to be the extreme deviations introduced from this source.

With some knowledge of the half-life, two other checks of the isotopic assignment become possible. These are the identification of electron capture and alpha-decay daughters and the observation that amounts, which grow in during successive time intervals, fall off with the half-life of the parent. The electron

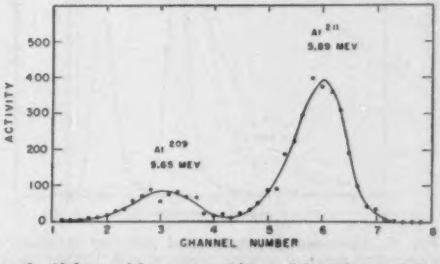

FIG. 3. Alpha-particle spectrum from alpha-pulse analysis of astatine made with 65-Mev helium ions on bismuth.

[5] E. L. Kelly and E. Segrè, Phys. Rev. 75, 999 (1949).
[6] G. T. Seaborg and I. Perlman, Revs. Modern Phys. 20, 585 (1948).
[7] E. L. Kelly, University of California Radiation Laboratory Unclassified Report UCRL-277 (January, 1949) (unpublished).
[8] Templeton, Howland, and Perlman, Phys. Rev. 72, 758 (1947).

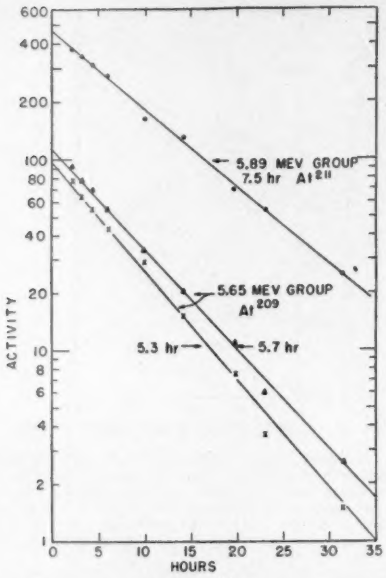

FIG. 4. Decay curves of At^{211} and At^{209} from data obtained by successive pulse analyses (see Fig. 3). ● 5.89-Mev group. ▲ Total activity under 5.65-Mev peak. × Activity under 5.65-Mev peak after subtracting a maximum possible tailing from At^{211}.

capture product[5] is Po^{209}, which, because of its long half-life, estimated to be about 200 yr, makes accurate measurement difficult with the amounts of At^{209} that could be prepared. Nevertheless, Po^{209} was definitely identified and the proper half-life for At^{209} reproduced. The particular astatine sample was prepared at 120 Mev, and at approximately 5-hour intervals an aliquot of polonium was purified and plated on a disk where it was allowed to undergo complete decay. The resulting polonium activities were analyzed according to energy, and a typical plot is shown in Fig. 5. The Po^{208} peak

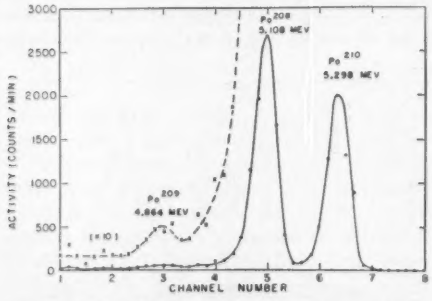

FIG. 5. Alpha-particle spectrum of polonium activities remaining after decay of astatine produced with 120-Mev helium ions on bismuth. (Broken line is on tenfold expanded ordinate scale.)

resulted from the decay of At^{208} to be discussed below, and the Po^{210} came from the decay of 8.3 hr At^{210}. The energies shown for Po^{208} and Po^{209} are probably more accurate than those which have been reported previously. Other astatine isotopes formed in the bombardment were either too short-lived, or their polonium daughters were too short-lived, to be seen under the conditions of the chemical separations. The amounts of Po^{209} that grew during each period could be calculated from the pulse analysis curves. In order to overcome variations in chemical yield, the data for Po^{210} were adjusted to the 8.3-hr half-life of its parent and other yields were normalized to them. These curves are shown in Fig. 6 in which a 5.7-hr half-life is found for At^{209}. This is in excellent agreement with the half-life obtained by following the decay of the alpha-particle peak at 5.65 Mev considering the uncertainties in

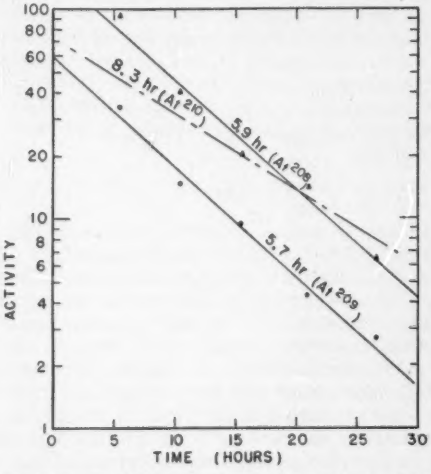

FIG. 6. Half-lives for At^{209} and At^{208} determined by yields of polonium daughters. —— – —— Yield of Po^{210} (normalized). —— ● —— 100×yield of Po^{209}. —— ▲ Yield of Po^{208}.

resolving the weak Po^{209} peaks. The alpha-branching of At^{209} was calculated from the ratio of its alpha-particles to that of the Po^{209} by assuming the Po^{209} half-life to be 200 yr as estimated from yield considerations by Kelly and Segrè.[5] It is from this calculation that the alpha-branching was found to be 5 percent.

The alpha-decay daughter can be used in as similar a manner as the electron capture daughter to determine mass number and half-life of the parent. The alpha-decay product is Bi^{205}, shown by Karraker and Templeton[4] to be an electron capture activity with a 14.5-day half-life. The Bi^{205} was separated in two ways: by chemical separation from the astatine and other decay products, and by collecting the recoils from the alpha-decay. In both cases the ~14-day period was identified without difficulty. Decay curves of the parent deter-

mined by yields of Bi^{205} gave, for two experiments, 5.4 hr and 6.2 hr, which is considered to be satisfactory agreement.

At^{208}

This isotope formed by the $(\alpha,5n)$ reaction had no discernible alpha-decay, but the limits of detection are poor, particularly if its energy is close to that of At^{209}. It was detected at 55 Mev, the lowest energy used in these studies, and at higher energies through its electron capture decay daughter, Po^{208}. Its excitation function (Fig. 2) agrees with this assignment in that it appears at lower energies than an activity assigned to At^{207} and does not drop off in yield as fast as At^{209}.

It has not been possible to resolve the radiation of At^{208} from the complex mixture so that its half-life could be determined only by successive removal and yield measurement of the Po^{208} daughter. Figure 6 shows a plot of such data in which a 5.9-hr half-life for the parent is noted. Another similar experiment indicated a half-life of 6.7 hr. For the present, we assume the half-life to be 6.3±0.5 hr.

As mentioned, no alpha-particles attributable to At^{208} have been noted. If the alpha-energy falls in a gap between others present, the alpha-branching could be as low as 1 percent; but if the alpha-group is obscured by the other isotopes present, it could be considerably higher, say 10 percent. No experiments, to measure the alpha-decay daughter 12-hr Bi^{204}, were performed which could shed some light on the alpha-branching.

It is interesting to note that Hyde, Ghiorso, and Seaborg[9] have reported another set of properties for At^{208}. Their activity arose from the alpha-decay of Fr^{212} and had a 1.7-hr half-life and alpha-particle of 5.65 Mev. The evidence for mass number assignments for the two activities are fairly convincing and we shall assume that they are isomers of At^{208}. It is not surprising that only one isomer should be seen from the alpha-decay of Fr^{212}, but we would expect both to be formed in an appreciable yield in the bombardment of bismuth. However, if the 1.8-hr isomer were formed in lower yield than the 6.3-hr period, it might not have been picked up through the Po^{208} daughter and its alpha-particles would have been submerged in those of At^{209}, which has the same energy. As mentioned below, there is some scanty evidence that there is some activity at 5.65 Mev with a shorter half-life than that of At^{209}.

At^{207}

At 75 Mev a new activity appeared having a half-life of about 2 hr, and this has been assigned to At^{207} formed by the $(\alpha,6n)$ reaction (Fig. 2). An alpha-pulse analysis of astatine prepared at 85 Mev is shown in Fig. 7, in which a new group at 5.75 Mev has appeared. In Fig. 8 are plotted the decay data of the individual peaks of Fig. 7, from which it is seen that the 5.75-Mev group

[9] Hyde, Ghiorso, and Seaborg, Phys. Rev. 77, 765 (1950).

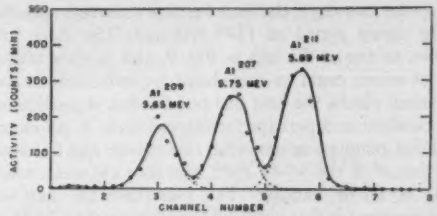

FIG. 7. Alpha-particle spectrum of astatine prepared with 85 Mev helium ions on bismuth.

decays with a 2.0-hr half-life. It will be noted that the early points of the 5.65-Mev peak indicate a short-lived component at this energy. This may be the 1.8-hr isomer of At^{208} reported by Hyde, Ghiorso, and Seaborg and formed in sufficiently favorable yield to make its appearance.

Along with the excitation function, the identification of the alpha-decay and electron capture decay daughters have served to assign the mass number 207 to this activity. In one experiment, bismuth recoils were caught over two time intervals and after decay (of 12-hr Bi^{208}), 52-hr Pb^{203} was identified and the decrease in yield corresponded to a half-life of somewhat under 2 hours for the parent. To obtain larger amounts of Pb^{203} in order to prove its identity, chemical separation of combined bismuth, lead, and polonium was made from a sample of astatine prepared at 110 Mev. These fractions were removed at 2-hr intervals, allowed to

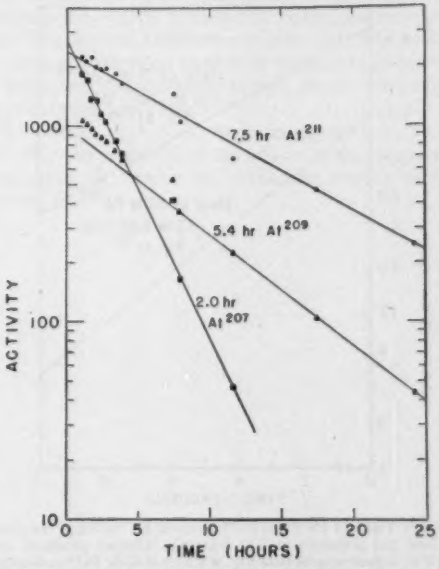

FIG. 8. Decay curves of At^{211}, At^{209}, and At^{207} from data obtained by successive pulse analyses (see Fig. 7).

decay for two days, the lead fraction removed, and the 52-hr decay period of Pb^{203} followed. The data are shown as one of the sets in Fig. 9, and in view of the errors which could be introduced by variations in the chemical yields, the best line of 1.9 hours is considered an excellent and perhaps fortuitous check. A polonium fraction removed in a similar experiment was followed for decay[9] of the 5.7-hr Po^{207}, and its yield went down with a 1.7-hr half-life. The most reliable half-life measurement is that obtained by following the 5.75-Mev peak on the pulse analyzer rather than the more complex procedures involving chemical separations just discussed.

No serious attempt has been made to determine the degree of alpha-branching of At^{207}. The best estimate from the alpha-particles of At^{207} and the yield of Po^{207} is 10 percent alpha-branching. This involves considerable uncertainty because of the unknown counting efficiency of the Po^{207} radiation. The cross sections for At^{207} in Fig. 2 are based on 10 percent alpha-branching.

At^{206}

In the same experiment (110-Mev helium ions) in which the astatine fraction yielded Pb^{203}, indirectly, from the alpha-decay at At^{207}, the polonium fraction[8] showed the presence of 9-day Po^{206} from the electron capture decay of At^{206}. Other polonium isotopes, Po^{210} and Po^{203}, were also present. Figure 9 shows that the yield of Po^{206} goes down with a half-life of 2.6 hr for the parent, At^{206}. No radiations directly attributable to At^{206} could be observed because of the complex mixture of other activities.

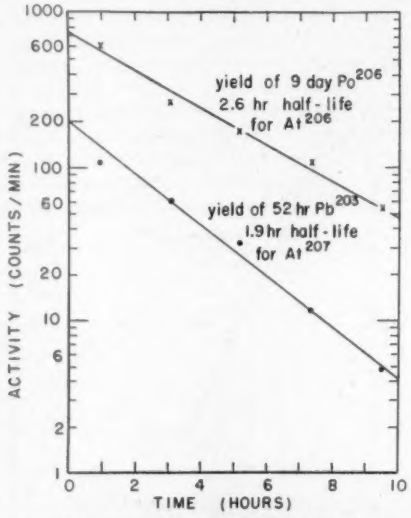

FIG. 9. Yields of Pb^{203} and Po^{206} observed by "milking" astatine for lead and polonium at 2-hr intervals (astatine produced by 110 Mev helium ions on bismuth). ● Yields of 52-hr Pb^{203} indirectly from alpha-decay of At^{207}. × Yields of 9-day Po^{206} from electron capture decay of At^{206}.

At^{205} and At^{204}

At higher bombardment energies other astatine isotopes were formed. These were, of course, farther from beta-stability and would be expected to have shorter half-lives toward electron capture decay. In addition, the alpha-energies would be expected to become progressively higher, and consequently, the half-lives would become shorter.[1]

Using 150-Mev helium ions, the astatine fraction was subjected to chemical separations in which polonium fractions were removed at short intervals. Each polonium fraction was allowed to decay for five hours, and then the bismuth fraction was removed and its decay followed. It was the object of this experiment to find the half-lives of the At^{205} and At^{204}, grandparents of 14-day Bi^{205} and 12-hr Bi^{204}. The bismuth decay curves were resolved and the yields plotted, as in Fig. 10 in which it is seen that half-lives of about 25 min are indicated for both At^{205} and At^{204}. Alpha-pulse analysis of another higher energy bombardment showed a single peak at 5.90 Mev with this half-life. Considerable further work would need to be done to establish the mass number to which the 5.90-Mev alpha-particle belongs and to establish whether, indeed, it may have two components which cannot be resolved.

For the present, we shall attribute the alpha-particle,

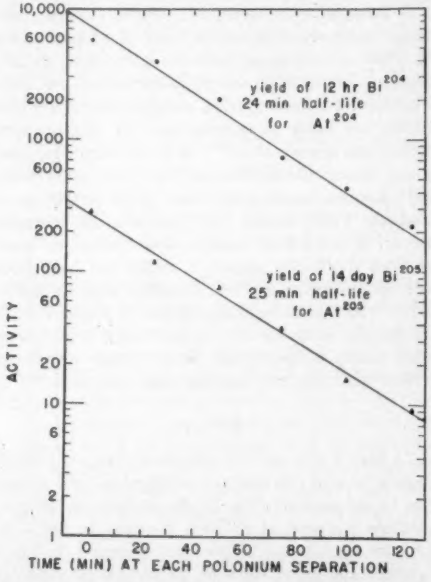

FIG. 10. Yields of Bi^{204} and Bi^{205} separated from polonium fractions which were in turn separated from an astatine sample prepared with 150 Mev helium ions on bismuth.

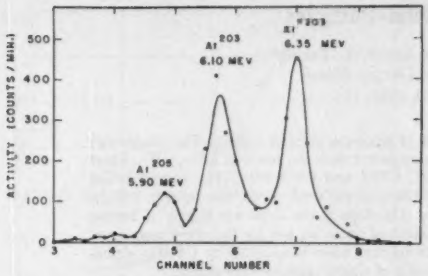

FIG. 11. Alpha-pulse analysis of astatine prepared with 275-Mev helium ions on bismuth.

which was found to decay with a 25-min half-life, to At^{205} and leave the At^{204} with its 25-min half-life and no alpha-particles indicated. The arguments are not very strong for this assignment over the reverse and have to do with the generally shorter half-lives for alpha-decay of the odd-even nuclei as compared with the odd-odd ones of the same or similar decay energy. For example, the alpha-particles of At^{211}, At^{209}, and At^{207} are seen; those of At^{210}, At^{208} (one of the isomers), and At^{206} are not. The argument is admittedly weak.

A^{203} and Lighter Isotopes

An irradiation with 275-Mev helium ions produced still other astatine isotopes. This bombardment and others at higher energies were made with pneumatic tube targets in order that the short half-lives might be seen. Figure 11 shows the alpha-pulse analysis of the astatine fraction in which new groups at 6.10 and 6.35 Mev appeared. The decay curves of these peaks are plotted in Fig. 12 along with part of that of 23-min At^{205}.

Since these new activities first appeared at higher energies than At^{205} and At^{204}, it is necessary to assign lower mass numbers to them. Their alpha-energies are in conformity with this assignment. For the present we shall assume the 7-min 6.10-Mev group to be At^{203}

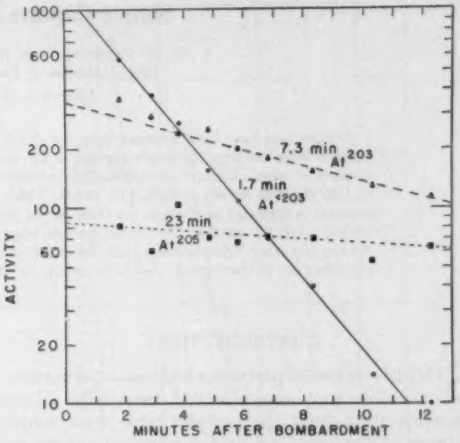

FIG. 12. Decay of the alpha-groups shown in pulse analysis of Fig. 11. ——— ● $At^{<203}$ 6.35-Mev α. — — — ▲ At^{203} 6.10-Mev α. - - - - - ■ At^{204} 5.90-Mev α.

and designate the 6.35-Mev group with 1.7-min half-life as $At^{<203}$. None of the decay products of these activities have been examined.

Using the full energy helium ions of the 184-in. cyclotron (380 Mev), other short-lived activities appeared. One, which we shall designate $At^{<202}$, has a 43-sec half-life and alpha-particles of 6.50 Mev.

Other alpha-particle groups of lower energy and half-lives in the range 1 to 3 minutes were also observed. Although one or more of these may be astatine isotopes, their energies and half-lives are such that they could be polonium daughters of short-lived astatine isotopes, or polonium contamination carried in the extremely rapid chemical procedure.

We wish to express our appreciation to J. T. Vale and the other members of the 184-in. cyclotron operating group for making the irradiations used in these studies.

Simple Capture of Alpha-Particles

W. E. Bennett, Paul A. Roys, and B. J. Toppel*
Illinois Institute of Technology, Chicago, Illinois

(Received October 30, 1950)

Gamma-rays have been observed from the simple capture of alpha-particles in lithium. The gamma-ray energies were too large for simple capture in Li^8, but not inconsistent with the reaction $Li^7(\alpha,\gamma)B^{11}$. Three resonances were observed at bombarding energies of 0.401, 0.819, and 0.958 Mev. The corresponding excited states in B^{11} are at 8.90, 9.16, and 9.25 Mev. The yields were too small to use thin targets, but the resonances appeared as steps in the thick target yield curve. The slope of the steps was largely of instrumental origin for the first two resonances and suggested a width of about six kev for the upper resonance. Among the other light elements, only Be and B yielded gamma-rays when bombarded by 1.4-Mev alpha-particles; but in these cases, the sharp resonances characteristic of simple capture were absent.

I. INTRODUCTION

SIMPLE capture of particles with emission of gamma-radiation has been observed frequently. Many elements throughout the periodic table show simple capture of neutrons, and proton capture has been reported in many of the lighter elements. Theory does not suggest any reason why simple capture should not be observed for alpha-particles in light nuclei. The Q values are positive except for atomic number below three, while the competing reactions involving heavy particle emission have negative Q values in most cases. The only problem is to find whether or not the nuclei produced in the reaction have excited states of appropriate energy in which the alpha-particles can be captured. The yield of gamma-rays from simple capture should be independent of the penetrability of the potential barrier as long as the width of the level remains much larger than a few electron volts.[1]

Natural sources of alpha-particles are unsuitable for a study of simple capture because the yield of gamma-radiation is always small and because the yield curves usually show sharp resonances.

II. EXPERIMENTAL ARRANGEMENT

The alpha-particles were produced by accelerating singly charged helium atoms in the Illinois Institute of Technology electrostatic generator. The beam to be used was bent magnetically and was passed through a narrow slit. The part of the beam which struck the edges of the slit was used as the signal for a controlled corona system of the type described by McKibben, *et al.*[2] Using this regulating system kept the energy of the beam constant to about ± 1.2 kev.

Thick targets were used containing the elements Li, Be, B, C, N, and O. For the first three the metals were used, and for the last three, graphite, urea, and quartz. The lithium metal probably formed a carbonate which decomposed under bombardment. A black spot formed on each target under bombardment, but this was minimized by using a dry-ice cold trap between the pump and the target chamber and by changing to new spots

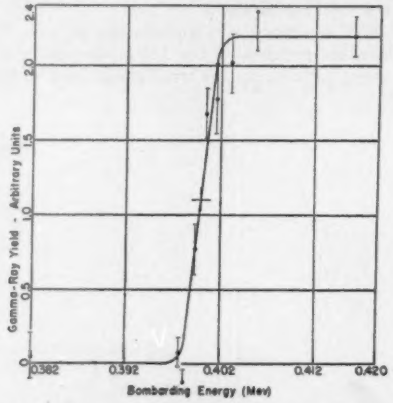

FIG. 1. The lower $Li^7(\alpha,\gamma)B^{11}$ resonance. The resonance energy is 0.401 Mev.

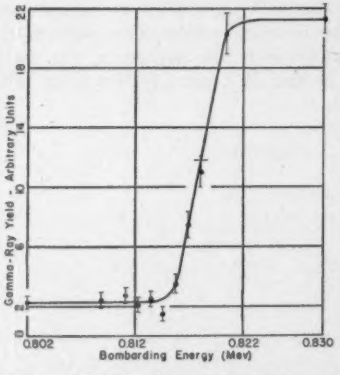

FIG. 2. The middle $Li^7(\alpha,\gamma)B^{11}$ resonance. The resonance energy is 0.819 Mev.

* AEC Predoctoral Fellow.

[1] Bröström, Huus, and Tangen, Phys. Rev. 71, 661 (1947).

[2] McKibben, Frisch, and Hush, U. S. Atomic Energy Commission Declassified Document No. MDDC-222 (1946) (unpublished).

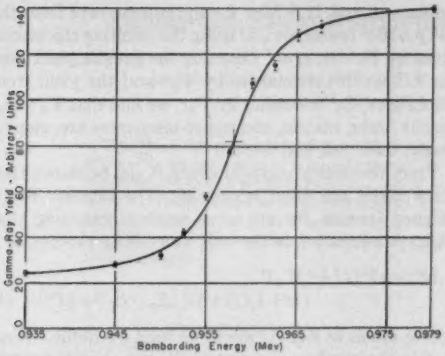

FIG. 3. The upper $Li^7(\alpha,\gamma)B^{11}$ resonance. The resonance energy is 0.958 Mev. The curve was calculated for $\Gamma=6$ kev.

on the target frequently. The yield of gamma-radiation from lithium was found to increase with time when the targets were new. This was caused by decomposition rather than by contamination, since the common contaminants gave no gamma-rays at all. Lithium fluoride targets were also used to facilitate calibration of the generating voltmeter. The beams falling upon the targets were measured by a current integrator of the type described by Watt.[3]

The gamma-rays were detected by a pair of coincidence beta-counters placed immediately outside the target holder in line with the analyzed beam. The absorption between the two counters owing to the walls was equivalent to 0.3 mm of aluminum. The counters were 4 cm apart and between them was placed an aluminum absorber 1.6 mm thick to reduce the background caused by x-rays from the electrostatic generator.

III. PROCEDURE AND RESULTS

When the lithium target was used, three resonances were observed for bombarding energies below 1.4 Mev. These resonances are shown in Figs. 1–3, and will be referred to as the lower, middle, and upper resonances, respectively. In all three figures, the abscissa interval is 10 kev. Although the yields of gamma-rays are in arbitrary units, the same arbitrary scale has been used in all three diagrams, so that each figure is a continuation of the preceding one. The vertical lines on the experimental points represent the probable error due to statistics of counting. The data have been corrected for background counts.

The voltage was measured by a generating voltmeter[4] which was calibrated from observations on the $F^{19}(p\alpha',\gamma)O^{16}$ resonance[5] at 0.8735 Mev. The calibration changed gradually during the day in a way which suggested that it was caused by the heating-up of the electrostatic generator during operation. The effect was eliminated by recalibration of the generating voltmeter immediately before and after each determination of the position of the resonance in question. Only a few minutes were required to change from hydrogen to helium in the ion source. To avoid changing of the target, a LiF target was used. Consistent results were obtained and the final values for the positions of the resonances were 0.401, 0.819, and 0.958 Mev. The errors are ± 0.001 Mev except for the lower resonance in which there may be an additional error caused by nonlinearity of the generating voltmeter.

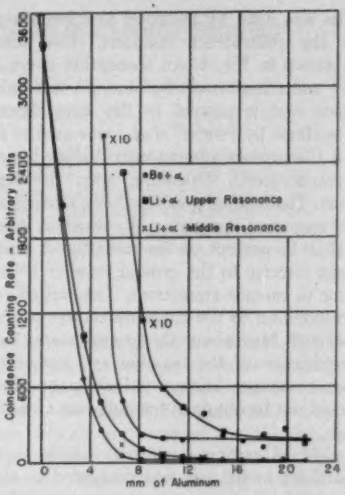

FIG. 4. Absorption curve in aluminum of the secondary electrons produced by gamma-radiation. The lower curve is for 4.45-Mev gamma-rays.

The slope of the step in a thick target yield curve can be used to get the width of the resonance if correction is made for the slope owing to instrumental fluctuations. From the slope of the lower and middle resonances, upper limits of 1 kev can be set to the true width of these resonances. The upper resonance is much broader, and the corresponding width can be determined. The best value in the room coordinate system is 6 kev. The line drawn in Fig. 3 is of theoretical shape for a thick target, obtained by integrating a Breit-Wigner dispersion function with $\Gamma=6$ kev and including the effect of instrumental fluctuations. The shape fits the experimental points quite closely.

Targets of the common contaminants (carbon, nitrogen, and oxygen) yielded no gamma-rays when bombarded by 1.4-Mev alpha-particles. Either Li^6 or Li^7 was the nucleus responsible for the observed effects. It was possible to identify the reaction as $Li^7+He^4 \rightarrow \gamma+B^{11}+8.64$ Mev rather than $Li^6+He^4 \rightarrow \gamma+Be^{10}+4.36$ Mev by measuring the energies of the gamma-

[3] B. E. Watt, Rev. Sci. Instr. 17, 334 (1946).
[4] Trump, Safford, and Van de Graaff, Rev. Sci. Instr. 11, 54 (1940).
[5] Herb, Snowdon, and Sala, Phys. Rev. 75, 246 (1949).

rays. This was done by inserting aluminum absorbers between the coincidence counters. The absorption curve is shown in Fig. 4. An absorption curve for the 4.45-Mev radiation[6] from $Be^9(\alpha,n)C^{12}$ was taken for comparison and is plotted in the same figure. The method outlined by Fowler, *et al.*,[7] was used to find the energy of the capture gamma-rays. Values from 5 to 7 Mev were obtained, depending upon the degree of absorption. The method gives too low a maximum value when the spectrum is complex. A consistent interpretation is that 15 percent of the radiation is emitted in transitions directly to the ground state of B^{11} and the rest is due to cascade transitions. The excited states in B^{11} corresponding to the three resonances are at 8.90, 9.16, and 9.25 Mev above the ground state. However, the identification of the reaction was less certain for the lower resonance because an accurate absorption curve could not be obtained for radiation of such feeble intensity.

The yield of gamma-rays from simple capture of alpha-particles in lithium was compared to the yield from the 440-kev resonance in the reaction $Li^7(p,\gamma)Be^8$ using the same target and detector. The counting rates above the three resonances were 0.9, 9, and 60×10^{-4} of the counting rates for 0.54-Mev protons. With these low counting rates it was not feasible to use thin targets to study the resonances.

The beryllium and boron targets yielded gamma-rays when bombarded with 1.4-Mev alpha-particles, but in these cases the sharp resonances characteristic of simple capture were absent. From the beryllium target there were no observable gamma-rays of energy greater than the 4.45-Mev energy expected from the $Be^9(\alpha,n)C^{12}$ reaction. The measured energy of the boron gamma-rays was about 3.8 Mev. They were probably produced in the $B^{10}(\alpha,p)C^{13}$ reaction, since excited states in C^{13} at 3.95 and 3.18 Mev are known.

IV. DISCUSSION OF RESULTS

The yield of photons from each resonance can be obtained from the counting rates quoted above. Since the counting rate for the $Li^7(p,\gamma)Be^8$ reaction was obtained considerably above the resonance, a correction is necessary so that only the step yield due to the resonance is involved. Since all the data was obtained for 1.60 mm of aluminum absorber between the counters, the values must be corrected to zero absorber thickness. Finally, the efficiency of counting is different for the two reactions, since the gamma-ray energy is different. This final correction was made by taking 5.3 Mev for the average energy of the gamma-rays from the $Li^7(\alpha,\gamma)B^{11}$ resonances and 17.5 Mev for the gamma-rays from the $Li^7(p,\gamma)Be^8$ resonance and using the counting efficiencies given by Fowler, *et al.*[7] Denoting the gamma yield from the $Li^7(\alpha,\gamma)B^{11}$ resonances by $Y_\gamma{}^\alpha$ and the yield from the $Li^7(p,\gamma)Be^8$ resonance by $Y_\gamma{}^p$, we find that $Y_\gamma{}^\alpha/Y_\gamma{}^p$ for the lower, middle, and upper resonances are, respectively, 0.65, 5.6, and 36×10^{-3}.

From theoretical considerations, it can be shown that these ratios are quite reasonable. The familiar Breit-Wigner formula for an (α,γ) reaction assuming that alpha—re-emission is the only competing process, is

$$\sigma_\gamma(E)=\pi\lambda^2(2J+1)\Gamma_\gamma\Gamma_\alpha/(2s+1)(2i+1)[(E_\alpha-E_r)^2+\tfrac{1}{4}\Gamma^2]. \quad (1)$$

The symbols in Eq. (1) are those used by Bethe.[8] Now, if N is the number of target nuclei per cc in the target and $R=dE/dx$ is the rate of loss of energy per cm of target with dE in the relative coordinate system, then,

$$Y_\gamma{}^\alpha=(N\hbar^2/R4M_\alpha E_\alpha)(\omega\gamma)_\alpha,$$

where we have taken R and λ to be constant over a narrow resonance, and have set

$$\omega=(2J+1)/(2s+1)(2i+1), \quad \gamma=\Gamma_\gamma\Gamma_\alpha/\Gamma_\alpha+\Gamma_\gamma.$$

Writing a similar expression for $Y_\gamma{}^p$ and assuming the target to be the same gives

$$Y_\gamma{}^\alpha/Y_\gamma{}^p=R_pM_pE_p(\omega\gamma)_\alpha/R_\alpha M_\alpha E_\alpha(\omega\gamma)_p,$$

where E is the energy at resonance in the relative coordinate system and M is the reduced mass. Using the measured yield ratios and obtaining the ratios of the R's from the range-energy relation of Bethe,[9] and using the value 8.9 ev for $(\omega\gamma)_p$ as given by Fowler, *et al.*,[7] we find the $(\omega\gamma)_\alpha$ for the lower, middle, and upper resonances to be, respectively; 0.04, 0.6, and 4.7 ev. These figures lie within the range of values quoted by Broström, *et al.*, for the corresponding quantity for the $Al^{27}(p,\gamma)Si^{28}$ reaction. One concludes, therefore, that there is no intrinsic difference between simple capture of protons and simple capture of alpha-particles. The yield of gamma-rays from an alpha-capture reaction will always be expected to be smaller than from the corresponding proton capture reaction because of the higher rate of energy loss per cm and the smaller wavelength associated with alpha-particles as compared with protons. The only compensating factor is the fact that, since the spins of the alpha-particle and proton are, respectively, 0 and $\frac{1}{2}$, it might be expected that on the average $(\omega\gamma)_\alpha$ would be double $(\omega\gamma)_p$. This last point would require much more experimental evidence than is available at this writing.

[6] C. E. Bradford and W. E. Bennett, Phys. Rev. **78**, 302 (1950).
[7] Fowler, Lauritsen, and Lauritsen, Revs. Modern Phys. **20**, 236 (1948).
[8] H. A. Bethe, Revs. Modern Phys. **9**, 69 (1937).
[9] H. A. Bethe, Revs. Modern Phys. **22**, 213 (1950).

Angular and Radial Distributions of Particles in Cascade Showers*

L. Eyges and S. Fernbach
Radiation Laboratory, Department of Physics, University of California, Berkeley, California
(Received November 16, 1950)

This paper is concerned with the calculation of the angular and radial distributions of electrons and photons at the maximum of a cascade shower. In Sec. II(A) we calculate the moments of the distribution functions in a shower neglecting collision loss of electrons, i.e., for energies E much greater than the critical energy ϵ. In Sec. II(B) we derive expressions for the moments when collision loss is not negligible. These expressions are in the form of a series in ϵ/E, and are valid down to a few times the critical energy. In Sec. III we use the moments to calculate the distribution functions for energies down to a few times the critical energy.

I. INTRODUCTION

IN interpreting experiments on large air showers, one often must know something about the angular and radial distributions of the electrons and photons in them. A considerable amount of work has been done on this subject. Some of this work has been concerned with finding the mean squares of the quantities of interest rather than the distribution functions themselves. Roberg and Nordheim,[1] for example, have calculated quite accurately the mean square angles and displacements integrated over the shower for electrons and photons down to rather low energies. Belenky[2] has done the same for electrons, although somewhat less accurately. Also, there have been several calculations of the mean squares at the shower maximum for very high energies[3] and some calculation of the mean squares as a function of depth.[4]

There have also been attempts to calculate the distribution functions at the maximum. Belenky[5] has calculated the angular distribution of electrons under[6] Approximation A and in the same approximation Molière[7] has calculated the radial distributions of both electrons and photons and the angular distributions of electrons.

Although it is quite difficult to calculate the distribution functions, it is easy to calculate their moments accurately in Approximation A. If one does this, and compares the moments derived from Molière's functions with the accurate ones, it appears that Molière's high energy functions are in error, particularly for the large values of the argument. This is shown in Sec. II. Now, knowing the moments of the distribution functions one might be tempted to see how much he can deduce from them about the nature of the function. Of course, there are recondite theorems which state that under certain conditions (which are satisfied for the functions we consider) the functions are uniquely determined from the moments. These theorems are useless for our purposes, since to use them one must have fairly simple analytic expressions for the general moment. These are not available. It appears, however, for the functions we consider—which we can assume on physical grounds to be monotonically decreasing and "smooth"—that one can deduce the function over most of its range with considerable accuracy from a knowledge of only the first few moments. Only the behavior at very small arguments is not determined. We have no rigorous proof for this statement, but several test examples which we have tried successfully have given us considerable confidence that it is true. These are discussed in Sec. III. In Sec. II(A) we have calculated the moments under Approximation A, and compared our results with the moments derived from Molière's functions. In Sec. II(B) we show how one can obtain expressions for the moments in the form of "asymptotic" expansions[8] which hold to two or three times the critical energy. Finally, in Sec. III(A) and III(B) we calculate the actual distribution functions for energies down to about twice the critical energy using the moments found in Sec. II.

The basic assumptions of our calculations are that the scattering angles are small and that the asymptotic expressions for radiation and pair production are valid. The calculations hold for any element for which, at the energy considered, these assumptions are valid.

II. MOMENTS OF THE DISTRIBUTION FUNCTIONS IN SHOWERS

(A) Approximation A

In this section we derive expressions for the moments of the angular and radial distribution functions in a

* This work was supported by the AEC.

[1] J. Roberg and L. Nordheim, Phys. Rev. **75**, 444 (1949).

[2] S. Belenky, J. Phys. (U.S.S.R.) **8**, 9 (1944).

[3] Nordheim, Osborne, and Blatt, Proceedings of the Echo Lake Cosmic Ray Symposium, p. 273; L. Janossy, *Cosmic Radiation* (Oxford University Press, 1948); G. Molière, *Cosmic Radiation*, edited by W. Heisenberg (Dover Publications, New York, 1946); and Z. Physik **125**, 250 (1948).

[4] A. Borsellino, Nuovo cimento **6**, 543 (1949) and **7**, 638 (1950). John Blatt (private communication).

[5] S. Belenky, J. Phys. (U.S.S.R.) **8**, 347 (1944).

[6] Following B. Rossi and K. Greisen, Revs. Modern Phys. **13**, 240 (1941), we call Approximation A that in which ionization loss of electrons is neglected.

[7] G. Molière, *Cosmic Radiation*, edited by W. Heisenberg (Dover Publications, New York, 1946); Phys. Rev. **77**, 715 (1950).

[8] We have not been able to prove that the series we derive are asymptotic in the strict sense, although they appear to be useful for computation; by analogy to the German term *halb-konvergent* they might better be called *half-asymptotic*. We shall, however, simply call them *"asymptotic."*

large shower for energies much greater than the critical energy.[9] We shall consider the distribution functions which have been integrated over the length of the shower. These will also be the distribution functions at the shower maximum, since the dE/E^2 energy spectrum of particles at the maximum is the same as the energy spectrum integrated over the length. Also, it will be convenient to assume that the showers we consider are initiated by a single electron of energy E_0; but the results are really independent of this particular boundary condition so long as the initiating particles have energies much larger than the energies of the electrons or photons in which we are interested.

We specify the lateral position and direction of an electron or photon in the shower by the coordinates x and y in a plane perpendicular to the shower axis and angles θ_x and θ_y in two perpendicular planes whose intersection is parallel to the shower axis. We call $\mathbf{r}$ the vector (x, y) and $\boldsymbol{\theta}$ the vector (θ_x, θ_y). We denote by $\pi(E, \theta_x, \theta_y, x, y)$ or, more briefly, $\pi(E, \boldsymbol{\theta}, \mathbf{r})$ the number of particles of energy E at the point (x, y) in $dxdy$ traveling at an angle (θ_x, θ_y) in $d\theta_x d\theta_y$ and by $\gamma(E, \theta_x, \theta_y, x, y)$ the analogous quantity for photons. Then, the diffusion equations which describe the propagation and scattering in the shower are[10]

$$\delta(E_0-E)\delta(x)\delta(y)\delta(\theta_x)\delta(\theta_y)=L_1(\pi,\gamma)+\frac{E_s^2}{4E^2}\left(\frac{\partial^2\pi}{\partial\theta_x^2}+\frac{\partial^2\pi}{\partial\theta_y^2}\right)-\theta_x\frac{\partial\pi}{\partial x}-\theta_y\frac{\partial\pi}{\partial y}, \quad (1a)$$

$$0=L_2(\pi,\gamma)-\theta_x(\partial\gamma/\partial x)-\theta_y(\partial\gamma/\partial y). \quad (1b)$$

Using the notation of Rossi and Greisen,[11] we find the integral operators L_1 and L_2 to be

$$L_1(\pi,\gamma)=2\int_0^1\gamma(E/u,\boldsymbol{\theta},\mathbf{r})\psi(u)du/u-\int_0^1[\pi(E,\boldsymbol{\theta},\mathbf{r})-(1/1-v)\pi(E/1-v,\boldsymbol{\theta},\mathbf{r})]\phi(v)dv+\epsilon\partial\pi(E,\boldsymbol{\theta},\mathbf{r})/\partial E, \quad (2a)$$

$$L_2(\pi,\gamma)=\int_0^1\pi(W/v,\boldsymbol{\theta},\mathbf{r})\phi(v)(dv/v)-\sigma\gamma(W,\boldsymbol{\theta},\mathbf{r}). \quad (2b)$$

In this section we will set ϵ equal to zero. This is Approximation A of Rossi and Greisen. Defining $\pi_{mn}(E)$ as

$$\pi_{mn}(E)=\int\int\int\int\int\pi(E,\theta_x,\theta_y,x,y)\times(x^m\theta_x{}^n+y^m\theta_y{}^n)d\theta_x d\theta_y dxdy, \quad (3)$$

we have

$$(x^m\theta_x{}^n+y^m\theta_y{}^n)_{\substack{\text{average for}\\ \text{electrons}}}=\pi_{mn}/\pi_{00}\equiv\langle\pi_{mn}\rangle, \quad (4)$$

where π_{00} is just *twice* the electron track length; i.e.,

$$\pi_{00}=2\cdot Z_s(E_0,E)=2\cdot(0.437E_0/E^2). \quad (5)$$

$\langle\gamma_{mn}(W)\rangle$ is defined analogously. Now we get a recursion relation for π_{mn} and γ_{mn}. We multiply Eqs. (1a, b) by $(x^m\theta_x{}^n+y^m\theta_y{}^n)$ and integrate over x, y, θ_x, θ_y. The terms containing derivatives with respect to the spatial variables are then transformed by integration by parts and we find that our equations become

$$0=L_1(\pi_{mn}(E),\gamma_{mn}(W))+(E_s^2/4E^2)n(n-1)\pi_{m,n-2}(E)+m\pi_{m-1,n+1}(E), \quad (6a)$$

$$0=L_2(\alpha_{mn}(E),\gamma_{mn}(W))+m\gamma_{m-1,n+1}(E). \quad (6b)$$

Equations (6a, b) have a solution of the following form:

$$\pi_{mn}(E)=\alpha_{mn}E_s^{m+n}/E^{m+n+2}, \quad (7a)$$

$$\gamma_{mn}(W)=\beta_{mn}E_s^{m+n}/W^{m+n+2}, \quad (7b)$$

where α_{mn} and β_{mn} are independent of E and W. If we substitute from Eqs. (7a, b) into Eqs. (6a, b), we are led to the following equations, for $E\neq E_0$:

$$0=-A(m+n+1)\alpha_{mn}+B(m+n+1)\beta_{mn}+\tfrac{1}{4}E_s^2n(n-1)\alpha_{m,n-2}+m\alpha_{m-1,n+1}, \quad (8a)$$

$$0=C(m+n+1)\alpha_{mn}-\sigma\beta_{mn}+m\beta_{m-1,n+1}. \quad (8b)$$

The functions A, B, C appearing here are the same as those in ordinary shower theory and are defined by Eq. (2.17) of Rossi and Greisen's article.

Since π_{00} and γ_{00} are known, one can solve Eqs. (8a, b) by successively putting: $m=0$, $n=2$; $m=1$, $n=1$; $m=2$, $n=0$; $m=4$, $n=0$; $m=3$, $n=1$, etc. We have calculated α_{mn} and β_{mn} for m, n up to $m+n=10$, and then used Eq. (4) to find $\langle\pi_{mn}\rangle$ and $\langle\gamma_{mn}\rangle$ over the same range. The moments for which $m+n$ is odd vanish by symmetry.

The infinite sequence of moments thus obtainable determines in principle the distribution functions which we desire. We shall see in the next sections what can be deduced concerning the distribution functions from the partial sequence actually calculated.

Here we shall use these moments to check Molière's and Belenky's calculations of the distribution functions. Molière has derived expressions for the radial distribution functions, integrated over all angles, for both electrons and photons and the angular distribution function, integrated over all lateral displacements, for electrons.[7] Belenky has calculated the angular distribution of electrons.[5] To assess the correctness of Molière's and Belenky's calculation of these functions we have calculated[12] $\langle r^n\rangle_{Av}$ and $\langle\theta^n\rangle_{Av}$ from their distributions and compared these moments with those derived from

[9] The essential results of Sec. II(A) appear in an unpublished thesis by one of us (L. Eyges, Dissertation, Cornell University, 1948). These results were derived independently by Professor John Blatt and incorporated into his lecture notes. We are very grateful to Professor Blatt for allowing us to see copies of these notes. We have profited from several illuminating observations in them, as well as from suggestions for notation.

[10] L. Landau, J. Phys. (U.S.S.R.) **3**, 237 (1940).

[11] B. Rossi and K. Greisen, Revs. Modern Phys. **13**, 240 (1941).

[12] $r^2=x^2+y^2$ and $\theta^2=\theta_x{}^2+\theta_y{}^2$.

TABLE I. Exact moments in Approximation A and comparison with those derived from the distribution functions calculated by Molière and Belenky.[a]

s	Electrons: $\langle r^s\rangle_{Av}\cdot(E/E_s)^s$ Molière	Exact[a]	Electrons: $\langle r^s\rangle_{Av}\cdot(E/E_s)^s$ Molière	Belenky	Exact	Photons: $\langle r^s\rangle_{Av}\cdot(W/E_s)^s$ Molière	Exact	Photons: $\langle r^s\rangle_{Av}\cdot(W/E_s)^s$ Exact
0	1	1	1	1	1	1	1	1
2	0.830	0.725	0.602	0.655	0.570	1.02	1.13	0.176
4	6.40	7.24	1.72	1.43	0.959	16.0	26.4	0.178
6	1.06×10^2	4.95×10^2	30.4	6.56	3.10	5.45×10^2	3.34×10^3	0.415
8	2.76×10^3	1.38×10^3	1.12×10^3	51.6	16.1	3.19×10^4	1.36×10^4	1.69
10	1.03×10^5	1.03×10^5	5.42×10^4	620	121	2.85×10^6	1.34×10^5	10.4

[a] Similar results for the exact radial moments of electrons have been obtained by Nordheim, Osborne, and Blatt, Proceedings of the Echo Lake Cosmic Ray Symposium, December, 1949.

the above calculations, using, e.g., for electrons

$$\langle \pi_{m0}\rangle=\langle x^m+y^m\rangle_{Av}=2\langle x^m\rangle_{Av}=2\langle r^m\rangle_{Av}\langle\cos^m\phi\rangle_{Av} \tag{9a}$$

$$\langle \pi_{0n}\rangle=\langle \theta_x{}^n\rangle_{Av}+\langle\theta_y{}^n\rangle_{Av}=2\langle\theta_x{}^n\rangle_{Av}=2\langle\theta^n\rangle_{Av}\langle\cos^n\phi\rangle_{Av}. \tag{9b}$$

The results are given in Table I.

(B) Asymptotic Expansions for the Moments

We now consider the problem of finding the moments for energies where collision loss of electrons is not negligible, i.e., when we retain the term $\epsilon\partial\pi/\partial E$ in Eq. (2a). First, consider the equations for the track lengths, neglecting scattering. We call the electron track length $Z_\pi(E_0, E)$ and the photon track length $Z_\gamma(E_0, W)$. They satisfy the following equations:

$$\delta(E_0-E)=L_1(Z_\pi, Z_\gamma), \tag{10a}$$

$$0=L_2(Z_\pi, Z_\gamma). \tag{10b}$$

How to obtain an asymptotic solution for these equations which is valid down to energies a few times the critical energy is well known.[13] One assumes that Z_π and Z_γ have their high energy forms, modified by a correction factor in the form of a series in ϵ/E and ϵ/W; i.e.,

$$Z_\pi(E_0, E)=\frac{0.437E_0}{E^2}\sum_{n=0}^{\infty}a_n\left(\frac{\epsilon}{E}\right)^n, \tag{11a}$$

$$Z_\gamma(E_0, W)=\frac{0.437E_0}{\sigma W^2}\sum_{n=0}^{\infty}b_n\left(\frac{\epsilon}{E}\right)^n. \tag{11b}$$

If one substitutes these expressions into Eqs. (2a, b), one gets the following infinite set of equations:

$$\left.\begin{aligned}&[b_nB(n+1)/\sigma]-a_nA(n+1)\\&\qquad=(n+1)a_{n-1}\end{aligned}\right\}n=1, 2\cdots. \tag{12a}$$

$$b_n=C(n+1)a_n \tag{12b}$$

These equations can be solved for a_n and b_n. Setting $a_0=1$, one gets for the electron track length:

$$Z_\pi(E_0, E)=\frac{0.437E_0}{E^2}\left(1-1.638\frac{\epsilon}{E}+2.799\frac{\epsilon^2}{E^2}-5.312\frac{\epsilon^3}{E^3}+11.18\frac{\epsilon^4}{E^4}+\cdots\right). \tag{13}$$

[13] Reference 11, p. 293.

It is possible to take forms somewhat different from Eqs. (11a, b) for Z_π and Z_γ. Following Rossi and Greisen, e.g., one can assume

$$Z_\pi(E_0, E)=0.437E_0/E^2\left(1+\alpha_1\frac{\epsilon}{E}+\alpha_2\frac{\epsilon^2}{E^2}+\cdots\right)^2. \tag{14}$$

Using the binomial expansion, Eq. (14) can be brought into the form (11a) and the relationship between a_n and α_n can be determined. Doing this, one gets the well-known expressions of Rossi and Greisen; namely, Eq. (2.96) of their paper. Similar results can be obtained for Z_γ.

We would like to emphasize that this last form for the track length is arbitrary in that one could assume series expansions in ϵ/E and ϵ/W, raised to *any* power, and then determine the coefficients in the same manner as above. The essential behavior of the series is not changed by writing it in a form other than that of Eq. (13). Thus, both Eq. (13) and Eq. (2.96) of Rossi and Greisen, seem to be valid down to $\epsilon/E\sim\frac{1}{3}$, and break down for higher values. It is true that for numerical computation one sometimes needs fewer terms in the series when it is in the latter form. On the other hand, the coefficients in Eq. (13) increase more slowly and in any computation, if one continues either of the series up to the point where the terms begin to increase, they give the same answer.

Now let us turn to the problem of calculating the moments when energy loss is taken into account. One transforms Eq. (1a, b) by integration by parts and defines π_{mn} and γ_{mn} as before. Equation (2a, b) still holds with the understanding that in the operator $L_1(\pi_{mn}, \gamma_{mn})$ one retains the term $\partial\pi_{mn}/\partial E$. One can find a formal solution of these equations by setting

$$\pi_{mn}(E)=\frac{\alpha_{mn}E_s{}^{m+n}}{E^{m+n+2}}\sum_{l=0}^{\infty}a_{mn}{}^{(l)}\left(\frac{\epsilon}{E}\right)^l, \tag{15a}$$

$$\gamma_{mn}(W)=\frac{\beta_{mn}E_s{}^{m+n}}{W^{m+n+2}}\sum_{l=0}^{\infty}b_{mn}{}^{(l)}\left(\frac{\epsilon}{W}\right)^l. \tag{15b}$$

On putting these expressions into Eqs. (6a, b) and equating to zero various powers of ϵ/E and ϵ/W, one

TABLE II. Electron moments including correction for ionization loss.

$$\langle(r^m)_{kl}\rangle_\epsilon = \frac{[\langle r^m\rangle_{kl}]_{\epsilon=0}}{[1+\sum_{l=1}^{\infty}\alpha_{m0}^{(l)}(\epsilon/E)^l]^m}, \qquad \alpha_{m0}^{(l)}$$

m \	2	4	6
1	1.73	1.60	1.52
2	−1.16	−2.02	−2.53
3	2.57	5.42	6.62
4	−7.60	−19.6	−30.8

$$\langle(\theta^n)_{kl}\rangle_\epsilon = \frac{[\langle\theta^n\rangle_{kl}]_{\epsilon=0}}{[1+\sum_{l=1}^{\infty}\alpha_{0n}^{(l)}(\epsilon/E)^l]^n}, \qquad \alpha_{0n}^{(l)}$$

n \	2	4	6
1	0.813	0.915	1.02
2	−0.747	−0.950	−1.17
3	1.46	2.09	2.88
4	−3.73	−6.05	−9.31

TABLE III. Photon moments including correction for ionization loss.

$$\langle(r^m)_{kl}\rangle_\epsilon = \frac{[\langle r^m\rangle_{kl}]_{\epsilon=0}}{[1+\sum_{l=1}^{\infty}\beta_{m0}^{(l)}(\epsilon/W)^l]^m}, \qquad \beta_{m0}^{(l)}$$

m \	2	4	6
1	1.32	1.16	1.21
2	−0.766	−1.10	−1.95
3	1.54	2.52	2.66
4	−3.80	−7.71	−13.0

$$\langle(\theta^n)_{kl}\rangle_\epsilon = \frac{[\langle\theta^n\rangle_{kl}]_{\epsilon=0}}{[1+\sum_{l=1}^{\infty}\beta_{0n}^{(l)}(\epsilon/W)^l]^n}, \qquad \beta_{0n}^{(l)}$$

n \	2	4	6
1	0.836	0.916	1.01
2	−0.556	−0.755	−0.952
3	0.949	1.50	2.23
4	−2.15	−3.98	−6.70

gets the following set of equations, for $l=0, 1, 2\cdots$:

$$\alpha_{mn}a_{mn}^{(l)}A(m+n+l+1)-\beta_{mn}b_{mn}^{(l)}B(m+n+l+1)+(m+n+l+1)\alpha_{mn}a_{mn}^{(l-1)}=\tfrac{1}{4}E_s^2n(n-1)\alpha_{m,n-2}a^{(l)}{}_{m,n-2}+m\alpha_{m-1,n+1}a^{(l)}{}_{m-1,n+1}; \quad (16a)$$

$$\alpha_{mn}a_{mn}^{(l)}C(m+n+l+1)-\sigma\beta_{mn}b_{mn}^{(l)}+m\beta_{m-1,n+1}b^{(l)}{}_{m-1,n+1}=0. \quad (16b)$$

In these equations $a_{mn}^{(0)}=b_{mn}^{(0)}=1$ and $a_{mn}^{(-1)}=0$. For $l=0$, Eqs. (16a, b) are identical with Eqs. (8a, b). Thus, the quantities α_{mn} and β_{mn} are known from the work in Sec. II(A). The quantities $a_{mn}^{(l)}$ and $b_{mn}^{(l)}$ can then be determined successively in the following sequence:

$$a_{02}^{(1)}, b_{02}^{(1)}; a_{02}^{(2)}, b_{02}^{(2)}; \cdots\rightarrow a_{11}^{(1)}, b_{11}^{(1)}; a_{11}^{(2)}, b_{11}^{(2)}\cdots\rightarrow a_{20}^{(1)}, b_{20}^{(1)}; a_{20}^{(2)}, b_{20}^{(2)}\cdots\rightarrow a_{04}^{(1)}, b_{04}^{(1)}; a_{04}^{(2)}, b_{04}^{(2)}\cdots, \text{etc.}$$

As before, we are not directly interested in π_{mn} and γ_{mn} but in these quantities divided by π_{00} and γ_{00}, respectively. If we then formally carry out this division using $\pi_{00}=2Z_\pi$, $\gamma_{00}=2Z_\gamma$ as given by Eq. (13), we get expressions for π_{mn} and γ_{mn} again in the form of the high energy expressions multiplied by a series in powers of ϵ/E or ϵ/W. For convenience in computation we can convert these series to the form

$$\langle\pi_{mn}(E)\rangle_\epsilon=\langle\pi_{mn}\rangle_{\epsilon=0}\Big/\left[\sum_{l=0}^{\infty}\alpha_{mn}^{(l)}\left(\frac{\epsilon}{E}\right)^l\right]^{m+n},$$

$$\langle\gamma_{mn}(W)\rangle_\epsilon=\langle\gamma_{mn}(W)\rangle_{\epsilon=0}\Big/\left[\sum_{l=0}^{\infty}\beta_{mn}^{(l)}\left(\frac{\epsilon}{W}\right)^l\right]^{m+n}.$$

We will not present here our numerical results for all the quantities $\alpha_{mn}^{(l)}$ and $\beta_{mn}^{(l)}$, since they are probably of no great interest. The quantities of real interest are $\langle r^n(E)\rangle_{kl}$ and $\langle\theta^n(W)\rangle_{kl}$. In the Tables II and III we present our results for these quantities.

It is hard to estimate the range of validity of the series in the denominators of the expressions in Tables II and III. First, we have derived them purely formally, and in the process have divided dubiously convergent series into one another. Also, it is clear that for small values of E/ϵ and W/ϵ they diverge rather violently, particularly for the higher radial moments. Nevertheless, it is probably satisfactory to compute with them, provided one terminates the series when the terms start to increase. The reason we believe this to be so is that the series for the track lengths in Eq. (13) seems to show the same dubious convergence, but they have been checked and found to be quite accurate for E/ϵ greater than two or three. As a further check we have compared our results for the mean squares with the fairly accurate calculations of Roberg and Nordheim and have found good agreement down to about five times the critical energy, and even at twice the critical energy our results do not differ from theirs by more than 20 or 30 percent.

It is worth noting that our results for the moments of the angular distribution are valid down to somewhat lower energies than for the radial distribution. This is also true for the higher order moments; from Tables II and III we see that the series for the higher radial moments converges more poorly than for the angular moments of the same order.

III. THE DISTRIBUTION FUNCTIONING

(A) Approximation A

We now turn to the problem of calculating the actual distribution functions under Approximation A, using the moments found in Sec. II(A). We shall concern ourselves with the angular distributions integrated over all displacements; from symmetry this distributions are a function only of $\theta=(\theta_x^2+\theta_y^2)^{\frac{1}{2}}$. Similarly, the radial distributions are a function only of $r=(x^2+y^2)^{\frac{1}{2}}$. Moreover, from the structure of the equations, the distributions depend on (E, r) and (W, r) through the combinations Er/E_s and Wr/E_s. We can denote both of these quantities by x without confusion. The angular distributions depend on $E\theta/E_s$ and $W\theta/E_s$, both of which we call y; r is measured in radiation units and θ in radians. We shall call $P_r(Er/E_s)\equiv P_r(x)$ the radial distribution of electrons and $P_\theta(E\theta/E_s)\equiv P_\theta(y)$ the angular distribution of electrons. Similarly, we call $Q_r(Wr/E_s)\equiv Q_r(x)$ the radial distribution of quanta and $Q_\theta(W\theta/E_s)$ the angular distribution. The distribution functions are defined so that $P_r(Er/E_s)rdr$ is proportional to the number of electrons of energy E in the annular ring between r and $r+dr$, and $P_\theta(E\theta/E_s)\theta d\theta$ is proportional to the number of electrons of energy E in the solid angle between θ and $\theta+d\theta$. We will choose

normalization so that $\int_0^\infty P_r(x)x dx = 1$ and $\int_0^\infty P_\theta(y)y dy = 1$ and similarly for the photons.

We assume that knowledge of the first few moments of a "reasonable" function essentially determines the function over a limited range. This assumption is based on the results of several "experiments" in which we tried to reconstruct known functions from a knowledge of the first four even moments alone. The functions chosen for this test were roughly of the same form as the expected distribution function. After trying various analytical schemes[14] we found that the most convenient method for reconstructing the function was simply to graph an arbitrary function, calculate its moments numerically, alter the function as indicated by the discrepancies from the correct moments, etc.

If one can extrapolate conclusions from the examples we tried, it would appear that it is readily feasible to fit a function over most of its range to within a few percent, even when not much care is taken in fitting the highest moment.[15] One cannot determine the behavior at the origin, however, with any certainty. This fact is particularly bothersome because one often wants to know the cosmic-ray distribution functions near the origin. The reason that the behavior at the origin is not determinable is as follows. The integrand for the nth moment is of the form $x^{n+1}f(x)$, and for increasing n the maximum of this function moves farther and farther along the x-axis. Moreover, this integrand vanishes very strongly for small x, so the high moments are essentially independent of the behavior of the function at the origin. Thus, most of the information about the origin is contained in the second moment; but the integrand even of this vanishes very strongly at the origin. For example, if $f(x)$ has a $1/x$ singularity, the integrand behaves like x^3. We feel particularly keenly here the fact that we know only the even moments. Knowledge of f_1 would help considerably in the fitting the function for small x.

Consider now the radial distribution of electrons. As we have explained, our method of fitting functions by their moments does not give the behavior near the origin. For the higher moments Molière's function seems to be quite inaccurate; but the second moment, which depends most sensitively on the behavior near the origin, differs from the correct value by only 12 percent. It seems reasonable then to assume that Molière's function is essentially correct for small x, and to start calculations on this basis. Actually, we reversed the procedure and used the higher moments first; i.e., we found the form of the function for large x and worked down toward the origin. If one can base an estimate on the examples cited, our function should be quite accurate down to about an x of 0.4. Our function also joins smoothly to Molière's at this point. In Table IV we present our results.

In calculating the radial distribution of photons there is again the difficulty that the distribution function has a singularity at the origin. For this case also the second moment as calculated from Molière's distribution function is not far off. We have felt justified in assuming his distribution function to be correct up to $x=0.4$, and calculating the function for higher values from the moments. The results are given in column 3 of Table IV.

The calculations of the angular distribution of electrons is somewhat simpler than for the above two cases, since there is no singularity at the origin. Our results are given in the fourth column of Table IV.

The angular distribution of photons can, of course, be calculated by the same methods we have used for the other distributions. Alternatively, it is clear on physical grounds that it is determined once the angular distribution of electrons is known, since photons are not scattered, but inherit their angular distribution from parent electrons of higher energy. Mathematically,

TABLE IV. Distribution functions in Approximation A.

x or y	$x=Er/E_s$ or Wr/E_s		$y=E\theta/E_s$ or $W\theta/E_s$	
	$P_r(x)$[a]	$Q_r(x)$[b]	$P\theta(y)$	$Q\theta(y)$[c]
0			9.27	
0.1			7.13	
0.2	7.62	7.33	5.35	8.60
0.4	2.74	1.12	2.78	2.19
0.6	1.01	3.73×10^{-1}	1.52	7.68×10^{-1}
0.8	4.84×10^{-1}	1.96	8.20×10^{-1}	2.86
1.0	2.52	1.21	4.46	1.18
1.2	1.47	8.58×10^{-2}	2.32	4.56×10^{-2}
1.4	8.72×10^{-2}	6.04	1.18	1.96
1.6	5.36	4.55	6.04×10^{-3}	8.6×10^{-3}
1.8	3.49	3.48	2.90	3.82
2.0	2.26	2.67	1.46	1.72
2.2	1.53	2.08	7.13×10^{-3}	7.82×10^{-4}
2.4	1.02	1.62	3.56	3.58
2.6	7.20×10^{-3}	1.29	1.74	1.66
2.8	5.16	1.02	8.29×10^{-4}	7.79×10^{-6}
3.0	3.73	8.25×10^{-3}	3.92	3.59
3.5	1.74	4.70		
4.0	8.72×10^{-4}	2.73		
4.5	4.52	1.57		
5.0	2.51	9.70×10^{-4}		
5.5	1.46	6.04		
6.0	8.80×10^{-5}	3.82		
6.5		2.46		
7.0		1.60		

[a] For $0\leq x\leq0.2$ we assume Molière's distribution function to be valid. In expanded form it is

$$P_r(x)=21.37x^{-1/2}-30.79+66.75x^{1/2}-66.99x^1+\cdots.$$

[b] For $0\leq x\leq0.2$ we again use Molière's distribution function (renormalized); viz.,

$$Q_r(x)=\frac{31.94\exp[-2x/(0.1)^{\frac{1}{2}}]}{2x/(0.1)^{\frac{1}{2}}}+\frac{0.806\exp[-2x/(3.25)^{\frac{1}{2}}]}{3.25}.$$

[c] For $0\leq y\leq0.2$

$$Q\theta(y)\approx(3.44/y)e^{-3.44y}.$$

[14] While this work was being prepared for publication, we received a copy of a paper by L. V. Spencer and U. Fano entitled "Penetration and diffusion of x-rays: VII. Calculation of space distributions by polynomial expansion." One of the points of their paper seems to be the same as that of this section; viz., the first few moments of a reasonable function essentially determine the function over a limited range. Unfortunately, the neat method of polynomial expansions that they describe is not directly applicable to our problem, since our functions may be singular at the origin.

[15] For further details see L. Eyges and S. Fernbach, UCRL Report No. 943, *Angular and Radial Distributions of Particles in Cascade Showers*.

TABLE V. Distribution functions for $E=10\epsilon$. Normalization of $P_r(x)$, $Q_r(x)$ is arbitrary. $\int_0^\infty P_\theta(y)ydy=1$. $x=10\sigma/E_s$, $y=10\epsilon\theta/E_s$.

x or y	$P_r(x)$	$Q_r(x)$	$P_\theta(y)$
0	...	...	10.0
0.1	...	...	7.42
0.2	9.0	7.33	5.51
0.3	4.5	2.50	4.24
0.4	2.45	1.12	3.08
0.5	1.35	6.36×10^{-1}	2.17
0.6	8.7×10^{-1}	3.73	1.56
0.7	5.7	2.63	1.11
0.8	3.85	1.96	7.95×10^{-1}
0.9	2.72	1.53	5.73
1.0	1.98	1.21	4.14
1.2	1.10	8.1×10^{-2}	2.01
1.4	6.5×10^{-2}	5.73	9.54×10^{-2}
1.6	3.85	4.13	4.29
1.8	2.35	3.13	1.96
2.0	1.53	2.33	8.80×10^{-3}
2.4	7.2×10^{-3}	1.37	1.64
2.8	3.43	8.22×10^{-3}	3.02×10^{-4}
3.2	1.75	5.28	5.40×10^{-5}
3.6	9.3×10^{-4}	3.32	
4.0	5.32	2.15	
4.5	2.77	1.30	
5.0	1.53	8.03×10^{-4}	
5.5		4.89	
6.0	5.04×10^{-5}	3.06	

this is clear from Eqs. (2b) and (3b), which give

$$Q_\theta(E\theta/E_s)=(1/\sigma)\int_0^1 P_\theta(E\theta/E_s v)\phi(v)dv/v.$$

If we take $\phi(v)=1/v$ and write $y=E\theta/E_s$, we have

$$Q_\theta(y)=(1/\sigma)\int_0^1 P_\theta(y/v)dv/v^2.$$

Now to a rough approximation $P_\theta(y)$ is just an exponential,

$$P_\theta(y)\approx 12\exp[-(12)^{\frac{1}{2}}y].$$

Therefore,

$$Q_\theta(y)\approx(12/\sigma)\int_0^1 \exp[-(12)^{\frac{1}{2}}y/v]\frac{dv}{v^2}\propto y^{-1}\exp[-(12)^{\frac{1}{2}}y]$$

is a rough approximation to the angular distribution of photons. We have improved on this approximation by the method of moments, assuming that the above expression for $Q_\theta(y)$ is approximately correct near the origin. Our results are given in the last column of Table IV.

It is interesting to compare the results of our calculations of the distribution functions with those of Molière. For the sake of brevity we shall simply describe the main features of this comparison. Consider first $P_\theta(y)$. Our calculations agree with Molière's to within a few percent up to about $y=1.7$. Beyond this point Molière's function becomes smaller than ours, by a factor 0.91 at $y=2$ and 0.36 at $y=2.5$. Around $y=3$ Molière's function becomes negative. Our calculations of $Q_r(x)$ also agree with Molière's to within a few percent up to $x=0.5$, where they begin to differ; but at no point up to $x=5$ do they differ by more than 25 percent. Our values for $P_r(x)$ show the greatest disagreement with those of Molière. There is good agreement up to about $x=0.6$, but at this point Molière's function begins to drop below ours and becomes lower by a factor 0.85 at $x=1.2$. Molière's curve then approaches ours, crosses at $x=1.8$ and becomes larger by a factor 2 at $x=3.5$. Then, it again approaches ours and crosses it at $x=5.5$.

(B) Effect of Collision Loss

Now we turn to the problem of calculating the distribution functions for energies where collision loss is not negligible, using the moments derived in Sec. II(A). There are no essential differences in this work from that of Sec. III(A); the main difficulty here is that for the lowest energies with which we deal the behavior of our series for the moments is rather dubious. For energies down to about five times the critical energy the latter difficulty is probably not very serious; our expressions for the moments are probably accurate within a few percent. Moreover, we are helped by the following fact: as one goes down in energy the distribution functions become steeper and their shape over the range of interest becomes less sensitive to the less accurate higher moments.

Also, when collision loss is included, we have less knowledge of the behavior of the functions at the origin. In Approximation A we could rely more or less on Molière's calculations; in the present case we must guess. The best guess seems to be that the singularities

TABLE VI. Distribution functions for $E=5\epsilon$. Normalization of $P_r(x)$, $Q_r(x)$, $Q_\theta(y)$ is arbitrary. $\int_0^\infty P_\theta(y)ydy=1$. $x=5\sigma/E_s$, $y=5\epsilon\theta/E_s$.

x or y	$P_r(x)$	$Q_r(x)$	$P_\theta(y)$	$Q_\theta(y)$
0	...	...	11.2	...
0.1	...	...	8.29	...
0.2	9.9	7.33	6.05	9.0
0.3	4.7	2.50	4.37	4.2
0.4	2.4	1.12	3.14	2.15
0.5	1.4	6.36×10^{-1}	2.24	1.20
0.6	8.0×10^{-1}	3.73	1.57	6.60×10^{-1}
0.7	4.8	2.63	1.10	3.70
0.8	3.3	1.96	7.7×10^{-1}	2.00
0.9	2.34	1.53	5.4	1.20
1.0	1.70	1.21	3.75	7.20×10^{-2}
1.2	9.00×10^{-2}	7.87×10^{-2}	1.74	2.80
1.4	5.1	5.43	7.7×10^{-2}	1.10
1.6	3.10	3.90	3.36	4.5×10^{-3}
1.8	1.90	2.83	1.40	1.7
2.0	1.20	2.06	5.6×10^{-3}	6.7×10^{-4}
2.4	5.3×10^{-3}	1.15	7.8×10^{-4}	8.0×10^{-5}
2.8	2.50	6.57×10^{-3}	1.12	7.2×10^{-6}
3.2	1.27	3.98		
3.6	6.70×10^{-4}	2.45		
4.0	3.70	1.57		
4.5	1.88	9.17×10^{-4}		
5.0	1.05	5.35		
5.5		3.13		
6.0	3.47×10^{-5}	1.87		

at the origin is the same as for high energies. Thus, from Table II we see that the effect of collision loss on the moments is least for the lower order moments, i.e., for small distances and angles. It does not seem unreasonable then to guess that the behavior of the distribution functions for small values of their arguments is unchanged from that when collision loss is neglected. At the very least, it seems certain that, since $P_r(x)$, $Q_r(x)$, and $Q_\theta(y)$ are all singular at the origin in Approximation A, they will also be singular when collision loss is included. This is confirmed by our calculations. We cannot determine the *order* of the singularity by our method of moments, but can determine that the singularity exists. This shows up when one reconstructs the distribution functions for large values of the argument and then tries to continue the function in toward the origin. It turns out to be impossible to fit all of the moments with a function which is not singular. We have reconstructed $P_r(x)$, $Q_r(x)$ and $Q_\theta(y)$ for $E=10\epsilon$ and the first two of these functions for $E=5\epsilon$ in the manner indicated above, i.e., by starting with large values of the arguments and working toward the origin. If we can judge from the examples mentioned above, our functions should be quite accurate down to about x or y about 0.4 and not be off more than by about 50 percent down to 0.2. Our results are presented in Tables V and VI.

In Approximation A, $P_\theta(y)$ is finite at the origin. As far as one can tell from the moments, it is also finite when collision loss is taken into account. If one assumes this, it is possible to reconstruct the function down to $y=0$. Unfortunately, we cannot estimate the accuracy of our function for very small y. The results are given in Tables V and VI for $E=10\epsilon$ and $E=5\epsilon$.

For $E=10\epsilon$, $x=0.2$ corresponds to a distance of $r=0.2E_s/10\epsilon$ radiation lengths. For air at sea level, for which $\epsilon=88$ Mev and $r=300$ meters, this corresponds to a distance of 1.4 meters. For Pb for which $\epsilon=6.7$ Mev and $r=0.51$ cm, this corresponds to a distance of 0.3 mm. We should like to remind the reader that the assumptions implicit in our calculations of the distribution functions are that the scattering angles are small, the asymptotic expressions for pair production are valid, and that Compton effect is negligible. The distribution functions given in Table V and VI are thus more accurate for light elements than for heavy ones. For air, for example, $E=2\epsilon$ corresponds to 176 Mev, where the assumptions above are fairly well satisfied. For Pb, on the other hand, $E=2\epsilon$ corresponds to 13 Mev; at this energy the scattering angles cannot be considered small nor are the asymptotic cross sections valid.

TABLE VII. Distribution functions for $E=2\epsilon$. Normalization of $P_r(x)$, $Q_r(x)$, $Q_\theta(y)$ is arbitrary. $\int_0^\infty P_\theta(y)y\,dy=1$. $x=2\sigma r/E_s$, $y=2\epsilon\theta/E_s$.

x or y	$P_r(x)$	$Q_r(x)$	$P_\theta(y)$	$Q_\theta(y)$
0	...	...	11.8	...
0.1	...	...	9.0	...
0.2	11.0	7.33	6.8	9.4
0.3	5.6	2.50	5.1	4.0
0.4	2.85	1.12	3.65	1.90
0.5	1.55	6.36×10^{-1}	2.6	9.5×10^{-1}
0.6	8.0×10^{-1}	3.73	1.80	5.2
0.7	4.35	2.63	1.18	2.87
0.8	2.30	1.96	7.1×10^{-1}	1.58
0.9	1.30	1.53	4.4	8.8×10^{-2}
1.0	8.5×10^{-2}	1.21	2.70	5.0
1.2	4.0	7.6×10^{-2}	1.08	1.5
1.4	2.18	5.04	3.9×10^{-2}	4.7×10^{-3}
1.6	1.28	3.48	1.42	1.38
1.8	8.0×10^{-3}	2.37	5.0×10^{-3}	4.1×10^{-4}
2.0	5.1	1.64	1.65	1.33
2.4	2.33	8.03×10^{-3}	1.70×10^{-4}	1.15×10^{-5}
2.8	1.14	4.10	2.10×10^{-5}	1.15×10^{-6}
3.2	5.85×10^{-4}	2.18		
3.6	3.14	1.24		
4.0	1.80	7.65×10^{-4}		
4.5	9.2×10^{-5}	4.28		
5.0	4.9	2.52		

We have also calculated the distribution functions for $E=2\epsilon$. For this case, the expressions for the radial moments are probably very inaccurate, and our radial distributions may very well be quite inaccurate. The numbers in Table VII thus represent more a guess at an extrapolation than a calculation. The angular distribution functions are probably somewhat more accurate than the radial functions since the expressions for the angular moments converge much better than for the radial moments. But even so, one cannot put much faith in even the angular functions for the reasons given in the last paragraph. The remarks made above concerning normalization and the behavior of the functions at the origin apply here also.

On the Ionization Yields of Heavy Particles

JULIAN K. KNIPP AND RUFUS C. LING
Institute for Atomic Research and Department of Physics, Iowa State College, Ames, Iowa
(Received October 18, 1950)

Since the energy loss of a slow heavy particle is due predominantly to recoiling atoms, ionization by secondary heavy particles contributes a large fraction of the total ionization resulting from a slow heavy particle that is stopped in a gas. If the secondary heavy particle ionization efficiency is low, the over-all efficiency for the production of ion pairs is greatly reduced for low energies of the primary particle. The secondary heavy particle ionization efficiency satisfies an integro-differential equation in which the ratio of electronic to atomic stopping cross sections plays a critical role. Data by Madsen on the ionization by recoiling particles in alpha-decay are used to set limits on the ionization by slow argon particles in argon, from which it is possible to make crude estimates of the energy of fission fragments which fails to give rise to ionization at the usual rate. In argon, ionization defects of the order of several Mev are to be expected.

I. INTRODUCTION

A PARTICLE in its passage through a gas produces direct excitation and ionization of the atoms of the gas and also gives rise to recoil atoms. A fast heavy particle ($v \gg v_0 = e^2/\hbar$) loses energy primarily to electrons. Ion pairs are produced at a rate per unit energy loss $(-dI/dE)$ which is very close to that for alpha-particles, for the energy loss per ion pair ω is largely independent of mass, charge, and velocity of fast particles of fixed charge and the process of capture and loss of electrons contributes relatively little to the energy loss and ionization processes when the average particle charge is large. For high velocities, ω tends to approach a value ω^e which depends on the nature of the gas and is practically independent of the nature of the particle. When the velocity of the particle falls below a velocity of the order of v_0, energy loss to recoiling atoms predominates because of the neutralization of the particle through the capture of electrons. Ionization then proceeds through the quasi-adiabatic interpenetration of the electron clouds of the particle and the gas atoms and by means of secondary ionization arising from the recoil atoms. If the secondary ionization efficiency is low, the over-all efficiency for the production of ion pairs is greatly reduced for low energies of the primary particle. A heavy particle of velocity v_0 has an energy of the order of millions of electron volts (a proton of this velocity has an energy of 25 kev). Hence, the energy which fails to give rise to ionization at the high velocity rate $1/\omega^e$ can be rather large unless the secondary ionization is highly efficient, as might be expected for light gases, or there is a marked increase in the efficiency of primary ionization, which seems unlikely for ordinary gases.

II. IONIZATION EFFICIENCY

We write for the energy loss of the particle per unit length of path

$$-dE/dx = N[b^e + b^r], \tag{1}$$

where N is the number of atoms per unit volume of the gas, and b^e and b^r are the energy stopping cross sections per atom for the loss of energy to electrons (inelastic collisions) and to recoiling atoms (elastic collisions), respectively, such a distinction being possible to a high degree of approximation. Similarly, for the ionization per unit length of path

$$-dI/dx = N\left[\sigma^e + \int_0^{E_{M'}} dE'\sigma(E, E')I'(E')\right], \tag{2}$$

where σ^e is the cross section for the production of ion pairs (including ionization produced by ejected electrons) in the collision of the particle with a gas atom, and $\sigma(E, E')$ is the cross section per unit energy range for the production of a recoil atom of energy E' in such a collision. The quantity $I(E)$ is the total ionization, primary and secondary, resulting from the stopping in the gas of the particle of energy E; and $I'(E')$ is the total ionization resulting from the stopping of a gas particle of energy E' in the same gas.[1] All secondary ionization is associated with that part of the path of the primary particle from which the secondary particles, whether electrons or atoms, producing the ionization originate, although some of the ion pairs may be widely removed therefrom because of the motion of the secondary particles. The maximum energy transferred in elastic collisions is

$$E_{M'} = 4MM'E/(M+M')^2, \tag{3}$$

where M and M' are the masses of the particle and gas atom, respectively. On combining the above relations, we obtain

$$dI/dE = \left[\sigma^e + \int_0^{E_{M'}} dE'\sigma(E, E')I'(E')\right] \Big/ [b^e + b^r] \tag{4}$$

for the ionization, arising from both primary and secondary processes, per unit energy loss of the primary particle.*

[1] In this discussion all the gas atoms are to be assumed identical.

* *Note added in proof.* A treatment based on the statistics of ionization gives integral equations for I and I' from which Eq. (4) follows at high energies. The expressions derived from the statistical treatment have minor differences with those obtained from the simpler arguments of this paper.

The ionization efficiency is conveniently defined as $\eta=\omega^s I/E$. At very low energies all collisions are practically adiabatic and the ionization efficiency is zero. It is seen from the definition of the constant ω^s that the ionization efficiency approaches unity at high energies.

We introduce the two functions of the energy

$$\mu=\omega^s\sigma^s/(b^s+b^r), \quad \text{and} \quad \lambda=b^r/(b^s+b^r), \tag{5}$$

the second of which is less than unity by definition. It follows from Eq. (4) that the ionization efficiency satisfies the equation

$$d(E\eta)/dE=\mu+\lambda\int_0^{E_M'} dE'k(E,E')\eta'(E'), \tag{6}$$

to which is added the boundary condition $\eta(0)=0$. The kernel is

$$k(E,E')=\sigma(E,E')E'\Big/\Big[\int_0^{E_M'} dE'\sigma(E,E')E'\Big]; \tag{7}$$

and $\eta'=\omega^s I'/E'$ is the ionization efficiency of a gas particle of energy E' in its own gas.[2]

The ionization efficiency η' of a gas particle satisfies the integro-differential equation

$$d(E'\eta')/dE'=\mu'+\lambda'\int_0^{E'} dE''k'(E',E'')\eta'(E''), \qquad \eta'(0)=0, \tag{8}$$

obtained from Eq. (6) by regarding the initial particle as identical in nature with the recoil atom. The quantities μ' and λ' are functions of the energy E' of the gas particle and are defined in a manner corresponding to the definitions of μ and λ given above. Likewise, the kernel $k'(E',E'')$ for a gas particle is defined in a manner similar to that given for the kernel for the primary particle.

It is thus seen that the problem of the determination of the ionization efficiency of a heavy particle requires the solution of Eq. (8) for the ionization efficiency of a gas particle. Once this solution is obtained, the ionization efficiency of the primary particle is obtained from Eq. (6) by simple integration.

III. IONIZATION DEFECT

The quantity $\Delta=E-\omega^s I$, which we term the ionization defect, is of particular interest, since it is a measure of the degree to which the total ionization, when converted to energy units by the use of the factor ω^s, fails to give a true measure of the particle energy. An ionization efficiency less than unity corresponds to a positive defect; if $\eta>1$, the defect is negative.

If we write $\Delta=E\chi$ with $\chi=1-\eta$, Eq. (6) becomes

$$d(E\chi)/dE=(1-\mu-\lambda)+\lambda\int_0^{E_M'} dE'k(E,E')\chi'(E'), \tag{9}$$

with $\chi(0)=1$; $\chi'=1-\eta'$.

[2] Any difference in ω^s for the primary particle and for the recoil atoms is neglected.

The quantity λ is nearly unity for the low velocities at which energy loss to recoiling atoms predominates, and approaches zero for very high velocities. The quantity $1-\mu-\lambda=(b^s-\omega^s\sigma^s)/(b^s+b^r)$ is zero everywhere if the rate of energy loss to electrons and the rate of primary ionization (including ionization by ejected electrons) are strictly proportional with the proportionality constant ω^s. In any case, $1-\mu-\lambda$ is small for velocities at which energy loss to recoiling atoms is highly predominant, and approaches zero rapidly for high velocities. In the intermediate range it may conceivably have values positive or negative which are appreciably different from zero. In the discussion that follows, $1-\mu-\lambda$ in Eq. (9) is assumed to be negligible and is set equal to zero for all energies.

Under these conditions the ionization defect is simply

$$\Delta=\int_0^E dE\lambda\int_0^{E_M'} dE'k(E,E')\chi'(E'). \tag{10}$$

If $1-\mu'-\lambda'$, which refers to the gas particles, is also set equal to zero, the quantity χ' is determined by

$$d(E'\chi')/dE'=\lambda'\int_0^{E'} dE''k'(E',E'')\chi'(E''), \qquad \chi'(0)=1. \tag{11}$$

It is then readily seen that both Δ and $\Delta'=E'\chi'$ are not negative, monotonically increasing, bounded functions of E and E', respectively, provided λ and λ' go to zero sufficiently rapidly for high energies. Moreover, if λ' is a monotonically decreasing function of E', and if $dk'(E',E'')/dE'\leq 0$, χ' is a positive, monotonically decreasing function of E'. Also under similar conditions, χ is a positive monotonically decreasing function of E.

IV. THE KERNEL $k(E,E')$ AND THE STOPPING CROSS SECTION b^r

An elastic collision can be described with considerable accuracy as the direct action of the screened nuclear coulomb field of the particle on the screened nuclear charge of the atom. The process is conveniently discussed with the aid of Bohr's screening parameter[3] $\zeta=b/a$, in which b is the collision diameter

$$[(M+M')/M'](ZZ'e^2/E),$$

and a is the screening length $a_0\bar{Z}^{-\frac{1}{2}}$. In terms of $E_S=ZZ'e^2/a$, the screening parameter is simply

$$\zeta=(M+M')E_S/M'E=E_2/E, \tag{12}$$

where $E_2=(M+M')E_S/M'$. In these expressions Z and Z' are the atomic numbers of the particle and gas atom, respectively, $\bar{Z}=(Z^{\frac{1}{2}}+Z'^{\frac{1}{2}})^2$, and $a_0=\hbar^2/me^2$.

For $\zeta\gg 1$, which is the condition of almost complete shielding, the collision cross section is essentially the

[3] N. Bohr, Kgl. Danske Videnskab. Selskab, Mat.-fys. Medd. 18, nr. 8 (1948).

kinetic theory area πd^2, with $d \approx a_0 Z_k^{-\frac{1}{3}}$, where $Z_k = (Z^{\frac{1}{2}}+Z'^{\frac{1}{2}})^2$; the mean energy transferred in a collision is $E_M'/2$. For $\zeta > \sim 1$, which Bohr describes as a condition of excessive screening, the principal scattering is at a separation distance of about the screening length a; the cross section is estimated by Bohr to be of the order of $\pi a^2\zeta/2.72$, and the scattering is still approximately uniform in the center-of-gravity system. For smaller values of ζ, coulomb scattering takes place with a limitation of the minimum energy transferred due to the effect of shielding on distant collisions (minor screening).

Correspondingly, the order of magnitude of the differential scattering coefficient is given by

$$\sigma(E, E') \sim \begin{cases} \pi d^2/E_M', \\ \pi a^2(M+M')E_S/M'EE_M', \\ \pi a^2 M E_S^2/M'EE'^2, \end{cases} \tag{13}$$

for the three conditions of complete, excessive, and minor screening, respectively, except that for minor screening, scattering with recoil energies less than $ME_S^2/M'E$ is negligible. For $E < E_2$, the scattering coefficient is practically independent of E' in the entire range 0 to E_M'. However, for $E_2 < E$, it is practically zero from 0 to $ME_S^2/M'E$ and proportional to $1/E'^2$ from the latter value to E_M'. It might seem reasonable to compensate somewhat for the discontinuous behavior at $E = E_2$ in these estimates by requiring that the collision cross section, which is the integral of the scattering coefficient over E', be continuous. This requirement could be satisfied by multiplying the value in (13) for excessive screening, which is the most uncertain of the three expressions, by the number $\frac{3}{4}$. However, it is more satisfactory in the present discussion to require that the stopping cross section b' be continuous. For this purpose the appropriate factor is $\log 2 = 0.69$.

Since the kernel $k(E, E')$ is independent of factors of proportionality, only the dependence of $\sigma(E, E')$ on E' is important in its determination. Thus, in the approximation here described,

$$k(E, E') \approx \begin{cases} 2E'/E_M'^2, & 0 \le E' \le E_M', \quad 0 \le E < E_2, \\ 0, & 0 \le E' \le E_m' \\ \dfrac{1}{2E' \log(2E/E_2)}, & E_m' \le E' \le E_M' \end{cases} E_2 < E, \tag{14}$$

where

$$E_m' = ME_S^2/M'E = MM'E_2^2/(M+M')^2E \tag{15}$$

is the effective value of the minimum energy transferred in an elastic collision in a screened coulomb field.

The stopping cross section, as calculated from Eq. (13) with the additional factor $\log 2$ for the intermediate condition, is

$$b' \approx \frac{4MM'}{(M+M')^2} \begin{cases} \frac{1}{2}\pi d^2 E, & 0 \le E \le E_1, \\ \frac{1}{2}\pi a^2 E_2 \log 2, & E_1 \le E \le E_2, \\ \frac{1}{2}\pi a^2 (E_2^2/E) \log(2E/E_2), & E_2 \le E, \end{cases} \tag{16}$$

in which $E_1 = (a/d)^2 E_2 \log 2$ has been so chosen to make the first two approximate expressions pass continuously from one to the other. For an argon particle in argon $E_1 = 113$ ev, and the corresponding velocity is $v_0/95$. It is of interest to note that for $E = E_1$, the screening parameter, which is $\zeta = E_2/E$, has the value

$$d^2/a^2 \log 2 \approx 1.45 Z_k^{\frac{1}{3}} Z^{\frac{1}{3}}, \tag{17}$$

which is much greater than unity for a heavy particle ($Z \gg 1$) in any gas. The stopping cross section as given by Eq. (16) increases linearly with E to E_1, is constant to E_2, rises to a maximum at $1.36E_2$ (the increase being only 6 percent), and then decreases. It should be emphasized that the particular features of Eq. (16) are highly arbitrary and that this entire description is at the best only semiquantitative.

V. THE ELECTRONIC STOPPING CROSS SECTION

Inelastic collisions are possible for particle energies above $(M+M')/M'$ times the energy ϵ of the first excited level of the particle or atom, whichever has the lower energy. The corresponding threshold velocity is

$$v_t = [2m\epsilon/\mu\epsilon_0]^{\frac{1}{2}} v_0,$$

where $\mu = MM'/(M+M')$, and $\epsilon_0 = me^4/\hbar^2$. The threshold velocity for argon particles in argon is $v_0/210$.

An energetic heavy particle loses energy primarily through the action of its average charge. The average charge decreases as the particle velocity decreases through the process of capture and loss of electrons.[4] The electronic-stopping cross section in a gas of high atomic number is approximately a linear function of the velocity in the velocity range corresponding to electron capture, giving rise to the familiar linear portion of the range-velocity curves for fission fragments.

As the particle velocity falls below about $v_a = v_0 Z^{-\frac{1}{3}}$, which is a measure of average velocity of the slowest electrons in the neutral particle, the mechanism for inelastic collisions is no longer through an average charge, which is practically zero, but rather through the relative kinetic energy which induces transitions during the interpenetration of the electron clouds of the particle and atom. Statistical arguments indicate that here again the electronic stopping cross section might be expected to be proportional to the particle velocity.

These considerations suggest that the electronic stopping cross section be expressed in ascending and

[4] N. Bohr, Phys. Rev. **58**, 654 (1940); **59**, 270 (1941). W. E. Lamb, Phys. Rev. **58**, 696 (1940); **59**, 687 (1941). J. K. Knipp and E. Teller, Phys. Rev. **59**, 659 (1941). Brunings, Knipp, and Teller, Phys. Rev. **60**, 657 (1941).

descending powers of the velocity in the following manner:

$$b^s=\begin{cases}0, & 0\le v\le v_i,\\ b_1(v-v_i/v_a)+b_2(v-v_i/v_a)^2+\cdots, & \\ & v_i\le v\le v_a,\\ B_1(v/v_a)+B_0+B_{-1}(v_a/v)+\cdots, & \\ & v_a\le v<\sim Zv_0,\ Z'v_0.\end{cases} \quad (18)$$

Except for B_1, we have very little theoretical basis for the calculation of the coefficients in these series because of the intrinsic difficulty of the theory of quasi-adiabatic processes.

For B_1 we have the expression

$$B_1\approx(4\pi e^4/mv_a v_a')\langle\log\rangle_M, \quad (19)$$

which is obtained from the familiar formula for the energy loss of a charged particle by replacing the particle charge by $(v/v_a)e$ and estimating the number of atomic electrons effective in an encounter as $(2v/v_a')$; $\langle\log\rangle_M$ is an average value of the usual logarithmic factor for these electrons. It has been shown by Bohr[3] that such a factor can be calculated from the stopping of alpha-particles by means of

$$(2v/v_a')\langle\log\rangle_M=[(3/4\kappa^3)+(1/4\kappa)]L_\alpha, \quad (20)$$

where L_α is the total logarithmic factor for alpha-particles. In this expression, $\kappa\approx 2Z^{\frac{1}{3}}$. Measurements in argon give[5] $L_\alpha\approx 13.9(v/v_0)$. From Eq. (20) we find $\langle\log\rangle_M\approx 1.21$ for argon particles in argon. For the average light fission fragment in argon $\langle\log\rangle_M$ is found to be 1.15 and for the average heavy fragment 1.10.

VI. IONIZATION BY SLOW HEAVY PARTICLES

The atomic scattering of a heavy particle is nearly spherically symmetrical in the center-of-gravity system if $v<v_2$, where $v_2=[ZZ'Z^{\frac{1}{3}}2m/\mu]^{\frac{1}{2}}v_0$. The equation for χ, when written in terms of velocities, is

$$\chi=\frac{8}{v^2}\int_0^v dv\frac{1}{(1+b^s/b^v)v^3\gamma'^4}\int_0^{\gamma' v}dv'v'^3\chi'(v'),\ v<v_2, \quad (21)$$

in which $\gamma'=2M/(M+M')$. Moreover, the secondary atomic scattering is also spherically symmetrical if $\gamma' v<v_2'$, where $v_2'=[(2)^{\frac{1}{2}}Z'^{7/3}4m/M']^{\frac{1}{2}}v_0$. The equation for χ' is

$$(1+b^{s'}/b^{v'})(d/dv')(v'^3\chi')=(8/v'^3)\int_0^{v'}dv''v''^3\chi'(v''),$$

$$\chi'(0)=1,\quad v'<v_2'. \quad (22)$$

For simplicity, we neglect v_i in Eq. (18) for b^s and suppose that b^v is practically constant; we treat $b^{v'}$ and $b^{s'}$ similarly. For $v'<v_2'$ and $v<v_2$, we write

$$b^{s'}/b^{v'}=\beta_1'(v'/v_2')+\beta_2'(v'/v_2')^2+\cdots, \quad (23)$$
$$b^s/b^v=\beta_1(v/v_2)+\beta_2(v/v_2)^2+\cdots,$$

and seek expressions in series form:

$$\chi'=1-\alpha_1'(v'/v_2')-\alpha_2'(v'/v_2')^2-\cdots,$$
$$\chi=1-\alpha_1(v/v_2)-\alpha_2(v/v_2)^2-\cdots. \quad (24)$$

From Eq. (22) we find for the coefficients in χ':

$$\alpha_1'=\frac{10}{7}\beta_1',\quad \alpha_2'=\frac{45}{28}\beta_1'^2+\frac{3}{4}\beta_2',\ \text{etc.} \quad (25)$$

Using these, we obtain from Eq. (21) for the coefficients in the expansion of χ:

$$\alpha_1=\frac{2}{3}\beta_1+\frac{16}{21}\beta_1'\gamma,$$
$$\alpha_2=-\frac{1}{2}\beta_1^2-\frac{4}{7}\beta_1\beta_1'\gamma-\frac{15}{28}\beta_1'^2\gamma^2+\frac{1}{2}\beta_2+\frac{1}{4}\beta_2'\gamma^2,\ \text{etc.}, \quad (26)$$

in which $\gamma=\gamma' v_2/v_2'$.

In argon with a five percent admixture of air, the ionization by single recoil particles in the alpha-decay of Po, ThC, and ThC′ has been measured by Madsen.[6] The recoil energies are 104 kev, 118 kev, and 170 kev, respectively, and correspond to a velocity range of $0.14v_0$ to $0.18v_0$. We take[7] $Z=82$, $Z'=18$, $M=208$ proton masses, and $M'=40$ proton masses and find $v_2=0.493v_0$, $v_2'=0.255v_0$, and $v_2'/\gamma'=0.151v_0$. Hence, it is seen that the primary atomic scattering is spherically symmetrical but that some nonspherically symmetrical secondary scattering is beginning to set in. We fit the Madsen data with $\alpha_1=0.91$ and $\alpha_2=-0.3$. It does not seem unreasonable to suppose that the values so determined are accurate enough to be used in Eq. (26), which applies to lower velocities. The first expression in Eq. (26) places upper limits on β_1 and β_1', since it gives

$$(\beta_1/1.36)+(\beta_1'/0.37)=1. \quad (27)$$

The most that can be obtained from the second is that

$$0.6\le(\beta_2/1.3)+(\beta_2'/0.3)\le 1, \quad (28)$$

indicating that quadratic terms in Eq. (23) are not negligible even at these low velocities.

VII. IONIZATION BY ARGON IN ARGON

We discuss first the behavior of χ' for velocities below v_2' on the assumption that terms in the velocity higher than quadratic are negligible in both $b^{s'}/b^{v'}$ and χ'. We assume also that β_2 and β_2' in Eq. (28) have the same sign; they then are positive and $\beta_2'\le 0.3$. We seek a lower bound for χ' in the range $0\le v'\le v_2'$. Using the

[5] G. Mano, Ann. phys. 11, 407 (1934). N. O. Lassen, Kgl. Danske Videnskab. Selskab, Mat.-fys. Medd. 25, nr. 11 (1949).

[6] B. S. Madsen, Kgl. Danske Videnskab. Selskab, Mat.-fys. Medd. 23, nr. 8 (1945).

[7] R. C. Ling and J. K. Knipp, Phys. Rev. 80, 106 (1950).

optimum value of β_1' and the maximum value of β_2', we find 0.53 for α_1' and approximately zero for α_2', indicating that $\chi' > \sim -0.5$ on this basis. In any case

$$\chi' > \sim [1-0.53(v'/v_2')] \text{ if } v' \leq v_2'.$$

Above the velocity v_2' the equation for χ' is

$$\frac{1}{v'}\log\left(\frac{\sqrt{2}v'}{v_2'}\right)\left(1+\frac{b^{e\prime}}{b^{r\prime}}\right)\frac{d(v'^2\chi')}{dv'} = \int_{v_2'^2/2v'}^{v'} \chi'(v'')dv''/v'', \quad (29)$$

the solution of which is to have the value $\chi'(v_2')$ at v_2', as determined by the solution of (22). For an argon particle in argon, $v_2'=0.255v_0$ and $v_a'=0.382v_0$. We write

$$\frac{b^{e\prime}}{b^{r\prime}} = \frac{1}{\log[(2)^{\frac{1}{2}}v'/v_2']}\left(\frac{v'}{v_2'}\right)\left[\gamma_1'\left(\frac{v'}{v_2'}\right)+\gamma_0'+\cdots\right], \quad v_2' < v, \quad (30)$$

where, if the descending series in Eq. (18) extends down to v_2',

$$\gamma_1' \approx (v_2'/v_a')B_1'/\pi a'^2E_2', \quad \gamma_0' \approx B_0'/\pi a'^2E_2', \text{ etc.} \quad (31)$$

From Eq. (19) the value of γ_1' for an argon particle in argon is found to be 0.127.

It is readily seen that

$$v_2'^2\chi'(v_2') + \chi'(v_2'/\sqrt{2})\int_{v_2'/\sqrt{2}}^{v'} v'\lambda' dv' \leq v'^2\chi' \leq 2\int_0^{v'} v'\lambda' dv'. \quad (32)$$

The integral in the lower bound has the asymptotic value $7.8v_2'^2$ for large values of v' if Eq. (30) is used in λ', with $\gamma_1'=0.13$, $\gamma_0'=0$, etc.

VIII. IONIZATION BY FISSION FRAGMENTS

Extensive studies have been made of the ionization produced by fission fragments when they are stopped in various gases. Ionization yields are usually converted to energies by comparison with the ionization of an alpha-particle of known energy. The ionization of an alpha-particle is directly proportional to its energy over a very wide energy range because the energy lost to recoiling atoms is but a small fraction of the energy of the alpha-particle and hence, even if the recoiling atoms have a reduced ionization efficiency, the total ionization yield of the primary particle is largely unaffected. The situation is quite different with fission fragments in a heavy gas such as argon. A reduced efficiency of the recoiling gas atoms brings about an appreciable decrease in the ionization yield of the fragments.

There is some indication, from experiments on fission fragments from U^{235} produced by thermal neutrons, that these particles have positive ionization defects. Estimates of the energy based on ionization yields[8] are appreciably smaller than the calorimetric measurement of Henderson.[9] Recently Leachman[10] has shown that certain differences between fission fragment mass and ionization distributions can be attributed to a variation in ω, the energy loss per ion pair, with fragment mass.

For $v < v_2$, the quantity χ is given by Eq. (21). For $v_2 < v$, we have

$$\chi = \frac{8}{v^2}\int_0^{v_2} \frac{dv}{(1+b^e/b^r)v^3\gamma'^4}\int_0^{\gamma' v} v'^3\chi'(v')dv' + \frac{1}{v^2}\int_{v_2}^{v} \frac{dv}{(1+b^e/b^r)v^{-1}\log(\sqrt{2}v/v_2)} \times \int_{\gamma' v^2/2v}^{\gamma' v} (v')^{-1}\chi'(v')dv', \quad v_2 < v. \quad (33)$$

Lower and upper bounds for the ionization defect are given by

$$E_2[\chi(v_2)+\chi'(\gamma' v_2/(2)^{\frac{1}{2}})v_2^{-2}\int_{v_2}^{v} v\lambda dv] \leq \Delta \leq 2E_2v_2^{-2}\int_0^{v} v\lambda dv. \quad (34)$$

The integral in the lower bound has the asymptotic value $9.6v_2^2$ for large values of v if an expression similar to Eq. (30) is used in λ, with $\gamma_1=0.10$, $\gamma_0=0$, etc., where

$$\gamma_1 \approx (v_2/v_a)B'/[4MM'\pi a^2E_2/(M+M')^2]. \quad (35)$$

The value 0.10 for γ_1 is the result obtained from Eq. (35) for both the average light and the average heavy fission fragments in argon.[11]

IX. NUMERICAL ESTIMATES

Owing to our lack of knowledge concerning the ratio of the stopping cross sections for velocities below v_a, which is the velocity at which the neutralization of the particle by electron capture is practically complete, it is not possible to do better than make very rough estimates of the actual magnitudes of the ionization efficiencies and ionization defects for various particles. We describe briefly a sample calculation which has been made on the basis of what would seem to be reasonable, although quite arbitrary, assumptions.

[8] Flammersfeld, Jensen, and Gentner, Z. Physik **120**, 450 (1943); W. Jentsche, Z. Physik **120**, 165 (1943); M. Deutsch and M. Ramsey, MDDC 945 (1946); D. C. Brunton and G. C. Hanna, Can. J. Research **A28**, 190 (1950).

[9] M. C. Henderson, Phys. Rev. **58**, 744 (1940).

[10] R. B. Leachman, Phys. Rev. **79**, 197 (A) (1950).

[11] We use $Z=37$ and $M=95$ proton masses for the average light fission fragment, which give $v_a=0.300v_0$ and $v_2=0.330v_0$; and $Z=55$ and $M=139$ proton masses for the average heavy fragment, which give $v_a=0.363v_0$ and $v_2=0.400v_0$.

Equations (22) and (29) are solved numerically for an argon particle in argon using, for $b^{\nu\prime}/b^{\nu\prime}$, only the first terms in the series (23) and (30), with $\beta_1'=0.24$ and $\gamma_1'=0.13$. The value for β_1' is that obtained from Eq. (27) under the assumption that $\beta_1'/v_2'=\beta_2/v_2$. One sees that there is introduced a discontinuity in $b^{\nu\prime}/b^{\nu\prime}$ at v_2', which might be expected to be smoothed out by higher terms in the series, were they included. It is found that $\chi'=0.78$ at $v'=v_2'/\sqrt{2}$, 0.72 at v_2', 0.53 at $2v_2'$, 0.40 at $3v_2'$, etc., and that $\chi'\to 12(v_2'/v')^2$ as $v'\to\infty$, corresponding to an ionization defect of 780 kev for an argon particle of very high velocity. The asymptotic value $v'^2\chi'$ is very closely the mean of the values obtained from the upper and lower bounds in Eq. (32).

For the average light fission fragment, we take $\beta_1=0.31$ and $\gamma_1=0.10$, and for the average heavy fission fragment, we take $\beta_1=0.38$ and $\gamma_1=0.10$, other coefficients in the series expressions being put equal to zero. We then obtain, in argon, an ionization defect of 2.5 Mev for a light fragment of energy 98 Mev and an ionization defect of 4.2 Mev for a heavy fragment of energy[12] 67 Mev. These quantities are rather insensitive to the the behavior of b^{ν}/b^{ν} for velocities below v_2, since the contribution of the second integral of Eq. (33) is much larger than that of the first. However, a behavior of $b^{\nu\prime}/b^{\nu\prime}$ which is radically different than that assumed would lead to quite different values for the ionization defects of both argon and the fission fragments.

[12] Knipp, Leachman, and Ling, Phys. Rev. **80**, 478 (1950).

PHYSICAL REVIEW VOLUME 82, NUMBER 1 APRIL 1, 1951

A Rapid Method of Calculating log(ft) Values for β-Transitions

S. A. Moszkowski
Institute for Nuclear Studies, University of Chicago, Chicago, Illinois
(Received July 17, 1950)

This paper contains several graphs and nomographs which make it possible to obtain, very quickly, log(ft) values for most β-decays. The use of these figures is discussed.

I. INTRODUCTION

BETA-DECAYS can be divided into several classes of allowedness and forbiddenness according to their $\log_{10}(ft)$ values.[1,2] In conjunction with Gamow-Teller selection rules, such a classification agrees, in nearly all cases, with predictions from the nuclear shell model.[2-4] This paper contains several graphs and nomographs which make it possible to obtain, very quickly, log(ft) values for most β^+ emissions, β^- emissions, and K-captures.

Log(ft) can be written as the sum of three additive terms. The first term, $\log(f_0t)$, is the value for a β-decay if the effect of the coulomb field is ignored and if there is no branching. The second term, log(C), is the coulomb correction term. The third term, $\Delta\log(ft)$, appears if there is branching. In this paper all logarithms are taken to the base 10.

II. CONSTRUCTION OF THE FIGURES

(a) Construction of Nomograph for $\log(f_0t)$

f_0 for β^+ emission is given by the formulas:

$$f_0=\int_1^{W_0} W(W^2-1)^{\frac{1}{2}}(W_0-W)^2dW,$$

and

$$f_0=[(W_0^4/30)-(3/20)W_0^2-(2/15)][(W_0^2-1)]^{\frac{1}{2}}+(2.302/4)W_0\log[W_0+(W_0^2-1)^{\frac{1}{2}}],$$

where W_0 is the maximum energy of the β-particles, including rest mass, in units of mc^2.

For K-capture, f_0 is given by $f_0=(W_0+E_K)^2$. Here E_K is the binding energy of a K-electron, which, of course, depends on the atomic number of the decaying nucleus. f_0 depends only on W_0 for $\beta^\pm$ emission. For K-capture, one can write for f_0, instead of the above expression:

$$f_0=W_0^2.$$

The error introduced by ignoring E_K in the expression for f_0 is negligible except for large Z and small W_0, as discussed in Sec. III. Here t is the half-life in seconds for all modes of decay.

The nomograph of Fig. 1, for getting $\log f_0t$ values, consists of three columns; a, b, and c. Column a contains two sets of entries of energies E_0. For $\beta^\pm$ emission, E_0 is the maximum energy of the β-particles in Mev, not including the rest mass, and the entries on the right side apply. For K-capture, E_0 is the decay energy in Mev, and the entries on the left side apply. The spacing of energies on Column a is not uniform but is proportional to $\log(f_0)$. Column b gives t in seconds, days, etc. The spacing is uniform in $\log(t)$. Column b is constructed exactly halfway between Columns a and c. Column c

[1] E. Konopinski, Revs. Modern Phys. **15**, 209 (1943).
[2] L. Nordheim, Phys. Rev. **78**, 294 (1950).
[3] M. G. Mayer, Phys. Rev. **78**, 16 (1950).
[4] E. Feenberg and K. C. Hammack, Phys. Rev. **75**, 1877 (1949).

FIG. 1. Log(f_0t) as a function of E_0 and t.

contains log(f_0t), spaced uniformly. These spacings are such that for equal geometrical intervals,

$$d(\log f_0t)=\tfrac{1}{2}d(\log t)=-d(\log f_0),$$

where $d(X)$ denotes the change in X. It is then possible to get log(f_0t) by drawing a straight line through the proper values of E_0 (Column *a*) and t (Column *b*), noting its crossing point with Column *c*.

(b) Construction of Graphs for log(C)

Log(C) is the coulomb correction term, dependent upon W_0, and Z, the the atomic number of the initial nucleus, and is different for β^- emission, β^+ emission, or K-capture. For β^- or β^+ emission, it is a relatively slowly varying function of W_0, and Z given by

$$C=\int^{W_0} F(Z',W)W(W^2-1)^{\frac{1}{2}}(W_0-W)^2dW/f_0.$$

$F(Z',W)$, the density of electrons at the edge of the nucleus, is given by

$$F(Z',W)=\frac{1+S}{2}\frac{4}{|\Gamma(2S+1)|^2}[2(W^2-1)^{\frac{1}{2}}R]^{2S-2}$$
$$\times\exp\left(\frac{\pi\alpha Z'W}{(W^2-1)^{\frac{1}{2}}}\right)\left|\Gamma\left(S+\frac{i\alpha Z'W}{(W^2-1)^{\frac{1}{2}}}\right)\right|^2,$$

where $Z'=\mp Z+1$ for $\beta^\pm$ emission, $S=(1-\alpha^2Z'^2)^{\frac{1}{2}}$, α=fine structure constant=1/137, R=nuclear radius in units of $\hbar/mc=0.0039A^{\frac{1}{3}}$, and Γ=the gamma-function. Figures 2(a) and 2(b) show log(C) as a function of maximum energy for various values of Z, for β^- and β^+ emission.

The calculation of log(C) was done as follows. In the expression for C given above, the factor $F(Z',W)$ can be replaced by $a(W-1)^b$, where a and b depend only slightly on W, and more strongly on Z'. This is apparent from graphs for $F(Z',W)$, which are not shown here. To get C for a given value of Z and W_0, it is necessary in principle, to integrate $F(Z',W)$, multiplied by the weighting factor $W(W^2-1)^{\frac{1}{2}}(W_0-W)^2$ over the energy. C is equal to the resulting integral divided by

$$f_0=\int_1^{W_0} W(W^2-1)^{\frac{1}{2}}(W_0-W)^2dW.$$

The weighting factor has a maximum for $W-1\sim0.3(W_0-1)$ and, in fact, most of the contribution to the integral comes from values of $W-1$ between

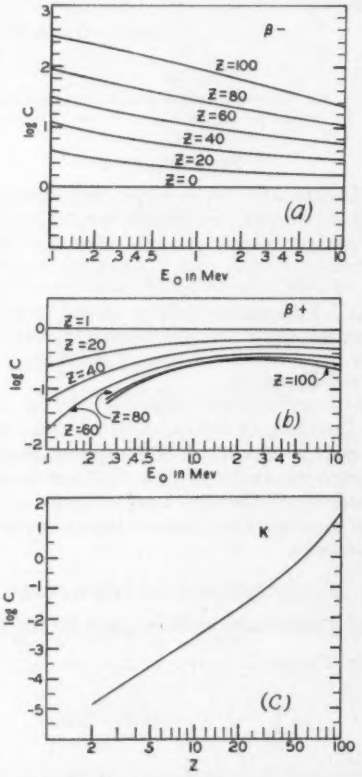

FIG. 2. (*a*) Log(C) as a function of E_0 and Z for β^- emission. (*b*) Log(C) as a function of E_0 and Z for β^+ emission. (*c*) Log(C) as a function of Z for K-capture.

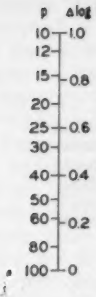

FIG. 3. $\Delta \log(ft)$ as a function of p.

$0.2(W_0-1)$ and $0.5(W_0-1)$, which is a relatively small range of values. It is therefore permissible to approximate $F(Z', W)$ by $a(W-1)^b$, where a and b are constants read off the graph for F. The constants should be read off at $Z'=\mp Z+1$ for $\beta^\pm$ emission and in the neighborhood of $W=1+0.3(W_0-1)$.

It is not desirable to carry out the integration explicitly, since the integrals depend so strongly on W_0, and the integration can be performed analytically only for $W_0-1 \ll 1$ and for $W_0 \gg 1$. Instead, $C(Z, W_0)$ may be written as $F(Z', W_{Av})$, where W_{Av} is some average value of the energy. If W_{Av} is written as $1+r(W_0-1)$, using the definition for C given above with $F(Z', W) = a(W-1)^b$, it is seen that r is given as a function of b and W_0:

$$r=\left[\frac{\int_1^{W_0}(W-1)^b W(W^2-1)^{\frac{1}{2}}(W_0-W)^2 dW}{(W_0-1)^b f_0}\right]^{1/b}.$$

r can be calculated analytically in the limit $W_0-1 \ll 1$ as well as for $W_0 \gg 1$. r depends only slightly on W_0 in contrast to the integrals separately. Therefore, in the intermediate case of $W_0-1 \sim 1$, r can be obtained quite accurately by interpolation. Then $C(Z, W_0)$ can be read off from the graph for F using the value of r obtained here.

For K-capture, with 2 electrons in the K-shell initially, C is given by

$$C=2\pi(\alpha Z_K)^3(2\alpha Z_K R)^{2S_0-2}\frac{2+E_K}{\Gamma(2S_0+1)}e^{-2\alpha Z_K R},$$

where $Z_K=Z-0.35$, $S_0=(1-\alpha^2 Z_K^2)^{\frac{1}{2}}$, $E_K=-\alpha^2 Z_K^2/2$. α, R and Γ are defined as for $\beta^\pm$ emission. Log(C) as a function of Z for K-captures is shown in Fig. 2(c).

(c) Construction of Table for the Branching Correction Term, $\Delta \log(ft)$

If there are several modes of decay occurring simultaneously with a half-life t, and the percentage p of total decay occurring in the mode under consideration is known, the term $\Delta \log(ft)$ appears and is given by

$$\Delta \log(ft)=2-\log p.$$

TABLE I. The function $E_0'(Z)$.

Z	E_0' (Mev)
60	0.18
70	0.24
80	0.32
90	0.40
100	0.50

This is shown in Fig. 3. If only one mode of decay occurs, $p=100$ and $\Delta \log ft=0$.

III. RANGE OF USEFULNESS OF THE FIGURES

The figures can be used for $\beta^\pm$ maximum energy of 120 kev to 9 Mev, and give results accurate to within 0.1 of the true value of $\log(ft)$. For K-captures, results to within 0.2 are obtained for energies of 200 kev to 10 Mev, with certain qualifications which are due to the approximations for f_0 made in Sec. II (a). Let $E_0'(Z)$ be the value of E_0 below which $\log(ft)$ for K-capture, as obtained from the figures, deviates by more than 0.2 from the correct value. Table I shows E_0' for various values of Z.

The branching correction obtainable from Fig. 3 is not restricted to values of $p>10$, since if p is replaced by $10^{-n}p$, $\Delta \log(ft)$ is replaced by $n+\Delta \log(ft)$.

IV. USE OF THE FIGURES

For a given type decay, given energy, half-life, etc., the figures of this article permit calculation of $\log(ft)$. Here the following notation is used: E_0 for $\beta^\pm$ emission is the maximum kinetic energy of the particles in Mev; E_0 for K-capture is the decay energy in Mev.

When a β^+ emission and K-capture go from and to the same level; E_0 for K capture$=E_0$ for β^+ emission $+1.02$ Mev; t is the total half-life in seconds (s), minutes (m), hours (h), days (d), or years (y); Z is the atomic number of the initial nucleus; and, p is the percentage of decay occurring in the mode under consideration. When no branching occurs, $p=100$.

V. PROCEDURE FOR OBTAINING LOG(FT)

(1) To obtain $\log(f_0 t)$, use Fig. 1. E_0 is read off the left-hand side of the E_0 column for K-capture, and off the right-hand side for $\beta^\pm$ emission. Put a straight edge over the given values of E_0 and t and note where it crosses the column of $\log(f_0 t)$ values.

(2) Read off $\log(C)$ from Figs. 2(a), 2(b), and 2(c), for β^- emission, β^+ emission, and K-capture, respectively.

(3) Get $\Delta \log(ft)$ from Fig. 3 if $p<100$. When $p=100$, $\Delta \log(ft)=0$.

(4) $\text{Log}(ft)=\log(f_0 t)+\log(C)+\Delta \log(ft)$.

The author wishes to express his appreciation to Dr. M. G. Mayer for valuable advice given in the preparation of the paper and to Mr. B. A. Meadows for the preparation of the figures.

The Absorption of Slow π^- Mesons in Deuterium

S. TAMOR,*†
University of Rochester, Rochester, New York
(Received October 5, 1950)

The possible mechanisms for absorption of π^- mesons in deuterium are considered. A phenomenological treatment of the simple "neutron absorption" enables one to calculate the competition between the processes independently of the value of the π^- nucleon coupling constant. It is found that various meson theories for the charged meson lead to markedly different predictions for the fraction of events leading to gamma-ray emission. The results are compared with experiment and lead to the conclusion that the charged meson is either pseudoscalar or pseudovector. Comparison with the $(\pi^0:\gamma)$ ratio from the absorption in hydrogen indicates that if the charged meson is pseudoscalar the neutral meson is also pseudoscalar.

I. INTRODUCTION

THE recent experiments on the absorption of π^- mesons in hydrogen[1] provide a very sensitive method of determining the π^0 rest mass. Furthermore, the $(\pi^0:\gamma)$ ratio enables one to calculate the strength of the π^0 nucleon coupling for any assumed theories of the charged and neutral meson.[2] The experiment does not, however, provide any clearcut information concerning the properties of the charged meson. It has been suggested[3] that an investigation of the absorption process in deuterium would lead to a method of determining the spin and parity of the charged meson.

There are three ways in which this process can go: "neutron absorption" (simple disintegration of the deuteron into two neutrons), radiative absorption (absorption accompanied by gamma-emission), and mesic absorption (absorption accompanied by emission of a neutral meson). In a completely field-theoretic calculation the lowest order in which the neutron absorption can take place is the third. The radiative and mesic processes can be treated as second-order processes, as in hydrogen. In this calculation the nucleon-nucleon interaction is treated phenomenologically, by means of an empirical potential. If this potential is included in the unperturbed nucleon hamiltonian, the neutron absorption can be treated as a first-order process in complete analogy with the photo-disintegration of the deuteron.[4] This method has the advantage that all three modes of absorption are of first-order in the π^- coupling constant, so that the ratios of the transition probabilities are independent of the strength of this coupling.

The observed decay of the neutral meson into two gamma-rays shows that the π^0 cannot have spin one. However, no such conclusion can be drawn for the charged meson. Calculations are, therefore, performed for neutral mesons of the type $S(S)$, $PS(PS)$, and $PS(PV)$, and for charged mesons of the type $S(S)$, $PS(PS)$, $PS(PV)$, $V(V)$, and $PV(PV)$. [$PS(PV)$ denotes pseudoscalar meson with pseudovector coupling, and similarly is for the others.] Gradient couplings for the S, V, and PV fields do not lead to any essentially new results.

II. THE METHOD OF CALCULATION

It has been shown by Wightman[5] that a meson passing through liquid hydrogen or deuterium will be slowed down, captured into a Bohr orbit, and cascade down to the K shell in much less time than the natural $\pi-\mu$-decay time. We, therefore, assume that all mesons are absorbed from the $1S$ state of the mesic deuterium atom. It is true that the $2S$ state is metastable so that an appreciable fraction of the mesons may be absorbed from this level. However, everything said about the $1S$ level also applies to all other S states except for a normalization factor.

Since the deuteron wave function is a ${}^3S_1+{}^3D_1$ state, the spatial wave function of the initial state has even parity. However, the exclusion principle applied to the final neutrons requires that the wave function be completely antisymmetric in their coordinates. This, combined with parity conservation, introduces selection rules which strongly affect the probability for neutron absorption.

The entire method of treatment is inherently nonrelativistic. The problem, therefore, resolves itself into two parts: first, to find the nonrelativistic approximation to the interaction operator for the process under consideration, and second, to evaluate the integral representing the overlap of the initial and final wave functions. If the interaction operator is odd, its nonrelativistic form is most easily found by application of the canonical transformation discussed by Foldy and Wouthuysen.[6] The exclusion principle is taken into account by explicitly antisymmetrizing the final neutron wave function. Since the deuteron wave function is completely symmetric with respect to interchange of

* AEC predoctoral fellow.
† Now at Oak Ridge National Laboratory, Oak Ridge, Tennessee.
[1] Panofsky, Aamodt, and York, Phys. Rev. **78**, 825 (1950).
[2] R. Marshak and A. Wightman, Phys. Rev. **76**, 114 (1949) and Marshak, Tamor, and Wightman, Phys. Rev. **80**, 765 (1950).
[3] B. Ferretti, "Report on the International Conference on Low Temperatures and Fundamental Particles," Cambridge (1946), p. 75.
[4] C. Marty and J. Prentki, J. phys. et rad. **10**, 156 (1949).
[5] A. Wightman, Phys. Rev. **77**, 521 (1950); and private communication.
[6] L. L. Foldy and S. A. Wouthuysen, Phys. Rev. **78**, 29 (1950).

the nucleon coordinates, only that part of the interaction which is antisymmetric in the nucleon coordinates leads to nonvanishing matrix elements. For the two-step processes of radiative and mesic absorption, it is important to use the relativistic interactions and only to pass to the Pauli approximation after the sum over intermediate states has been performed. Otherwise, transitions through states of negative energy, which are frequently important, will not be included. All matrix elements are calculated to the lowest nonvanishing order in the nucleon velocities and μ/M, where μ and M are the meson and nucleon masses respectively. Since the radius of the mesic Bohr orbit is much larger than the radius of the deuteron, the meson wave function may be replaced by its value at the origin, and terms involving the gradient of the meson wave function may be neglected.

(A) Neutron Absorption

The nonrelativistic forms of the $S(S)$ and $PV(PV)$ interactions may be written down immediately as ϕ and $\boldsymbol{\sigma}\cdot\boldsymbol{\phi}$ respectively; the Foldy-Wouthuysen transformation gives for the $PS(PV)$ and $V(V)$ cases

$$PS(PV)\ (\hbar/Mc)\boldsymbol{\sigma}\cdot\mathbf{p}\phi, \quad V(V)\ (\hbar/Mc)\boldsymbol{\phi}\cdot\mathbf{p},$$

where the vectors $\boldsymbol{\sigma}$ and $\mathbf{p}$ are respectively the nucleon spin and momentum operators, and

$$\phi=\frac{\hbar c}{(2E_l)^{\frac{1}{2}}}(a_l+b_l^*)\varphi_l\tau^-, \quad \boldsymbol{\phi}=\frac{\hbar c}{(2E_l)^{\frac{1}{2}}}\mathbf{e}(a_l+b_l^*)\varphi_l\tau^-.$$

Here, φ_l is the wave function of a meson in the l'th Bohr orbit, and $\mathbf{e}$ is a unit vector in the direction of polarization of the meson; for a meson at rest, the fourth component of the vector meson field is zero.

The matrix element for the absorption of a $PS(PS)$ meson is found by use of the equivalence theorem.[7] Dyson has pointed out, however, that the equivalence theorem must be modified in the presence of a phenomenological nucleon-nucleon interaction which has a charge exchange character. Application of his transformation to a system with a potential interaction V, having an arbitrary spin and charge dependence, leads to the modified equivalence relation (keeping only terms to first order in g)

$$\boldsymbol{\sigma}\cdot\boldsymbol{\nabla}\phi-(1/c)\gamma_0(\partial\phi/\partial t)=2iM\beta\gamma_5\phi+\gamma_5[V,\phi].$$

The commutator vanishes when the potential V does not contain isotopic spin operators.

After antisymmetrizing the interactions, the matrix elements become (except for factors of i)

$$(4\pi)^{\frac{1}{2}}g[\hbar c/(2E)^{\frac{1}{2}}](\chi_f^*|Q|\chi_0)\varphi(0)\int\psi_0\psi_f d\tau,$$

where χ_0 and χ_f are the initial and final nucleon spin functions, ψ_0 and ψ_f are the spatial part of the initial and final wave functions, and the operator Q is given by

$$\begin{aligned} &S(S) && 0,\\ &PS(PV) && (\hbar/Mc)\tfrac{1}{2}(\boldsymbol{\sigma}_1+\boldsymbol{\sigma}_2)\cdot\mathbf{K},\\ &V(V) && (\hbar/Mc)\mathbf{e}\cdot\mathbf{K},\\ &PS(PV) && \tfrac{1}{2}(\boldsymbol{\sigma}_1-\boldsymbol{\sigma}_2)\cdot\mathbf{e}. \end{aligned}$$

Here $\mathbf{K}$ denotes the final nucleon momentum in the center-of-mass system of the final neutrons (which in this case coincides with the laboratory system). If one assumes a nucleon-nucleon interaction of the form[8] $V(r)(1+P_M)/2$ (P_M is the Majorana operator), the $PS(PS)$ matrix element becomes

$$(4\pi)^{\frac{1}{2}}g\frac{\mu}{2M}\frac{\hbar}{Mc}\left(\chi_f^*\left|\frac{\boldsymbol{\sigma}_1+\boldsymbol{\sigma}_2}{2}\cdot\mathbf{K}\right|\chi_0\right)\varphi(0)\times\int\psi_0\left(1-\frac{V(r)}{\mu c^2}\right)\psi_f d\tau.$$

After squaring the matrix element, we find that the sums over initial and final spins proceed in exactly the same manner as in the photo-disintegration of the deuteron.[9] On multiplication by the density of final states, the transition probabilities per unit time are in units of $\frac{1}{2}(g^2/\hbar c)N^2(\hbar/\mu c)^3\cdot c\cdot|\varphi(0)|^2$;

$$\begin{aligned} &S(S) && 0,\\ &PS(PS) && 2\pi(\mu/M)^2(\hbar K/\mu c)^3|I'|^2\\ &PS(PV) && 8\pi(\mu/M)(\hbar K/\mu c)^3|I|^2,\\ &V(V) && 4\pi(\mu/M)(\hbar K/\mu c)^3|I|^2,\\ &PV(PV) && 12\pi(M/\mu)(\hbar K/\mu c)|I|^2; \quad (J=0), \end{aligned}$$

where

$$I=\int(u_0(r)/r)\psi_f(\mathbf{r})d\tau,$$

$$I'=\int(u_0(r)/r)(1-V(r)/\mu c^2)\psi_f(\mathbf{r})d\tau.$$

u_0 denotes the radial part of the deuteron wave function, and N is its normalization factor.

It should be noted that for mesons of spin one there are three possible values for the total angular momentum of the meson-deuteron system. For the case of pseudovector mesons the above matrix elements correspond to absorption from the state $J=0$ of the meson-deuteron system. Since the deuteron is partially in a $^3D_1$ state, neutron absorption from the state $J=2$ is also possible. This is calculated by replacing χ_0 by $2^{-\frac{1}{2}}S_{12}\chi_0$ (S_{12} is the tensor operator) and using the appropriate radial wave function for the $^3D_1$ state. Neutron absorption from the state $J=1$ is forbidden.[10]

[7] F. J. Dyson, Phys. Rev. **73**, 929 (1948); K. M. Case, Phys. Rev. **76**, 14 (1949).

[8] R. S. Christian and E. W. Hart, Phys. Rev. **77**, 441 (1950).

[9] W. Rarita and J. Schwinger, Phys. Rev. **59**, 436 (1941).

[10] The author is indebted to Dr. K. A. Brueckner for calling his attention to this point.

(B) Radiative Absorption

Both the radiative and mesic absorptions may be treated as second-order processes. Here, only the proton takes part in the interaction, since interactions of the neutron with the meson or electromagnetic fields can only occur in higher order. It is easy to see that if the depth of the nucleon-nucleon potential is small compared to Mc^2, the deuteron may be treated as a superposition of free Dirac wave functions with a momentum distribution corresponding to the fourier transform of the nonrelativistic deuteron wave function. For every value of the final relative momentum of the nucleons, $\mathbf{K}$, and of the γ-ray (or meson) momentum, $\mathbf{k}$, there corresponds a matrix element for the interaction which can be expressed as a function of $\mathbf{K}$ and $\mathbf{k}$. If this is a slowly varying function of $\mathbf{K}$, it is possible to write the matrix element for the absorption of the meson and emission of a quantum of momentum $\mathbf{k}$ as

$$\int d\mathbf{K} M(\mathbf{k},\mathbf{K}) \int \psi_0(\mathbf{r}) e^{-i(\mathbf{k}\cdot\mathbf{r})} \psi_f(\mathbf{r}) d\tau,$$

where M is the corresponding matrix element for a free proton, and ψ_f is the final neutron wave function which is asymptotically a plane wave representing a relative momentum $\mathbf{K}$. The magnitudes of $\mathbf{K}$ and $\mathbf{k}$ are related to one another through the requirement of energy conservation.

Thus, the problem is again separated into two parts; the determination of the nonrelativistic matrix element and the evaluation of an overlap integral. The matrix element $M(\mathbf{k},\mathbf{K})$ is calculated in the same way as in the hydrogen case except that the proton can no longer be considered to be initially at rest. The calculation is easily performed using either the standard methods of perturbation theory or the new techniques of Feynman.

In this calculation the anomalous magnetic moment of the nucleon is treated phenomenologically by adding an additional interaction between the nucleon and the radiation field.[11] A completely field-theoretic calculation would require consideration of higher order processes involving the virtual emission and absorption of mesons. In view of the fact that, at present, meson theory does not give quantitatively the correct nucleon moments, and since higher order terms would defeat the purpose of the present calculation by introducing higher powers of g, we simply add this anomalous interaction to the ordinary spin moment of the nucleon.

After summing over intermediate states and passing to the Pauli approximation, we find for the matrix elements for the absorption of a meson with the emission of a gamma-ray of wave number $\mathbf{k}$,

$$2\pi e g \frac{\hbar c}{(2E)^{\frac{1}{2}}(2\hbar\omega)^{\frac{1}{2}}} \frac{\hbar}{Mc} (\chi_f^* | Q | \chi_0) \int \psi_f e^{-i(\mathbf{k}\cdot\mathbf{r})} \psi_0 d\tau,$$

where Q is given by

$S(S)$	$\Gamma(\hbar/\mu c)\boldsymbol{\sigma}_1\cdot\mathbf{k}\times\boldsymbol{\varepsilon}$,
$PS(PS)$	$\boldsymbol{\sigma}_1\cdot\boldsymbol{\varepsilon}$,
$PS(PV)$	$(2M/\mu)\boldsymbol{\sigma}_1\cdot\boldsymbol{\varepsilon}$,
$V(V)$	$(M/\mu)\mathbf{c}\cdot\boldsymbol{\varepsilon}+i\boldsymbol{\sigma}_1\cdot\mathbf{c}\times\boldsymbol{\varepsilon}$,
$PV(PV)$	$(M/\mu)\boldsymbol{\sigma}_1\cdot\boldsymbol{\varepsilon}(\mathbf{k}\cdot\mathbf{c})/\lvert k\rvert$.

Here, Γ is the difference of the neutron and proton magnetic moments in units of the ordinary Dirac moment ($\Gamma=4.7$), and $\boldsymbol{\varepsilon}$ is a unit vector in the direction of polarization of the gamma-ray.

The probabilities for transitions to the singlet state are, in units of $\frac{1}{3}(g^2/\hbar c)N^2(\hbar/\mu c)^3 c\,|\varphi(0)|^2\,|I_s(k)|^2$,

$S(S)$	$2\Gamma^2(\mu/M)(\hbar/\mu c)^5 K k^2 dk$,
$PS(PS)$	$2(\mu/M)(\hbar/\mu c)^3 K k dk$,
$PS(PV)$	$8(M/\mu)(\hbar/\mu c)^3 K k dk$,
$V(V)$	$(4\mu/3M)(\hbar/\mu c)^3 K k dk$,
$PV(PV)$	$(2M/\mu)(\hbar/\mu c)^5 K k^2 dk$, $\quad (J=1)$

where

$$I_s = \int (u_0(r)/r) e^{-i(\mathbf{k}\cdot\mathbf{r})} \psi_s(\mathbf{r}) d\tau,$$

and ψ_s is the symmetric part of the final neutron wave function.

Similarly, if we replace I_s by I_t, where the neutron wave function is now antisymmetric in space, the transition probabilities to triplet states are, in the same units,

$S(S)$	$4\Gamma^2(\mu/M)(\hbar/\mu c)^5 K k^2 dk$,
$PS(PS)$	$4(\mu/M)(\hbar/\mu c)^3 K k dk$,
$PS(PV)$	$16(M/\mu)(\hbar/\mu c)^3 K k dk$,
$V(V)$	$2(M/\mu)(\hbar/\mu c)^3 K k dk$,
$PV(PV)$	$2(M/\mu)(\hbar/\mu c)^5 K k^2 dk$. $\quad (J=0, 2)$

Since the deuteron is a loosely bound system, the most probable transitions are those in which the gamma-ray carries off most of the available energy. Therefore, the final state is predominantly S, and the most important transitions (except in the vector case) are those to the singlet state.

(C) Mesic Absorption

The calculation of the probability for mesic absorption proceeds in exactly the same way as for the radiative case. Since there are so many possible combinations of π^0 and π^- meson theories, we shall not list all the matrix elements but simply discuss the important features of the interactions.

As a first approximation, the matrix elements for mesic absorption in deuterium should be the same as those for hydrogen, except for the operation of the exclusion principle. The antisymmetrization in most cases simply introduces a factor of $\frac{1}{2}$ arising from the averaging over initial spins. The only exceptions occur when both mesons are scalar or both pseudoscalar. In these cases, transitions to singlet states are impossible so that the P parts of the final nucleon and meson wave

[11] W. Pauli, *Handbuch der Physik*, Vol. 24/1, p. 233.

functions contribute to the integral. This reduces the probabilities for these processes by a large factor. In the other cases, one would expect the $(\pi^0:\gamma)$ ratios to be about the same as in the hydrogen case. However, the binding energy of the deuteron uses up a considerable fraction of the $(\pi^- - \pi^0)$ mass difference so that the volume of phase space available to the meson is diminished. This has the effect of decreasing all the mesic absorption probabilities by factors of 10 to 100.

III. RESULTS

The various integrals were evaluated using the deuteron wave function $u_0(r)=N(e^{-\gamma r}-e^{-\beta r})$ corresponding to the Hulthén potential $(\gamma^2-\beta^2)/(e^{(\beta-\gamma)r}-1)$. This potential closely approximates the Yukawa potential but has the advantage of permitting an analytic solution of the wave equation. The parameters γ and β are determined from the effective range and scattering length of the $n-p$ interaction.[12] In the case of neutron absorption, the energy available in the center of mass system is 138 Mev so that the final neutron wave function is very nearly a plane wave. However, in the radiative and mesic processes the neutrons carry off very little energy, and the distortion of the wave function due to mutual interaction may be large. The S part of the wave function may be approximated at low energies by

$$(1-e^{-\eta r})\sin(Kr+\delta)/Kr,$$

where the parameter η is determined from the effective singlet range of the $n-n$ interaction. The parameters for the $n-n$ interaction are obtained by assuming that this interaction is the same as the nuclear part of the $p-p$ interaction. The phase shift, δ, is obtained from

$$K\cot\delta=-\alpha+\tfrac{1}{2}Kr_0^2,$$

where r_0 is the effective range of the singlet interaction, and α is the reciprocal scattering length. These approximations are valid throughout the range of energies available for the mesic absorption process. For radiative absorption the approximation breaks down for nucleon energies much over 10 Mev, but this is already well beyond the peak in the gamma-ray spectrum. At these energies the distortion of the P state wave function may be neglected.

The integrals have been evaluated using a meson mass of $277m_e$, a deuteron binding energy of 2.24 Mev, and a neutron-proton mass difference [13] of 1.31 Mev. For the triplet interaction an effective range of $1.60\cdot10^{-13}$ cm was used, while for the singlet interaction $r_0=2.43\cdot10^{-13}$ cm, $\alpha=-0.421\cdot10^{12}$ cm^{-1}, and $\eta=12.8\cdot10^{12}$ cm^{-1}. In Table I are listed the transition probabilities for neutron absorption, and the integrated radiative absorption probabilities. The energy spectrum of the gamma-rays from the absorption of pseudoscalar mesons is shown in Fig. 1. The shapes of the spectra arising from scalar and pseudovector mesons are almost indistinguishable from this, because k is essentially constant over the width of the maximum. The singlet probabilities were also calculated using undistorted wave functions for the final state. The effect of ignoring the neutron-neutron interaction is to increase the half-width of the maximum from something less than 2 Mev to about 12 Mev, but the integrated transition probabilities are relatively unaffected.

TABLE I. Transition probabilities for neutron and radiative absorption in units of $\frac{1}{4}(g^2/\hbar c)N^2(\hbar/\mu c)^3c|\varphi(0)|^2=0.91\cdot10^{16}$ sec^{-1}.

Meson theory	$S(S)$	$PS(PS)$	$PS(PV)$	$V(V)$	$PV(PV)$
Neutron absorption	0	$2.7\cdot10^{-4}$	0.25	0.12	$2.5(J=0)$ $0\ (J=1)$ $0.15(J=2)$
Radiative	0.012	$6.6\cdot10^{-4}$	0.12	$2.2\cdot10^{-4}$	$2.10\cdot10^{-4}(J=1)$ $2.4\cdot10^{-4}(J=0,2)$
Ratio	0	4.1	2.1	55	2

The probabilities for mesic absorption are given in Table II. The integrals were evaluated for $(\pi^- - \pi^0)$ mass differences of 4.25 and 4.75 Mev.[1,14] These numbers were all obtained using the distorted wave function for the S wave. The effect of ignoring the $n-n$ interaction is to decrease the transition probability by a factor of 5 to 20.

These results indicate that the relative probabilities for the three absorption mechanisms depend strongly upon the assumed spin and parity of the charged meson.

(A) Scalar Mesons

Here, all absorption leads to either gamma-rays or neutral mesons. If the π^0 is also scalar, no neutral mesons should be found, but the assumption of a pseudoscalar neutral meson leads to a probability for

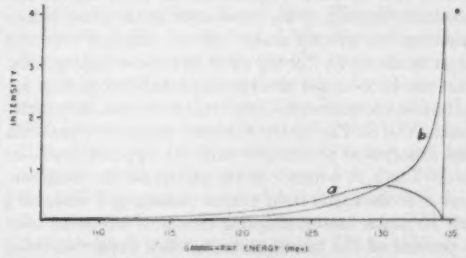

FIG. 1. Energy distribution of gamma-rays from the absorption of pseudoscalar mesons in deuterium. (a) Calculated using plane waves for final neutrons. (b) Calculated using distorted wave for S part of neutron wave function.

[12] J. M. Blatt and J. D. Jackson, Phys. Rev. 76, 18 (1949); H. A. Bethe and C. Longmire, Phys. Rev. 77, 647 (1950). Where possible, the notation of these papers is used here.

[13] R. Bell and L. Elliot, Phys. Rev. 74, 1552 (1948).

[14] W. Panofsky, private communication. According to the newest data, the $(\pi^- - \pi^0)$ mass difference is closer to 6 Mev. This will have the effect of increasing the probabilities for mesic absorption by about a factor of 2 compared to those given for a mass difference of 4.75 Mev. None of the qualitative features of the results are changed however.

TABLE II. Transition probabilities for mesic absorption for various meson theories in units of $g^2/\hbar c \cdot 0.91 \cdot 10^{16}$ sec^{-1}. $\Delta\mu$ is the $(\pi^- - \pi^0)$ mass difference. In the last column are given the appropriate π^0 coupling constants and their values as determined from the absorption of mesons in hydrogen (reference 2). The notation here is the same as in ref. 2; $\Delta g = g_n - g_p$, $\bar{g} = g_n + g_p$. The actual probability is the product of column 3 or 4 with column 5.

π^-	π^0	$W(\Delta\mu=4.25$ Mev)	$W(\Delta\mu=4.75$ Mev)	Coupling constant
$S(S)$	$S(S)$	$1.0 \cdot 10^{-6}$	$6.8 \cdot 10^{-6}$	$(\Delta g)^2 = 0.008$
$PS(PS)$	$PS(PS)$	$0.59 \cdot 10^{-7}$	$3.9 \cdot 10^{-7}$	$(\bar{g})^2 = 0.06$
$PS(PV)$	$PS(PV)$	$0.59 \cdot 10^{-7}$	$3.9 \cdot 10^{-7}$	$(\bar{g})^2 = 11$
$PS(PS)$	$PS(PV)$	$0.59 \cdot 10^{-7}$	$3.9 \cdot 10^{-7}$	$(\Delta g)^2 = 0.06$
$PS(PV)$	$PS(PS)$	$0.59 \cdot 10^{-7}$	$3.9 \cdot 10^{-7}$	$(\Delta g)^2 = 11$
$S(S)$	$PS(PS)$	$1.1 \cdot 10^{-6}$	$3.9 \cdot 10^{-6}$	$(\Delta g)^2 = 27$
$S(S)$	$PS(PV)$	$1.9 \cdot 10^{-6}$	$6.8 \cdot 10^{-6}$	$(\Delta g)^2 = 0.15$
$PS(PS)$	$S(S)$	$0.62 \cdot 10^{-7}$	$2.2 \cdot 10^{-7}$	$(\Delta g)^2 = 210$
$PS(PV)$	$S(S)$	$1.1 \cdot 10^{-6}$	$3.9 \cdot 10^{-6}$	$(2g_p)^2 = 210$
$V(V)$	$S(S)$	$1.8 \cdot 10^{-6}$	$6.9 \cdot 10^{-6}$	$(\Delta g)^2 = 52$[a]
$V(V)$	$PS(PS)$	$2.0 \cdot 10^{-3}$	$3.6 \cdot 10^{-3}$	$(\Delta g)^2 = 0.93$
$V(V)$	$PS(PV)$	$2.0 \cdot 10^{-3}$	$3.6 \cdot 10^{-3}$	$(\bar{g})^2 = 0.93$
$PV(PV)$	$S(S)$	0.35	0.64	$(\Delta g)^2 = 0.005$
$PV(PV)$	$PS(PS)$	$0.73 \cdot 10^{-6}$	$2.6 \cdot 10^{-6}$	$(\bar{g})^2 = 26$[b]
$PV(PV)$	$PS(PV)$	$1.3 \cdot 10^{-3}$	$4.5 \cdot 10^{-3}$	$(\bar{g})^2 = 0.15$[b]

[a] This assumes a symmetric theory. A neutral theory applied to the hydrogen experiment gives the same π^0 coupling constant but in deuterium gives a zero transition probability in this approximation.
[b] Here, a neutral theory is assumed. A symmetric theory for the hydrogen experiment gives coupling constants half as large but gives zero for the deuteron absorption.

mesic absorption of about 10 percent. There are two effects which tend to invalidate the selection rule against neutron absorption of scalar mesons. The first is the possibility of absorption from states of higher angular momentum, especially from the $2P$ state. The absorption probability from the $2P$ state has been calculated and is $(g^2/\hbar c)1.71 \cdot 10^{10}$ sec^{-1}. This is to be compared with the probability of radiative transitions to the $1S$ state. The probability for the $2P-1S$ transition is given by [15]

$$W_{2P-1S} = c(\mu c/\hbar)(e^2/\hbar c)^5(\tfrac{2}{3})^8$$

and is $1.75 \cdot 10^{11}$ sec^{-1}. Therefore, in order for an appreciable fraction of the mesons to be absorbed before reaching the ground state, the π^- coupling constant must be about 10. For higher P states it is easy to show that the ratio of the absorption probability to that for radiative transitions to lower states is essentially independent of n. For states of higher angular momentum the absorption probability falls off approximately as $1/(2l)!\,(r/a_0)^2$, where r is the radius of the deuteron, and a_0 is the mesic Bohr radius. Assuming a value of $\frac{1}{4}$ for the scalar meson coupling constant, not more than 4 percent of the mesons are absorbed before reaching either the $1S$ or the $2S$ state.

The other effect tending to invalidate the selection rule is the presence of relativistic terms in a correct field theoretic calculation. The relativistic matrix element for the third-order process is easily calculated, and again turns out to be identically zero. (This result was first obtained by A. S. Wightman.) We can conclude, therefore, that if the charged meson is scalar, the vast majority of absorptions would lead to gamma-ray emission, with about 10 percent neutral mesons if the π^0 is pseudoscalar.

[15] H. A. Bethe, *Handbuch der Physik*, Vol. 24/1, p. 440.

(B) Pseudoscalar Mesons

In this case the neutron and radiative processes compete. The $PS(PS)$ case gives a ratio of neutron to radiative absorption of 4.1 to 1, or 20 percent gamma-emission, while the $PS(PV)$ theory gives a ratio 2.1 to 1, or 32 percent gamma-emission. If the equivalence theorem were valid, both would give a ratio of 2.1 to 1. The assumption of a pseudoscalar neutral meson gives no observable number of mesic absorptions. However, the probability of emission of a scalar π^0 is about 10 percent of the radiative.

The neutron absorption probability in the $PS(PV)$ case was also calculated using a square well for the $n-p$ interaction. This leads to a neutron radiative ratio of 1.4 to 1 or a probability for gamma-emission of 42 percent. (The probability for radiative absorption is quite insensitive to the shape of the potential.) If the charged meson is pseudoscalar, we would, therefore, expect to observe a high energy gamma-ray in 20 to 40 percent of the events. A pseudoscalar neutral meson would not be observed, but a scalar meson should be detectable

(C) Vector Mesons

The absorption of a vector meson should lead to no observable number of either gamma-rays or neutral mesons.

(D) Pseudovector Mesons

Here, the crucial effect is not the relative rates of the neutron and radiative absorptions but the relative populations of the states $J=0, 1, 2$. If one assumes them to be populated according to their statistical weights, the ratio of neutron to radiative absorption is 2 to 1. Strictly speaking, however, the populations of these states depend on the previous history of the meson during its cascade to the ground state. To see how much difference this makes, one can assume that in some higher energy level the degenerate states are populated according to their statistical weights (this should be true for very high levels) and then trace the meson down to the ground state (or $2S$ state). This was done for several initial energy levels, and in no case was a significant deviation from the statistical distribution found.

Radiative absorption can, indeed, take place from the states $J=0$ and 2, but this matrix element brings down additional powers of the nucleon momentum and, therefore, leads to a smaller transition probability than for $J=1$. The absorption probability for $J=2$ was calculated by numerical integration using the D state wave function given by Rarita and Schwinger.[9] While

the result is admittedly very approximate, it does show that from the state $J=2$ the predominant process is neutron absorption.

The number given for the mesic absorption probability also represents absorption from the $J=0$ state and is much smaller than the neutron probability. For states of higher J, additional powers of the meson and nucleon momenta appear which make the probability for mesic absorption extremely small. We may, therefore, say that no neutral mesons should be observed, regardless of their parity.

IV. CONCLUSIONS

Preliminary results of the experiment of Panofsky, Aamodt, and Hadley on the absorption of π^- mesons in deuterium[14] indicate a gamma-ray spectrum with a large peak in the neighborhood of 130 Mev, while there is no detectable peak in the spectrum at 70 Mev where the decay quanta from the neutral meson would appear. They estimate that of the total number of absorption events, about $\frac{1}{3}$ actually give rise to gamma-rays. These results are inconsistent with the assumption of either a scalar or vector character for the charged meson but do fit with both the pseudoscalar and pseudovector theories. If the charged meson is assumed to be pseudoscalar, the absence of neutral mesons indicates that they too are pseudoscalar. If, on the other hand, the charged meson is assumed to be pseudovector, nothing can be said about the parity of the neutral meson field.

The author wishes to express his appreciation to Professor R. E. Marshak for having suggested this problem and for his guidance throughout the course of the work. He also wishes to thank Dr. A. S. Wightman for a number of helpful conversations and Professor W. Panofsky for having communicated his new results on the absorption in hydrogen and deuterium.

Note added in proof:—Owing to failure to correct for the $n-p$ mass difference, all energies in Fig. 1 are too high by 1.3 Mev.

PHYSICAL REVIEW VOLUME 82, NUMBER 1 APRIL 1, 1951

Energy Levels of B^{10}

FAY AJZENBERG
University of Wisconsin, Madison, Wisconsin*
(Received December 14, 1950)

The neutron spectrum at 0° and at 80° from the $Be^9(d,n)B^{10}$ reaction has been investigated by means of nuclear emulsions. Energy levels of B^{10} at 0.77, 1.79, 2.22, 3.59, 4.79, 5.12, 5.91, 6.11, 6.57, and 6.81 Mev have been observed as have possible levels at 5.58, 5.68, and 6.38 Mev. There is evidence for multiplicities at 5.12 and, possibly, at 6.11 Mev. No neutron groups were observed which would correspond to levels at 1.4 and 2.85 Mev. This result is in disagreement with the picture of equally spaced levels in B^{10}. An attempt is made to explain the results that led to this picture.

I. INTRODUCTION

IN the past few years, much attention has been devoted to the energy levels of B^{10}. The low-lying levels with excitation energies (E_x) of less than 6 Mev have been investigated by means of the reactions $Be^9(d,n)B^{10}$ and $Li^7(\alpha,n)B^{10}$, while the high energy levels ($E_x \geq 6.5$ Mev) have been studied by bombarding Be^9 with protons. Studies of the neutron spectrum by observation of proton recoils in Wilson cloud chambers[1,2] or in nuclear emulsions[3,4] have indicated the presence of levels at approximately 0.7, 2.2, 3.5, and 5.1 Mev above the ground state of B^{10}. Haxel and Stuhlinger[5] have detected neutrons from the $Li^7(\alpha,n)B^{10}$ reaction by means of a boron counter. This work indicated levels at approximately 0.8, 1.3, and 2.1 Mev. Bonner *et al.*,[6] using the method of neutron thresholds to study the neutrons from the $Be^9(d,n)B^{10}$ reaction, have investigated the range from 5 to 6 Mev. They have located levels[7] at 5.098, 5.156, and 5.920 Mev. Rasmussen, Hornyak, Lauritsen, and Chao[8,9] have studied the gamma-rays from the same reaction by means of a magnetic lens spectrometer. They have attributed to B^{10*} gamma-rays of energies 413.5, 716.6, 1022, 1433, 2151, 2871, 3604, 3970, 4470, and 5200 kev, and have assigned corresponding levels to all but the 3970 and the 4470-kev gamma-rays which they assumed to be due to cascade transitions. Rasmussen *et al.*[8,10] state that the levels corresponding to the 716.6, 1433, 2151, 2871, and 3604-kev gamma-rays appear to constitute an equally spaced set of levels leading to the picture of a harmonic oscillator.

* Work supported by the AEC and the Wisconsin Alumni Research Foundation.

[1] T. W. Bonner and W. M. Brubaker, Phys. Rev. **50**, 308 (1936).
[2] H. Staub and W. E. Stephens, Phys. Rev. **55**, 131 (1939).
[3] C. F. Powell, Proc. Roy. Soc. (London) **A181**, 344 (1942).
[4] W. D. Whitehead and C. E. Mandeville, Phys. Rev. **77**, 732 (1950).
[5] O. Haxel and E. Stuhlinger, Z. Physik **114**, 178 (1939).
[6] Bonner, Butler, and Risser, Phys. Rev. **79**, 240 (1950).
[7] T. W. Bonner, private communication.
[8] Rasmussen, Hornyak, and Lauritsen, Phys. Rev. **76**, 581 (1949).
[9] Chao, Lauritsen, and Rasmussen, Phys. Rev. **76**, 582 (1949).
[10] Hornyak, Lauritsen, Morrison, and Fowler, Revs. Modern Phys. **22**, 291 (1950).

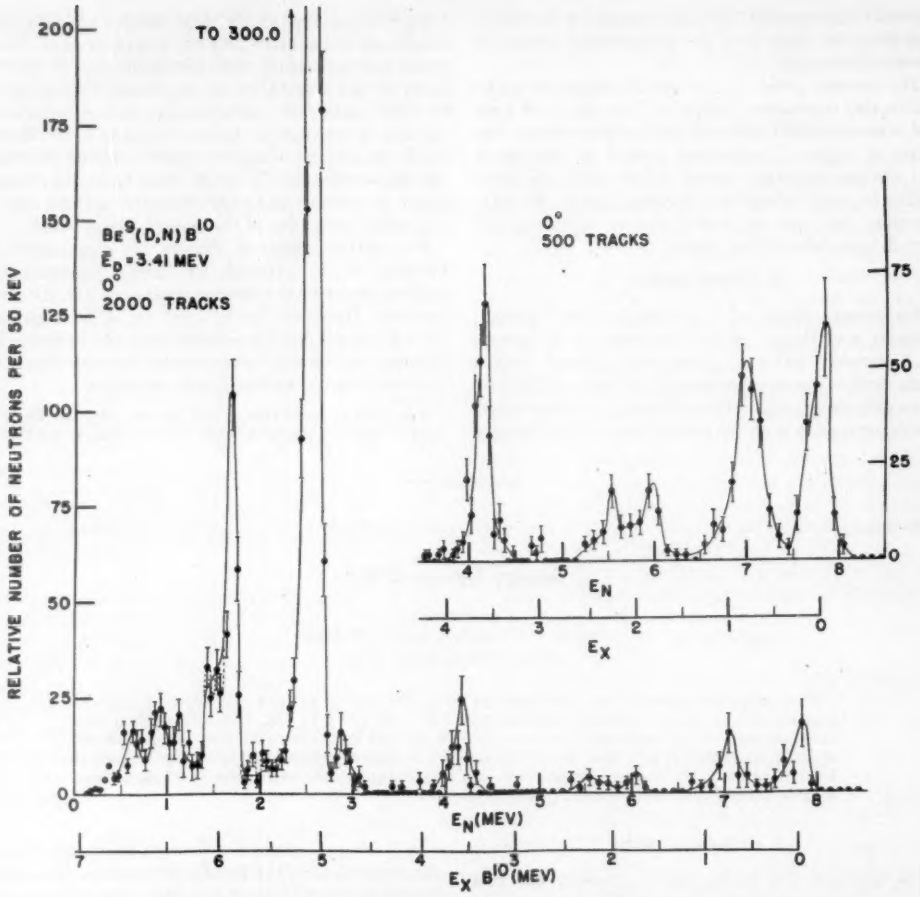

FIG. 1. Relative number of neutrons per 50-kev interval *versus* neutron energy at 0°.

The purpose of this experiment was twofold: (1) to cover, continuously, the energy region from 0 to 7 Mev above the ground state of B^{10} by bombarding beryllium with higher energy deuterons that have been used previously, and, (2) to ascertain whether the assignment of levels to the reported gammas was consistent by obtaining a better resolution for the neutron groups than in previous recoil measurements.

II. EXPERIMENTAL PROCEDURE

A 50-kev thick[10a] foil of beryllium mounted on a tantalum backing was bombarded by 3.436-Mev deuterons from the Wisconsin electrostatic generator. The resultant neutron spectrum was observed by means of 200μ Eastman NTA nuclear emulsions mounted 10 cm from the target and at angles of 0° and 80° to the direction of the beam. In addition, background plates were exposed to deuterons hitting bare tantalum. The criteria for the measurements of the recoil proton tracks have been discussed previously.[11] The neutron energies are calculated from the energies of the proton recoils and from the angles which these recoils make with the incident neutrons. The range-energy relation used in this experiment was found as follows: from previous work,[11,12] the range-energy relation was known for low energy proton tracks ($E_p \leq 2.5$ Mev). The value (7.76 Mev) for the average neutron energy ($\bar{E}_n$) corresponding to the ground state of B^{10} was calculated

[10a] For deuterons of 3.4-Mev energy.

[11] Johnson, Laubenstein, and Richards, Phys. Rev. **77**, 413 (1950).

[12] Johnson, Ajzenberg, and Laubenstein, Phys. Rev. **79**, 187 (1950).

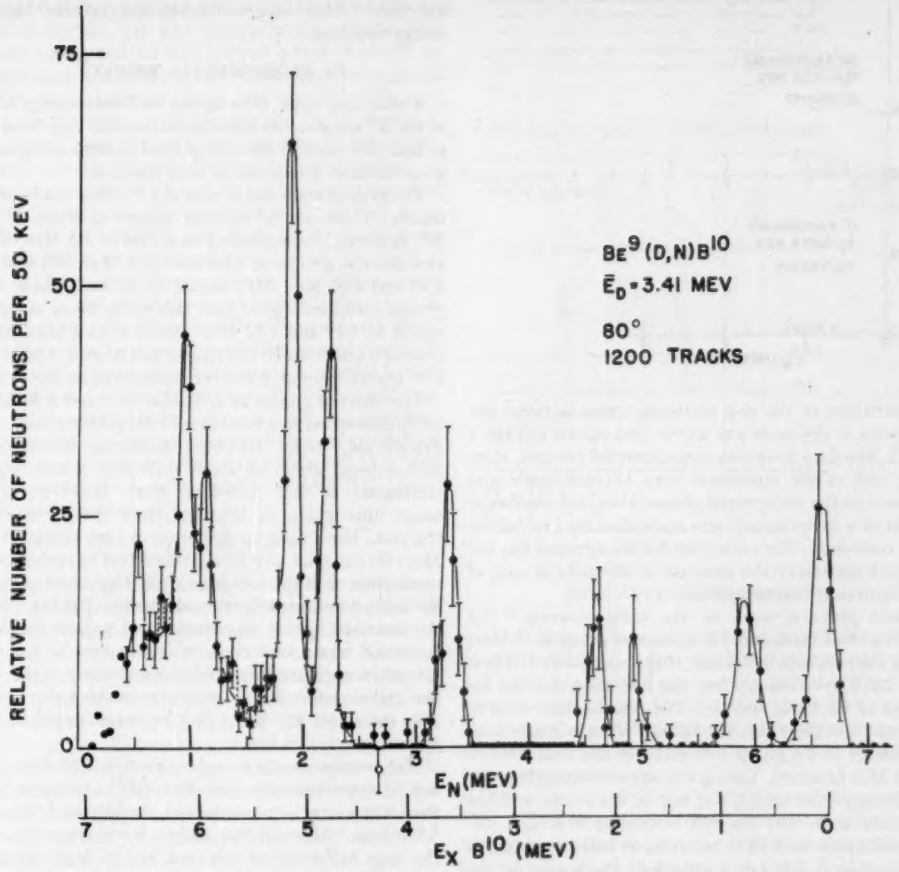

FIG. 2. Relative number of neutrons per 50-kev interval *versus* neutron energy at 80°.

using[12] $Q=4.35$ Mev. A mean value (390 microns) of the ranges of the ground-state tracks which were observed was assumed to correspond to this value of $\bar{E}_n$. The low energy range-energy curve was then extrapolated to this point with a shape similar to that of the Lattès curve.[14] At high energies, this curve is approximately 4.5 percent higher (i.e., 4.5 percent lower energy for a given range) than the Lattès curve for Ilford emulsions. The agreement between the values of $\bar{E}_n$ for groups at 0° and 80° is quite good. $\Delta(\bar{E}_n)$ is ≤ 40 kev, and the average $\Delta(\bar{E}_n)$ for all levels is approximately 20 kev. Taking into account the differences between our values and the more accurate gamma-ray values observed by Rasmussen *et al.*[8] and the uncertainty in the range-energy curve, it is felt that the value of E_n for levels below 3 Mev is known to better than ± 100 kev and to better than ± 50 kev for the levels of higher energy.

Two thousand tracks have been measured on the 0° plates and 1200 on the 80° plates. In order to improve the statistics for high energy neutrons at 0°, an additional 382 tracks, due to neutrons of energy greater than 3.5 Mev, have been measured. The data, corrected for variation of neutron-proton scattering cross section,[15] geometry,[16] and background, is shown as Fig. 1 for 0° (the inset shows the high energy data, including the 382 additional long tracks which were measured), and Fig. 2 for 80°.

Figure 3 shows the distribution of the background tracks at 0° and at 80°. The data have been corrected

[12] Tollestrup, Fowler, and Lauritsen, Phys. Rev. **78**, 372 (1950).
[14] Lattès, Fowler, and Cuer, Proc. Phys. Soc. (London) **59**, 883 (1947).
[15] R. K. Adair, Revs. Modern Phys. **22**, 249 (1950).
[16] H. T. Richards, Phys. Rev. **59**, 796 (1941).

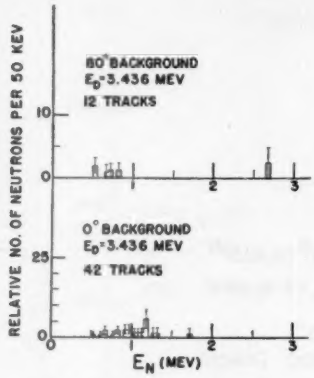

FIG. 3. Background at 0° and at 80°.

for variation of the n–p scattering cross sections and geometry in the same way as the data shown in Figs. 1 and 2. The data have also been corrected for area, since only half of the equivalent area at each angle was scanned on the background plates. Thus, the number of tracks of a given energy was multiplied by two for the area correction. The correction for background has not affected materially the location or intensity of any of the significant neutron groups.

From previous work by the same observer,[12] the width at half-maximum for a neutron group at 2 Mev, using the emulsion technique, is approximately 100 kev. It is not known exactly how the resolution changes for higher or for lower energies. The present data seem to indicate that the width at half-maximum increases with the energy of the group, but that it is less than 300-kev for 8-Mev neutrons. Taking into account straggling, the thickness of the target, the size of the source and the scanning area, and multiple scattering effects, a calculated width for 8-Mev neutrons, at half-maximum, of approximately 200 kev is obtained. The reason for the larger observed width is not understood. The data has been plotted in 50-kev intervals for neutrons of energies less than 5 Mev, and in 100-kev intervals for higher energy neutrons.

TABLE I. Intensities of the neutron groups at 0° and at 80° (lab) in the center-of-mass system.

Level at:	Relative intensity at 0°	Relative intensity at $\phi°$	$\phi°$	Ratio $0°/\phi°$
0	15	10	85.5	1.5
0.77	14	7	85.6	2.0
1.79	3	2	85.7	1.5
2.22	5	4	86.0	1.2
3.59	14	8	87.2	1.7
4.79	10	12	89.1	0.8
5.12	195	19	90.0	10.0
5.58	4	1	91.2	4.0
5.68	4	3	91.5	1.4
5.91	37	7	92.5	5.3
6.11	20	13	94.0	1.5
6.38	11	4	96.8	2.8
6.57	12	6	99.1	2.0
6.81	8			

III. EXPERIMENTAL RESULTS

A secondary scale, showing the excitation energy (E_x) of the B^{10} nucleus, has been drawn on both Figs. 1 and 2 so that the value of the energy level corresponding to a given neutron group can be seen directly.

The ground state and a level at 0.77 Mev can be seen clearly. There are no neutron groups at either 0° or 80°, however, corresponding to a level at 1.4 Mev. The two neutron groups at 6.00 and 5.55 Mev (0°) and at 4.95 and 4.60 Mev (80°) should be noticed. These two groups correspond to at least two levels whose energies would be 1.79 and 2.22 Mev. No neutron groups were observed which would correspond to a level at 2.85 Mev. The known level at 3.59 Mev is observed again.

The neutron groups at 2.90 Mev (0°) and 2.20 Mev (80°) correspond to a level at 4.79 Mev. Whitehead and Mandeville,[4] using 1.15-Mev deuterons, observed a proton recoil group at about 0.70 Mev which might correspond to this 4.79-Mev level. However, they assign this group to neutrons from the $C^{12}(d,n)N^{13}$ reaction. Their data for deuterons of high energy (1.62 Mev) do not show any groups due either to carbon contamination or to the 4.79-Mev level. The target used by Whitehead and Mandeville was thicker (100 kev) than the one used in this experiment, and apparently their resolution was poorer. Bonner[7] states that he has not yet taken accurate threshold measurements below 730 kev and therefore has no evidence on this point at all. The threshold for the 4.79-Mev level would be at approximately 525 kev.

The neutron group at approximately 2.55 Mev (0°) and at approximately 1.88 Mev (80°) corresponds to the known, but here unresolved, doublet at 5.098 and 5.156 Mev.[7] Although the doublet is not resolved at 0°, the large half-width of this peak and its high intensity may indicate the presence of several closely spaced levels. It is interesting to note that the half-width of the corresponding peak at 80° is smaller by a factor of two. It should also be noticed that this neutron group is very definitely bunched forward in the center of mass system (Table I).

If the groups at $\bar{E}_n$=2.05 Mev and 1.92 Mev (0°) and $\bar{E}_n$=1.47 and 1.37 Mev (80°) are real, levels at 5.58 and 5.68 Mev are indicated. The neutron groups at 1.68 Mev (0°) and 1.12 Mev (80°) correspond to a level at 5.91 Mev which has been observed, independently, by Bonner, though he finds no evidence for levels at 5.58 and 5.68 Mev.[7] The groups with $\bar{E}_n$=1.48 Mev (0°) and 0.94 Mev (80°) correspond to a level with $\bar{E}_x$=6.11 Mev. The width at half-maximum, larger than expected for a single level, may indicate a doublet.

Other high energy levels undoubtedly exist, but the interpretation of the data is not clearcut owing to poorer statistics. The following is a tentative interpretation of the data obtained at both 0° and 80°: (1) A possible

level at 6.38-Mev excitation. (2) A probable level at 6.57-Mev excitation. (3) The known level[17] at 6.81 Mev would correspond to the neutron group observed at approximately 0.62 Mev at 0°. The corresponding group at 80° would have an energy less than 0.5 Mev and, therefore, could not be observed reliably by this method.

Table I shows the relative intensities in the center-of-mass system of the neutron groups observed at laboratory angles of 0° and 80°. The same table also shows the ratio of the intensities at 0° to that at ϕ, where ϕ is the center-of-mass angle for the given group corresponding to the laboratory angle of 80°. Only a few of the neutron groups show a large difference in intensity at the two observation angles in the center of mass system. The data for 80° will correspond qualitatively to the total cross section because of the small anisotropy and the large solid-angle weighting factor.

No neutron groups were observed which would correspond to ground-state neutrons from the reactions (1) $H^2(d,n)He^3$ (these neutrons would appear at 6.6 Mev at 0° and at 3.7 Mev at 80°), (2) $C^{12}(d,n)N^{13}$ (3.1 Mev —0°—and 2.5 Mev—80°), and (3) $O^{16}(d,n)F^{17}$ (1.7 Mev —0°—and 1.4 Mev—80°).

IV. DISCUSSION

Because a high bombarding energy was used, deuterons of high angular momentum would be effective in forming states of a wide range of angular momenta and of either parity in the compound nucleus. Since the excitation of the compound nucleus is approximately 19 Mev, one expects a large density of overlapping levels in that nucleus. Hence, it is difficult to see why there should not be neutron groups corresponding to all existing levels of B^{10}. The fact that no neutron groups were observed which would correspond to levels at 1.4 and 2.85 Mev appears, therefore, to be strong evidence that the picture of equally-spaced levels in B^{10} is incorrect.

Still, it is necessary to account, in some way, for the gamma-rays observed by Rasmussen, Hornyak, Lauritsen, and Chao. Figure 4 shows a possible level scheme which is consistent with our neutron data and

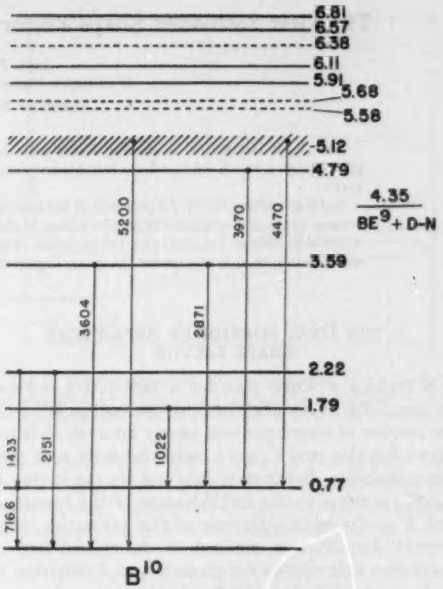

FIG. 4. Energy level diagram of B^{10}.

with all gamma-rays observed by Rasmussen *et al.*, except possibly for the 413.5-kev gamma-ray. The 413.5-kev gamma-ray may result from the transition between the 2.22- and the 1.79-Mev levels. However, it is somewhat surprising that this gamma-ray competes successfully in intensity with the 1433- and the 2151-kev gamma-rays.

One of the results of the transitions suggested in Fig. 4 is that the 716.6-kev gamma-ray should be relatively very intense, since several of the other gamma-rays are explained as cascades to the 0.77-Mev level. This appears to be the case.[18]

The author is extremely grateful to V. R. Johnson for his assistance in the exposure of the plates, and to Professor H. T. Richards, who suggested this problem and whose criticisms and suggestions throughout all stages of this work were invaluable.

[17] Thomas, Rubin, Fowler, and Lauritsen, Phys. Rev. 75, 1612 (1949).

The First Forbidden Shape Factor and the $f_n t$ Products for Beta-Decay*

JACK P. DAVIDSON, JR.
Washington University, St. Louis, Missouri
(Received November 6, 1950)

The shape factor used in making Kurie plots for first forbidden beta-decay transitions with maximum spin change is expressed in a form suitable for computation. Graphs of the function for various Z and W are given.

Approximations for the $f_n t$ products of beta-decay are derived enabling one to compute these products for certain types of transitions from the values of the allowed f_0 function. Finally, these results are used to compile a table of 1st, 2nd, and 3rd forbidden transitions exhibiting the unique spectral shapes associated with maximum spin change for the given degree of forbiddenness.

I. THE FIRST FORBIDDEN BETA-DECAY SHAPE FACTOR

IN making a Kurie plot for a beta-active isotope, one plots $(N/C_{nX}F_0)^{\frac{1}{2}}$ against the energy W. N is the number of counts per unit energy interval, F_0 is the Fermi function, and C_{nX} is a correction term such that the probability distribution function for the energy is $C_{nX}F_0$; n refers to the forbiddenness of the transition and X to the relativistic form of the interaction.[1] The present discussion is confined to the special case of maximum spin change for given n and X referring to tensor or axial vector coupling.

Many critical experiments have shown that C_{nX} must indeed be appropriate to the degree of forbiddenness under consideration in order that the Kurie plot may have the desired constant-slope form. For $n=1([\Delta I]_{\max}=\pm 2$, yes), the correction term C_{1T} has the asymptotic form

$$C_{1T}=[(W_0-W)^2+(W^2-1)]/12, \tag{1}$$

which is valid only[2] for $\alpha Z \ll 1$. In many applications this condition does not hold, and in some calculations made for Osoba,[3] a better fit was obtained by using the accurate form

$$C_{1T}=[(1+S_0)/24][(W_0-W)^2+A(W^2-1)]. \tag{2}$$

The exact expression for A is[2]

$$A=\frac{S_1+2}{2S_0+2}\left(\frac{12\Gamma(2S_0+1)}{\Gamma(2S_1+1)}\right)^2 \times(2p\rho)^{2(S_1-S_0-1)}\left|\frac{\Gamma(S_1+iy)}{\Gamma(S_0+iy)}\right|^2, \tag{3}$$

in which $y=\alpha ZW/p$, $p=(W^2-1)^{\frac{1}{2}}$, $S_0=(1-\alpha^2Z^2)^{\frac{1}{2}}$, $S_1=(4-\alpha^2Z^2)^{\frac{1}{2}}$, and ρ is the nuclear radius.[4] By making use of the natural logarithm of the complex gamma-function and the logarithmic derivative,[5] one obtains from Eq. (3) the following expression which is suitable for computational purposes:

$$A=\frac{S_1+2}{2S_0+2}\left[\frac{12\Gamma(2S_0+1)}{\Gamma(2S_1+1)}\right]^2(2p\rho)^{\alpha^2Z^2/2}\left|1-\tfrac{1}{4}\alpha^2Z^2+iy\right|^2 \times\left[1-\tfrac{1}{2}\alpha^2Z^2C+\tfrac{1}{2}\alpha^2Z^2y^2\sum_{n=1}^{\infty}\frac{1}{n(n^2+y^2)}\right], \tag{4}$$

where C is the gauss number. This expression is identical with that used by Osoba[3] through terms in α^2Z^2. Figure 1 shows A plotted against W for $Z=0$, 30, 60, and 90, while in Fig. 2 A is plotted for the same values of A but for small W. Certain points should be noted. Firstly, one has

$$\lim_{Z\to 0}A(W,Z)=1 \text{ for all } W. \tag{5}$$

Secondly, one can replace the gamma-functions in Eq. (3) through Stirling's formula and can compute the limit of the A function as W approaches unity. In this manner it can be shown that as W approaches unity (y increases without limit), A behaves asymptotically as y^2. Finally, as W becomes unboundedly large, A again increases but only as $W^{\alpha^2Z^2}$. These characteristics are seen in the graphs of the A function. Similar curves are given by Laslett and his co-workers.[6] It is important to note that for any Z not zero, $A\gg 1$ will hold for sufficiently small energies.

Finally, as a check, the A function was computed at $Z=90$ keeping all terms through α^4Z^4. If A_2 be the approximation containing terms through α^2Z^2, and A_4 the approximation containing terms through α^4Z^4, it was found that

$$\begin{aligned} A_4/A_2&=0.94 \quad 1.2\lesssim W\lesssim 2.0,\\ A_4/A_2&=0.99 \quad W\gtrsim 6.0. \end{aligned} \tag{6}$$

The accuracy of the first approximation, A_2, is sufficient for almost all applications. For $Z<90$, it is, of course, even more accurate than is indicated by Eq. (6).

* Part of a thesis submitted in partial fulfillment of the requirements for the degree of Master of Arts in Physics in the Graduate School of Washington University.

[1] This notation is used by E. Greuling, Phys Rev. **61**, 568 (1942).

[2] E. J. Konopinski and G. E. Uhlenbeck, Phys. Rev. **60**, 308 (1941).

[3] J. S. Osoba, Phys. Rev. **76**, 345 (1949).

[4] The units used in this article are the usual dimensionless ones; i.e., energy is in units of mc^2, lengths in units of $\hbar/mc$, etc.

[5] Jahnke and Emde, *Tables of Functions* (B. G. Teubner, Leipzig, 1938).

[6] Laslett, Jensen, and Paskin, Phys. Rev. **79**, 412 (1950).

II. THE f_0t PRODUCTS

(A) The Averaging Approximation

If one defines the function f_0 for a beta-transition as

$$f_0=\int_1^{W_0} C_0F_0(W,Z)pW(W_0-W)^2dW, \qquad (7)$$

then the product of f_0 by the half-life of the transition is relatively constant for allowed transitions (both favored and unfavored). However, one does not expect the same constancy for forbidden transitions because the term C_0 in Eq. (7) must be replaced by C_{nX}, which is appropriate to the transition under consideration. The generalization of the f_0-function to any transition is immediate:

$$f_{nX}=\int_1^{W_0} C_{nX}F_0(W,Z)pW(W_0-W)^2dW. \qquad (8)$$

However, the complexity of the correction terms C_{nX} makes most calculations out of the question (the general expression for the C_{nX} is given by Greuling[1]).

A very great simplification is obtained if one considers those interaction types which permit the greatest ΔI for a given degree of forbiddenness n. One then notes that for all n the tensor and axial vector interactions allow $(\Delta I)_{\max}=\pm(n+1)$, which is greater by one unit than for any of the other three interactions. For these two cases all of the nuclear matrix elements but one vanish, and this forms a symmetrical tensor with zero spur. The correction term is of the form

$$C_{nT\text{ or }A}=|Q_{n+1}(\sigma,\mathbf{r})/(n+1)!|^2\sum_{\nu=0}^{n}(B_{n\nu}K^{2(n-\nu)}L_\nu), \qquad (9)$$

with

$$B_{n\nu}=\frac{2^{n-2\nu}(2\nu+1)!}{(2n-2\nu+1)!(\nu!)^2},\quad K=W_0-W$$
$$L_\nu=(F_\nu/F_0)\left(\frac{2^\nu(\nu!)}{(2\nu+1)!}p^\nu\right)^2\frac{\nu+1+S_\nu}{2\nu+2}, \qquad (10)$$

with $Q_{n+1}(\sigma,\mathbf{r})$ a tensor of rank $(n+1)$, symmetric in all indices and having zero spur. For $Z\to0$, $S_\nu\to\nu+1$, and $(F_\nu/F_0)\to1$, then

$$\lim_{Z\to0}L_\nu=\left(\frac{2^\nu(\nu!)}{(2\nu+1)!}p^\nu\right)^2. \qquad (11)$$

Thus, for $n=1$, 2, 3 and $Z=0$, one has

$$12C_{1T,A}=(W_0-W)^2+(W^2-1),$$
$$5\cdot6^3C_{2T,A}=(W_0-W)^4+(10/3)(W_0-W)^2(W^2-1)+(W^2-1)^2,$$

and (12)

$$70\cdot72^2C_{3T,A}=(W_0-W)^6+7(W_0-W)^4(W^2-1)+7(W_0-W)^2(W^2-1)^2+(W^2-1)^3.$$

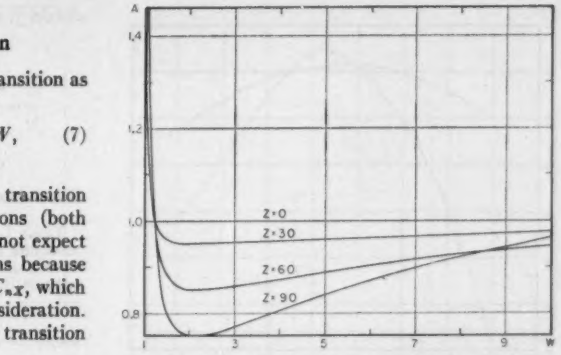

FIG. 1. The function $A(W,Z)$ plotted against W for $Z=0$, 30, 60, and 90. $C_{1T}=[(1+S_0)/24][(W_0-W)^2+A(W,Z)(W^2-1)]$ is the beta-decay shape factor for unique first forbidden transitions.

The function $\mathfrak{F}(W)=(W-1)(W_0-W)$ looks very much like the energy distribution function for beta-decay and has been used[7] to compute an approximate formula for f_1. Replacing F_0 by $\mathfrak{F}$ in the general expressions

$$f_n=\int_1^{W_0} C_nF_0(W,Z)pW(W_0-W)^2dW$$
$$=\bar{C}_n\int_1^{W_0}F_0(W,Z)pW(W_0-W)^2dW=\bar{C}_nf_0, \qquad (13)$$

one obtains simple approximate formulas for $\bar{C}_n$. The

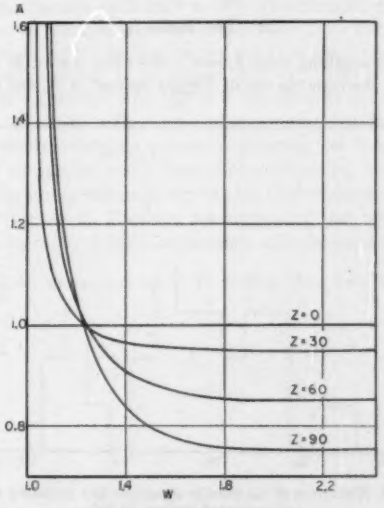

FIG. 2. The function $A(W,Z)$ for low values of W.

[7] F. B. Shull and E. Feenberg, Phys. Rev. 75, 1768 (1949).

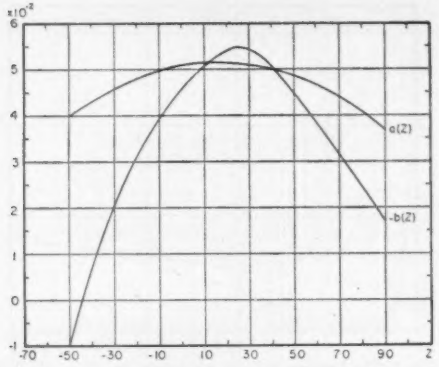

FIG. 3. The coefficients $a(Z)$ and $-b(Z)$ plotted against Z, where $f_1/f_0=a(Z)(W_0^2-1)+b(Z)(W_0-1)$.

$\bar{C}_n$ are

$$12\bar{C}_{1T}(W_0)=(6/10)(W_0^2-1)-(1/5)(W_0-1),$$

$$5\cdot 6^2\bar{C}_{2T}(W_0)=(3/7)(W_0^2-1)^2-(26/105)(W_0^2-1)(W_0-1)-(2/105)(W_0-1)^2, \quad (14)$$

and

$$70\cdot 72^2\bar{C}_{3T}(W_0)=(1/3)(W_0^2-1)^3-(9/35)(W_0^2-1)^2(W_0-1)-(2/35)(W_0^2-1)(W_0-1)^2+(8/105)(W_0-1)^3.$$

(B) The Ratio f_1/f_0

If something were known concerning the ratio f_1/f_0, then, through the use of Trigg's curves[8] of f_0, one could obtain f_1 and hence the f_1t products. Consider the ratio

$$\frac{f_1}{f_0}=\frac{\int_1^{W_0} C_1F_0(W,Z)pW(W_0-W)^2dW}{\int_1^{W_0} C_0F_0(W,Z)pW(W_0-W)^2dW}=\frac{\bar{C}_1}{C_0}. \quad (15)$$

Since this ratio was expected to be fairly independent of Z, two new functions, $a(Z)$ and $b(Z)$, were defined by

$$f_1/f_0=R(W_0,Z)=a(Z)(W_0^2-1)+b(Z)(W_0-1), \quad (16)$$

and were computed from exact values of f_1 and f_0 at $Z=0$, ± 25, ± 50, and 90 and for $W_0=1.5$, 5, and 10. The functions $a(Z)$ and $b(Z)$ are shown in Fig. 3 plotted against Z. It should be noted that the average value of the coefficient $a(Z)$ is almost equal to the coef-

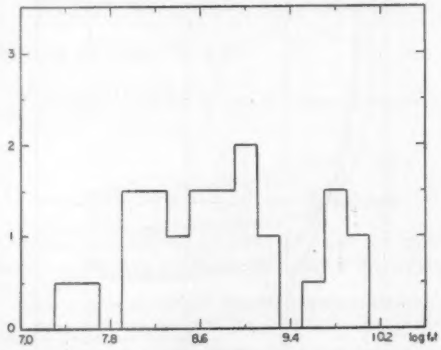

FIG. 4. Histogram of the number of unique first forbidden transitions plotted against $\log(ft)$.

[8] E. Feenberg and G. L. Trigg, Revs. Modern Phys. 22, 399 (1950).

TABLE I. A table of ft products for forbidden transitions with maximum spin change for the degree of forbiddenness (classification derived from spectral shapes, known spin changes, and comparative half-lives).

Nucleus	W_0	$\log(fa)$	$\log[(W_0^2-1)fa]$	$\log(f_0t)$[a]	Ref.
		Forbidden transitions with $n=1$, $\Delta I=\pm 2$.			
C^{14}	10.43	7.44	9.48	8.15	f, o
A^{39}	2.11	8.66[b]	9.10[b]	7.56[b]	t
K^{40}	8.02	8.02	9.82	8.49	f
Kr^{85}	2.36	9.09	9.75	8.30	u, x
Rb^{86}	4.57	8.51	9.81	8.43	f
Sr^{89}	3.93	8.57	9.73	8.34	h, i
Sr^{90}	2.04	9.86[c]	10.48[c]	8.89[c]	g, j
Y^{90}	5.40	8.03	9.48	8.11	g, i, j
Y^{91}	4.02	9.19[c]	10.37[c]	8.98[c]	i, k, l
Sn^{122}	3.78	8.88	10.00	8.60	m, v
Sn^{125}	5.57	8.86	10.34	8.96	m, v
I^{134d}	5.31	8.11	9.54	8.11	n
Cs^{137}	2.02	9.83[c]	10.32[c]	8.85[c]	f, k
Tl^{204}	2.51	9.60	10.32	8.85	w
		Forbidden transitions with $n=2$, $\Delta I=\pm 3$.			
Be^{10}	2.10	14.50[c]	15.03[c]	12.08[c]	o
Na^{22c}	4.7	13.6	14.96	12.85	o, p
		Forbidden transitions with $n=3$, $\Delta I=\pm 4$.			
K^{40}	3.64	18.46	19.54	15.60	f, q, r, y

[a] $f_0=f_1=f_0[a(Z)(W_0^2-1)+b(Z)(W_0-1)]$ for $n=1$,
$=\bar{C}_nT(W_0)f_0$ for $n=2, 3$.

[b] These products are lower limits as the reported half-life is given as a minimum value.

[c] These products contain the term $(2I_f+1)/(2I_i+1)$, I the nuclear spin. This factor must be included because $I_f>I_i$.

[d] Corrected for K-capture.

[e] A branching ratio of one in 11,000 used.

[f] G. T. Seaborg and I. Perlman, Revs. Modern Phys. 20, 585 (1948).

[g] Braden, Slack, and Shull, Phys. Rev. 75, 1964 (1949).

[h] Slack, Braden, and Shull, Phys. Rev. 75, 1965 (1949).

[i] L. M. Langer and H. C. Price, Jr., Phys. Rev. 76, 641 (1949).

[j] E. U. Jensen and L. J. Laslett, Phys. Rev. 75, 1949 (1949).

[k] Reference 3.

[l] L. M. Langer and H. C. Price, Jr., Phys. Rev. 75, 1109 (1949).

[m] J. C. Lee and M. L. Pool, Phys. Rev. 76, 606 (1949).

[n] Reference 10.

[o] L. J. Laslett, Phys. Rev. 76, 858 (1949).

[p] Reference 11.

[q] L. H. Ahrens and R. D. Evans, Phys. Rev. 74, 279 (1948).

[r] D. E. Alburger, Phys. Rev. 79, 236(A) (1950).

[s] L. M. Langer, Phys. Rev. 77, 50 (1950).

[t] Zeldes, Ketelle, and Brasi, Phys. Rev. 79, 901 (1950).

[u] Reference 9.

[v] Ketelle, Nelson, and Boyd, Phys. Rev. 79, 242(A) (1950).

[w] D. Saxon and J. Richards, Phys. Rev. 76, 982 (1949).

[x] I. Bergström (private communication from Dr. Kai Siegbahn).

[y] Bell, Weaver, and Cassidy, Phys. Rev. 77, 399 (1950).

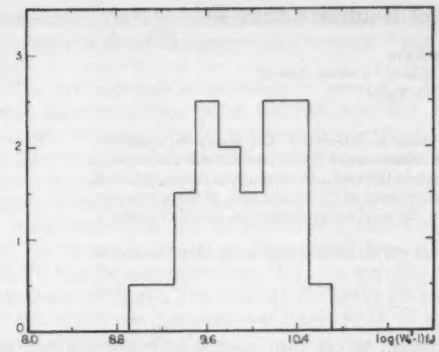

FIG. 5. Histogram of the number of unique first forbidden transitions plotted against $\log[(W_0^2-1)f_0t]$.

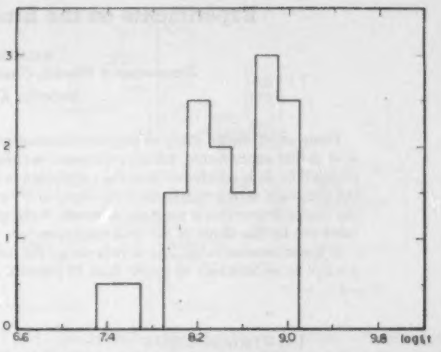

FIG. 6. Histogram of the number of unique first forbidden transitions plotted against $\log(f_1t)$.

ficient of the term in (W_0^2-1) in $\bar{C}_{1T}$, indicating the suitability of the approximate averaging process based on the distribution function $\mathcal{F}$.

(C) Discussion of the Results

In Eq. (9) the nuclear matrix elements for $n=1$ contain the nucleon space coordinates to the first power. Thus, one might expect the product $A^{\frac{1}{3}}f_1t$ to be more constant than the f_1t product alone. To check this, the spread of values for the products $A^m f_1t$ (A the atomic number) was investigated. It was found that $m=0$ resulted in a smaller spread for this product (when applied to the experimental information for the isotopes listed in Table I) than any other value. The total region investigated was $-1\leq m\leq 1$.

In Table I the low ft products for A^{39} must be considered lower limits because the half-life reported is only a minimum value.[9] Using Trigg's curves for[6] f_k+f_+, the branching ratios for the two low energy transitions found by Mitchell and his co-workers in I^{124} can be corrected for K-capture.[10] This correction reduces the branching ratio for the high energy, first forbidden transition from 51 to 14 percent, and raises all of the ft products for this isotope. If K-capture does indeed give rise to the gamma-ray line at 1.72 Mev, as suggested in Reference 10, this would have the effect of further reducing the branching ratio for the first forbidden transition and increasing the value of f_1t.

Figures 4–6 are histograms in which the number of transitions with the shape factor $C_{1T \text{ or } A}$ is plotted against $\log(f_0t)$, $\log[(W_0^2-1)f_0t]$, and $\log(f_1t)$. From the broad distribution in the f_0t plot it seems evident that the f_0t product is not as suitable a criterion for the unique first forbidden type transition as are the other products.

Nothing at all can be said for the third forbidden transition of K^{40} as there is no other known transition with which to compare it. The situation is different for the second forbidden transitions. The transition of Na^{22} to the ground state of Ne^{22} is in fair agreement with the similar transition of Be^{10} to B^{10}. The branching ratio given by Morganstern and Wolf[11] has been corrected for masking by the low energy positron spectrum, and the ratio of one to an upper limit of 11,000 is used. While agreement with the Be^{10} transition is not excellent, it would seem that the uncertainty in the approximate averaging process is probably far less than that arising naturally from the experimental method.

The author wishes to express his sincere appreciation to Professor E. Feenberg for suggesting this problem and for many helpful suggestions and discussions.

[9] Brosi, Zeldes, and Ketelle, Phys. Rev. **79**, 902 (1950).
[10] Mitchell, Mei, Maierschein, and Peacock, Phys. Rev. **76**, 1450 (1949).
[11] K. H. Morganstern and K. W. P. Wolf, Phys. Rev. **76**, 1261 (1949).

Experiments on the Emission of Neutrinos from P^{32}

CHALMERS W. SHERWIN
Department of Physics, University of Illinois, Urbana, Illinois*
(Received December 18, 1950)

These experiments study energy and momentum conservation in beta-decay. The apparatus, improved over earlier experiments, permits increased accuracy in the measurement of the neutrino-electron angular correlation. It is concluded that the correlation is approximately $(1+\cos\theta)$. Determination of the nature of the dominant interaction in the beta-decay of P^{32} awaits measurement of the nuclear spin. If the spin is one, the tensor interaction is uniquely selected. If the spin is zero, the axial vector dominates. Spin 2 or higher is ruled out by the shape of the beta-spectrum.

It is also demonstrated that in beta-decay the missing energy and the missing momentum obey the relation $p=E/c$ to an accuracy of better than 10 percent.

I. INTRODUCTION

THE neutrino is unique among all the particles studied in physics in that its existence is inferred entirely from the emission process. All other particles can be observed both in emission and absorption. The effect of the neutrino on the parent nucleon and the accompanying electron is the only presently available process by which one can discover anything about the characteristics of this remarkable particle. Since we have only one avenue of approach to the neutrino, it deserves exhaustive exploration. This paper is the third in a series[1] describing experiments of neutrino emission from P^{32}. Each paper in this series is the result of a repetition of the same basic experiment with improved apparatus. The hope is that the experimental errors can be reduced, and so more reliable information about the neutrino can be obtained.

These experiments consist essentially in a measurement of the energy and momentum of the recoil nucleus and of the electron. One then uses only the basic principles of conservation of energy and momentum to infer the momentum and energy of the neutrino. Theoretical predictions regarding the outcome of possible experiments are made with a pair of dividers and a ruler in a simple manner. Appeal to only the most elementary and fundamental physical concepts always makes the interpretation of experiments more convincing.

In these experiments, a surface layer of P^{32} is evaporated in a vacuum on a thin supporting film. The electrons can escape through the film with little scattering, but the recoil ions can be scattered violently as they escape the surface. Even one collision with some surface molecule can either stop the recoil ion (maximum energy about 78 ev) completely, or scatter it so badly that it loses all memory of its original momentum. The most important experimental problem is to distinguish between those recoil ions which have been scattered and those which escape the surface with no substantial change in their original momenta. If one can identify clearly those recoil ions which are not scattered, he can then reach definite conclusions concerning the relation of energy and momentum of the neutrino and also concerning the angular correlation that the neutrino has with the electron.

An effort has been made to work with the lowest possible electron energy, and therefore with a neutrino having the highest possible energy. The neutrino thus produces the greatest possible effect on the recoil ion. A further advantage of this situation is that one can work exclusively with high energy recoil ions, since the recoil momentum is kept quite near its maximum value over quite a range of electron-neutrino angles. When inferring the electron-neutrino angular correlation, one must compare the relative intensities of groups of recoil ions. If these groups all have nearly the same momentum, one has some confidence that their relative intensities are due to neutrino characteristics and not to surface effects.

Electrons going in several different directions are studied simultaneously. This reduces errors due to progressive changes at the surface (e.g., slow adsorption of gas molecules) and also speeds the collection of data. Since it requires three or four days of continuous observation to get even barely adequate statistics for one particular setting of the apparatus, and since even the best surfaces often show deterioration after this length of time, it is important to collect the maximum amount of information in the first few days.

The equipment is completely automatic, and all the data are recorded photographically.

II. THE EXPERIMENTAL EQUIPMENT

Figures 1 and 2 show the apparatus in which the measurements are made. A glass film (300 to 500 $\mu g/cm^2$) is successively coated with aluminum (barely visible), lithium fluoride (100 to 1000 atomic layers), and finally with P^{32} (preferably less than one atomic layer). This is all done by evaporation in the upper chamber, Fig. 1. The radiant heater wires are mounted 2 or 3 mm behind the film. They are kept at a red heat except during the evaporation processes. A rough estimate of the temperature of the film when this heater is operating is about 100°C. However, it is effective in

* This work was supported by the joint program of the ONR and AEC.
[1] C. W. Sherwin, Phys. Rev. **73**, 216 (1948); **75**, 1799 (1949).

preventing what is probably van der Waals adsorption for days at a time.[3] The pressure is 2 to 6×10^{-7} mm of Hg.

The LiF substrate is necessary to provide a high work function surface which will not neutralize the escaping S^{32} ions. If the P^{32} is deposited directly on the aluminum, no recoil ions are observed. If the aluminum film is omitted, electrostatic surface charge effects completely distort the recoil ion momentum spectrum.

After preparation, the radiant heater is turned back on, the source is lowered to the common focal point of the four beta-spectrometers (Fig. 2), and the observations are begun. The magnetic field over the path of the recoils was measured and found to be of negligible importance.

The scintillation counters use anthracene crystals. They detect the magnetically selected electrons and start the sweep on a cathode-ray tube. The pulse, owing to the arrival of a positive ion at the Allen-type electron multiplier, appears as an intensified spot $\frac{1}{2}$ μsec in duration on the cathode-ray tube. This measures the time of flight of the recoil ion. The distance is known exactly, so the velocity is then determined. Each of the recoil ion pulses appearing on the cathode-ray tube is followed by code pulses. These code pulses identify that scintillation counter which initiated the sweep on which the recoil ion pulse appears. The same cathode-ray tube and the same moving film camera record the complete time of flight data of the recoil ions associated with the four different electron directions. In practice, the electrons at the 110° position (Fig. 2) never give any useful information, so that only the three remaining spectrometers were used.

The spectrometers are all operated at the same magnet current, and all select the same momentum interval. Calibration with the 625-kev line of Cs^{137} gives a momentum resolution in which the full width at half-maximum is 15 percent. This spread is mainly due to the fact that the exit slits of the spectrometers are 2 cm wide.

The entire vacuum system is heated to about 100°C to speed outgassing. This process usually continues for several days. Only after the vacuum system is returned to room temperature is a surface formed. Helium is used to fill the system whenever it is brought up to atmospheric pressure.

The P^{32} is purified in an auxiliary system by vacuum evaporation, during which process it is deposited on one of the evaporation filaments eventually used in Fig. 1. Thus, the final surface is formed after two evaporations, each of which has been carefully studied to provide maximum separation from impurities.

[3] H. Frauenfelder has shown (private communication) that the rate of Cd^{109} recoil emission from a surface is greatly increased by raising its temperature one to two hundred degrees C. See also P. B. Smith and J. S. Allen, Phys. Rev. 81, 381 (1951).

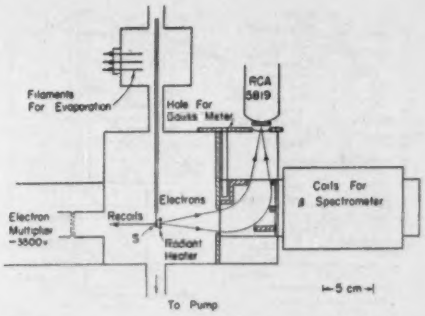

FIG. 1. Apparatus for measuring the momentum of the electrons and recoil ions in beta-decay. The radioactive atoms are on the surface S facing the electron multiplier. The electrons go through S, are deflected in 90° spectrometers, and leave the vacuum through a thin window at the focal point. The velocity of the recoil ion is measured by observing its time of flight from S to the first dynode of the electron multiplier.

III. SOME RESULTS WITH POOR SOURCES

Most of the sources of P^{32} gave no useful information about the neutrino. Apparently all recoil ions that escape these surfaces are badly scattered. Such a surface gives results like those shown in Fig. 3. Here, broad peaks of recoil ions appear above the chance background. This background is determined by those events occurring before true coincidences are possible (0 to $3\frac{1}{2}$ μsec from the start of the sweep). In Fig. 3, the recoil ion momentum distribution is quite insensitive to the direction of the electrons. This is just what is to be expected if violent scattering occurs, and we conclude that this source is "thick" or overlayed with some adsorbed molecules. The latter explanation is made probable by the fact that, every time a source gives results similar to Fig. 3, it is also observed that the recoil ion counting rate drops steadily from its initial

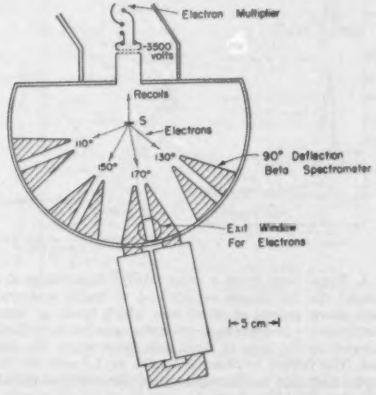

FIG. 2. Plan view of the experimental apparatus. The four beta-spectrometers are all in the same vacuum and have a common focus at the source S.

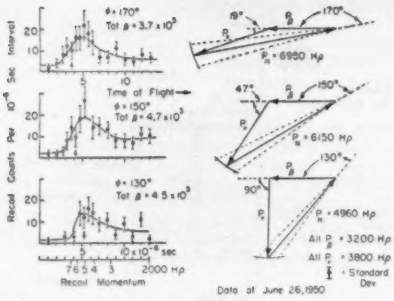

FIG. 3. Time of flight of recoil ions from a poor source. The short arrows along the time axis show where peaks of recoil ions should occur if the predictions based on the vector diagrams are fulfilled. The dotted lines bounding P_N show the over-all angular resolution set by the slit systems.

rate. This decrease in the recoil ion counting rate is noticeable in 20 min to one hour, and continues for many hours or even days before reaching a steady value of 30 to 70 percent of the initial rate. Since it takes 10 to 20 hours to observe enough events to reach any conclusions about the recoil spectra, the nature of the surface during the first hour or so of its existence is not known. This adsorbed contamination may be chemically bonded, since even violent heating by the radiant heater does not drive it off.[3]

For the "good" surfaces, shortly to be described, the recoil ion counting rate is always observed to be constant for days at a time (except for the normal beta-decay).

Many efforts at making a surface resulted in too weak an activity, so that even in 5 or 10 days of observation no significant results were obtainable.

Some surfaces were too intense. This causes the coincident events to sink down into the background; and although the statistical accuracy increases, systematic errors become enormously important. Most of the good data were obtained when the true events were 3 to 30 times the random background.

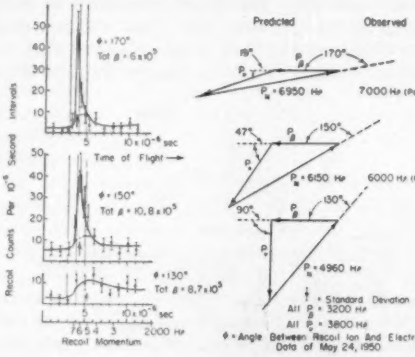

FIG. 4. Recoil ions from a good source. Superimposed on the background due to chance events and to badly scattered ions, there are sharp groups of recoil ions which occur at times that are quantitatively in agreement with the neutrino hypothesis. The short arrows on the time of flight axis show where the peaks are expected. The failure to observe a peak at 5.3 μsec for the 130° case is probably due to the weakness of the neutrino radiation at 90° with respect to the electron.

[3] Diffusion into the surface is also a possibility. See H. Frauenfelder, Helv. Phys. Acta **23**, 347 (1950).

IV. SOME RESULTS WITH GOOD SOURCES

The recoil time of flight spectra for two "good" surfaces are shown in Figs. 4 and 5. Here one still sees the background of badly scattered recoil ions which seems to be much the same for all directions of electrons. However, superimposed upon this background are peaks of recoil ions which are nicely accounted for

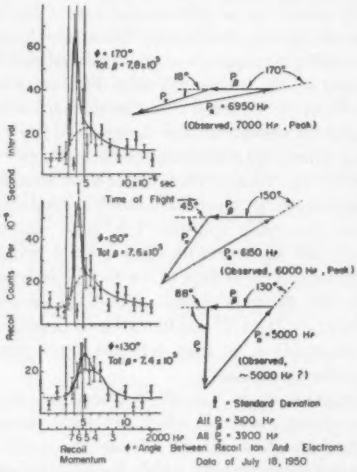

FIG. 5. Recoil ions from a second good source. Here the background of badly scattered recoil ions is much higher than for the source in Fig. 4; but fairly sharp groups of recoil ions, coming at the times predicted by the neutrino hypothesis, are clearly visible.

by the electron and the neutrino. The most convincing thing about these peaks is that they come exactly at those times, predicted by the accompanying vector triangles, which are based simply on the conservation of momentum and energy. The shift of the peak from the 170° case to the 150° case (from 3.75 to 4.25 μsec) is very clear. This shift of 0.5 μsec is much larger than either the relative or absolute experimental errors, which are both less than 0.1 μsec. The peak at 130° is so weak that its existence is uncertain. It does serve to set up some upper limit to the intensity of neutrino radiation at 90° with respect to the electron.

In order to work with still higher neutrino energies, we turn to electrons of only 2150-oersted-cm momentum. Figure 6 shows the results from the best surface that was obtained under these conditions. The experimental

difficulties are greater than for the 3150 $H\rho$ electrons in Figs. 4 and 5, since there are fewer electrons at this energy, and also since the neutrino must enter a smaller solid angle to make an observable recoil ion. However, we again obtain agreement with the predictions of the neutrino hypothesis within experimental error. A peak of recoil ions due to neutrinos which are emitted at 70° with respect to the electrons is definitely observed. The recoil ions caused by these neutrinos have a momentum only 17 percent smaller than those recoil ions for which the electron-neutrino angle is 15°. One has some confidence, therefore, that their much lower intensity is due to the weakness of the neutrino radiation at wide angles with respect to the electron. Here v/c for the electron is 0.78, so that any angular correlation due to relativistic effects is not greatly reduced. The average scattering of the electrons as they pass through the 400 $\mu g/cm^2$ glass film is less than 3°, using the data of Groetzinger, Berger, and Ribe[4] for scattering in argon. This is less than half of the angular resolution of 8° set by slit widths.

A further advantage in using larger neutrino energies is that the solid angle corrections which are necesssary to compute the electron-neutrino angular correlation become nearly the same for the different angles involved.

V. THE ANGULAR CORRELATION OF ELECTRONS AND NEUTRINOS

The experimental angular correlation of electrons and neutrinos is shown in Fig. 7. The neutrino intensity is inferred from the intensity of the recoil ion groups after correction is made for the solid angles involved. This correction is nearly the same for all the points in Fig. 7, and therefore can introduce little relative error. The interpretation of these data in terms of beta-decay theory will be discussed in the next section. Meanwhile, it suffices to note that the experimental points are fitted adequately by an angular correlation of the approximate form $(1+\cos\theta)$.

This same conclusion was reached by earlier experiments,[1] where the correction for the effects of surface scattering was made by an indirect method. Also, the earlier experiments differed from these in that the recoil ions, which were used to infer the neutrino intensity at wide angles with respect to the electron, had much lower momenta than they do here. Thus, the refinement of the beta-spectrometer apparatus, the simple and direct method of correcting for the badly scattered recoil ions, and the use of the highest possible recoil ion momenta all confirm the conclusions reached earlier by more tenous reasoning from less reliable data.

Statistical errors are indicated in Fig. 7. Systematic errors cannot be determined exactly. The most likely source of error arises from the fact that the recoil ion groups on which the neutrino intensity is based do not all have the same momentum for different directions of

[4] Groetzinger, Berger, and Ribe, Phys. Rev. 77, 584 (1950).

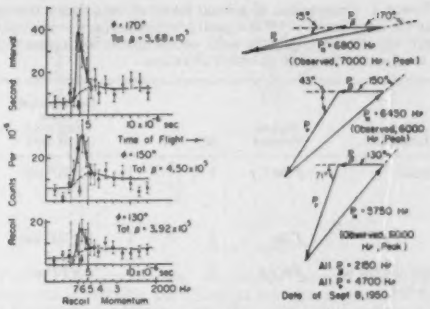

FIG. 6. Recoil ions from a third good source. Here the neutrino has over two times the momentum of the electron. The short arrows on the time axis indicate the predicted times at which the recoil ion peaks should occur. The recoil ions associated with neutrinos going at 71° with respect to the electrons have a momentum only 17 percent smaller than those associated with neutrinos going at 15° with respect to the electron.

the neutrino with respect to the electron. That this source of error is probably not significant is shown by the fact that the recoil ion momenta vary over a range of 17 percent in the upper part of Fig. 7, 28 percent in the lower part of Fig. 7, and 50 percent in the data of the previous paper; but all give the same result regarding the electron neutrino angular correlation. Furthermore, even though the intensity of the badly scattered recoil ions varies widely (Figs. 4 and 5), one still obtains the same angular correlation for the electron and the neutrino.

The fraction of the total recoil ions that escape the surface with little scattering is really quite small. About 1 percent of the total expected number are actually observed in the sharp peaks due to unscattered ions.

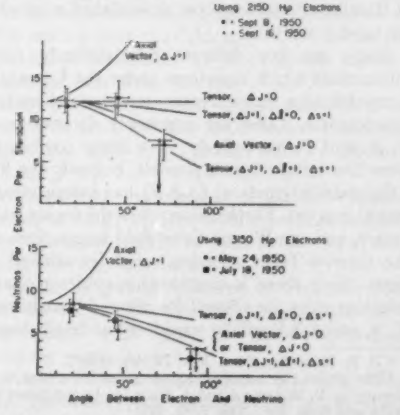
Using 2150 Hρ Electrons
Using 3150 Hρ Electrons
Neutrinos Per Steradian Per Electron
Angle Between Electron And Neutrino

FIG. 7. The experimental neutrino-electron angular correlation for P^{32}. The error limits plotted are statistical. Only the tensor interaction with $\Delta J=1$, $\Delta l=1$, and $\Delta s=1$, and the axial vector interaction with $\Delta J=0$ agree with the observations. Each unit of the ordinate scale is 10^{-4} electron per neutrino per steradian.

TABLE I. Comparison of several forms of beta-decay theory with experiment. One assumption, common to all the calculations, is that the beta-decay of P^{32} is a parity forbidden ($\pi_i = -\pi_f$) transition. If $\Delta J = 1$, only the tensor interaction is in agreement with experiment; but if $\Delta J = 0$, only the axial vector interaction agrees with all experimental observations. The estimates of *ft* values are good only to within a factor of 30 in either direction.

Form of interaction	Matrix element	ΔJ	Δl	Δs	Estimated *ft* value (Exp. $=8.5\times10^7$ sec)	Calculated beta-spectrum shape (Exp. =allowed)	Calculated electron-neutrino angular correlation. $Z=0$. Exp. $=(1+\cos\theta)$
Tensor	$\int\beta\sigma\times r$	1	1	1	5×10^7 sec	Less than 4 percent deviation from allowed Kurie plot	$[1+(v/c)\cos\theta](p^2+q^2+2pq\cos\theta)+pq(v/c)\sin^2\theta \cong 1+(4/3)\cos\theta+\frac{1}{3}\cos^2\theta$
	$\int\beta\alpha$	1	0	1	5×10^7 sec	Allowed	$1+\frac{1}{3}(v/c)\cos\theta$
Axial vector or A-S-P	$\int\sigma\times r$	1	1	1	5×10^7 sec	Easily observable deviation from allowed	$[1-(v/c)\cos\theta](p^2+q^2+2pq\cos\theta)-pq(v/c)\sin^2\theta \cong (1-\cos^2\theta)$
Tensor	$\int\beta\sigma\cdot r$	0	1	1	5×10^7 sec	Easily observable deviation from allowed	$[1-(v/c)\cos\theta](p^2+q^2+2pq\cos\theta)-2pq(v/c)\sin^2\theta =$ constant for $\rho = 2150\ H\rho$ and $\cong(1+\cos\theta)$ for $\rho = 3140\ H\rho$.
Axial vector or A-S-P	$\int\gamma_5$	0	0	0	5×10^7 sec	Allowed	$[1+(v/c)\cos\theta]$
	$\int\sigma\cdot r$	0	1	1	5×10^7 sec	Less than 4 percent deviation from allowed Kurie plot	$[1+(v/c)\cos\theta](p^2+q^2+2pq\cos\theta)+2pq\sin^2\theta \cong (1+\cos\theta)$

About 10 percent of all those that should be available, judging from the beta-activity, are badly scattered. These are "smeared" in both time and angle and are easily distinguished, since they merely raise the background somewhat. The remaining 90 percent or so of the recoil ions probably never escape at all from what must be, on an atomic scale, a fantastically rough surface of aluminum, lithium fluoride, and impurities evaporated along with the P^{32}.

VI. THE INTERPRETATION OF THE ANGULAR CORRELATION

For the interpretation of the experimental results of Fig. 7, in terms of beta-decay theory, the calculations of Hamilton,[6] and some yet unpublished work of Blatt[6] are used.

There are five different relativistically covariant interactions which transform under the Lorentz transformation as a scalar, vector, tensor, axial vector, and pseudoscalar. These are commonly denoted by *S*, *V*, *T*, *A*, and *P*, respectively. Any linear combination of these five interactions is possible, but only the Wigner-Critchfield interaction[7] (A-S-P) has independent theoretical support. Furthermore, only the tensor, the axial vector, and the Wigner-Critchfield interactions require the Gamow-Teller selection rules[8] for allowed transitions. Since there is considerable evidence that these selection rules are obeyed for allowed transitions, only T, A, and A-S-P will be considered in detail. Also, these choices are in agreement with the electron-neutrino angular correlation for the allowed He^6 decay as measured by Allen.[9]

The interpretation hinges on the spin and parity of P^{32} and the daughter nucleus S^{32}. The final nucleus, S^{32}, has a measured spin of zero.[10] Since P^{32} is an odd-odd nucleus, it must have an integral spin.

P^{32} cannot have a spin of two or greater, since this would cause the beta-spectrum to have an easily observed deviation from the experimentally measured allowed shape.

We are thus left with the possibility that the spin of P^{32} is either one or zero.

There are three experimental observations which must be predicted correctly by the successful form of the theory: (1) the *ft* value[3] (experimentally 8.5×10^7 sec), (2) the shape of the beta-spectrum (experimentally allowed),[11] and (3) the electron neutrino angular correlation (experimentally, $1+\cos\theta$). Table I lists the interactions with their theoretical predictions regarding these three items. We have assumed that the transition must be parity forbidden ("yes") in order to account for the long half-life of P^{32}.

It should be realized however that an allowed transition with an unusually small matrix element is a possibility. The square of the matrix element would have to be about 1000 times smaller than usual for the allowed but unfavored transitions. In addition, the experimental electron-neutrino angular correlation, Fig. 7, disagrees with both the allowed tensor inter-

[6] D. R. Hamilton, Phys. Rev. **71**, 456 (1947).
[6] The relevant formulas will appear as part of a book on nuclear physics by V. Weisskopf and J. Blatt (to be published by John Wiley and Sons, Inc., New York, 1951).
[7] C. L. Critchfield and E. P. Wigner, Phys. Rev. **60**, 412 (1941); **63**, 417 (1943).
[8] E. J. Konopinski, Revs. Modern Phys. **15**, 209 (1943). G. Gamow and C. L. Critchfield, *Theory of Atomic Nucleus and Nuclear Energy Sources* (Oxford University Press, 1949).
[9] Allen, Paneth, and Morrish, Phys. Rev. **75**, 570 (1949).
[10] E. Olsson, Z. Physik **100**, 656 (1936).
[11] The excess of electrons below 300 kev observed by H. M. Agnew, Phys. Rev. **77**, 655 (1950), and also by Warshaw, Chen, and Appleton, Phys. Rev. **80**, 288 (1950) is unexplained; but in any case the spectrum shape above 300 kev is indistinguishable from the allowed form.

action $(1+(v/c)\frac{1}{3}\cos\theta)$ and with the allowed axial vector interaction $(1-(v/c)\frac{1}{3}\cos\theta)$.

The Wigner-Critchfield interaction (A-S-P) is grouped with the pure axial vector, since for this case the A term dominates (i.e., it has an appreciably smaller ft value than the S or the P terms). The exact shapes of the various theoretical angular correlation functions are plotted in Fig. 7, using the exact values of p the electron momentum, q the neutrino momentum, and v/c, where v is the electron velocity. It should be noted that in Table I the estimates of the ft values are good only to a factor of 30 in either direction.

If the spin of P^{32} is one, the tensor interaction gives agreement with all the experimental facts, but only if the $\int\beta\sigma\times\mathbf{r}$ matrix element dominates, since the $[1+(\frac{1}{3})(v/c)\cos\theta]$ angular correlation is improbable. For this same case, the axial vector interaction can be ruled out conclusively on two counts: the beta-spectrum shape, and the angular correlation.

If the spin of P^{32} is zero, only the axial vector (or the A-S-P) interaction gives agreement with the experimental facts. For this case, the tensor interaction is ruled out on both the beta-spectrum shape, and also the electron-neutrino angular correlation observed with 2150 oersted-cm electrons. Curiously enough, for the 3150 oersted-cm electrons, the tensor interaction predicts approximately a $(1+\cos\theta)$ correlation. Because of this fact, and because even for 2150 oersted-cm electrons the theoretical angular correlation is only a constant, the tensor interaction is not as convincingly rejected for this case as is the axial vector interaction for the case where the spin of P^{32} is one.

The theoretical angular correlation functions in Table I are all calculated for the case where $Z=0$. Rose[12] has shown that for $\Delta l=0$ transitions at least, there is no appreciable effect of the nuclear charge on the angular correlation. It would be very valuable to have exact information regarding possible coulomb effects on $\Delta l=1$ transitions.

Thus, it appears that if the spin of P^{32} is one, it is fairly certain that the tensor interaction dominates the transition; and if the spin is zero, it is very probable that the axial vector interaction dominates.

VII. THE RELATIONSHIP OF THE ENERGY AND MOMENTUM OF THE NEUTRINO

Since these experiments measure both the missing energy and the missing momentum in the beta-decay of P^{32}, it is interesting to see how they are related. A few representative points out of many separate observations are plotted in Fig. 8. If all the experimental data are included, the theoretical relationship, $p=E/c$, is verified to an accuracy of 10 percent or better, the limit being set by the possibility of systematic errors. Only the statistical uncertainties are indicated in the

[12] M. E. Rose, Phys. Rev. 75, 1444 (1949).

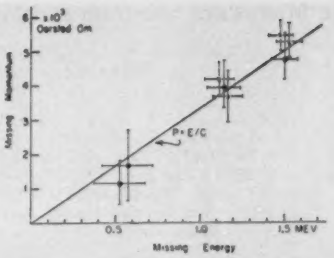

FIG. 8. The experimental relationship between the missing energy and the missing momentum in beta-decay, compared with the fundamental relativistic equation. The points indicated by circles are for cases where the missing momentum goes in nearly the same direction as the electron. The points indicated by x are for cases where the missing momentum goes 50° to 70° with respect to the electron.

figure. It is interesting that this law is obeyed equally well for neutrinos which make an appreciable angle with respect to the electron as well as those which go in the same direction. Since the minimum energy of the neutrinos used in these experiments is of the order of 0.5 Mev, one can draw no inferences regarding the rest mass of the neutrino, which is known, from other measurements, to be very much smaller than this.

VIII. CONCLUSIONS

The neutrino energy and momentum are related by $p=E/c$ to an accuracy of better than 10 percent for neutrino energies above 0.5 Mev.

For P^{32}, the electron and neutrino strongly favor the same hemisphere, having an angular correlation of the approximate form $(1+\cos\theta)$.

Adequate agreement with all the experimental data on P^{32} (the energy and half-life, the beta-spectrum shape, and the electron-neutrino angular correlation) is attained if one assumes that the spin of P^{32} is one and that the tensor interaction ($\int\beta\sigma\times\mathbf{r}$ matrix element) dominates the beta-decay process.

Agreement with experiment is also obtained if the spin of P^{32} is zero and the axial vector interaction dominates the beta-decay process (matrix elements $\int(\mathbf{r}\cdot\sigma)$ and $\int\gamma_5$).

An experimental measurement of the total angular momentum of the P^{32} nucleus could determine uniquely whether the axial vector or the tensor interaction dominates the beta-decay of P^{32}.

The author is greatly indebted to Professor John Blatt for several valuable discussions and for the use of his calculations which apply the general beta-decay theory to the special case of P^{32}.

The author is also indebted to the Oak Ridge National Laboratory for the numerous shipments of carrier free material which made the experiments possible.

The Microwave Spectrum and Molecular Constants of Trifluoromethyl Acetylene*

WALLACE E. ANDERSON,† RALPH TRAMBARULO, JOHN SHERIDAN,‡ AND WALTER GORDY
Department of Physics, Duke University, Durham, North Carolina

(Received December 8, 1950)

Pure rotational transitions, $J=4\rightarrow5$, $6\rightarrow7$, and $8\rightarrow9$ have been measured for CF_3CCH and $J=5\rightarrow6$ and $8\rightarrow9$ for CF_3CCD. These yield for CF_3CCH, $B_0=2{,}877.948$ Mc/sec, $D_J=0.2_4$ kc/sec, $D_{JK}=6.3$ kc/sec, and for CF_3CCD, $B_0=2{,}696.073$ Mc/sec, $D_J=0.2_8$ kc/sec, $D_{JK}=6.2$ kc/sec. If $\angle FCF$ is tetrahedral, $d(C\equiv C)$ and $d(CH)$ are assumed to be 1.207A and 1.056A, respectively, then the bond lengths $d(CF)=1.330$A and $d(C-C)=1.493$A are obtained. Rotational frequencies of molecules in excited bending vibration modes have been measured and found to agree with Nielsen's theory of *l*-type doubling.

I. INTRODUCTION

TRIFLUOROMETHYL acetylene is a new compound prepared the first time in 1950 by Haszeldine.[1] Consequently, little is known of its physical properties. The present study was undertaken in the hope of determining its molecular structure. This has been only partly achieved, since measurements on only two isotopic species have been made. As expected, its microwave spectrum is that characteristic of a symmetric top rotator. The moments of inertia, I_B, and centrifugal stretching constants of the forms CF_3CCH and CF_3CCD have been obtained. Rotational transitions of molecules in excited bending vibration states have been measured and found to agree with Nielsen's theory of *l*-type doubling.

II. EXPERIMENTAL PROCEDURE

The absorption lines were observed with a video detection sweep spectroscope,[2] and were measured with a frequency standard[3] monitored by comparison with station WWV. Measurements were made at dry ice temperature with pressures of about 10^{-3} mm of Hg.

The sample of trifluoromethyl acetylene was prepared by the method devised by Haszeldine.[1] Trifluoromethyl acetylene-*d* was obtained by exchange with a solution of sodium carbonate in heavy water. The completeness of the conversion was indicated by failure to detect lines caused by CF_3CCH in the CF_3CCD sample.

III. RESULTS FOR THE GROUND VIBRATIONAL STATE

Table I lists the measured frequencies of CF_3CCH and CF_3CCD for the ground vibrational state. Rotational constants calculated from these appear in Table II. For the calculation of I_B the value of Planck's constant used was $h=6.62373\times10^{-27}$ ergsec.

If the CF_3 group is assumed to be tetrahedral and $d(C\equiv C)=1.207$A and $d(CH)=1.056$A, as in methyl acetylene,[4] the lengths obtained for the other bonds are

$$d(C-F)=1.330\text{A}, \quad d(C-C)=1.493\text{A}.$$

TABLE I. Observed frequencies for the rotational transitions of trifluoromethyl acetylene and trifluoromethyl acetylene-*d* in the ground vibrational state.

Species	Transition		Frequency* Mc/sec
CF_3CCH	$J=4\rightarrow5$	$K=0\rightarrow0$, $K=1\rightarrow1$	28,779.31
		$K=2\rightarrow2$	27,779.14
		$K=3\rightarrow3$	27,778.76
		$K=4\rightarrow4$	27,778.32
	$J=5\rightarrow6$	$K=0\rightarrow0$, $K=1\rightarrow1$	34,535.09
		$K=2\rightarrow2$	34,534.86
		$K=3\rightarrow3$	34,534.47
		$K=4\rightarrow4$	34,533.91
		$K=5\rightarrow5$	34,533.23
	$J=8\rightarrow9$	$K=0\rightarrow0$, $K=1\rightarrow1$	51,802.26
		$K=2\rightarrow2$	51,801.90
		$K=3\rightarrow3$	51,801.32
		$K=4\rightarrow4$	51,800.54
		$K=5\rightarrow5$	51,799.56
		$K=6\rightarrow6$	51,798.26
		$K=7\rightarrow7$	51,796.78
		$K=8\rightarrow8$	51,795.10
CF_3CCD	$J=5\rightarrow6$	$K=0\rightarrow0$, $K=1\rightarrow1$	32,352.62
		$K=2\rightarrow2$	32,352.36
		$K=3\rightarrow3$	32,352.01
		$K=4\rightarrow4$	32,351.47
		$K=5\rightarrow5$	32,350.82
	$J=8\rightarrow9$	$K=0\rightarrow0$, $K=1\rightarrow1$	48,528.42
		$K=2\rightarrow2$	48,528.08
		$K=3\rightarrow3$	48,527.56
		$K=4\rightarrow4$	48,526.74
		$K=5\rightarrow5$	48,525.74
		$K=6\rightarrow6$	48,524.54
		$K=7\rightarrow7$	48,523.08
		$K=8\rightarrow8$	48,521.44

* Absolute frequencies are accurate to ±0.10 Mc/sec.

* The research reported in this document has been made possible through support and sponsorship extended by the Geophysical Research Directorate of the Air Force Cambridge Research Laboratories. It is published for technical information only and does not represent recommendations or conclusions of the sponsoring agency.

† Present address: The Citadel, Charleston, South Carolina.

‡ Present address: Department of Chemistry, University of Birmingham, England.

[1] R. N. Haszeldine, Nature **165**, 152 (1950). We are indebted to Dr. Haszeldine for furnishing us details of this preparation.

[2] W. Gordy and M. Kessler, Phys. Rev. **72**, 644 (1947).

[3] R. R. Unterberger and W. V. Smith, Rev. Sci. Instr. **19**, 580 (1948).

[4] R. Trambarulo and W. Gordy, J. Chem. Phys. **18**, 1613 (1950).

The assumptions made appear to be reasonable. The CC triple bond length is quite insensitive to conjugation effects and has been found to be 1.21A in a large number of similar molecules, and the $\equiv C-H$ distance has not been found to vary significantly from molecule to molecule. The greatest error is caused by the assumption of the angle.

Measurement of lines with C^{13} in each of the three carbon positions would allow a complete determination of the structure. The video detection spectrometer used did not have quite enough sensitivity to detect lines of the molecules with C^{13} in natural abundance. An attempt was made to detect these on a Stark modulation spectrograph. With this method the weak C^{13} lines were so obscured by the many Stark components of the C^{12} lines that identification was uncertain. We expect to detect them later with a superheterodyne receiver.

The cathode-ray scope display of a part of the $J=8\rightarrow9$ rotational transition of CF_3CCH shown in Fig. 1 illustrates the separation by centrifugal distortion of the lines of different K in a symmetric top molecule as well as the effects of nuclear spin on the relative intensities of these lines. The $K=0$, 1, and 2

TABLE II. Rotational constants for the ground vibrational states of trifluoromethyl acetylene.

Species	B_0 (Mc/sec)	D_J (kc/sec)	D_{JK} (kc/sec)	I_B(×10^{+40} g-cm^2)
CF_3CCH	2877.948	0.2_4	6.3	291.4_{84}
CF_3CCD	2696.073	0.2_6	6.2	311.1_{88}

lines were not well resolved and are omitted. The relative intensities of the $K=3$ and $K=6$ lines compared with the intensities of the others are those predicted with a spin of $\frac{1}{2}$ for F^{19}. This photograph, therefore, provides objective confirmation by microwave spectroscopy of the F^{19} spin.

IV. ROTATIONAL SPECTRA FOR AN EXCITED VIBRATIONAL STATE

Two groups of lines, weaker than those for the ground vibrational state, were found centered about 28,834 Mc/sec and 51,902 Mc/sec. Each group consisted of a number of closely spaced lines approximately midway between two more widely spaced lines. The patterns were typical of the rotational spectra resulting from an excited degenerate bending vibration. These lines were interpreted as the $J=4\rightarrow5$ and $8\rightarrow9$ rotational transitions of CF_3CCH for the first excited $C-C\equiv C$ bending mode.

The method of treatment for the interaction of degenerate vibrations with rotation has been set forth by Nielsen,[5] and the term values for $J=1$ and $J=2$ calculated by him. The order of the secular equation of the submatrix is $4J+2$, and for high values of J the

[5] H. H. Nielsen, Phys. Rev. 77, 130 (1950).

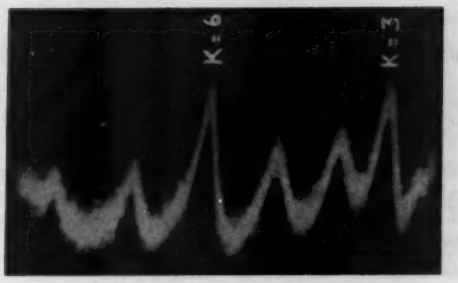

FIG. 1. Part of the $J=8\rightarrow9$ rotational transition of CF_3CCH showing lines for $K=3$ to 8.

solution by direct methods becomes prohibitive. Nevertheless, since only the levels corresponding to the same angular momentum of the framework interact, the secular equation may be factored by inspection. The rotational term values for the vibrational quantum numbers $v=1$ and $l=\pm1$ are

$$F_v(J,K,l)=B_vJ(J+1)-(B_v-C_v)K^2-2C_vKl\xi$$
$$-D_JJ^2(J+1)^2-D_{JK}J(J+1)K^2-D_KK^4$$
$$+2\{(2D_J+D_{JK})J(J+1)+(2D_K+D_{JK})K^2\}Kl\xi$$
$$+P(J,K,l),$$

where

$$P=\pm J(J+1)B_e^2a/\omega_t \quad \text{for} \quad K=\pm1, \quad l=\pm1;$$

TABLE III. Frequencies and assignments for the $J=4\rightarrow5$ and $8\rightarrow9$ rotational transitions of CF_3CCH for the excited bending vibration $V_{10}=1$.

J	Transition K	Transition l	Observed freq. (Mc/sec)[a]	Calculated freq. (Mc/sec)
4→5	±1	±1	28,816.48	28,816.52
			28,852.61	28,852.72
	0	±1	28,835.26	28,835.31
	±1	∓1	28,834.45	28,834.65
	±2	±1	28,833.81	28,833.78
	±2	∓1		28,833.94
	±3	±1	28,834.20	28,834.12
	±4	±1		28,834.03
	±3	∓1	28,833.22	28,833.19
	±4	∓1	28,832[b]	28,832.48
8→9	±1	±1	51,869.14	51,869.10
			51,934.48	51,934.20
	0	±1	51,906.64	51,906.69
	±1	∓1	51,903.42	51,903.55
	±2	±1	51,896.86	51,896.89
	±2	∓1	51,901.68	51,901.87
	±3	±1	51,899.44	51,899.26
	±5	±1		51,899.42
	±3	∓1	51,899.99	51,900.36
	±4	±1		51,899.68
	±4	∓1	51,898.61	51,898.77
	±6	±1		51,898.74
	±5	∓1	...	51,896.06
	±6	∓1	51,894.95	51,895.04
	±7	±1	51,897.63	51,897.72
	±7	∓1	51,892.88	51,892.71
	±8	±1	...	51,896.39
	±8	∓1	51,890.62	51,890.42

[a] All frequencies except that marked [b] are accurate to ±0.20 Mc/sec.
[b] Frequency accurate to ±1 Mc/sec.

and

$$P=\pm\frac{\{J(J+1)-K(K\mp1)\}\{J(J+1)-(K\mp1)(K\mp2)\}}{2(K\mp1)\{(1-\xi)C_\nu-B_\nu\}}\times\left(\frac{B_e^2a}{\omega_e}\right)^2$$

for K other than ±1 and $l=\pm1$, the upper sign being taken for $l=+1$ and the lower for $l=-1$. This holds for K different from ±1 only when P is small. The frequencies of the transitions are then

$$\nu=2B_\nu(J+1)-4D_J(J+1)^3-2D_{JK}(J+1)K^2+4(2D_J+D_{JK})(J+1)Kl\xi+\Delta P(J,K,l),$$

where

$$\Delta P=\pm2(J+1)B_e^2a/\omega_e \quad \text{for} \quad K=\pm1, \quad l=\pm1$$

$$\Delta P=\pm\frac{(J+1)\{(J+1)^2-(K\mp1)^2\}}{(K\mp1)\{(1-\xi)C_\nu-B_\nu\}}(B_e^2a/\omega_e)^2,$$

for K other than ±1 and $l=\pm1$. As before, the upper sign is taken for $l=+1$ and the lower for $l=-1$.

The assignments of the excited vibrational lines, the observed frequencies, and the calculated positions of the lines are given in Table III. The parameters used to give the calculated line positions are: $B_\nu=2883.46$ Mc/sec, $D_J=0.2$ kc/sec, $D_{JK}=7.0$ kc/sec, $\xi=1.5$, $B_e^2a/\omega_e=1.81$ Mc/sec, and $(B_e^2a/\omega_e)^2/\{(1-\xi)C_\nu-B_\nu\}=7.0$ kc/sec. The parameters listed are those which gives the best fit to the data. Although the upper limit for ξ is $+1$ from theoretical considerations, it is not possible to fit the observed data using values of $\xi\leq+1$. From the value of B in the ground state and this excited state, $\alpha_{10}=-6.51$ Mc/sec.

We would like to thank Mr. Charles Greenhow for suggesting the method of solution of the secular equations for the excited vibrational states.

PHYSICAL REVIEW VOLUME 82, NUMBER 1 APRIL 1, 1951

The Effective Range of Nuclear Forces. Effect of the Potential Shape

E. E. SALPETER
Cornell University, Ithaca, New York
(Received October 30, 1950)

Corrections to the theory of the effective range, which take account of the shape of the neutron-proton potential, are discussed. The following quantities are calculated for a Yukawa, exponential, and square well potential: (*a*) various triplet ranges compatible with the value obtained for $\rho_t(0,-\epsilon)$ from the latest experiments, $(1.72\pm0.035)\times10^{-13}$ cm. (*b*) The singlet effective range r_{0s} from neutron-proton scattering cross sections at energies up to 6 Mev. (*c*) r_{0s} from neutron absorption cross sections by hydrogen. (*d*) Photoelectric and photomagnetic disintegration cross sections for the deuteron for various γ-rays.

It is shown that a comparison of the values obtained for r_{0s} from (*b*) and (*c*) could, with a slight increase in experimental accuracy, give an estimate of the potential shape. Present, very tentative, indications are for a short-tailed potential and a value for r_{0s} of about $(2.7\pm0.5)\times10^{-13}$ cm.

I. INTRODUCTION

IN a previous paper[1] (quoted as **B**) Bethe developed formulas for nuclear scattering using the theory of the effective range. In a second paper[2] (quoted as **BL**) Bethe and Longmire applied the effective range theory to the photodisintegration of the deuteron. Throughout this paper we use, wherever possible, the same notation as in these references. In these two papers and in a paper[3] (quoted as **BJ**) by Blatt and Jackson it was shown that the effect of the shape of the nuclear potential on the various quantities which can be calculated from experiments is small; these effects were masked completely by the experimental inaccuracies in the results available at that time. In the meantime, many of the relevant experimental determinations have been repeated with greatly increased accuracy; notably the measurements of the deuteron binding energy, the coherent neutron–proton scattering amplitude, and the neutron–proton scattering cross section for neutron energies up to 5 Mev. It therefore seemed worthwhile to calculate the deviations from the simple formulas obtained on the effective range theory (quoted as *ERT*) for the various potential shapes.

In this paper we derive formulas for the evaluation of the effective singlet range r_{0s} for a neutron–proton potential of Yukawa, exponential-well, and square-well shape from two independent experimental measurements: (i) neutron–proton scattering cross sections for neutron energies up to 5 Mev. (ii) Cross section for the capture of slow neutrons by protons. We also derive expressions for the photomagnetic and photoelectric disintegration cross sections of the deuteron, for γ-rays of "classical" energies, for the potential shapes mentioned above.

[1] H. A. Bethe, Phys. Rev. **76**, 38 (1949), to be referred to as **B**.
[2] H. A. Bethe and C. Longmire, Phys. Rev. **77**, 647 (1950), to be referred to as **BL**.
[3] J. M. Blatt and J. D. Jackson, Phys. Rev. **76**, 18 (1949), to be referred to as **BJ**.

There are now at least three different accurate determinations of the deuteron binding energy ϵ which agree fairly well with each other. The corrected value obtained by Bell and Elliot,[4] by direct energy measurement of the γ-rays from the n–p capture reaction, is

$$\epsilon = (2.230 \pm 0.007) \text{ Mev}. \quad (1)$$

A direct determination of the threshold energy for photodisintegration by Mobley and Laubenstein,[5] using γ-rays obtained from an electrostatic generator, gives

$$\epsilon = (2.226 \pm 0.003) \text{ Mev}. \quad (2)$$

The accurate value for the neutron-proton mass difference obtained by Taschek *et al.*[6] using the $H^3(p,n)He^3$ reaction agrees fairly well now with the values from other nuclear cycles.[7] We take

$$n - H = (0.782 \pm 0.002) \text{ Mev}. \quad (3a)$$

Using the mass spectrographic result of Roberts and Nier[8]

$$2H - D = (1.442 \pm 0.005) \text{ Mev}, \quad (3b)$$

we obtain a third, accurate although indirect, value for the deuteron binding energy

$$\epsilon = (2.224 \pm 0.006) \text{ Mev}. \quad (3c)$$

The calculations throughout this paper are based on a value of

$$\epsilon = 2.227(1 \pm 0.0015) \text{ Mev} \quad (4)$$

(although 2.226 would probably be a better value now).

For the coherent scattering amplitude f, we use the accurate value obtained recently by Hughes *et al.*,[9] using the reflection of thermal neutrons from a liquid hydrocarbon mirror,

$$f = 2(\tfrac{3}{4}a_t + \tfrac{1}{4}a_s) = -3.76(1 \pm 0.008) \times 10^{-13} \text{ cm}. \quad (5)$$

For the scattering cross section σ_{free} of slow neutrons by free protons, we use the same value as that used in **B**, obtained by Melkonian,[10]

$$\sigma_{free} = \pi(3a_t^2 + a_s^2) = 20.36(1 \pm 0.005) \text{ barns} \quad (6)$$

The values chosen above give for the radius of the deuteron

$$1/\gamma = 4.314(1 \pm 0.0008) \times 10^{-13} \text{ cm}, \quad (7)$$

and for the two scattering lengths,

$$a_t = 5.388(1 \pm 0.0045) \times 10^{-13} \text{ cm}, \quad (8)$$

$$a_s = -23.68(1 \pm 0.0025) \times 10^{-13} \text{ cm}. \quad (9)$$

[4] R. E. Bell and L. G. Elliot, Phys. Rev. **79**, 282 (1950).
[5] R. C. Mobley and R. A. Laubenstein, Phys. Rev. **80**, 309 (1950).
[6] Taschek, Argo, Hemmendinger, and Jarvis, Phys. Rev. **76**, 325 (1940).
[7] Hornyak, Lauritsen, Morrison, and Fowler, Revs. Modern Phys. **22**, 291 (1950).
[8] T. R. Roberts and A. O. Nier, Phys. Rev. **77**, 746 (1950).
[9] Hughes, Burgy, and Ringo, Phys. Rev. **77**, 291 (1950); Phys. Rev. **79**, 227 (1950); and private communication.
[10] E. Melkonian, Phys. Rev. **76**, 1744 (1949).

TABLE I. $\rho_t(E_1, E_2)$ and b_t in 10^{-13} cm for three potential shapes; $\rho_t \equiv \rho_t(0, -\epsilon)$ being 1.720×10^{-13} cm.

	$\rho_t' = \rho_t(-\epsilon, -\epsilon)$	$r_{0t} = \rho_t(0, 0)$	$\rho_t(0, 5 \text{ Mev})$	b_t
Yukawa	1.787	1.653	1.578	2.99
Exponential	1.737	1.703	1.684	2.40
Square well	1.697	1.743	1.768	2.07

Equation (B, 19) gives for $\rho_t(0, -\epsilon)$ (which we shall simply denote by ρ_t)

$$\rho_t \equiv \rho_t(0, -\epsilon) = (1.720 \pm 0.035) \times 10^{-13} \text{ cm}. \quad (10)$$

The experimental errors in the measurements of σ_{free} and of f now contribute about equally to the stated probable error for ρ_t (and similarly for a_t and a_s); the uncertainty in ϵ contributes a much smaller error for ρ_t. The accuracy of the measurement[9] of f will probably be increased somewhat further in the near future.*

With the help of Eq. (B, 19) we have found a value (10) for ρ_t which is the same for all potential shapes. To determine the effective range $\rho_t(E_1, E_2)$ for other energies, we use the approximate formula [see Eq. (B, 33)]

$$\rho(E_1, E_2) = r_0 - 2Pr_0^3(k_1^2 + k_2^2). \quad (11)$$

The values of P, which depend on the shape and strength of the potential, were taken from the graphs and formulas of **BJ**. In Table I we give the values of r_{0t}, $\rho_t(-\epsilon, -\epsilon)$ (which we shall denote by ρ_t') and of $\rho_t(0, 5 \text{ Mev})$ for central triplet potentials of Yukawa well, exponential well, and square well shapes, respectively. The experimental errors of these numbers are practically the same as those of ρ_t and are now *smaller* than the differences between the values for the different potential shapes and also somewhat smaller than the dependence of ρ_t on the energy in the region considered. The effect of potential shape on the values for r_{0t} and for disintegration cross sections, which we shall derive in this paper, is largely due to the fact that ρ_t' or $\rho_t(0, E)$, and not ρ_t, occurs in some relevant formula.

In Table I we also give the values for the intrinsic triplet range b_t for the three different potential shapes considered. For the Yukawa potential the value of b_t corresponds to a value of the meson mass μ_t of

$$\mu_t = (274 \pm 12)m_e. \quad (12)$$

This is very close to the best experimental value[11] for the mass of the π-meson, $(276 \pm 6)m_e$, but this excellent agreement is almost certainly fortuitous.

II. NEUTRON-PROTON SCATTERING

The total cross section $\sigma_{tot}(E)$ for the scattering of neutrons of energy E Mev (wave number k) by sta-

* *Note added in proof:*—A more recent value of $-(3.78 \pm 0.02) \times 10^{-13}$ cm for f would give a value of $(1.704 \pm 0.030) \times 10^{-13}$ cm for ρ_t.

[11] Smith, Barkas, Bishop, Bradner, and Gardner, Phys. Rev. **78**, 86 (1950).

TABLE II. r_{0s} obtained from total n–p scattering cross sections σ_{tot} for a neutron energy of 5.000 Mev.

σ_{tot} (in barns)	r_{0s} (in 10^{-13} cm) for ERT	Yuk.	Exp.	Sq. well	Error in r_{0s}
1.6487	2.00	1.55	1.90	2.11	±0.20
1.6290	2.50	2.11	2.41	2.58	±0.20
1.6086	3.00	2.66	2.92	3.04	±0.20

tionary protons is given by the expression

$$\sigma_{tot}(E)=3\pi\{k^2+[a_t^{-1}-\tfrac{1}{2}\rho_t(0,E)k^2]^2\}^{-1}+\pi\{k^2+[a_s^{-1}-\tfrac{1}{2}\rho_s(0,E)k^2]^2\}^{-1}. \quad (13)$$

The three constants ρ_t, a_t, and a_s are now known with sufficient accuracy so that a completely precise experimental value of $\sigma_{tot}(E)$ for E about 3 Mev or more would yield values of $\rho_s(0, E)$ uncertain by only about $(\pm 0.2)\times 10^{-13}$ cm for any given potential shape. In Table II we give values of r_{0s}, obtained by assuming certain values of σ_{tot} for E equal to 5 Mev and using Eqs. (11) and (13). It is seen that the different potential shapes yield values for r_{0s} which differ, for any given value of σ_{tot}, by considerably more than the uncertainty $(\pm 0.2)\times 10^{-13}$ cm which arises from the constants ρ_t, a_t, and a_s. We also give r_{0s} as calculated by means of the simpler formulas of the effective range theory (denoted by ERT) which involve putting P in Eq. (11) equal to zero both for the singlet and triplet states.

Williams *et al.*[12] have recently measured $\sigma_{tot}(E)$ for various energies E between 0 and 5 Mev. In Table III we give values of r_{0s} derived from these values of $\sigma_{tot}(E)$. The probable errors for r_{0s} quoted in Table II are now due almost exclusively to experimental errors in these "high energy" experiments; at 5 Mev the experimental uncertainty of σ_{tot} and of E contribute about equally, while at the lower energies the error is mainly in σ_{tot}. The mean values of r_{0s} for the different potential shapes differ from each other only by amounts small compared with the probable error; this is mainly due to the fact that the more accurate measurements of Williams *et al.*[12] were done for neutron energies of the order of magnitude of 1 Mev for which the effect of potential shape on the value of r_{0s} is much less marked than for energies of about 3 Mev or more.

TABLE III. Values of r_{0s} obtained from measurements of the total n–p scattering cross section, by the Minnesota group, at various energies E.

E (in Mev)	σ_{tot}	r_{0s} (in 10^{-13} cm) for ERT	Yukawa	Exp.	Sq. well	Error (in 10^{-13} cm)
0.798	4.79	2.5_5	2.4_5	2.5_5	2.5_5	±1.0
1.078	4.09	2.4	2.3	2.3_5	2.4_5	±1.0
1.340	3.66	2.1_5	2.0	2.1	2.2	±1.0
1.578	3.32	2.5	2.3	2.4_5	2.5_5	±1.0
4.92	1.64	2.7	2.3	2.6	2.8	±1.5
4.97	1.56	4.3	4.3	4.3	4.2	±1.5
Weighted mean for r_{0s}		2.6	2.4_5	2.5_5	2.6_5	±0.5
b_s			2.2_5	2.4	2.5_5	±0.5

[12] Lampi, Freier, and Williams, Phys. Rev. **80**, 853 (1950).

In Table III we also give the values for the intrinsic singlet range b_s for the three potential shapes considered. For the Yukawa potential the value of the corresponding meson mass μ_s is

$$\mu_s=(365\pm 80)m_e. \quad (14)$$

For the exponential shape the intrinsic singlet and triplet ranges (and hence the radii of the singlet and triplet potentials) agree well. For the Yukawa and square well shapes, b_t and b_s differ (in opposite directions), but only by about the combined probable error of b_t and b_s.

III. PHOTOMAGNETIC CAPTURE

Let σ_H be the cross section for the photomagnetic capture of a slow neutron of velocity v by a stationary proton. We assume that a fraction ϵ_3 of the total cross section σ_H is due to the presence of a magnetic exchange moment (see below). The remainder of the cross section is then given by

$$\sigma_H v(1-\epsilon_3)=2\pi(e^2/Mc)(\hbar/Mc)(W_1/Mc^2)^{\frac{1}{2}}\times(\mu_P-\mu_N)^2[\gamma+\beta'-\gamma^2 D]^2/(1-\rho_t'\gamma)\beta'^2, \quad (15)$$

where $\rho_t'\equiv\rho_t(-\epsilon,-\epsilon)$ and the other symbols are as defined in **BL**. Equation (15) is the same as the approximate expression (**BL**, 47), except that ρ_t' has not been replaced by r_{0t} and D is the function defined in (**BL**, 25)

$$D=\int_0^\infty(\psi_s\psi_t-u_0u_s)dr. \quad (16)$$

For $\sigma_H v$ we take the value obtained from the experiments of Whitehouse and Graham,[13]

$$\sigma_H v=6.81\times 10^{-20}\ (\mathrm{cm^3/sec})(1+\epsilon_4). \quad (17)$$

In **BL** the probable error, ϵ_4, in the measurement[13] of $\sigma_H v$ was taken to be ±0.04 and the measurement agrees to within this accuracy with earlier results by Walker and Frisch.[14] On the other hand, Halban *et al.*[15] consider that the possibility of a somewhat larger error cannot be excluded. For γ, a_t, and a_s we use the values (7), (8), and (9), respectively, for ρ_t' the values given in Table I and for $(\mu_P-\mu_N)$ a value[16] of 4.706. The relation for D is then

$$D=\{[1.064+0.78\delta+6.8\epsilon_1+5.2\epsilon_2-0.92\epsilon_3]+[1-(1+\epsilon_4-\epsilon_3)^{\frac{1}{2}}][4.04-0.8\delta-10\epsilon_1-6\epsilon_2-0.9\epsilon_3]\}, \quad (18)$$

where

$$\delta\equiv\rho_t'-\rho_t \quad (19)$$

and ϵ_1, ϵ_2, ϵ_3 are as defined in **B**.

[13] W. J. Whitehouse and G. A. R. Graham, Can. J. Research **A25**, 261 (1947).
[14] R. L. Walker, MDDC—414, unpublished.
[15] G. R. Bishop *et al.*, Phys. Rev. **80**, 211 (1950); **81**, 219 (1951).
[16] J. E. Mack, Revs. Modern Phys. **22**, 64 (1950).

Some calculations have been carried out, and more are in progress by Austern and Sachs[17] and by Gray[18] to relate the contribution of magnetic exchange moments to n–p capture, ϵ_s, to the experimentally known value of the exchange moment in the ground state of H^3 and He^3 on a general phenomenological theory. After adjusting the parameters of such a theory to give the correct value for the H^3 exchange moment, the value obtained for ϵ_s still depends to some extent on (a) the shape of the wave functions for the deuteron and for the triton and hence on the shape of the neutron-proton potential; (b) a distribution function $\Phi(\rho)$. This function $\Phi(\rho)$ enters in all calculations concerning exchange magnetic moments and is not known theoretically unless a specific meson theory is used. Austern and Sachs[17] have shown that, for specific deuteron and triton wave functions, the value obtained for ϵ_s does not depend very much on the actual shape of $\Phi(\rho)$ as long as $\Phi(\rho)$ is appreciable only for $\rho<2\times10^{-13}$ cm, and ϵ_s is then approximately $(+0.04)$. If $\Phi(\rho)$ has a "longer tail," larger values are obtained for ϵ_s, but it may be possible to get an upper limit for the size of the "tail" of $\Phi(\rho)$ for $\rho>2\times10^{-13}$ cm from other considerations (see Sec V). Separate values are being calculated by Gray[18] for ϵ_s for various potential shapes, making some reasonable assumptions about $\Phi(\rho)$, and using consistent pairs of triton and deuteron wave functions corresponding to the same potential.

Because of the present uncertainties both in ϵ_t and ϵ_s, we give values obtained for D for various values of $(\epsilon_t-\epsilon_s)$ in Table V, using (18) and the values obtained for δ for the three potential shapes from Table I.

To use the values obtained for D from Table V to calculate a value for r_{0s}, we still need an expression for D in terms of r_{0t} (or ρ_t) and of r_{0s}. In **BL** an approximation to such an expression is given (which we denote by ERT) which can be written in the following form

$$D=0.430+0.250r_{0s}+0.250(r_{0t}-1.72), \quad (20a)$$

where D, r_{0t}, and r_{0s} are all in units of 10^{-13} cm. The exact expression for D depends on r_{0t} and r_{0s} in a very complicated way, which is different for the different potential shapes, and moreover depends somewhat on the values of a_t and a_s. However, if a_t and a_s have values near those given in (8) and (9), if ρ_t lies between 1.5 and 2.0 and r_{0s} between 2 and 3 (ρ_t and r_{0s} again expressed in units of 10^{-13} cm), an approximate expression can be found for D, which is more accurate than (20a), in the form

$$D=a+br_{0s}+c(\rho_t-1.720)-d(\rho_t-1.720)r_{0s}. \quad (20)$$

The four coefficients a, b, c, and d were calculated, separately for each of the three potential shapes, by Mr. Newcomb by evaluacting D directly from the wave functions for two slightly different values of ρ_t and two different values of r_{0s} with a_t and a_s given by (8) and (9) in each case. For the square-well potential, D was calculated analytically, using exact wave functions, for values of ρ_t of 1.67 and 1.82 and for values of r_{0s} of 2.49 and 2.72. For the exponential potential, D was calculated by numerical integration, using exact wave functions, for values of ρ_t of 1.807 and 1.460 for which the bessel functions occuring in the wave functions are of order $\frac{1}{3}$ and $\frac{1}{4}$, respectively. The values used for r_{0s} were 2.0 and 2.7. For the Yukawa potential, the approximate wave functions (**BL**, 33c) and (**BL**, 34b), which are exact solutions for the Hulthén potential, were used, but for the constant P defined in (11), the value for the Yukawa potential itself was used. The two values of ρ_t and the two values of r_{0s} used for the Yukawa potential were approximately the same as those used for the exponential potential. The values of a, b, c, and d thus calculated are given in Table IV.

Table IV. Values of the coefficients in Eq. (20) for three potential shapes.

	a	b	c	d
Yukawa (Hulthén)	0.686	0.146	0.57	0.09
Exponential	0.649	0.154	0.53	0.06
Square well	0.579	0.176	0.55	0.06

In Table V we give the values obtained for r_{0s}, using Eqs. (18) and (20), for various values of $(\epsilon_t-\epsilon_s)$. Present indications are for a large value of r_{0s}, of the order of magnitude of 3×10^{-13} cm, but in view of the present uncertainties both in ϵ_t and ϵ_s no reliable conclusions can as yet be derived. The presence of the tensor force in the deuteron problem has the effect, as was shown in **BL**, of increasing the values obtained for r_{0s} in this section by about 0.1×10^{-13} cm. It should be emphasized that the calculations in this section take account of magnetic exchange effects but are based on the assumption that there are no other relativistic effects which alter the magnetic moments of the neutron and proton in the deuterium nucleus appreciably.

IV. PHOTODISINTEGRATION AT MODERATE ENERGIES

In **BL** a simple approximation is derived for σ_s, the photoelectric disintegration cross section of the deuteron, for γ-rays of a few Mev energy. We assume that the proton–neutron potential is zero for a P-state. We can

Table V. Values of r_{0s} and of D (both in 10^{-13} cm) for n–p capture cross section σ_H given by $\sigma_H v=6.81(1+\epsilon_t)$ cm³/sec and with a fraction ϵ_s of this cross section due to magnetic exchange moments.

	D (in 10^{-13} cm) for				r_{0s} (in 10^{-13} cm) for			
$\epsilon_t-\epsilon_s$	ERT	Yuk.	Exp.	Sq. well	ERT	Yuk.	Exp.	Sq. well
−0.10	1.271	1.320	1.284	1.254	3.36	4.34	4.12	3.83
−0.05	1.166	1.217	1.179	1.148	2.95	3.64	3.45	3.22
0	1.064	1.116	1.077	1.046	2.54	2.94	2.79	2.66
+0.05	0.964	1.017	0.977	0.946	2.14	2.27	2.14	2.08
+0.10	0.867	0.922	0.881	0.848	1.75	1.62	1.51	1.53

[17] N. Austern and R. G. Sachs, Phys. Rev. **81**, 710 (1951).
[18] E. P. Gray, private communication.

then write this approximation in the form[18a]

$$\sigma_e=\sigma_{e0}/(1-\rho_t'\gamma), \tag{21}$$

where σ_{e0} is the theoretical cross section for zero range, given in Eq. (**BL**, 7). In **BL** the further approximation was made of neglecting the differences between ρ_t, ρ_t' and r_{0t}. In Table VI we give values for σ_e for various γ-ray energies calculated from Eq. (21) but with the value for ρ_t' taken from Table I for each of the potential shapes, separately.

The only error in expression (21) is due to having replaced the correct wave functions in the matrix element (**BL**, 1) by their asymptotic expression. We have estimated this error once more by computing the matrix element (**BL**, 1) directly by using either exact wave functions (for the square well) or approximate wave functions remaining accurate at small distances (for exponential and Yukawa). The calculation showed that, if the potential in the P-state is really zero, and if the γ-ray energy is near threshold, the approximate formula (21) is correct to about 0.03 percent for the square well and to about 0.1 percent for the exponential and Yukawa potential; for γ-rays of 4 or 5 Mev the equivalent errors are about 0.1 percent and 0.4 percent, respectively, and increase approximately with the square of the γ-ray energy. The values for σ_e calculated from (21) are given, without any corrections, in Table VI, for a γ-ray energy of 6.14 Mev although the values may be wrong by more than 1 percent at such high energies.

The correct expression for the *photomagnetic* cross section for disintegration of the deuteron, σ_m, by γ-rays of energy $(2.227+E)$ Mev involves the expression (16) for D where ψ_s and u_s now represent wave functions corresponding to an energy E. In general, therefore, the expression in terms of r_{0s} and ρ_t to be used for D will depend on E. Furthermore, the effect of the magnetic exchange moments on σ_m will, in general, vary with the energy E. However, it is probable that, for E small compared with the deuteron binding energy (which is the case for the Ga^{72}, ThC″, and Na^{24} γ-rays), the percentage of σ_m which is due to magnetic exchange moments is practically the same as that for zero energy ϵ_5. Similarly, Eq. (20), with the coefficients given in Table IV, should be a good approximation for D for such low values of E. We write for σ_m at an energy of E Mev (wave number k)

$$\sigma_m(E)=R(E)\times\sigma_{m0}(E), \tag{22}$$

where $\sigma_{m0}(E)$, the cross section for zero range, is given by the expression (**BL**, 56). Substituting the latest values for the constants in this expression we get, to an accuracy better than 0.2 percent,

$$\sigma_{m0}(E)=6.94\times10^{-28}\frac{E^{\frac{1}{2}}}{(E+2.227)(E+0.0739)}\ \text{cm}^2. \tag{23}$$

Making the above approximations then,[18b]

$$R(E)=R(0)[1+k^2(\tfrac{1}{2}r_{0s}-D)/(\gamma+\beta'-\gamma^2D)]\times[1+(\tfrac{1}{4}r_{0s}^2k^4+\beta'r_{0s}k^2)/(k^2+\beta'^2)]^{-1}, \tag{24a}$$

$$R(0)=[1-\gamma^2D/(\gamma+\beta')]^2\times(1-\rho_t'\gamma)^{-1}\times(1-\epsilon_5)^{-1}. \tag{24b}$$

$R(0)$, the value of $R(E)$ for zero energy, is equal to the ratio of the actual total magnetic capture cross section at zero energy to the theoretical expression for zero range of forces. We therefore have as an alternative to (24b),

$$R(0)=1.041(1+\epsilon_4)\{1-2.4\epsilon_1-0.8\epsilon_2-0.05\epsilon_3\}. \tag{25}$$

In Table VI we give values of σ_m, for the three potential shapes discussed, calculated with the help of Eqs. (22), (23), (24a), and (25) for some energies at which experimental results[15] are available. In (25) we have put ϵ_4 equal to zero and the values for D and r_{0s} used in (24a) are those obtained from Table V for $(\epsilon_4-\epsilon_5)$ equal to zero, since no very definite values are as yet available for ϵ_5 and since $(\epsilon_4-\epsilon_5)$ equal to zero gives values for r_{0s} in rough agreement with those obtained from n–p scattering. Because of the large uncertainty in ϵ_4 and ϵ_5 at the present time the values for σ_m in Table VI are not yet accurate enough for an accurate comparison with experimental results and are given mainly to show the dependence of the values on the potential shape. It is seen that the magnetic cross section is very nearly independent of the potential shape, mainly because it is tied to the capture cross section at low energies; the electric cross section varies by about 4 percent, this variation being due to the difference between ρ_t and ρ_t'. The uncertainty in the γ-ray energies contributes a probable error of about ±2 percent to σ_e, the uncertainty in ρ_t slightly less than ±2 percent. The probable error in σ_m is mainly due to the uncertainty in the capture cross section and is somewhat larger than ±5 percent. Values of σ_m are included for 6.14 Mev γ-rays, for the sake of comparison, also calculated using the above formulas, which are probably not good approximations at such high energies.

The theoretical formulas derived in this paper for the case of a Yukawa potential are of course not quite as accurate as the results of Hansson and Hulthén,[19] who perform more direct calculations using very good approximations for the neutron-proton wave functions. However, the differences between the numerical values for σ_m, etc., obtained in this paper and in that of

[18a] It has been brought to our attention that H. Hall [Revs. Modern Phys. 8, 358 (1936)] was the first to recognize the main feature of Eq. (21), namely, that the photoelectric cross section depends on the range of the forces only through the normalization of the ground state, and that this dependence is similar to the dependence of the elastic triplet cross section on range.

[18b] In the equivalent expression to (24a) in reference **BL**, (**BL**, 55), the last factor was inadvertently omitted.

[19] I. F. E. Hansson and L. Hulthén, Phys. Rev. **76**, 1163 (1949); I. F. E. Hansson, Phys. Rev. **79**, 909 (1950).

TABLE VI. Photoelectric and photomagnetic cross sections, σ_e and σ_m, in 10^{-28} cm^2 for various γ-ray energies and potential shapes. (ϵ is taken to be 2.227 Mev.)

γ-ray	Ga^{72}		ThC''		Na^{24}		F+H	
Energy (Mev)	2.507		2.615		2.757		6.14	
	σ_e	σ_m	σ_e	σ_m	σ_e	σ_m	σ_e	σ_m
ERT	5.91	3.99	8.51	3.42	11.39	2.91	21.0	0.55
Yukawa	6.07	3.97	8.74	3.40	11.70	2.90	21.6	0.59
Exponential	5.95	3.98	8.57	3.41	11.47	2.91	21.2	0.59
Square well	5.86	3.99	8.43	3.42	11.29	2.92	20.8	0.58
Experimental	7.2±1	4.4±1	10.1±1.5	3.8±1	12.5±1	3.3±0.5	20.9±1.5	0.6±1

Hansson and Hulthén,[19] are due mainly to the fact that Hansson and Hulthén assume the triplet and singlet intrinsic ranges to be the same (whereas in this paper the singlet and triplet ranges are determined separately from experiments) and to a much smaller extent (at least for low enough values of E) to the inaccuracy of the formulas of this paper.

In Table VII we give some of the experimental results for $(\sigma_m+\sigma_e)$ and for σ_m/σ_e available at present. Values for σ_e and σ_m are given in Table VI, using as experimental values for $(\sigma_m+\sigma_e)$ and σ_m/σ_e the weighted means of the appropriate values in Table VII. The four results quoted for σ_m/σ_e for the Na^{24} γ-ray do not all lie within each others stated experimental errors. Dr. W. M. Woodward advised us that an evaluation of the relative accuracies of these experimental results is rather difficult and hence their unweighted arithmetic mean was taken. The accuracies of these "experimental" values for σ_e and σ_m are now considerably less than of the equivalent "theoretical" values, but further experiments are in progress. For the three lower energies considered, all experimental cross sections appear to be higher than the theoretical ones, but the discrepancies are slightly less than the experimental errors at present.

V. DISCUSSION

We have seen in the foregoing sections that two independent methods are now available for the determination of the singlet effective range r_{0s} from experiment; the one method being based on precision measurements of the neutron–proton scattering cross sections for neutron energies up to 5 Mev, the other on precision measurements of the neutron–proton capture cross section at very low neutron velocities. We have also seen that the values obtained for r_{0s} from each of these two experiments depend somewhat on the shape of the neutron–proton potential. A given value for the scattering cross section for neutron energies of 3 to 5 Mev leads to a value for r_{0s} about 0.4×10^{-13} cm *larger* for a square-well potential than for a Yukawa potential, with an intermediate value for an exponential potential. A given value of the neutron–proton capture cross section, on the other hand, leads to a value for r_{0s} about 0.3×10^{-13} cm *smaller* for a square-well than for a Yukawa potential, the value for an exponential potential being again intermediate. The errors in r_{0s} due to to the experimental inaccuracies in ρ_t, a_t, and a_s at the present time are only about $(\pm0.2)\times10^{-13}$ cm for the determination from the scattering cross section and about $(\pm0.1)\times10^{-13}$ cm for that from the capture cross section. Furthermore, these errors in r_{0s} are in the same direction for the two determinations, and these errors will probably be reduced further later this year when the coherent scattering length will be remeasured.[9]

Since the difference in r_{0s} for "long tailed" and "short tailed" potentials are in opposite directions for the two different methods, we have, in principle, a way for estimating the shape of the neutron–proton potential. That is, we merely have to see for which of the three potential shapes discussed in this paper the two values for r_{0s}, obtained by the two methods, are in closest agreement. This, of course, would not determine the actual dependence of the neutron–proton potential on distance, but it would at least give a rough measure of the extent to which the potential is "long tailed" or "short tailed." This method gives a considerably more sensitive test for potential shape than an attempt to determine the variation of $\rho_t(0, E)$ with energy directly from neutron–proton scattering cross sections at different energies, since the corresponding variations of cross sections are still very small compared with the experimental errors. At present, the values of r_{0s} agree

TABLE VII. Experimental values for the total photodisintegration cross section σ_{tot} (in 10^{-28} cm^2) and for the ratio, σ_m/σ_e, of the magnetic to the electric cross section.

γ-ray	Ga^{72}	ThC''	Na^{24}	F+H
Energy (Mev)	2.507	2.615	2.757	6.14
$\sigma_{tot}\times(10^{28}$ cm$^{-2})$	(11.9±0.8)[a] (10.6± ?)[b]	(13.9±0.6)[a]	(15.9±0.6)[a] (14.3±1.5)[b] (17.2±1.5)[d]	(21.5±1.2)[a]
σ_m/σ_e	(0.61±0.14)[c]	(0.37±0.12)[b]	0.20[e], 0.27[f] 0.32[f], 0.26[f]	(0.03±0.06)[h]

[a] See reference 15 (1950).
[b] Snell, Barker, and Sternberg, Phys. Rev. **80**, 637 (1950).
[c] See reference 15 (1951).
[d] Shinohara *et al.*, J. Phys. Soc. (Japan), **4**, 77 (1949).
[e] C. A. Barnes *et al.*, Nature **165**, 69 (1950).
[f] G. A. R. Graham and H. Halban, Revs. Modern Phys. **17**, 297 (1945).
[g] F. Genevese, Phys. Rev. **76**, 1288 (1949) (with corrections calculated by W. M. Woodward).
[h] Hammermesh and Wattenberg, Phys. Rev. **76**, 1408 (1949) (corrected).
[i] E. P. Meiners, Phys. Rev. **76**, 259 (1949).
[j] N. O. Lassen, Phys. Rev. **75**, 1099 (1949).
[k] P. V. C. Hough, thesis, Cornell 1950, unpublished.

best for a very short tailed potential (like the square well), but the present inaccuracies in both the scattering and capture cross sections are still somewhat too large to come to a definite conclusion about the potential shape. The following three improvements would suffice, at least for distinguishing between a very long tailed potential, like the Yukawa, and a very short tailed one, like the square well.

(1) Measurements of the neutron–proton scattering cross section would be needed at a few energies in the 3 to 5 Mev region. If each of these cross sections could be measured to an accuracy of about 1 percent and if the corresponding energies were also known to within 1 percent or better then r_{0s} would be known to within about $(\pm 0.3)\times 10^{-13}$ cm for each potential shape assumed. At these energies the value obtained for r_{0s} depends much more on potential shape than at lower energies. (2) The contribution to the neutron–proton capture cross section due to magnetic exchange moments would have to be known, theoretically, to within about 1 percent of the total cross section for each of the potential shapes considered. Calculations to this accuracy may be completed soon. (3) The ratio of the capture cross section of neutrons by hydrogen to that by boron would have to be remeasured, as well as the absolute value of the boron cross section. An accuracy of 1 or 2 percent in the neutron–proton capture cross section would give an error in r_{0s} of only about $(\pm 0.2)\times 10^{-13}$ cm.

The arguments in this section are, of course, based on the assumption that there are no very strong relativistic effects which alter the magnetic properties of bound neutrons and protons. Even if such effects are present there is at least some hope that their neglect will be compensated, to a large extent, by the semi-empirical treatment of "exchange moments" discussed above. It has been shown[20] that, at low enough energies, the effects of tensor forces are similar to those of an "equivalent central potential." No detailed calculations have as yet been done, but it seems likely that the presence of tensor forces does not appreciably alter the results obtained in this paper, except that the value obtained for r_{0s} from the n–p capture cross section is increased by about 0.1×10^{-13} cm (and that any conclusions about potential shape now refer to the total equivalent central potential).

Another way of relating the shape of the neutron–proton potential to a property of nuclear magnetic moments is offered by a study of the hyperfine structure of hydrogen and deuterium. The ratio of the hyperfine structure separation has recently been measured very accurately by Prodell and Kusch.[21] These measurements, together with the latest value of the ratio of the magnetic moment of the deuteron to that of the proton,[22] gives the very accurate value of

$$\Delta \equiv 1-\left[\frac{(\nu_H/\nu_D)_{exp}}{(\nu_H/\nu_D)_{theor}}\right]=(1.703\pm 0.007)\times 10^{-4}, \quad (26)$$

where $(\nu_H/\nu_D)_{theor}$ is the theoretical result obtained on the assumption that the nucleus of deuterium, as well as of hydrogen, is a point particle without any structure. Low[23] has made a detailed study of the value which can be derived for Δ from our present knowledge of nuclear forces. Using the more accurate values quoted in this paper for r_{0t}, Low's result can be written in the form

$$\Delta=(1.88+\epsilon_6+\epsilon_7+\epsilon_8)\times 10^{-4}. \quad (27)$$

Here ϵ_6 is a term which depends on the shape of the neutron–proton potential and can be calculated fairly accurately for each of the potential shapes commonly discussed. For a short tailed potential ϵ_6 is of the order of magnitude of $(+0.15)$, for a long tailed potential (-0.15). Any finite spread of the magnetic moment of a bare neutron or a bare proton (or at least of the "anomalous" part of the proton moment) gives a negative value for ϵ_7. This value[24] is roughly proportional to the radius up to which the proton moment is spread out, and for a radius of 1×10^{-13} cm, ϵ_7 is of the order of magnitude of (-0.4). The remaining inaccuracies in the calculation and uncertainties in the theory contribute the term ϵ_8, which is somewhat smaller than (± 0.1). Using (26) and (27) we have

$$\epsilon_6+\epsilon_7=-0.18\pm 0.08. \quad (28)$$

We therefore have a means for finding an estimate of the spread of the magnetic moment of a bare proton corresponding to each shape we might consider for the neutron–proton potential. It might in turn be possible to find a relation between this spread of the moment of a bare nucleon with the distribution function[17] $\Phi(\rho)$ for the exchange moment between two nucleons; such a relation might be less sensitive to the exact nature of the theory used than the results obtained for either quantity.

The author wishes to thank Professor H. A. Bethe for his advice on all aspects of this paper and Mr. W. A. Newcomb for deriving Eq. (20) and Table IV and for help with the numerical work involved in this paper. I am also grateful to Professors J. Blatt, W. A. Fowler, P. Morrison, J. H. Williams, and W. M. Woodward and to Drs. E. P. Gray, H. Halban, D. J. Hughes, L. Hulthén, and R. C. Mobley for valuable discussions or communications.

[20] R. S. Christian and E. W. Hart, Phys. Rev. **77**, 441 (1950); H. A. Bethe (unpublished work).
[21] A. G. Prodell and P. Kusch, Phys. Rev. **79**, 1009 (1950).
[22] Smaller, Yasaitis, and Anderson, Phys. Rev. **80**, 137 (1950).
[23] F. Low, Phys. Rev. **77**, 361 (1950).
[24] A. Bohr, Phys. Rev. **73**, 1109 (1948).

Activation Cross Sections Measured with Antimony-Beryllium Photoneutrons

VIRGINIA HUMMEL AND BERNARD HAMERMESH
Argonne National Laboratory, Chicago, Illinois
(Received December 6, 1950)

Activation cross sections for 15 isotopes have been measured by means of an antimony-beryllium photoneutron source. The cross sections have been determined relative to the values of the thermal neutron activation cross sections of each substance.

I. INTRODUCTION

PHOTONEUTRON sources[1] which will yield a sufficient number of neutrons for activation cross-section measurements will degrade the neutron energies sufficiently to cause a spread of 20 to 25 percent in energy. An electrostatic accelerator using the $Li^7(p,n)Be^7$ reaction to yield[2,3] 35-kev neutrons at 120° from a 10-kev thick lithium target, would give nearly the same spread over a cone of only 5° half-angle. Therefore, at 35 kev, the Sb—Be source competes favorably with an electrostatic accelerator as a neutron source for activation cross-section measurements. In addition, a photoneutron source used in this manner frees the accelerator for use in other experiments. For these reasons a program of activation cross-section measurements with Sb—Be photoneutrons has been undertaken.

II. METHOD

Figure 1 shows the details of the neutron source and foil holder. The aluminum cylinder containing 98 grams of fused antimony was irradiated in the Argonne heavy water pile. After removal from the pile, the source was allowed to cool for two weeks before any measurements were made. The only antimony activity that was important after this length of time was the one from 60-day Sb^{124}.

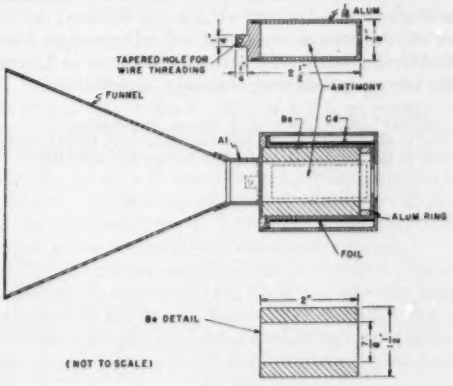

FIG. 1. Sb—Be photoneutron source.

The strength of the neutron source was measured by comparison with a Ra-Be standard by the method described by Hughes.[4] The source yielded 1.5×10^7 neutrons/sec one month after the pile irradiation was ended. The gamma-ray strength was about 8 curies at this time.

The flux from the source varied over the surface of the beryllium. An average flux over the cylindrical surface was determined in the following manner.

A rectangular indium foil placed on the source in the usual foil position shown in the figure was irradiated and then counted. Then an indium disk of the same thickness and covered with cadmium was placed over the flat end of the photoneutron source. The disk was then irradiated and counted. By comparing the saturated activities of the rectangle and the disk of indium, the ratio of the average flux on the two surfaces could be found. It was then assumed that the flux through the cylindrical surface was uniform over this surface and that the fluxes through the flat ends of the source were equal to each other and were also constant over the flat surfaces. With these assumptions, and the measured average flux ratio, an average flux over the region where the foils were irradiated could be calculated.

The irradiations were made outdoors to minimize the number of room scattered neutrons. The apparatus was suspended from a tall tree with the mouth of the funnel pointing upwards. The antimony was raised out of the lead pot in which it was stored and was lowered into the funnel. The whole apparatus was then raised to a height of nearly fifteen feet from the ground. After the irradiation was completed, the antimony was again separated from the beryllium, and the foil was then removed and counted with an efficiency which had been previously determined, as follows.

The counting system was calibrated for each substance in terms of the known[5] thermal neutron activation cross section for the substance. The same foil that was used in the Sb—Be activation was used for calibration purposes, so that the geometrical and absorption effects on the counting efficiency were the same.

The foil and a standard gold foil were irradiated in a

[1] A. Wattenberg, *Photoneutron Sources*, Preliminary Report No. 6, Nuclear Science Series, Division of Mathematics and Physical Sciences, National Research Council.
[2] The energy of the Sb—Be neutrons is still in doubt. See reference 1. Values of 25–35 kev are reported.
[3] Roberts, Hill, and McCammon, Phys. Rev. **80**, 9 (1950).
[4] D. J. Hughes, Nucleonics **6**, 50 (1950).
[5] Seren, Friedlander, and Turkel, Phys. Rev. **72**, 888 (1947).

beam from the thermal column of the Argonne uranium-graphite pile. The gold foil was counted in a counting system that had been standardized. The foil of the substance under study was counted in the experimental counting system. The irradiation was then repeated with cadmium-covered foils. The gold foil measurements allowed one to determine the value of the thermal flux and the measurements on the substance yielded a counting rate due to the thermal neutron activation. By using the value of the known thermal cross section of the substance, the counting efficiency could be found.

In most cases, the materials to be studied were in the form of metal foils. In those instances in which this was not feasible, samples of a powdered salt of the element were prepared as follows.

A backing for the powder was made by bending a sheet of nickel into a cylinder of approximately the same radius as the Geiger counter to be used to detect the activity. This cylinder, of 7.5-cm circumference and 5.5-cm height, was cut, parallel to the axis, into four equal sections.

A known amount of the powder to be studied was then placed on each section, and thoroughly mixed with dilute zapon. The zapon-powder mixture was spread as evenly as possible over one surface of the nickel and allowed to dry. When thoroughly dry, each section was wrapped in wide Scotch Tape to protect the powder surface. The four sections were then mounted on a Scotch Tape backing, which acted as a hinge. This allowed the holder to fit around the counter, the Sb—Be source, or on a flat surface for irradiation at the thermal column of the Argonne uranium-graphite pile.

III. RESULTS

Table I lists the isotopes studied, together with the half-life of the isotope that is formed by the neutron capture, and the results obtained for the natural atom cross section for the reaction at the energy of the Sb—Be neutrons.

The last column of Table I lists the percent error of the measurements, relative to the values given by Seren for the thermal cross section.

TABLE I. Natural atom cross sections for Sb—Be neutrons.

Item	Natural isotope	Half-life of $(A+1)$ isotope	Natural atom cross section (millibarns)	Percent error
1	$_{13}Al^{27}$	2.4 min	1.6	25
2	$_{23}V^{51}$	3.9 min	59	15
3	$_{25}Mn^{55}$	2.59 hr	78	12
4	$_{29}Cu^{65}$	5 min	20	20
5	$_{30}Zn^{68}$	57 min	6.1	20
6	$_{33}As^{75}$	26.8 hr	1.2×10^{3}	20
7	$_{42}Mo^{100}$	14 min	57	30
8	$_{45}Rh^{103}$	4.2 min	2.0×10^{2}	15
9	$_{46}Pd^{108}$	13 hr	3.6×10^{2}	25
10	$_{47}Ag^{107}$	2.3 min	1.1×10^{3}	17
11	$_{49}In^{115}$	54 min	1.0×10^{3}	10
12	$_{51}Sb^{121}$	2.8 day	1.6×10^{3}	20
13	$_{53}I^{127}$	25 min	2.2×10^{3}	20
14	$_{78}Pt^{196}$	31 min	20	10
15	$_{79}Au^{197}$	2.7 day	1.5×10^{3}	15

These errors result from uncertainties in the strength of the standard radium-beryllium source used to calibrate the antimony-beryllium source, from errors in the calibration of the standard counters on which the gold foils were counted, from small variations in geometry in counting the foils and in irradiating them, and from counting statistics. Errors in the half-lives of the isotopes were not considered.

IV. DISCUSSION

Only two of the measurements could be compared with other data that have been obtained on cross sections at this energy. The value obtained for gold is in excellent agreement with that reported by the Los Alamos group.[6] The cross section obtained for aluminum is considerably lower than that given by Henkel and Barschall.[7] The cross sections obtained with Sb—Be neutrons were compared with those published by Beghian and Halban[8] at 200 and 900 kev. As expected, the cross sections obtained with neutrons from the Sb—Be source were generally found to be higher. The two exceptions were aluminum and platinum.

[6] MIDDC-286, edited by K. I. Griesen (unpublished).
[7] R. L. Henkel and H. H. Barschall, Phys. Rev. **80**, 145 (1950).
[8] L. E. Beghian and H. H. Halban, Nature **163**, 366 (1949).

The Inelastic Scattering of 15-Mev Neutrons by Lead, Iron, and Aluminum*

P. H. STELSON† AND CLARK GOODMAN
Department of Physics and Laboratory for Nuclear Science and Engineering, Massachusetts Institute of Technology, Cambridge, Massachusetts

(Received December 19, 1950)

A tritium-zirconium target bombarded by 1.0-Mev deuterons from the Rockefeller electrostatic generator was used as a source of high energy (~15-Mev) neutrons. This source was surrounded by lead, iron, and aluminum scatterers with dimensions of approximately one mean free path for inelastic scattering. The resulting neutron spectra were measured by means of proton recoils in photographic emulsions. An exposure without scatterer permitted an evaluation of the upper limit for the neutron background. The spectra indicate that most of the neutrons are inelastically scattered to energies below 3 Mev in the case of the lead and iron scatterers and to below 5 Mev with the aluminum scatterer. The data can be represented by a curve of the form (const $Ee^{-E/T}$) as predicted by the Weisskopf statistical theory. The values obtained for the nuclear temperatures, T, are 0.7, 0.6, and 1.1 Mev for lead, iron, and aluminum, respectively. The fact that the measured temperatures for iron and lead are approximately the same supports the hypothesis that lead nuclei have a closed shell structure and therefore have properties similar to much lighter nuclei.

I. INTRODUCTION

THE process of inelastic scattering of neutrons with energy large compared to the spacing of the low-lying levels of the target nucleus has been treated in a quantitative manner by Weisskopf.[1] According to Weisskopf's statistical theory, the energy distribution of the inelastically scattered neutrons is approximately maxwellian with a mean energy $2(aE_0)^{\frac{1}{2}}$, where E_0 is the kinetic energy of the incident neutrons and a is a parameter dependent on the nuclear structure. The quantity $(aE_0)^{\frac{1}{2}}$ is therefore analogous to a temperature, T, and is interpreted as the temperature of the excited residual nucleus. From the available data on nuclei, it was estimated that $a \cong 0.05$ to 0.2 Mev for heavy nuclei ($A > 100$). The theory predicted, therefore, that 10-Mev neutrons incident on heavy nuclei should be inelastically scattered to a mean energy of about 2 Mev.

The statistical theory for the emission of neutrons from highly excited nuclei does not depend on the method of excitation and is therefore also applicable to (p, n), (d, n), and (α, n), etc., reactions, provided the energies of the incident particles are large enough to allow a statistical interpretation. Gugelot[2] has carried out an extensive investigation of the neutron spectra resulting from (p, n) reactions with incident protons of 16 Mev. The resulting spectra are maxwellian as predicted by the theory, but the nuclear temperatures obtained are somewhat lower than those predicted.

There have been comparatively few inelastic neutron scattering experiments which permit an effective comparison with the theory. The work of Barschall, *et al.*,[3] and that of Dunlap and Little,[4] in which incident neutron energies of 3 Mev or less were employed, have been interpreted by Feld[5] in terms of the statistical theory and in terms of a detailed theory of individual levels applicable when only a few levels of the target nucleus are involved. He finds that the inelastic scattering of wolfram at incident neutron energies of 1.5 and 3.0 Mev does agree with the prediction of the statistical theory; the value deduced for a is 0.08 Mev. However, the data on iron and lead do not fit the statistical theory and are more readily interpreted in terms of the detailed level theory, thus indicating a large level spacing for these nuclei.

Recently, Gittings, Barschall, and Everhart[6] performed an experiment in which 14.5±0.5-Mev neutrons produced by the $H^3(d, n)He^4$ reaction using low energy deuterons were scattered by lead and the resulting spectrum measured by threshold detectors. Two threshold detectors were used: the $Al(n, p)$ reaction with a threshold[6a] of about 3 Mev, and the $Cu^{63}(n, 2n)$ reaction with a threshold of about 11 Mev. Their result, which depends on the values assigned to the cross sections for the threshold reactions, suggests that the inelastically scattered neutrons which are degraded in energy below the copper threshold are also degraded below the aluminum threshold, indicating that a 14.5-Mev neutron loses at least 11 Mev in its first inelastic collision.

This paper presents the results of an experiment in which the fast neutrons produced by the $H^3(d, n)He^4$ reaction are scattered by the elements lead, iron, and aluminum and the resulting spectra measured by means of proton recoils within photographic emulsions.

II. EXPERIMENTAL METHOD

A diagram of the experimental arrangement is shown in Fig. 1. The dimensions of the scatterers were chosen

* This work was supported by the ONR and the Bureau of Ships.
† AEC Predoctoral Fellow.
[1] V. F. Weisskopf, Phys. Rev. 52, 295 (1937).
[2] P. C. Gugelot, Phys. Rev. 81, 51 (1951).
[3] Barschall, Battat, Bright, Graves, Jorgensen, and Manley, Phys. Rev. 72, 881 (1947); Barschall, Manley, and Weisskopf, Phys. Rev. 72, 875 (1947).
[4] H. F. Dunlap and R. N. Little, Phys. Rev. 60, 693 (1941).
[5] B. T. Feld, Phys. Rev. 75, 1115 (1949).
[6] Gittings, Barschall, and Everhart, Phys. Rev. 75, 1610 (1949).
[6a] The "thresholds" for the $Al(n, p)$ and $Cu^{63}(n, 2n)$ are also quoted as 4.5 Mev and 12 Mev, respectively. The value depends on the definition; i.e., whether this is the energy required just to initiate the reaction or to give a practical yield. See R. M. Kiehn, Technical Report No. 40, Laboratory for Nuclear Science and Engineering, M.I.T. (May 5, 1950).

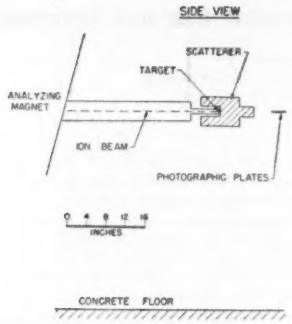

FIG. 1. Diagram, drawn to scale, of experimental arrangement used to measure the inelastic scattering of fast neutrons produced by the $H^3(d, n)He^4$ reaction.

to be approximately one mean free path for inelastic scattering λ_i of 15-Mev neutrons. Smaller dimensions reduce the ratio of the inelastically scattered neutron flux to the background neutron flux, while larger dimensions introduce distortion due to multiple inelastic scattering. Assuming $\lambda_i = 1/n\pi R^2$, where n is the number of nuclei per cm^3 and (the radius) $R = 1.4\times10^{-13}\,A^{\frac{1}{3}}$ cm, we obtain for Pb, Fe, and Al, $\lambda_i = 14$ cm, 13 cm, and 30 cm, respectively. Since $\lambda_i(\text{Pb}) \approx \lambda_i(\text{Fe}) \approx \lambda_i(\text{Al})/2$, the dimensions of the three scatterers were made identical in order to simplify geometrical considerations.

The fast neutrons from the $H^3(d, n)He^4$ reaction were produced by allowing 1.0-Mev deuterons from the Rockefeller electrostatic generator to strike a thick tritium target of the type described by Graves, *et al.*,[7] in which tritium gas is absorbed in a layer of zirconium metal on a wolfram backing. Since 1.0-Mev deuterons, the lowest energy deuterons for which an appreciable beam current could be obtained from the generator, were incident on a thick target and since the scatterers subtended a large solid angle, the incident neutrons had a considerable variation in energy. From a consideration of the variation of cross section with deuteron energy and the variation of neutron energy with emergent angle for the $H^3(d, n)He^4$ reaction,[8] it is estimated that with the scatterer arrangement used the neutron energy is about 15 Mev with a spread of approximately ± 1.5 Mev.

Eastman NTB emulsions of 200 microns thickness were used. In addition to exposures with the lead, iron, and aluminum scatterers, an exposure without a scatterer was made to obtain an evaluation of the neutron background. The four exposures were of the same duration (0.6 μamp-hr); and thus the spectra could be normalized in terms of the volume of emulsion measured. The background neutron flux is produced by (1) some of the deuteron beam striking objects within the generator system (sides of the accelerating tube, walls of the analyzing chamber, collimating slits, etc.) to produce (d, n) neutrons and (2) neutrons produced at the target and then scattered, elastically and inelastically, by the large nearby objects such as the concrete floor and the analyzing magnet. The (d, n) background is approximately the same with and without the scatterer; if anything, it is somewhat reduced with the scatterer present because of the partial shielding of the photographic plates by the scatterer. The more important background of scattered neutrons is appreciably different with and without scatterer, but it is difficult to estimate the change in the character of this background flux. Qualitative considerations indicate that the number of background proton recoil tracks is reduced with the scatterer present. The exposure made without a scatterer is therefore considered to be a measure of the upper limit of the background with a scatterer.

When the plates were measured, a given volume of the emulsion was carefully searched at 210× magnification and tracks within ten degrees of the forward direction were accepted for measurement. The acceptance angles and track lengths were measured at 950× with the exception of the very long tracks whose lengths were measured at 210×. The coordinates of the beginning of each track were used for identification to eliminate possible remeasurements. The range-energy relation used to convert proton recoil track lengths to neutron energies was obtained by measuring the $Li^7(p, n)Be^7$ spectrum at several proton bombarding energies and the $D(d, n)He^3$ and $F^{19}(d, n)Ne^{20}$ spectra at a single deuteron bombarding energy.[9] The correction resulting

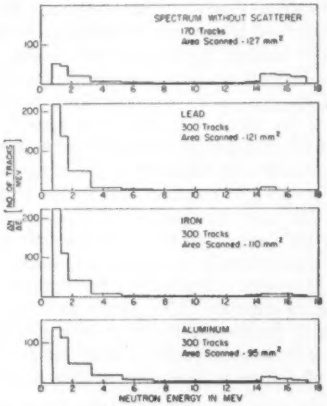

FIG. 2. Histograms of $\Delta N/\Delta E$ *vs* E, where N is the number of tracks and E is the neutron energy. The correction factors necessary to obtain relative neutron intensity have not been applied to these data. These factors result in a marked increase in the relative magnitude of high energy, primary neutron flux. A lower limit of $E_n = 0.75$ Mev was chosen in plotting the data.

[7] Graves, Rodriques, Goldblatt, and Meyer, Rev. Sci. Instr. **20**, 579 (1949).

[8] Hanson, Taschek, and Williams, Revs. Modern Phys. **21**, 635 (1949).

[9] P. H. Stelson, Ph.D. thesis, M.I.T. (1950), unpublished.

from the fact that the scatterer is an extended source was not applied to the data.

With a scanning magnification of 210×, the very short tracks ($E_n \lesssim 0.5$ Mev) tend to be overlooked because of the difficulty in distinguishing these tracks from the fog background. It is thought that the region above $E_n = 0.6$ Mev is not distorted by this effect; but, to insure its elimination, a lower limit of 0.75 Mev was chosen in plotting the data.

III. DISCUSSION

The data obtained are presented in Fig. 2 as histograms of $\Delta N/\Delta E$ *vs* E, where N denotes number of tracks and E is neutron energy. Two corrections must be applied to these data to obtain relative neutron intensity: the correction for the variation of the (n, p) collision cross section with energy and the correction for the different probability of leaving the emulsion for tracks of different length. The data were also normalized in terms of the volume of the emulsion measured. The corrected data are given in Fig. 3 as plots of ln [relative neutron intensity/neutron energy] *vs* neutron energy for the lower energy region, where the data are statistically significant. It is seen that the data are represented fairly well by straight lines; according to the statistical theory the negative reciprocal of the slope of these lines is equal to the nuclear temperature, T. The lines designated (1) are the data without the subtraction of the spectrum obtained without a scatterer, while the subtraction has been made for the lines designated (2). The nuclear temperatures calculated from these slopes are: for Pb, $T_1 = 0.8$ Mev, and $T_2 = 0.7$ Mev; for Fe, $T_1 = 0.7$ Mev, and $T_2 = 0.6$ Mev; and for Al, $T_1 = 1.2$ Mev, and $T_2 = 1.1$ Mev. It is seen that the subtraction of the spectrum obtained without a scatterer lowers the nuclear temperature in each case by 0.1 Mev, an amount which is within the statistical uncertainty of the measurements.

The high excitation energy used in the present experiment suggests that the $(n, 2n)$ process is important. The $(n, 2n)$ threshold, E_t, is equal to the (γ, n) threshold and this quantity has been measured for the Pb isotopes by Palevsky and Hanson[10] and for Al by McElhinney, *et al.*[11] The average value of E_t for the three principal Pb isotopes is 7.6 Mev, and the value of E_t for Al is 14.0 Mev. Unfortunately, a value for the (γ, n) threshold of the main iron isotope, Fe^{56}, has not been reported; a calculation of this threshold based on the semi-empirical mass formula gives a value of 11.6 Mev and is probably accurate to 1 Mev. The values for E_t indicate that the $(n, 2n)$ process is probably the principal mode of decay for lead and iron but is of less importance in the case of aluminum. The fact that a nucleus decays by the $(n, 2n)$ instead of (n, n') process complicates the interpretation of the measured nuclear

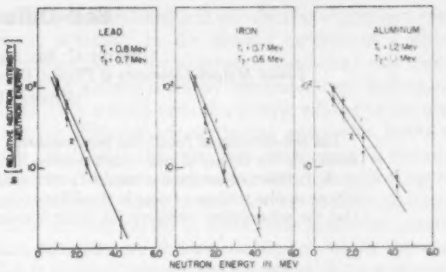

FIG. 3. Semilogarithmic plot of [relative neutron intensity/neutron energy] *vs* neutron energy. The negative reciprocal of the slope is the nuclear temperature, T.

temperature, T. The relatively large low-lying level spacing of Pb and Fe and the low average excitation energy available for the emission of the second neutron (~6.0 Mev for lead, ~2.0 Mev for iron) probably invalidates a statistical interpretation of the second neutron emission. One can state qualitatively that the $(n, 2n)$ process increases the number of lower energy neutrons and thus gives a somewhat lower value for the measured nuclear temperature and that, consequently, the quantity, a, calculated from the expression $T = (aE_0)^{\frac{1}{2}}$ is smaller than if the process were purely (n, n'), for which this formula was derived. The values of a obtained from this formula are 0.03, 0.02, and 0.08 Mev for lead, iron, and aluminum, respectively, where E_0 is taken to be 15 Mev and T is taken as T_2.

The nuclear temperature is related to the ratio of the level densities of the excited nucleus before and after emission of the neutron. The total excitation energy before emission of the neutron is equal to the kinetic energy of the incident neutron plus its binding energy which, for the present experiment, gives an initial excitation energy of about 22 to 23 Mev. The average excitation energy after the emission of the neutron is the kinetic energy of the incident neutron minus the average energy of the emitted neutron (~$2T$) which is about 13 to 14 Mev. This type of experiment therefore yields information on the ratio of level densities in nuclei at high excitation energies. It is of interest to note that lead, which has approximately four times as many nucleons as iron, has about the same nuclear temperature and hence about the same ratio of level densities at these excitation energies. This can be interpreted as additional support for the hypothesis that lead nuclei have a closed shell structure resulting in a relatively large level spacing characteristic of much lighter nuclei and that this property persists to rather high excitation energies.

The authors wish to thank W. M. Preston, T. T. Magel, H. B. Willard, J. J. McCue, and R. A. Peck, Jr. for their assistance. We also wish to thank Professors V. F. Weisskopf and B. T. Feld for helpful discussion and criticism.

[10] H. Palevsky and A. O. Hanson, Phys. Rev. **79**, 242(A) (1950).

[11] McElhinney, Hanson, Becker, Duffield, and Diven, Phys. Rev. **75**, 542 (1949).

Self-Diffusion in Cobalt*

FOSTER C. NIX AND FRANK E. JAUMOT, JR.
Randal Morgan Laboratory of Physics, University of Pennsylvania, Philadelphia, Pennsylvania
(Received December 4, 1950)

The self-diffusion of cobalt has been measured using radioactive Co^{60}. The radioactive Co^{60} was evaporated onto the surface of pure cobalt samples. The absorption coefficient in cobalt of the complex spectrum of the radioactive isotope was required in the mathematical analysis used. This was determined under conditions similar to those present in the diffusion samples. The data at 1050°C, 1150°C, and 1250°C, indicate that the self-diffusion coefficient for cobalt is given approximately by $D=0.37e^{-67000/RT}$ cm²-sec⁻¹.

I. INTRODUCTION

THE self-diffusion of metals is of great importance to both the physicist and the metallurgist. The physicist is concerned primarily with the mechanisms of the diffusion,[1] while the metallurgist[2] is primarily interested in the role which diffusion plays in such phenomena as recovery, recrystallization, creep, and sintering. Although much progress has been made in increasing our understanding of the mechanisms involved in diffusional phenomena, of which self-diffusion is the simplest, there still exists considerable doubt as to the relative role played by the presence of vacancies and interstitial atoms.[1] The experimental evidence to date does not lend support to the older concept of atomic interchange between neighboring atoms.

The present research dealing with the self-diffusion of cobalt was undertaken in order to obtain additional accurate experimental data with the hope of testing recent theories of metallic diffusion.

II. DESCRIPTION AND DISCUSSION OF PRESENT INVESTIGATION

Radioactive Co^{60}, which may be obtained from the Atomic Energy Commission[3] in the form of metallic wire, emits two gamma-spectra, one with an energy of 1.30 Mev, the other with an energy of 1.16 Mev, and a beta-spectrum of energy 0.31 Mev. The isotope has a half-life of 5.3 yr, which made it unnecessary to compare each measurement with a standard to allow for radioactive decay, since the time between counting any set of samples before and after diffusion did not exceed three days.

The radioactive cobalt was evaporated from a tungsten filament onto square samples of pure cobalt metal, $\frac{3}{8}''\times\frac{3}{8}''\times\frac{1}{8}''$, which had received a careful metallographical polish. The cobalt used for the samples was obtained in two purities, 99.06 percent cobalt in rondel form from African Metals Company, New York, New York, and 99.7 percent electrolytic cobalt in nodular form from Johnson-Matthey Company, England. The cobalt was melted in a hydrogen atmosphere in an induction furnace, cooled, and remelted with intermittent hydrogen flushing during melting, held at a temperature above the melting point for more than one hour in a vacuum to remove the majority of the adsorbed hydrogen, then cooled in a vacuum. After melting, both purity metals were of x-ray density within the limits of our measurements. No difference in the diffusion rates was obtained for the two different purities of cobalt. The evaporated radioactive layers were less than 0.05 micron in thickness and did not affect the appearance of the mirror surface. These layers were considered to be infinitely thin for calculational purposes.

The surface activity of the coated samples was determined by means of a standard commercial thin mica end window counter tube in conjunction with a scale of sixty-four counting circuit. The samples were placed in a specially built collimating device constructed of lead with an interchangeable base. The base had a socket into which the sample was a "slip fit." The collimating device fitted snugly into a standard counter tube holder. This arrangement allowed the geometry to be reproducible to within 0.005" in either direction, and the collimation reduced any edge effect to a minimum. The samples before diffusion displayed an activity of 7000 to 20,000 counts/min above background.

Two samples of nearly the same surface activity were placed with active faces together in a two piece Lavite "boat type" sample holder, and this placed in a refractory tube furnace, heated by a tubular Globar heating element. During the diffusion process the furnace was evacuated to a pressure of less than 10^{-5} mm Hg. The furnace temperature was controlled by a standard Leeds and Northrup two-point controller-recorder with both points being used in order to reduce the control time. The controllers operated on platinum, platinum-rhodium thermocouples placed in contact with the Lavite sample holder. Uncertainties in the temperature did not exceed 0.5 percent in most cases although they were as high as 2 percent in isolated cases. A certain error is introduced by the time taken to heat the samples and to cool them after diffusion, but this was minimized as far as the cooling was involved by the water-cooled

* This work was supported by the ONR.
[1] F. Seitz, Acta Crys. 3, 355 (1950).
[2] C. E. Birchenall and R. F. Mehl, Inst. Metals Div. 188, 144 (1950).
[3] U. S. Atomic Energy Commission, Isotopes Branch: Catalog and Price List No. 3 (July, 1949).

ends on the Globar element, and by an arrangement which allowed air to be forced past the furnace tube as well as the outside of the furnace using an ordinary blower fan. In no case did it take more than five minutes to reduce the temperature to 1000°C, or more than ten minutes to reduce the temperature to 800°C, below which diffusion proceeds very slowly. However, the error introduced by the time taken to bring the samples to the desired temperatures must be corrected for and this error is difficult to calculate exactly, although it is estimated not to exceed 1 percent.

After diffusion the activities of the samples were again determined, the counts now falling in the range 4000 to 17,000 counts/min above background.

Inasmuch as the samples were placed in the furnace in pairs to reduce the error due to evaporation from the surfaces, all calculations were based on the counts from a pair of samples, rather than from a single sample.

III. THEORY AND MEASUREMENT OF THE ABSORPTION COEFFICIENT

It has been shown by Steigman, Shockley, and Nix[4] that the diffusion constant, D, and the absorption coefficient, μ, can be related to the fraction, F, of the count remaining after diffusion, to a very good approximation by

$$F=e^{z}[1-P(\sqrt{z})], \tag{1}$$

where

$$P(\sqrt{z})=(2/\pi)\int_0^{\sqrt{z}}\exp(-y^2)dy, \tag{2}$$

$$z=\mu^2Dt. \tag{3}$$

The use of these equations assumes the sample to be thick compared with the depth of penetration of the diffusing atoms, which is certainly valid in the present investigation. Also, the use of expressions (1) and (3) requires that the measured activity decrease exponentially with absorber thickness to the depth of penetration of the diffusing atoms, or at least to the depth where contributions to the measured activity after diffusion will be small. This latter requirement of Eqs. (1) and (3) of course necessitates a very careful measurement of the absorption coefficient for very thin absorber thicknesses in the case of an isotope such as Co^{60} which has the three radiation spectra mentioned above. In this case it is not sufficient to employ the standard technique of using thin foils to measure this coefficient and then extrapolating to less thick materials since the logarithmic plot of μ against thickness is not a straight line from zero thickness to the thickness of the foils which we were able to obtain. Under similar circumstances Birchenall and Mehl[5] measured the absorption coefficient for aluminum, for which the mass coefficient for beta-rays is nearly the same as for iron, the metal under consideration. The contribution for x-rays was calculated and an effective absorption coefficient obtained. In the present experiment a direct determination of the absorption coefficient was made. This was accomplished by electroplating[6] radioactive cobalt onto a small area of a sample similar to the ones used for diffusion, electroplating successive layers of pure cobalt onto this, and then determining μ directly. Eighteen determinations were carried out, showing remarkable consistency. As a check on the method, cobalt was eventually plated to a thickness somewhat greater than the thinnest uniform cobalt foil which we were able to obtain. Although the absorption did not decrease exponentially to this thickness, 0.001", the curve obtained from the electroplated cobalt samples agreed with the curve obtained by using the foil to within 3 percent, after corrections for the difference in initial activity were made.

Since there are many sources of error in a determination of the absorption coefficient great accuracy cannot be claimed for the value. The value for μ^2 obtained by averaging the 18 values from the individual samples is probably no more than 10 percent in error and certainly within 15 percent.

The absorption curves obtained using this method were found to satisfy the condition imposed by Eqs. (1) and (3) to the depth of penetration of the diffusing atoms. Four typical curves obtained from samples of different initial activity are plotted in Fig. 1.

IV. RESULTS

Diffusion "runs" were carried out at three temperatures, 1050°C, 1150°C, and 1250°C for 18 hours. The diffusion constants, D, given in Table I were obtained by averaging the fractions, F, of all samples at a given temperature which did not show oxidation, reading z from a plot of F *vs* ln$z$ from Eq. (1), and calculating D from Eq. (3).

Table II gives A, the activation constant, and Q, the

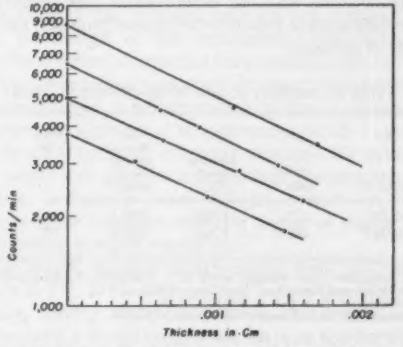

FIG. 1. Typical plots of counts per minute *versus* thickness of cobalt absorbing layer.

[4] Steigman, Shockley, and Nix, Phys. Rev. **56**, 13 (1939).

[5] Soderberg, Pinner, and Baker, *Modern Electroplating* (Journal of Electrochemical Society, 1942), pp. 145 ff.

TABLE I. Values of self-diffusion coefficient, D, for cobalt obtained using directly measured values of the absorption coefficient.

Temperature (deg. C)	μ^2 (cm^{-2})	D (cm^2-sec^{-1})
1050	2.68×10^{6}	3.22×10^{-12}
1150	2.68×10^{6}	1.78×10^{-11}
1250	2.68×10^{6}	9.18×10^{-11}

activation energy, as obtained from a plot of $\ln D$ against $1/T$, shown in Fig. 2. D, A, and Q are related by

$$D=Ae^{-Q/RT}. \tag{4}$$

The data lead to the self-diffusion constant for cobalt being represented approximately by

$$D=0.37e^{-67000/RT}\ \text{cm}^2\ \text{sec}^{-1}. \tag{5}$$

Table II also gives values for A and Q as obtained from the Langmuir-Dushman equation relating D and Q,

$$D=(Q/Nh)\delta^2e^{-Q/RT}, \tag{6}$$

where N is 6.06×10^{23} mole^{-1}, h is Planck's constant, and δ is the lattice constant for the face-centered cubic lattice, which is the stable phase at the diffusion temperatures.

V. DISCUSSION OF RESULTS

First, it should be noted that the agreement of the Q-value obtained from the Langmuir-Dushman equation with that found experimentally is probably fortuitous. It has been pointed out[6] that in the determination of Q by the Langmuir-Dushman equation the calculation is very insensitive to a change in the lattice constant, δ. More careful considerations of the mechanisms involved indicate the constant A should be of the order of $\delta^2\nu$, where ν is a lattice vibrational frequency not in general[7] equal to Q/Nh. Unfortunately, we know of no existing theoretical values of Q and A for comparison with our experimental data permitting us to differentiate between the various proposed mechanisms of diffusion.

TABLE II. Summary of data on self-diffusion in cobalt.

A (cm^2-sec^{-1})	Q (kcal-$mole^{-1}$)	T_m Melting point (°K)	E[a] Binding energy (kcal-$mole^{-1}$)	Q/T_m $\times10^2$	Q/E
0.37[b]	67[b]	1768	100.4	38	0.67
0.93[c]	69.6[c]	1768	100.4	39	0.69

[a] E computed from relations given in S. Dushman, *Vacuum Technique* (John Wiley and Sons, Inc., New York, 1949), p. 742.
[b] Determined from plot of $\ln D$ *vs* $1/T$ °K.
[c] Determined from Langmuir-Dushman equation.

[6] A. B. LeClaire, *Progress of Metals Physics* (Butterworth's Scientific Publications, London, 1949).
[7] J. Bardeen, private communication.

We have included in Table II the values of Q/T_m and Q/E, where T_m is the melting point in degrees Kelvin and E is the binding energy. The binding energy of a metal and its melting point are measures of the energy required to destroy the lattice, and since diffusion involves the escape of atoms from their proper lattice sites, the energy of activation should also be related to this energy. The values of Q/T_m and Q/E are approximately constant for most metals and the values we obtained for these ratios agree well with those given for other metals.[6] Owing to the uncertainty in the experimental values of Q, to date,† it has not been possible to say whether Q is more closely related[4,6] to E or T_m.

The errors in diffusion work are somewhat difficult to estimate with accuracy. As mentioned, the largest error is probably in the determination of μ^2, and is probably of the order of 10 to 15 percent. The error in the counting, including the statistical error, and the geometric effects, probably aggregate to 2 to 3 percent, and the error in the temperature and control to no more than 2 percent. Errors in the measurement of time are negligible. Thus the average uncertainty may be of the order of 15 percent for single points, but the error in the curve of $\ln D$ *vs* $1/T$ should be much less than this.

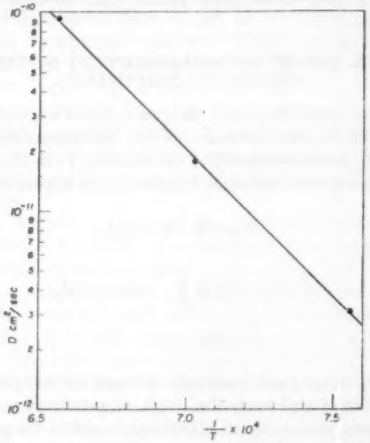

FIG. 2. Values of D *versus* $1/T$ °K.

† Since the writing of this article, G. J. Dienes [J. Appl. Phys. **21**, 1189 (1950)] has given an interesting empirical correlation between the activation constant A, which he calls the frequency factor, and the quantity Q/T_m. Dienes finds a correlation between these quantities by plotting $\log_{10}A/\nu\lambda^2$ *vs* $Q/2.303RT_m$, where λ is the interatomic distance and ν is the Debye frequency. Our data seem to lend support to the suggested correlation when plotted on Fig. 1 of Dienes' paper. Furthermore, a reasonable agreement with experiment, i.e., within an order of magnitude, is given for A when this quantity is computed from Eq. (2) of that paper.

Angular Yield of Deuterons and Alphas from the Proton Bombardment of Beryllium

J. A. NEUENDORFFER,* D. R. INGLIS,† AND S. S. HANNA
Department of Physics, Johns Hopkins University, Baltimore, Maryland‡
(Received November 13, 1950)

A photographic target chamber incorporating limited magnetic deflection of product particles was used to measure the angular yield of deuterons and alphas from the proton bombardment of beryllium at energies up to 1 Mev. The angular variation observed is of the form $1+A_1\cos\theta+A_2\cos^2\theta$, with relatively large values for A_1 indicating strong interference between states of the compound nucleus of opposite parity. The variation of the total cross sections with energy suggests the presence of a state of the compound nucleus at $E_p=0.68$ Mev, in addition to the states previously known at $E_p=0.33$ and 0.94 Mev. Range in emulsion vs energy measurements for the light nuclei observed in the reaction are also given.

I. INTRODUCTION

ENERGY levels in B^{10} have been studied by means of the $Be^9(d,n)B^{10*}$ and $Li^7(\alpha,n)B^{10*}$ reactions by several investigators.[1] In addition, levels in B^{10} above 6.5 Mev can be examined by means of the reactions produced by the proton bombardment of Be^9, in which B^{10} is formed as a compound nucleus:

$$\begin{aligned} &Be^9(p,\gamma)B^{10} \quad Q=6.49 \text{ Mev},\\ &Be^9(p,p)Be^9\\ &Be^9(p,d)Be^8 \quad Q=0.56 \text{ Mev},\\ &Be^9(p,\alpha)Li^8 \quad Q=2.12 \text{ Mev}. \end{aligned}$$

Measurements of the γ-ray yield[2] reveal resonances in the low energy range at 0.31, 0.67, 0.88, 1.00, and 1.09 Mev, indicating levels in B^{10} at 6.8, 7.1, 7.3, 7.4, and 7.5 Mev. Thomas, Rubin, Fowler, and Lauritsen[3] have measured the heavy particle yields at bombarding energies between 0.25 and 1.3 Mev and at a laboratory angle of 138°. The proton scattering cross section shows anomalies corresponding to the γ-ray resonances at 0.31, 1.00, and 1.09 Mev. The alpha- and deuteron yield curves are reproduced in Fig. 5. They both exhibit a strong resonance structure at 0.33 Mev and a considerably less pronounced structure in the region from 0.9 to 1.0 Mev. In addition, the deuteron yield shows a small anomaly at 0.47 Mev and appears to be rising toward a resonance above 1 Mev. It is possible that some of this structure in the differential cross section arises from interference effects and not from the presence of levels in the B^{10} nucleus. To investigate this question and to obtain information concerning the nature of the states involved, the variation of yield with angle has been studied for the alpha- and deuteron reactions.

II. METHOD AND PROCEDURE

In the method employed in observing the angular distributions, photographic plates were used as particle detectors. This choice makes it possible to observe the low energy particle groups in the target chamber vacuum, and the intensities can be recorded at several angles simultaneously.

In addition, it is necessary to identify reliably and rapidly the alphas, deuterons, and protons from the reaction. This cannot be done entirely by range in the emulsion alone, for the protons have approximately the same track length as do the alphas at the lower, and the deuterons at the higher bombarding energies. Appropriate photographic technique and careful analysis of track characteristics would facilitate the identification, but this was thought to be impracticable when thousands of tracks must be counted. Moreover, the protons, which are distributed approximately according to the Rutherford law, predominate and would almost completely mask the other particles at all but the most backward angles. For these reasons, limited magnetic deflections of the product particles was incorporated into the design of the experiment. The technique employed served to separate the scattered protons from the alphas and deuterons at all the energies investigated but contributed, to a lesser extent, to the discrimination between the alphas and the deuterons, which have approximately the same magnetic deflection for many of the angles and energies investigated. Electrostatic deflection, technically more difficult, would not have improved the situation over the range of angles and bombarding energies employed.

The target chamber incorporating these features is shown in Fig. 1. It was machined from a duraluminum casting, having an approximately semicircular cross section with a closed bottom and an open top for which an appropriate cover was provided. The iron pieces indicated in the diagram were shaped and arranged inside the chamber so as to provide seven radial gaps through which particles from the target could pass in

* Now with the Operations Evaluation Group, Office of the Chief of Naval Operations, Department of the Navy.
† Now at Argonne National Laboratory, Chicago, Illinois.
‡ Assisted by a contract with the AEC.
[1] O. Haxel and E. Stuhlinger, Z. Physik **114**, 178 (1939); T. W. Bonner and G. Brubaker, Phys. Rev. **50**, 308 (1936); H. Staub and W. E. Stephens, Phys. Rev. **55**, 131 (1939); Rasmussen, Hornyak, and Lauritsen, Phys. Rev. **76**, 581 (1949); Bonner, Butler, and Risser, Phys. Rev. **79**, 240 (1950).
[2] Herb, Kerst, and McKibben, Phys. Rev. **51**, 691 (1937); Curran, Dee, and Petrzilka, Proc. Roy. Soc. (London) **A169**, 269 (1939); W. J. Hushley, Phys. Rev. **67**, 34 (1945); Fowler, Lauritsen, and Lauritsen, Revs. Modern Phys. **20**, 236 (1948); S. Devons and M. G. N. Hine, Proc. Roy. Soc. (London) **A199**, 56 (1949).
[3] Thomas, Rubin, Fowler, and Lauritsen, Phys. Rev. **75**, 1612 (1949).

reaching the photographic plates. This internal iron constitutes the yoke of an external electromagnet of suitable design. The iron magnetic circuit is broken only by the walls of the chamber, there only $\frac{1}{4}$ in. thick, and the seven radial gaps, each approximately 0.15 in. wide. The target, a suspended beryllium foil either 15 or 30 microinches thick,[4] is mounted on a rod extending through a seal in the bottom of the chamber. The photographic plates are mounted on a platform which also can be raised and lowered from the outside, allowing several exposures to be made with one set of plates. The incident beam from the electrostatic accelerator arrives at the target through a tube passing through a hole in the iron yoke, and the beam is collimated by suitable apertures, the last of which is approximately 0.03 in.×0.06 in. Despite the smallness of this opening, which improves the resolution of the apparatus, adequate beam currents reached the target. Within each gap in the iron yoke several vertical baffles are placed to reduce scattering, and a single horizontal slit, about in the middle of the gap, completes the collimation of the product particles. The path followed by a typical particle through the magnetic field in a gap is illustrated in the cross section drawing in Fig. 1.

During most of the experimental runs, the target was set at an angle of about 55°, approximately midway between two of the gaps. To reduce the air gaps in the electromagnetic yoke, the width of each gap was adjusted to accommodate the varying projected target width as seen from the gap. This procedure restricts the settings of the target, however, and subsequent experience indicates that the precaution was not necessary. Fields up to at least 3000 gauss in each gap were readily obtainable, and this range proved to be more than adequate for the problem under investigation. Because all sections of the magnetic yoke within the vacuum were of the same thickness (1 in.), with no adequate provision for compensation for leakage flux, the deflecting field in the central gaps was somewhat weaker than in the forward and backward gaps.

Following an experimental run, in which the spectrum of the reaction is recorded photographically at each angle, the developed plates are viewed in a microscope. Particles having a given momentum and charge are observed within a well defined region or "plateau," the extent of which is determined by the size of the target spot and the collimating slits. Any portion of this region can receive particles from any portion of the

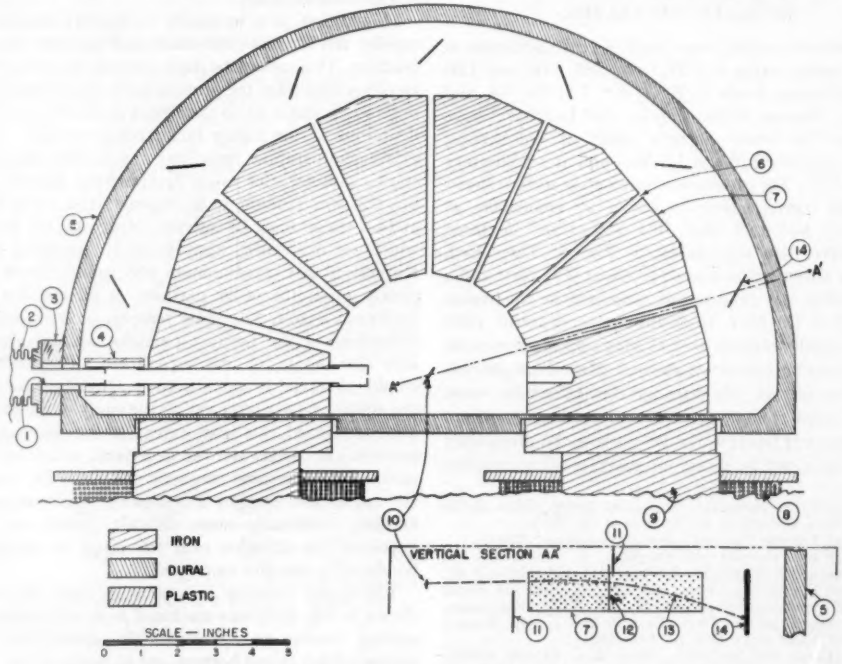

FIG. 1. Photographic chamber incorporating magnetic deflection. (1) Entrance tube; (2) Sylphon connection to accelerator; (3) Insulating washer; (4) Magnetic shield; (5) Chamber wall, 8 in. high; (6) Air gap in magnetic circuit; (7) Magnet pole piece; (8) Coil of electromagnet; (9) Core of electromagnet; (10) Target; (11) Shields; (12) Horizontal slit; (13) Typical particle path; (14) Nuclear plate.

[4] These foils were very generously supplied to us by Dr. Hugh Bradner of the University of California at Berkeley.

target spot. The shape of the plateau is that of a slightly skewed rectangle, since the collimated beam of rectangular cross section, after deflection in the magnetic field, is no longer horizontal when it strikes the plate set at 45°. Surrounding the plateau is a region of partial exposure, the extent of which depends on the particular geometry of the slit system.

The plates are analyzed by determining the extent of the plateau and measuring the particle density within it. Only two small geometric corrections need to be made to this density: an inverse square correction and an area correction, which are necessitated by slight irregularities in plate location and inclination in the target chamber. In principle, the particle density depends also on the deflection in the magnetic field. It was demonstrated that this effect is quite negligible when yields of a given particle are compared at different angles for which the deflections are approximately the same. The corrected densities are converted to the center-of-mass coordinate system,[5] and for convenience the yields are normalized to unity at the 90° angle in the center-of-mass system.

In addition to these routine corrections, several other questions required attention. It is well known that in traversing matter charged particles capture and lose electrons. In the range of energies encountered in this investigation the effect was appreciable only for the alpha-particles. Rutherford,[6] Henderson,[7] and Briggs[8] found that when alpha-particles traverse various kinds of matter, an equilibrium ratio is quickly established between the numbers of He^+ and He^{++} ions (the ratio depending on the alpha-energy and not significantly on the material traversed). In the present experiment, the alphas establish this equilibrium before leaving the target, and the subsequent passage through the magnetic field divides the beam into He^+ and He^{++} components. The He^+ ions are easily identified since they receive one-half of the deflection of the He^{++} ions, and they were counted on four different plates. The He^+ to He^{++} ratios thus determined were in agreement with the results of Henderson and of Briggs. The He^{++} yields on all of the plates were corrected accordingly, to give total alpha-yields, using the equilibrium curve of these authors.

Since the alpha-particles and deuterons receive approximately the same magnetic deflection at several angles and energies, identification was made by track length and appearance alone. It was felt that this was a reliable procedure, but in order to test its validity a series of plates was taken in which a 0.05-mil nickel foil was placed around the target. This foil served either to filter out the alphas completely or at least to separate them from the deuterons after magnetic deflection. Deuteron yields obtained in this manner agreed satisfactorily with those measured without a foil.

The most serious problem encountered in this work arose from the asymmetry introduced by the setting of the target. The effective target thickness for emergent

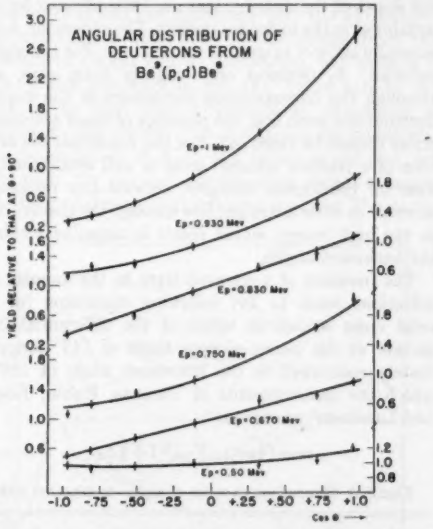

FIG. 2. Angular distributions in the center-of-mass system of the reaction $Be^9(p,d)Be^8$. Yields have been normalized to unity at 90°.

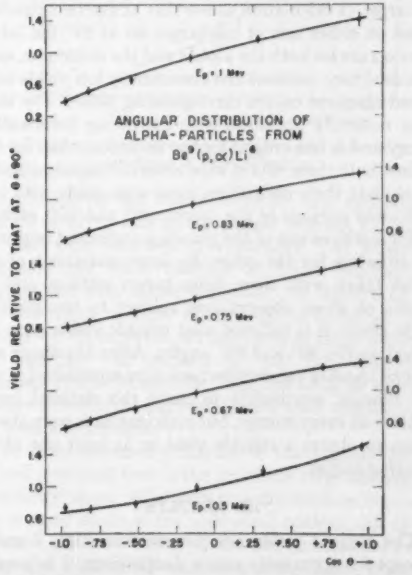

FIG. 3. Angular distributions in the center-of-mass system of the reaction $Be^9(p,\alpha)Li^6$. Yields have been normalized to unity at 90°.

[5] M. Moskow, Master's Thesis (Johns Hopkins University, 1948).
[6] E. Rutherford, Phil. Mag. 47, 277 (1924).
[7] G. H. Henderson, Proc. Roy. Soc. (London) A 109, 157 (1925).
[8] G. H. Briggs, Proc. Roy. Soc. (London) A 114, 341 (1927).

TABLE I. Coefficients in the expression

$$Y(\cos\theta) = Y(0)(1+A_1\cos\theta+A_2\cos^2\theta),$$

obtained from a least-square analysis of the angular yields. The values listed for $Y(0)$ were based on the measurements of Thomas, Rubin, Fowler, and Lauritsen at $\cos\theta = -0.80$. The values are 4π times the cross section in $cm^2 \times 10^{-27}$ per steradian.

	0.50 Mev	0.67 Mev	0.75 Mev	0.83 Mev	0.93 Mev	1.0 Mev
			Deuterons			
$Y(0)$	222	283	248	300	312	301
A_1	0.11	0.49	0.70	0.70	0.66	1.25
A_2	0.09	−0.06	0.25	0.02	0.21	0.52
			Alphas			
$Y(0)$	225	230	206	273	(354)	260
A_1	0.42	0.41	0.41	0.42		0.53
A_2	0.09	−0.09	0.01	−0.08		−0.11

particles varies with the angle of observation and becomes quite appreciable for the two glancing angles on either side of the target plane. For particles of low energy, originating at various depths within the target, this produces an appreciable spread in energy at these angles and a corresponding spread along the photographic plate. If this spread is smaller than the width of the plateau for monoenergetic particles, the effect is not serious and results chiefly in a narrowing of the plateau within which the particle density is to be computed. If, on the other hand, the spread exceeds the width of the "geometric plateau," a false plateau is created inside of which, at a given point, one observes only particles originating from a restricted layer within the target. A calculation shows that at the two glancing angles on either side of the target set at 55° the latter effect occurs for both the alphas and the deuterons, and, unsatisfactory plateaus and consistently low yields were indeed observed on the corresponding plates. The situation naturally improves with increasing bombarding energy and is less critical for the deuterons than for the alphas; both these effects were observed experimentally. To obviate these difficulties, runs were made with two additional settings of the target, 40° and 60°, each of which sacrifices one of the glancing angles but improves the situation for the other. By intercomparison of the plates taken with these three target settings and rejection of those observations subject to the glancing angle effect, it is believed that reliable yields were obtained at the 40° and 65° angles. After the shape and general trend of the distributions were established, it was not thought worthwhile to make this detailed investigation at every energy, but sufficient data were always taken to obtain a reliable yield at at least one of the glancing angles.

III. RESULTS

The angular yields are presented in Figs. 2 and 3. Except for apparently minor fluctuations, it is possible to fit the distributions by means of polynomials in $\cos\theta$ of the form $1+A_1\cos\theta+A_2\cos^2\theta$. The coefficients, obtained from a least-square analysis, are listed in Table I and plotted against bombarding energy in Fig. 4. The curves for A_1 are rather reliable inasmuch as the straight line slopes of the distributions are little affected by uncertainties in the individual points. The curves for A_2 are naturally subject to greater uncertainty. For the alpha-particles, A_2 deviates only slightly from zero, and although the corresponding curvatures in the angular distributions seem real, the presence of small systematic errors cannot be ruled out. For the deuterons the existence of a positive squared term is well established, at least for the highest energies, because any reasonable attempt to draw a straight line through the observations at the high energy would result in negative yields at the backward angles.

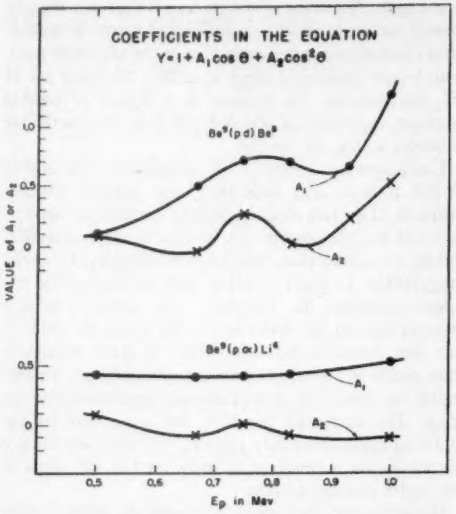

FIG. 4. Energy dependence of the coefficients A_1 and A_2 for the deuterons and alphas from the proton bombardment of beryllium.

The presence of a squared term in the angular distributions leads to the following expression for the total cross section in terms of the differential cross section at the center-of-mass angle of 143° (approximately equivalent to the laboratory angle of 138° at which the measurements of Thomas, Rubin, Fowler, and Lauritsen[3] were made):

$$\sigma_T = (4\pi\sigma_{143}/Y_{143})(1+\tfrac{1}{3}A_2).$$

TABLE II. Comparison of ratios of alpha- to deuteron yields.

E_p (Mev)	Y_α/Y_d (Thomas *et al.*, $\theta_L = 138°$)	Y_α/Y_d (JHU, $\theta_L = 140°$)
0.50	0.50	0.72
0.67	1.0	0.91
0.75	1.2	0.94
0.83	1.4	1.2
1.00	1.6	1.9

$4\pi\sigma_{143}$ are the values given by Thomas *et al.* Y_{143} is the yield at 143° relative to that at 90° and is given by $(1-0.80A_1+0.64A_2)$. The 143° angle is approximately equal to one of the angles of observation of the present experiment. A comparison of the ratios of alpha- to deuteron yields from the two experiments is given in Table II. The discrepancies are probably within the experimental error, except at the lowest energy where our measurement gives a proportionately greater alpha-yield. We have computed the total cross sections in three ways: in the first, the curves of Thomas *et al.* were used as given; in the second, their alpha-yields were adjusted to agree with our alpha- to deuteron ratios; and in the last, both yields were adjusted to give these ratios, but the combined alpha- and deuteron yield was kept the same. The three results differ chiefly in the general trend of the curves and not significantly in the structure displayed, and we present in Fig. 5 the total cross sections obtained in the last manner. The alpha-cross section varies smoothly, but the resonance structure between 0.9 and 1.0 Mev is enhanced. The deuteron curve exhibits more structure. The peak at 0.47 Mev results from the corresponding structure in the 143° curve and occurs in a region where the angular distribution measurements were extrapolated on the basis of rather sketchy observations at 0.44 and 0.40 Mev (these measurements and one at 0.30 Mev are not included in the results because the counting and identification of alphas and deuterons were too unreliable). The structure at 0.68 Mev results chiefly from the variation in the A_1 and A_2 coefficients, but there is a trace of this structure in the 143° curve and in the alpha-curves also, and a gamma-ray resonance is observed in this vicinity.[7] To investigate the possibility that the variation of A_2 in this region is not real, we have made the calculations assuming $A_2\simeq 0$ to agree with the measurements at adjacent energies. The result indicates a broadening and a shifting to higher energy for the resonance structure, but does not appear to eliminate it.

In the course of this investigation we had opportunity to observe the ranges in photographic emulsion of several different particles, H_1^+, H_2^+, He_4^+, He_4^{++}, Li_6^+, and Li_6^{++}, for a variety of known energies. The results of a series of range measurements are presented in Fig. 6. The proton and alpha-curves are in agreement with the measurements from other laboratories.[9] The deuteron curve agrees substantially with the theoretical prediction based on the proton curve. A comparison of these curves with the corresponding range-in-air curves shows that the stopping power of the emulsion relative to air varies only slightly from 1600. The lithium range-energy curve is not greatly displaced from the alpha-curve, which reflects the fact that at these energies the triply ionized state of lithium is somewhat improbable. This

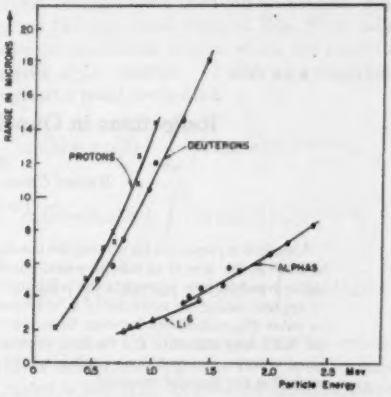

FIG. 6. Range *vs* energy curves for the light nuclei observed in this experiment in Ilford C2 plates.

is confirmed by the failure to locate any appreciable number of Li^{+++} ions on the plates, whereas Li^{++} and Li^+ ions were observed in abundance. Del Rosario,[10] observing the same reaction at lower bombarding energies and with higher resolution, did observe Li^{+++} ions but found that the other states of ionization predominated. As expected, no difference in range between He^+ and He^{++} or between Li^+ and Li^{++} ions were detected. This is because the mean free path for electron capture or loss in the emulsion is very much smaller than the total track length.[8]

The most interesting feature of the angular distributions presented here is the relatively large amount of asymmetry about 90°, indicating interference between two or more states of the compound nucleus, not all of the same parity. Because of the prominence and relatively high yield of the resonance at 0.33 Mev, it seems

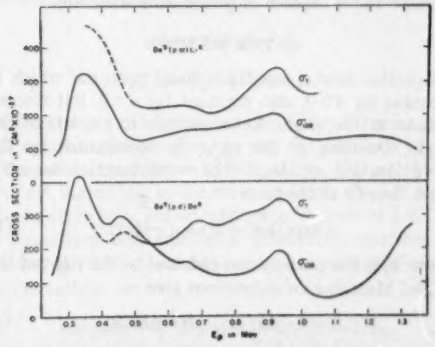

FIG. 5. Energy dependence of the cross sections for the alphas and deuterons from the proton bombardment of beryllium. σ_{138} is 4π times the differential cross sections at a laboratory angle of 138°, as given by Thomas, Rubin, Fowler, and Lauritsen, σ_T is the total cross section calculated from the 138° curves and the measured angular distributions.

[9] Lattes, Fowler, and Cuer, Proc. Phys. Soc. (London) 59, 883 (1947); N. Nereson and F. Reines, Rev. Sci. Instr. 21. 534 (1950).
[10] L. Del Rosario, Phys. Rev. 74. 304 (1948).

reasonable to attribute it to s-wave capture forming a state of the compound nucleus of odd parity. This assignment is confirmed by the observation of Jacobs, Malmberg, and Wahl[11] on the angular yield of the radiation from this state in that they found it to be essentially isotropic. In the interest of simplicity one would like to identify the alpha- and deuteron resonance at 0.94 Mev with the gamma-resonance at 1.00 Mev, although the difference in energy appears to be significant and not easily explained. Devons and Hine[12] attribute this gamma-resonance to s-wave capture also (with a small amount of d-wave penetration), on the basis of their observation that the yield of radiation is nearly isotropic. If this identification of states is correct, the observed interference in the alpha- and deuteron cross sections cannot arise between this state of odd parity and the one at 0.33 Mev; it must come from yet another state of even parity formed presumably by p-wave capture. For the deuterons, such a state is possible at bombarding energies of 0.47, 0.68, and 1.35 Mev; for the alphas, there is evidence for broad resonances, perhaps, at the latter two energies. To test whether the interfering state falls between or above the two odd states, calculations have been carried out to determine the trend of the coefficients. The gross features of the A_1- and A_2-curves seem to be explained best by assuming that the even state falls between the other two, the significant feature being the maxima displayed by the curves in passing through the intermediate resonance (the absence of an observed maximum in the A_1-curve of the alpha-particles is a difficulty which can be attributed partially to the greater width of the alpha-resonance).

[11] Jacobs, Malmberg, and Wahl, Phys. Rev. **73**, 1130 (1948).
[12] S. Devons and M. G. N. Hine, Proc. Roy. Soc. (London) A **199**, 73 (1949).

PHYSICAL REVIEW VOLUME 82, NUMBER 1 APRIL 1, 1951

Reflections in One-Dimensional Wave Mechanics

ROLF LANDAUER
*Harvard University, Cambridge, Massachusetts**
(Received May 31, 1950)

A method is presented for solving the one-dimensional Schroedinger equation. The method gives the wave function in the form of an infinite series. The first term of the series is the WBK approximation. Each of the higher terms in turn represents the reflections generated by the preceding term. The expansion is obtained by approximating the potential by a "staircase" potential, which is constant over short regions and changes its value discontinuously between these regions. The method is applied to periodic potentials. By taking the WBK approximation and the first reflection term into account, the zones of the periodic potential can be found in terms of a coefficient which gives the probability that a particle will be reflected in passing through one cell of the periodic potential.

I. INTRODUCTION

SCHELKUNOFF[1] and Brillouin[2] have recently given methods of supplying higher order corrections to the WBK approximation, so that a convergent series for the wave function can be obtained. The method to be presented serves the same purpose, but in addition has a simple physical interpretation. The same method had been arrived at independently by Bremmer.[3,4] The presentation below is along somewhat different lines from that given by Bremmer. Similar concepts have also been suggested by Hill.[5]

In a periodic potential a particle must have energies restricted to certain energy bands. The WBK method neglects the reflections that cause this, and is therefore inadequate for dealing with periodic potentials. The method given here takes distributed reflections into account and is capable of giving zone structure.

II. THE METHOD

Consider first a one-dimensional potential which is constant for $x>0$, also constant for $x<0$, but discontinuous at the origin. Let a particle to the left of the origin, traveling to the right, be represented by the wave function $\exp(ik_1x)$. The wave function for $x>0$ must then be of the form

$$A\exp(ik_2x)+B\exp(-ik_2x), \tag{1}$$

where k_2 is the propagation constant to the right of the origin. Matching considerations give

$$A=1-\Delta k/2k_2, \quad B=\Delta k/2k_2, \tag{2}$$

where $\Delta k=k_2-k_1$. If $k_2\gg\Delta k$, then A will be given by $(k_1/k_2)^{\frac{1}{2}}$, to first order in Δk. Under the same condition $A\gg B$. To a first approximation the term $B\exp(-ik_2x)$ can therefore be neglected. The wave function is then given by a wave which moves to the right everywhere

* Now with the National Advisory Committee for Aeronautics, Cleveland, Ohio.
[1] S. A. Schelkunoff, Q. Appl. Math. **3**, 348 (1946).
[2] L. N. Brillouin, Q. Appl. Math. **7**, 363 (1950).
[3] Presented at the Symposium on the Theory of Electromagnetic Waves, at New York University, June 7, 1950.
[4] H. Bremmer, Physica **15**, 593 (1949).
[5] E. L. Hill, Phys. Rev. **38**, 2115 (1931).

and has its amplitude inversely proportional to the square root of the classical momentum.

If we are given a smooth potential, $V(x)$, we can approximate it arbitrarily closely by a "staircase" function, which is constant over short regions of the x axis and changes its value discontinuously between them. We can solve the wave equation for this modified potential by finding two independent solutions in each region of constant potential and then matching at the discontinuities. We can then form a first approximation as in the example above. This gives us a wave which moves everywhere to the right and neglects the reflections which are generated at the discontinuities. Similarly, there will be an approximate solution giving a wave moving to the left. These waves are just the ordinary WBK approximations:

$$(p)^{-\frac{1}{2}} \exp\left[(i/\hbar)\int p dx\right], \quad (p)^{-\frac{1}{2}} \exp\left[(i/\hbar)\int p dx\right]. \tag{3}$$

To obtain the higher approximations, we could as suggested above, go through a matching and limiting process. A simpler procedure is, however, available. In each region of constant potential the wave function must be the sum of two free electron waves

$$\psi = A \exp(ipx/\hbar) + B \exp(-ipx/\hbar). \tag{4}$$

Within this small region of constant potential, the propagation constant, $p/\hbar$, does not change its value, nor do A and B; and, therefore,

$$d\psi/dx = (ip/\hbar)[A \exp(ipx/\hbar) - B \exp(-ipx/\hbar)]. \tag{5}$$

Two new functions, $\phi_R(x)$ and $\phi_L(x)$, can be defined in terms of A and B as follows:

$$\phi_R = Ap^{\frac{1}{2}} \exp(ipx/\hbar), \quad \phi_L = Bp^{\frac{1}{2}} \exp(-ipx/\hbar). \tag{6}$$

In terms of ϕ_R and ϕ_L, Eqs. (4) and (5) become

$$\psi = p^{-\frac{1}{2}}(\phi_R + \phi_L) \tag{7}$$

$$d\psi/dx = (ip^{\frac{1}{2}}/\hbar)(\phi_R - \phi_L). \tag{8}$$

Differentiating the right-hand side of Eq. (7) must give $d\psi/dx$, which is also given by Eq. (8). Similarly, if we differentiate the right-hand side of Eq. (8), we obtain $d^2\psi/dx^2$. According to the wave equation $d^2\psi/dx^2$ must also be given by $-p^2\psi/\hbar^2$, where ψ is as given by Eq. (7). We therefore have two linear differential equations in ϕ_R and ϕ_L. Taking suitable linear combinations of these two equations, we find

$$\begin{aligned} (d\phi_R/dx) - (i/\hbar)p\phi_R &= (1/2p)(dp/dx)\phi_L, \\ (d\phi_L/dx) + (i/\hbar)p\phi_L &= (1/2p)(dp/dx)\phi_R. \end{aligned} \tag{9}$$

These equations can be solved by a method of successive approximations. Let us, at first, neglect the right-hand side of the equations. This leaves two independent equations, whose solutions are

$$\phi_R = C \exp\left[(i/\hbar)\int p dx\right]$$

$$\phi_L = D \exp\left[-(i/\hbar)\int p dx\right]. \tag{10}$$

According to Eq. (7) these expressions must be divided by $p^{\frac{1}{2}}$ in order to obtain the wave function. These solutions are, therefore, again WBK approximations. Let us denote them by $\phi_{R0}(x)$ and $\phi_{L0}(x)$, respectively. Let us also assume that there is some point, $x=a$, at which $\phi_{R0}(a)$ and $\phi_{L0}(a)$, if substituted in Eqs. (7) and (8) give the correct value of the wave function and its derivative. The farther we move away from $x=a$, the more these zeroth approximations will be in error.

By substitution of these zeroth approximations into the right-hand side of Eqs. (9), and solution of these equations, the next approximation is obtained. That is, we regard the right-hand terms of Eqs. (9) as inhomogeneities or distributed sources which are known from the zeroth approximation. To this approximation we find that at a point $x=b$, $b>a$,

$$\phi_R(b) = \phi_{R0}(b) + \int_a^b dx \phi_{L0}(x)\rho(x)e^{i\theta(b,x)}, \tag{11}$$

$$\phi_L(b) = \phi_{L0}(b) + \int_a^b dx \phi_{R0}(x)\rho(x)e^{-i\theta(b,x)}, \tag{12}$$

where

$$\rho(x) = (1/2p)dp/dx, \quad \theta(b,x) = \int_a^b (p/\hbar)dx. \tag{13}$$

The terms present in the integral can be understood in terms of the staircase picture. To be specific, consider the integral in Eq. (12). At $x=a$ the zeroth approximation is correct. As the ϕ_{R0}-wave moves to the right, it generates waves moving in the opposite direction, at every discontinuity between a and b. The integral represents a summation over these discontinuities. The waves generated at the discontinuities are proportional to the incident wave that is generating them. Therefore, the zeroth approximation occurs in the integrand. The factor $\exp[-i\theta(b,x)]$ represents the phase shift of the generated waves between the point x at which they are generated and the point $x=b$ at which the wave function is being evaluated. The factor $\rho(x)$ arises from the factor $\Delta k/2k$ in Eq. (2) and represents the strength with which waves are generated at a discontinuity.

In this fashion, still higher approximations can be obtained and the wave function can be written

$$\psi = \sum_{n=0}^{\infty} (\phi_{Rn} + \phi_{Ln}), \tag{14}$$

where

$$\phi_{R(n+1)}(b) = \int_a^b dx \phi_{Ln}(x)\rho(x)e^{i\theta(b,x)} \tag{15}$$

and

$$\phi_{L(n+1)}(b)=\int_a^b dx\phi_{Rn}(x)\rho(x)e^{-i\theta(b,x)}. \quad (16)$$

We have, up to this point, assumed that we are discussing a region in which the classical momentum, p, is real. Classically forbidden regions can, however, be discussed in the same manner. There we will have

$$\psi=|p|^{-\frac{1}{2}}(\phi_u+\phi_d) \quad (17)$$

$$d\psi/dx=(|p|^{\frac{1}{2}}/\hbar)(\phi_u-\phi_d). \quad (18)$$

ϕ_u represents the component of the wave function increasing exponentially to the right; ϕ_d represents the component increasing exponentially to the left. The differential equations that these components obey are

$$\begin{aligned}(d\phi_u/dx)-|p|\phi_u/\hbar&=(1/2p)(dp/dx)\phi_d,\\ (d\phi_d/dx)+|p|\phi_d/\hbar&=(1/2p)(dp/dx)\phi_u.\end{aligned} \quad (19)$$

The quantum-mechanical current assumes in our notation the usual simple form associated with regions of constant potential. In the classically allowed region

$$j_x=(1/m)(\phi_R^*\phi_R-\phi_L^*\phi_L), \quad (20)$$

while in the classically forbidden region

$$j_x=(1/mi)(\phi_d^*\phi_u-\phi_u^*\phi_d). \quad (21)$$

It can be shown that our series expansion of the wave function, as given in Eq. (14), is uniformly and absolutely convergent if $[a, b]$ is a closed interval in which the logarithm of the momentum has a finite variation. The region cannot include a turning point or a singularity of the potential. To connect across a turning point, the ordinary WBK connection formulas must be used.[6] There is no obvious way in which the method described here can be used to give improved connection formulas.

III. LIMITATION OF THE WBK METHOD

Consider the integral for ϕ_{L1} given in Eq. (16). ϕ_{R0} in this integrand can be replaced by the use of Eq. (10). This gives

$$\phi_{L1}(b)=Ce^{i\theta(b,a)}\int_a^b \rho(x)e^{-2i\theta(b,x)}dx. \quad (22)$$

Now consider two points, x' and x'', included in the interval of integration. From the neighborhood of both points the integral receives a contribution. If x' and x'' are very close together, then the two expressions

$$\exp[-2i\theta(b,x')],\quad \exp[-2i\theta(b,x'')] \quad (23)$$

will have almost the same phase and the contributions will add. If, however, x' and x'' are a quarter of a wavelength apart, then their contributions are of opposite sign. Now the waves generated in that quarter wavelength have an upper bound which can be obtained by omitting the phase factors. This gives

$$|C|\int_x^{x+\frac{1}{4}\lambda}\rho(x)dx=\frac{|C|}{2}\log\left[\frac{p(x+\frac{1}{4}\lambda)}{p(x)}\right]. \quad (24)$$

If this quantity is small compared to $|C|$, or equivalently if

$$p(x+\tfrac{1}{4}\lambda)/p(x) \quad (25)$$

is close to unity, then the waves generated in that quarter-cycle are small compared with the amplitude of that quarter-cycle and do not change the wave shape appreciably. This is the type of criterion usually given for the validity of the WBK approximation. It must, however, be taken with caution. It does guarantee that the WBK approximation satisfies the Schroedinger equation with accuracy. It does not, however, guarantee that the WBK approximation is *everywhere* close to an exact solution.

While contributions from adjacent quarter-wavelengths will tend to cancel, they will not do so exactly. It is then possible that contributions coming from points x', x'', x''', etc., each of which is about half a wavelength from the next, can pile up. This is what takes place in the case of an electron suffering a Bragg reflection in a periodic potential.

IV. THE PERIODIC POTENTIAL

The application of the WBK approximation to a periodic potential has been considered by Jeffreys,[7] Goldstein,[8] and Strutt.[9] Their procedures yield the expected band structure for those energy levels which are low enough so that the particle is classically confined to a single potential trough. (The potential is considered to consist of a succession of identical potential wells.) These treatments require the use of the connection formulas without regard to the usual directional limitations. In the range of energies which are high enough so that the particle is classically free to move along the whole axis, the WBK method fails to give energy bands; and it will be necessary to use the method of distributed reflections which we have introduced above.

Consider a periodic potential. Let $x=a$ be the left edge of a unit cell and $x=b$ the right edge of the same cell. The zeroth, or WBK approximation, for the wave function is

$$\begin{aligned}\phi_{R0}(x)&=\exp[i\theta(x,a)]\phi_{R0}(a),\\ \phi_{L0}(x)&=\exp[-i\theta(x,a)]\phi_{L0}(a).\end{aligned} \quad (26)$$

For these two solutions

$$\begin{aligned}\phi_{R0}(b)&=\exp[i\theta(b,a)]\phi_{R0}(a),\\ \phi_{L0}(b)&=\exp[-i\theta(b,a)]\phi_{L0}(a).\end{aligned} \quad (27)$$

If we take our first-order correction into account by

[6] E. C. Kemble, *Fundamental Principles of Quantum Mechanics* (McGraw-Hill Book Company, Inc., New York, 1937), p. 97.

[7] H. Jeffreys, Proc. London Math. Soc. **23**, 437 (1924).

[8] S. Goldstein, Proc. London Math. Soc. **28**, 81 (1928).

[9] M. J. O. Strutt, Math. Ann. **101**, 559 (1929).

using Eqs. (11) and (12), we obtain

$$\phi_R(b)=\phi_R(a)e^{i\theta(b,a)}+\int_a^b dx\phi_{L0}(x)\rho(x)e^{i\theta(b,x)}, \quad (28)$$

$$\phi_L(b)=\phi_L(a)e^{-i\theta(b,a)}+\int_a^b dx\phi_{R0}(x)\rho(x)e^{-i\theta(b,x)}. \quad (29)$$

The equations can be simplified by the introduction of two new parameters:

$$A=\int_a^b dx\rho(x)e^{-2i\theta(x,a)}, \quad \theta=\theta(b,a). \quad (30)$$

In terms of these, Eqs. (28) and (29) become

$$\phi_R(b)=\phi_R(a)e^{i\theta}+\phi_L(a)Ae^{i\theta}, \quad (31)$$

$$\phi_L(b)=\phi_L(a)e^{-i\theta}+\phi_R(a)A^*e^{-i\theta}. \quad (32)$$

θ is the phase shift per cell given by the ordinary WBK method. $|A|^2$ is the probability that the particle changes its direction of motion in going through one cell.

Floquet's theorem tell us that the solutions to the wave equation for a periodic potential can always be written in the form $u(x)\exp[i\mu x]$, where $u(x)$ has the periodicity of the lattice and μ is either purely real or purely imaginary. It is real for the energy levels corresponding to allowed levels, and imaginary for the stop bands between them. Equations (31) and (32) represent a linear transformation whose characteristic values are $\lambda=\exp[\pm i\mu x]$. The secular equation obtained from Eqs. (31) and (32) is

$$\lambda^2-2\lambda\cos\theta+(1-|A|^2)=0. \quad (33)$$

The roots of this equation are

$$\lambda=\cos\theta\pm(|A|^2-\sin^2\theta)^{\frac{1}{2}}. \quad (34)$$

Whenever the quantity in parentheses is negative, the equation has two imaginary roots, complex conjugates of each other. In this case

$$\lambda=\cos\theta\pm i(\sin^2\theta-|A|^2)^{\frac{1}{2}} \quad (35)$$

which to first order in $|A|$ satisfies $|\lambda|=1$. Whenever the quantity in parentheses is negative, we will be in an allowed energy range. As the energy is varied, for a given potential, $\sin\theta$ will repeatedly go through zero. When $\sin\theta$ comes close enough to zero, the term in parentheses in Eq. (34) becomes positive and both roots will be real. The roots, when real, will have their extreme values (i.e., farthest removed from unity) when $\sin\theta=0$. For that value of energy, we have

$$|\lambda|=1\pm|A|\simeq e^{\pm|A|} \quad (36)$$

to first order in $|A|$. The zone boundaries occur when the quantity in parentheses is negative, we will be in an $\sin\theta=\pm|A|$.

The fact that we have taken into account only the first-order correction makes our solution an approximate one, which is valid only if the coefficient $|A|$ is small compared with unity. The method is therefore valid only when the region between bands is narrow. This condition is not as restrictive as the one applicable to the usual perturbation theory approach.

It is possible that $|A|$ can be zero. In this case a particle can travel through the lattice without being reflected. The reflections caused by different parts of the cell must cancel in such a case. If $|A|$ vanishes at an energy for which $\sin\theta=0$, the spacing between adjacent bands vanishes and they touch each other.

The author wishes to thank Professors Furry and Brillouin for helpful discussions, and the Atomic Energy Commission for a Predoctoral Fellowship.

PHYSICAL REVIEW VOLUME 82, NUMBER 1 APRIL 1, 1951

The Infrared Spectrum of Active Nitrogen

LEWIS M. BRANSCOMB*
Harvard University, Cambridge, Massachusetts
(Received December 22, 1950)

Thirty-one bands, including the (0, 0) band at 10,440A, of the N_2 first positive system have been photographed in the Lewis-Rayleigh afterglow of active nitrogen. There is no indication that the $v=0$ level of the $B^3\Pi$ state is preferentially populated as required by the "resonance" theory of atomic re-association using $D(N_2)=7.383$ volts. The analogy between the Lewis-Rayleigh glow and the spectrum of the airglow is discussed briefly.

I. INTRODUCTION

MOST investigators of active nitrogen accept the hypothesis that the primary reaction leading to the Lewis-Rayleigh afterglow of active nitrogen is the recombination of two nitrogen atoms in the presence of a third body, the walls being conditioned in such a way as to inhibit recombination at the walls and allow the reaction to proceed slowly in the volume.[1] This reaction may be expected to give rise to a nitrogen

* Junior Fellow in the Society of Fellows, Harvard University.

[1] S. K. Mitra, *Active Nitrogen—A New Theory* (Indian Assoc. for the Cultivation of Science, Calcutta, 1945), p. 68. Mitra's theory of active N_2 involving nitrogen positive ions was based to a substantial degree of an analogy with processes in the night sky and the ionosphere. New experimental data on the upper atmosphere show that this analogy is quite remote, as is pointed out in the present paper. For this and other reasons Mitra's theory is no longer in general favor.

molecule in either the metastable $A^3\Sigma$-level or in the $v=0$ level of $B^3\Pi$, providing the dissociation energy of nitrogen is 7.383 ev. Admittedly, the magnitude of the dissociation energy of N_2 is a controversial point, since Gaydon's proposal[2] that it is 9.765 ev. In the spectrum of active nitrogen, Kaplan[3] has reported a marked enhancement of the (0, 0) band of the first positive system ($B^3\Pi - A^3\Sigma$) at 10,440A. This observation indicates that the $v=0$ level of $B^3\Pi$ is preferentially populated by the afterglow reactions. This may be interpreted as evidence, for both the nitrogen reassociation theory of active nitrogen and for the 7.383-ev dissociation energy, by the following argument.

Since the $v=0$ level of the $B^3\Pi$-state of N_2 has an excitation energy of 7.35 ev, and the $v=1$ level of this state lies above 7.383 ev, the only nonmetastable state of N_2 which can be excited by a re-association which has 7.383-ev energy available is the $v=0$ level of $B^3\Pi$. Hence, the only allowed radiation which this process could produce is the 10,440A (0, 0) band of the N_2 first positive system. Thus, if X represents the third body in the collision,

$$N(^4S)+N(^4S)+X \rightarrow N_2(v=0\ B^3\Pi)+X \qquad (1)$$

followed by

$$N_2(v=0\ B^3\Pi) \rightarrow N_2(v\geq 0\ A^3\Sigma)+h\nu(\lambda \geq 10{,}440\text{A}). \qquad (2)$$

Of course, the dissociation energy may be divided between the third body and the newly formed molecule.

This alternative reaction does not lead to molecular radiation[4]

$$N(^4S)+N(^4S)+X \rightarrow N_2(v\geq 0\ A^3\Sigma)+X^{exc}. \qquad (3)$$

After reactions (1) and (2) or (3), the molecule is in the metastable $A^3\Sigma$-state. Subsequent collisions of the second kind, with atomic and molecular nitrogen in ground or metastable states, can be invoked to explain the excitation of the remainder of the afterglow spectrum (at least as far as the energetic requirements are concerned).[5] We conclude then, that *if* in the three-body collision the *entire* dissociation energy (of 7.383 ev) is given to the resulting nitrogen molecule in the form of electronic energy and none to the third body, then one would expect the strongest feature of the afterglow spectrum to be the 10,440A (0, 0) band of the first positive system.

Of course, the appearance of a very intense (0, 0) band of the first positive system of nitrogen in the afterglow would not in itself prove the correctness of the theory described above, nor would it prove that the dissociation energy of N_2 is 7.383 ev. However, the presence of this radiation with great intensity would make possible an experiment which would strongly support the 7.383-ev value for $D(N_2)$ if this is the correct value. The experiment is to study the infrared spectrum of the "dark modification" of active nitrogen. When active nitrogen is heated, or is subjected to a small electric current, the visible glow disappears or is greatly weakened, but the gas retains its activity.[1] This is demonstrated, in the first case, by the observation that when nitrogen flows through a tube, the central portion of which is heated, the glow is extinguished in the heated portion but recommences when the gas reaches the cooler part of the system. One assumes then that the primary reaction (three-body recombination in the volume) continues throughout the dark phase, and that the intermediate reactions leading to the excitation of visible light are interrupted by the heating (or the current.) The mechanism for this interruption might be the destruction of the metastable molecules which the recombination process produces. If the dissociation energy is 7.383 ev, then the primary reaction leads to radiation in the infrared only, so that the phase in which only the primary reaction proceeds would indeed appear "dark." An investigation of the infrared spectrum of the "dark modification" of active nitrogen should reveal the reportedly strong (0, 0) band of N_2 (first positive) at 10,440A with more or less undi-

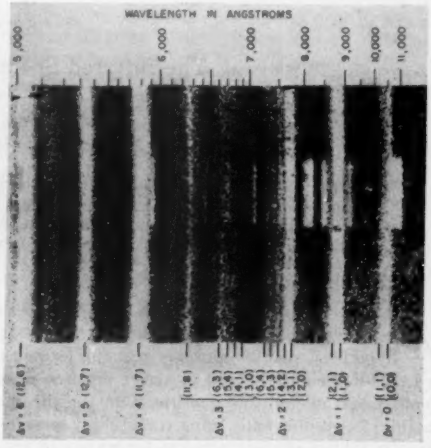

FIG. 1. Bands of first positive system of N_2 in active nitrogen. Type I–Z plate. Maximum infrared speed, 10,900A.

[2] G. Herzberg, *Spectra of Diatomic Molecules* (D. Van Nostrand Company, Inc., New York, 1950), p. 448. A. G. Gaydon, *Dissociation Energies* (John Wiley and Sons, Inc., New York, 1947), p. 152. Other values of $D(N_2)$ have been proposed, the most recent being 11.80 ev, by G. Glockler, J. Chem. Phys. 18, 1518 (1950).

[3] J. Kaplan, "*The Laboratory Production of Auroral Afterglows*," in *The Emission Spectra of the Night Sky and Aurorae* (The Physical Society, London, 1948), p. 118.

[4] It has often been stated that because the available dissociation energy is almost exactly equal to the excitation energy of a certain level of the product molecule, the reaction exciting this level by "resonance" is very probable. However, owing to the interchange between the kinetic energy of vibration and translation with the electronic energy, it is by no means obvious that all of the energy involved in the recombination process will be transformed into electronic energy. The most probable products of the reaction may be left in a state of strong vibration, as is indicated in Eq. (3).

[5] A complete discussion of the reaction scheme for active nitrogen (which will not be undertaken here) must include also an analysis of the role played by the metastable $a^1\Pi$-state of the molecule.

minished intensity, if the mechanism described is operative. Such an observation would suggest strongly the value 7.383 ev for $D(N_2)$.

The early work on the infrared spectrum of active nitrogen was carried by Kichlu, Acharya,[6] and Cario.[7] The infrared limit of their photographic plates was about 8900A, so they were only able to observe the (3, 1), (2, 0), and probably the (3, 2), (2, 1), and perhaps (1, 0) bands of the first positive system in addition to the well-known visible bands originating on $v'=6$, 11, and 12. They could not have detected the (0, 0) band even if it had been much more intense than the bands originating on $v'>0$. More recently, Kaplan[3] has investigated the infrared spectra of nitrogen afterglows and has compared them with airglow and auroral spectra. He mentions a strong enhancement of the (0, 0) band of the first positive system in the Lewis-Rayleigh afterglow, though no details are given. Before undertaking the spectroscopy of the "dark modification," we had to confirm the abnormal intensity of the 10,440A band in the normal afterglow. These spectra of the Lewis-Rayleigh glow in active nitrogen, photographed with I-Z plates, are described in this paper.

II. EXPERIMENTAL APPARATUS

Commercial tank nitrogen was flowed over hot platinized asbestos and then phosphorous pentoxide to remove all of the hydrogen in the gas. A remaining trace of oxygen in the gas was allowed to remain as a helpful impurity and appeared in the spectra as bands of NO. The gas was passed through a dry ice-acetone trap, then a controlled leak, and finally through an uncoated cylindrical Vycor vessel 3″ in diameter and 12″ long. A self-excited 7-Mc oscillator with a maximum power output of 750 watts excited a discharge in the cylindrical vessel. Microswitches, operated by a rotating cam, turned on the oscillator for ½ second. The oscillator was then turned off, and about 0.05 sec later a shutter between the discharge vessel and the spectrograph slit opened. The shutter remained open, with the oscillator off, for 2½ sec, after which the shutter closed and the cycle began again. In this way the apparatus operated continuously, the spectrograph photographing the integrated spectrum from 0.05 to 2.50 sec in the afterglow. A neon Geissler tube was next to one end of the discharge vessel so that neon lines would appear on the plate if the shutter opened while the neon tube was excited. The neon tube was periodically excited by the same oscillator which produced the nitrogen discharge, and the fact that no neon lines appeared on the afterglow spectrograms proves that the shutter did not leak light from the very intense direct discharge. When the cycling apparatus was turned off, the afterglow was easily visible in a darkened room for one minute.

The spectrograph was a glass prism Zeiss instrument with a speed of f:2.7, an aperture of about 6 cm, and a slit width of 0.08 mm. A 30-sec exposure showed the visible spectrum quite satisfactorily, but preliminary exposures of 48 hr on I-Z plates hypersensitized in an ammonia-ethyl alcohol solution were not sufficient to show the band at 10,440A. The hypersensitized plates were then pre-fogged by a controlled exposure to a tungsten lamp through two Wratten 87 infrared filters.[8] After this pre-exposure, a 48-hr exposure brought out the (1, 0) band as well as the (0, 0) band. Since only a qualitative measure of the relative intensity of the (0, 0) band and the bands from higher initial vibrational levels was sought, a heterochromatic photometry was not employed. The manufacturer's data on the spectral sensitivity of the hypersensitized emulsion, as well as comparison of afterglow plates with spectrograms of the direct discharge, afford a sufficient indication of the order of magnitude of the relative intensities involved. The speed of the I-Z plate (hypersensitized) is roughly uniform from 7000 to 11,000A with a slight maximum around 10,900A.

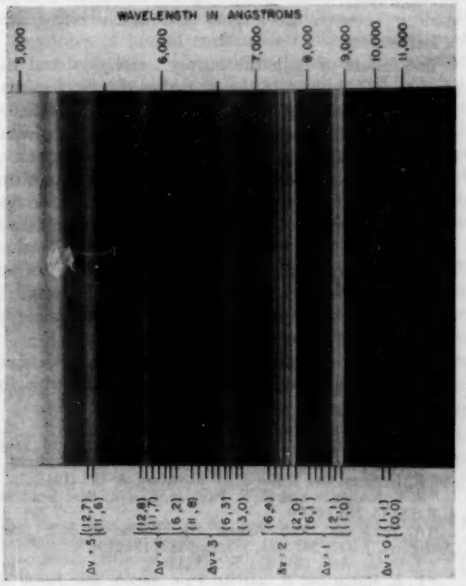

FIG. 2. Bands of first positive system of N_2 in active nitrogen. Type I-Z plate. Maximum infrared speed, 10,900A.

III. RESULTS

Figure 1 shows an enlargement of a spectrogram of the infrared afterglow. The short lines in the center of the spectrogram are comparison spectra of He, A, and

[6] Kichlu and Acharya, Nature **121**, 982 (1928); Proc. Roy. Soc. (London) **A103**, 168 (1929).
[7] G. Cario, Z. Physik **89**, 523 (1934).
[8] The details of the criteria used to determine the optimum pre-exposure will be published soon elsewhere.

Ne. The most prominent features of the spectrum are the well-known bands originating on $v'=12$ and 11. The characteristically anomalous intensity distribution in the progressions involving $v'=6$ are also apparent. In the infrared, the bands originating on $v'=1$, 2, and 3 are quite intense. Also, their intensity is quite comparable to that of the (0, 0) band. There is certainly no suggestion in this spectrum that the $v'=0$ level of $B^3\Pi$ is selectively populated, which the theory outlined above would require. Of the several two-day exposures which were made, the spectrum in Fig. 1 had the strongest (0, 0) band. The intensity distribution in the bands originating on levels with $v'<6$ appears very similar to the intensity distribution in the spectrum of the direct discharge.

Figure 2 shows an enlargement of another spectrogram in which (0, 0) appeared much weaker, although in this case it was at least in part due to an accidental fault in the hypersensitization procedure. This enlargement was made by mounting the printing paper on a rotating drum whose axis was perpendicular to the image of the spectral lines from the enlarger. In this way the effect of grain spoiling the resolution of the spectral lines was intentionally reduced, and many more bands are visible on careful inspection of the enlargement. In this spectrum the (1, 0) and (2, 1) bands were particularly intense, even more intense than the usually dominant (12, 7) and (11, 7) bands. The preferential population of $v'=6$ is particularly apparent, however. The $\Delta v=1$ and 2 progressions drop off abruptly in intensity at $v'=6$. The $\Delta v=3$ progression shows an abrupt decrease in intensity at $v'=6$ and then again at $v'=11$. The $\Delta v=4$ progression begins with (6, 2) and then gets much stronger at (11, 7) and (12, 8). A total of 31 bands of the N_2 first positive system are observed. In the green and blue regions of the spectrum, traces of the β-spectrum of NO and the violet system of CN appear. No atomic spectral lines were observed in the afterglow. Overlapping of NO and CN impurity bands and the very low dispersion make it impossible to exclude the possibility that N_2 second positive bands, or Vegard-Kaplan bands appear very faintly in the afterglow. These systems are not found by other authors in the Lewis-Rayleigh glow (though they may be found in the very short time afterglows). A weak feature at 4850A is unidentified and might be associated with the (2, 15) Vegard-Kaplan band which is degraded to the red and has its band head at 4837.1A. This band is listed by Pearse and Gaydon[9] as the most intense Vegard-Kaplan band observed by Bernard.

[9] R. W. B. Pearse and A. G. Gaydon, *The Identification of Molecular Spectra* (John Wiley and Sons, Inc., New York, 1941), p. 140.

IV. ACTIVE NITROGEN AND THE AIRGLOW

The excitation process for the 10,440A band described at the beginning of the paper was first proposed with reference to a very strong radiation of about this wavelength in the airglow of the earth's atmosphere. When this radiation was first discovered[10–13] it was interpreted as the (0, 0) band of the N_2 first positive system, assuming the above reaction scheme. The altitude of emission of the airglow was, at that time, very uncertain. The possibility that this altitude might be as high as 200 km or more gave encouragement to efforts to explain the existence of the required density of atomic nitrogen in the atmosphere at night. Also, there appeared to be a marked similarity between the spectra of the airglow and the Lewis-Rayleigh nitrogen afterglow in the laboratory, especially when a little oxygen is introduced into the active nitrogen. This similarity also appeared to support the atomic nitrogen theory of excitation of the airglow, since this theory appeared to apply well to active nitrogen. Our failure to find a marked enhancement of the (0, 0) band at 10,440A is not surprising in view of the recent discovery by Meinel[14,15] that the infrared spectrum of the airglow must be identified as due to OH and not to N_2. Also, recent work indicates that the altitude of emission of the airglow is in the neighborhood[16] of 100 km, and it is very unlikely that an appreciable density of atomic nitrogen exists at this height. Hence, it appears that the analogy between the airglow and active nitrogen is rather remote.

The failure of both the nitrogen afterglow and the airglow to demonstrate the resonance theory of excitation of the first positive (0, 0) band of N_2 by recombination of atoms does not contradict the 7.383-ev value of the dissociation energy of N_2. Nor does the lack of preferential excitation of the (0, 0) band in active nitrogen disprove the hypothesis that the primary reaction is the recombination of atoms in three-body collisions. For even if $D(N_2)=7.383$ ev, the recombination product may be in the metastable $A^3\Sigma$-state (see Sec. I). Construction of the correct reaction scheme for active nitrogen must await an independent and final determination of the dissociation energy of nitrogen.

The author is grateful to Professor O. Oldenberg for many helpful discussions in connection with the spectrum of active nitrogen and this paper.

[10] Stebbens, Whitford, and Swings, Astrophys. J. **101**, 39 (1945).
[11] Herman, Herman, and Gauzit, Nature **156**, 114 (1945).
[12] R. Herman, and J. Gauzit, J. phys. rad. **6**, 182 (1945).
[13] S. F. Rodionov and E. N. Pavlova, Compt. rend. acad. sci. U.R.S.S. **15**, 831 (1949).
[14] A. B. Meinel, Pub. Astron. Soc. Pacific **60**, 357 (1948); Astrophys. J. **111**, **207**, 433, 555, and **112**, 131 (1950).
[15] J. Dufay, Ann. Geophys. **5**, 183 (1949).
[16] F. E. Roach and D. Barbier, Pub. Astron. Soc. Pacific **61**, 88 (1949).

Some Theorems on the Free Energies of Crystal Surfaces

CONYERS HERRING
Bell Telephone Laboratories, Murray Hill, New Jersey
(Received December 18, 1950)

Although the interpretation of experiments in such fields as the shapes of small particles and the thermal etching of surfaces usually involves problems of kinetics rather than mere equilibrium considerations, it is suggested that a knowledge of the relative free energies of different shapes or surface configurations may provide a useful perspective. This paper presents some theorems on these relative free energies which follow from the Wulff construction for the equilibrium shape of a small particle, and some relations between atomic models of crystal surfaces and the surface free energy function used in this construction. Equilibrium shapes of crystals and of noncrystalline anisotropic media are classified, and it is pointed out that the possibilities for crystals include smoothly rounded as well as sharp-cornered forms. The condition is formulated for thermodynamic stability of a flat crystal face with respect to formation of a hill-and-valley structure. A discussion is presented of the limitations on the applicability of the results imposed by the dependence of surface free energy on curvature; and it is concluded that these limitations are not likely to be serious for most real substances, though they are serious for certain idealized theoretical models.

I. INTRODUCTION

MANY fields of physics, chemistry, and metallurgy encounter the need for an understanding of the surface structures of crystals which have been subjected to various kinds of heat treatment. Examples of such fields include thermionic emission, sintering, and many problems in adsorption and catalysis. A complete understanding of surface structures will not be easy to achieve, however; the many experimental studies which have been conducted on "thermal etching" and related phenomena indicate that the processes involved are quite varied and complex.[1,2] In fact, it has long been recognized that the shapes of growing crystals, the structures of heated surfaces, etc., are in most cases determined by a competition between the rates of various mechanisms of transport, such as condensation, diffusion, chemical reaction rates, and that a complete understanding of such structures usually requires a detailed knowledge of these kinetic factors.[3] Nevertheless, one can expect in many cases to gain a valuable perspective on problems of crystal form and surface structure by investigating the surface free energies of the various possible configurations of the surface of a crystal. The cases in which surface free energy is important are, of course, those in which the dimensions of the crystal grains, or of the surface irregularities, are sufficiently small. In such cases the tendency of the crystal to lower its surface free energy is often the principal motivation for changes in surface structure which take place—as seems to be the case in sintering, for example—and under proper conditions one may even approach an equilibrium configuration of minimum free energy. The present paper will be concerned merely with this rather limited problem of the relative free energies of various shapes and surface structures of a crystal, with inclusion of a few results applicable to noncrystalline anisotropic phases, such as liquid crystals and tactoids.

The most obvious problem in this field is that of determining what shape a small crystal must assume if its surface free energy is to be a minimum for a given volume. The solution to this problem was stated by Wulff[4] almost half a century ago; and as Wulff's theorem will serve as a foundation for some of the arguments to be presented here, a brief description of it is in order. The surface free energy of any body is an integral of the form

$$\int \gamma(\mathbf{n})dS \qquad (1)$$

extended over the surface of the body, where the specific surface free energy γ is, for anisotropic bodies, a function of the orientation of the unit outward normal $\mathbf{n}$ at each surface point. Let γ be plotted radially as a function of the direction of $\mathbf{n}$; for a crystalline body a two-dimensional cross section of this plot will look something like the outer curve in Fig. 1, with cusped minima in certain directions corresponding to surfaces of particularly simple structure. At each point of this polar plot construct a plane perpendicular to the radius vector at that point. Then the volume which can be reached from the origin without crossing any of the

[1] For a brief survey of the problem of surface structure of metals with special emphasis on topics important to the field of thermionic emission, see C. Herring and M. H. Nichols, Revs. Modern Phys. **21**, 185 (1949), Sect. II, 1 and II, 2 and especially Appendix III.

[2] A brief review of experimental work in this field has been given by R. Shuttleworth, Metallurgia **38**, 125 (1948).

[3] See, for example, K. Spangenberg, "Wachstum und Auflösung der Kristalle," in *Handwörterbuch der Naturwissenschaften* (Verlag Gustav Fischer, Jena, 1934), second edition, Vol. X.

[4] G. Wulff, Z. Krist. **34**, 449 (1901). The first rigorous proof of Wulff's result seems to have been given by H. Liebmann, Z. Krist. **53**, 171 (1914); see also M. v. Laue, Z. Krist. **105**, 124 (1943). These proofs, although they leave no doubt that the result is true in general, are a little unsatisfying logically in that they prove merely that no polyhedron can be an equilibrium shape unless it is geometrically similar to the polyhedron obtained from application of the Wulff construction to the set of normal directions occurring for the sides of the polyhedron. However, A. Dinghas, Z. Krist. **105**, 304 (1944), has shown how an inequality due to Brunn and Minkowski can be used to prove directly that any shape differing from that given by the Wulff construction has a higher surface free energy than the latter. Although Dinghas considers only a special class of polyhedral shapes, his method is easily extended to arbitrary shapes, since the Brunn-Minkowski inequality is true for convex bodies in general.

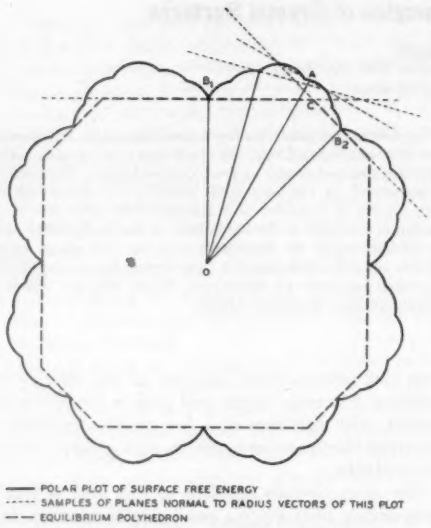

FIG. 1. Typical polar plot of surface free energy for a crystal and the Wulff construction based on it.

planes is, according to Wulff, geometrically similar to the ultimate equilibrium shape for the crystal; i.e., the shape which minimizes Eq. (1) for fixed volume. This construction is shown by the dashed line in the figure. The proofs of this theorem which have been given[4] have been formulated only for the case in which the equilibrium shape is a polyhedron, but they are easily generalized to apply to cases in which part or all of the equilibrium shape is bounded by smoothly curved surfaces.

This equilibrium shape is of direct practical interest only for very small crystals, since for a large crystal a significant alteration in shape can be achieved only by transporting a large number of atoms through a large distance, and the effort involved in doing this becomes very large in comparison with the decrease in Eq. (1) which rewards it. For large crystals it is of greater interest, therefore, to inquire how the free energies of neighboring configurations compare, even though none of these is at all close to the shape given by the Wulff construction. In Sec. II we therefore consider the question: when can the free energy of a plane surface be lowered by rearranging the atoms into hills and valleys of a size large compared with atomic dimensions but still small from the macroscopic standpoint?

Section III will be devoted to an investigation of the conditions under which the equilibrium shape can be bounded in part by continuously curved regions, or more generally, the conditions under which a continuously curved surface can be thermodynamically stable with respect to small distortions or roughenings.

In Sec. IV it will be shown that the often-used assumption that the atoms of a crystal interact attractively in pairs leads to a Wulff construction which has certain degenerate properties, so that conclusions based on this assumption may be qualitatively as well as quantitatively altered by slightly modifying the assumption. This will be illustrated in Sec. V by a discussion of the amount of rounding of edges and corners which is to be expected for surface structures in local thermodynamic equilibrium.

II. THERMODYNAMIC STABILITY OF A HILL-AND-VALLEY SURFACE STRUCTURE

To see under what circumstances it is possible to decrease the free energy of an initially flat surface by rearranging the atoms into hills and valleys, consider a polar plot of surface free energy such as that in Fig. 1. Let OA be the direction normal to the crystal surface in question. Consider any three other directions OB_1, OB_2, OB_3 (only the first two are shown in the plane of the drawing), having positive projections on OA. The planes normal to these three directions could form the sides of a hill-and-valley structure on a macroscopic surface normal to OA. The surface free energy of such a hill-and-valley structure would be, per unit area of the macroscopic surface,

$$\gamma_h = \gamma_1 f_1 + \gamma_2 f_2 + \gamma_3 f_3, \tag{2}$$

where γ_1, γ_2, γ_3 are the surface tensions of the three boundary planes just mentioned, and f_1, f_2, f_3 are the areas of surfaces of these three types in the hill-and-valley structure per unit projected area in the plane of the macroscopic surface. If we let $\boldsymbol{\sigma}_1$, $\boldsymbol{\sigma}_2$, $\boldsymbol{\sigma}_3$ be the unit normal vectors for the three boundary planes, the equations determining f_1, f_2, f_3 are

$$f_1\boldsymbol{\sigma}_1 + f_2\boldsymbol{\sigma}_2 + f_3\boldsymbol{\sigma}_3 = \boldsymbol{\sigma}, \tag{3}$$

where $\boldsymbol{\sigma}$ is the unit vector in the direction OA. Now if we let $\boldsymbol{\tau}_1$, $\boldsymbol{\tau}_2$, $\boldsymbol{\tau}_3$ be the system reciprocal to $\boldsymbol{\sigma}_1$, $\boldsymbol{\sigma}_2$, $\boldsymbol{\sigma}_3$, i.e.,

$$\boldsymbol{\tau}_1\cdot\boldsymbol{\sigma}_1 = \boldsymbol{\tau}_2\cdot\boldsymbol{\sigma}_2 = \boldsymbol{\tau}_3\cdot\boldsymbol{\sigma}_3 = 1, \quad \boldsymbol{\tau}_j\cdot\boldsymbol{\tau}_j = 0 \quad (i\neq j),$$

Eq. (2) can be written

$$\gamma_h = (\gamma_1\boldsymbol{\tau}_1 + \gamma_2\boldsymbol{\tau}_2 + \gamma_3\boldsymbol{\tau}_3)\cdot\boldsymbol{\sigma}. \tag{4}$$

The vector in parentheses is, however, identical with the vector $\mathbf{c}$ which joints the origin to the corner C defined as the intersection of the three planes drawn normal to OB_1, OB_2, OB_3, respectively, at the points where these directions intersect the polar plot of γ. For

$$\mathbf{c}\cdot\boldsymbol{\sigma}_1 = \gamma_1, \quad \mathbf{c}\cdot\boldsymbol{\sigma}_2 = \gamma_2, \quad \mathbf{c}\cdot\boldsymbol{\sigma}_3 = \gamma_3,$$

and the vector in parentheses satisfies these equations. Thus, finally

$$\gamma_h = \mathbf{c}\cdot\boldsymbol{\sigma}, \tag{5}$$

i.e., the surface free energy of the hill-and-valley structure is represented by the length OM from the origin to the foot M of a perpendicular drawn from C to OA.

Thus, if there exists any set of directions OB_1, OB_2, OB_3 with positive projections on OA, such that M lies inside the polar plot of γ, an ideal crystal surface normal to OA will be thermodynamically unstable with respect to formation of some sort of hill-and-valley structure. The converse is also true: if no such set of directions exists, the ideal surface normal to OA will be stable. The possibility of more than three types of surface for the sides of the hill-and-valley structure does not impair this conclusion, since the free energy of any hypothetical structure with more than three types of hill side can always be lowered by eliminating all but the three most favorable types. Now the condition that M be inside the polar plot of γ is the same as the condition that C be inside the plane drawn normal to OA at the point of its intersection with the γ-plot. If there exists a set OB_1, OB_2, OB_3 for which this is the case, the plane normal to OA cannot occur as a boundary plane in the Wulff construction for the equilibrium shape, i.e., it can neither form a flat portion of the boundary nor be tangent to a continuously curved portion; conversely, if OA is included among the normals of the equilibrium shape, some such set OB_1, OB_2, OB_3 must exist. We therefore have the result: *If a given macroscopic surface of a crystal does not coincide in orientation with some portion of the boundary of the equilibrium shape, there will always exist a hill-and-valley structure which has a lower free energy than a flat surface, while if the given surface does occur in the equilibrium shape, no hill-and-valley structure can be more stable.*

The implications of this result depend very much on the nature of the equilibrium shape. If the equilibrium shape is a polyhedron, as has usually been assumed to be the case for crystals, then a crystal surface chosen with a random macroscopic orientation will almost always prefer to have a hill-and-valley structure. At the other extreme, if the equilibrium shape has no sharp corners at all, then surfaces of every orientation will prefer to remain smooth.

III. QUALITATIVE CHARACTERISTICS OF THE γ-PLOT AND THE EQUILIBRIUM SHAPE

Let us now consider under what conditions a given direction will occur among the surface normals of the equilibrium shape. In Fig. 2, let O be the origin of the Wulff diagram and OA a normal direction to be investigated. Let A' be another point of the γ-plot infinitesimally distant from A. The plane normal to OA at A and that normal to OA' at A' will intersect along a line through P; a third such plane, constructed on a line OA'' lying outside the plane of the drawing (not shown, of course) would intersect the other two planes at some point P_s. The figure has been drawn for the case in which P_s and P coincide; but we shall use different symbols for them, since P_s does not in general lie in the plane OAA' of the drawing. Now if A is a point in whose neighborhood the slope of the γ-plot varies continuously with direction, $P_s(A, A', A'')$ will approach

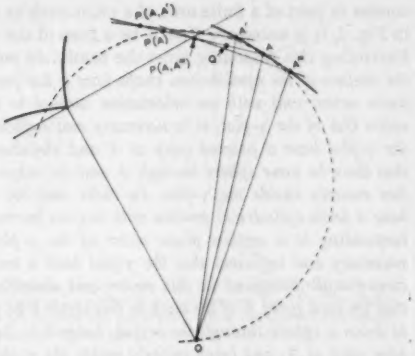

FIG. 2. Use of the tangent sphere to predict properties of the Wulff construction. The heavy curve shows two portions of the polar plot of surface free energy, and the dashed circle is a cross section of the sphere tangent to this plot at A and passing through the origin O.

a limiting position $P_s(A)$ as A' and A'' approach A. A sphere drawn with the origin and $P_s(A)$ as opposite ends of a diameter will be tangent to the γ-plot at A. If any point of the γ-plot, either in the neighborhood of A or in some more distant region, lies inside this sphere, $P_s(A)$ will lie outside the surface of the Wulff construction for the equilibrium shape; if the γ-plot is entirely outside the sphere, $P_s(A)$ will be on the periphery of the equilibrium shape. Since we are assuming the slope of the γ-plot to be continuous near A, no other point Q of the plane $AP(A)$ can be on the periphery of the equilibrium shape, for there can always be found an A''' in the neighborhood of A whose plane will pass inside Q. We therefore have the result: *If OA is a radius vector of the γ-plot in whose neighborhood the derivatives of γ are continuous, then a necessary and sufficient condition for the direction OA to occur among the normals of the equilibrium shape is that the γ-plot nowhere pass inside the sphere drawn through the origin and tangent to the γ-plot at A. When the γ-plot is outside this sphere at all points except A, all orientations in the neighborhood of OA will occur among the normals of the equilibrium shape; i.e., the latter will be continuously curved in the region where its normal has the direction OA.*

Combination of this result with that of the preceding Section gives the further conclusion: *A continuously curved surface with normals in the neighborhood of OA will be stable with respect to formation of a hill-and-valley structure if, and only if, the γ-plot nowhere passes inside the sphere through the origin and tangent at A.*

We consider next the conditions under which a plane region of finite area can occur as part of the boundary of the equilibrium shape. Since the position of the point $P_s(A)$, defined previously varies continuously with A (Fig. 2), except at points of the γ-plot where the derivatives of γ are discontinuous, it is clear that in order for the boundary of the equilibrium shape to

consist in part of a finite area of a plane such as $AP(A)$ in Fig. 2, it is necessary that A be a cusp of the γ-plot. Extending this reasoning gives the result: *In order that the surface of the equilibrium shape have a flat portion of finite extent and with an orientation normal to a given vector OA of the γ-plot, it is necessary and sufficient that the γ-plot have a pointed cusp at A and simultaneously that there be some sphere through A and the origin which lies entirely inside the γ-plot. In order that the surface have a finite cylindrical portion with surface normals corresponding to a certain plane sector of the γ-plot, it is necessary and sufficient that the γ-plot have a knife-edge cusp for all directions in this sector, and simultaneously that for each point A of the cusp in this sector it be possible to draw a sphere through the origin, tangent to the knife-edge cusp at A, and lying entirely inside the γ-plot.*

These results provide a convenient tool for exploring the possible types of equilibrium shapes for various types of γ-plots. We shall consider first the case where γ and its derivatives are continuous for all directions. As we shall show presently, this case cannot occur for crystals, for which γ may be expected to have cusped minima in crystallographically simple directions; however, it may occur for liquid crystals and for the anisotropic colloid phases known as tactoids.[6] For this case there are clearly two possibilities:

(a) All directions occur among the normals to the equilibrium shape, so that there are no sharp edges or corners. This will occur if the sphere tangent at any point of the γ-plot always lies inside it, a condition which will obviously be fulfilled if the γ-plot is sufficiently close to a sphere.

(b) The equilibrium shape is bounded by a number of smoothly curved (not flat) surfaces which intersect in sharp edges. This includes all cases not falling under (a); photographs of tactoids[6] usually show shapes of this type.

As has just been mentioned, the γ-plot for a crystal may be expected to have cusps; and it can, in fact, be argued that at sufficiently low temperatures point cusps occur for all orientations whose Miller indices are rational, and knife-edge cusps for orientations any two of whose Miller indices are rational. The argument is similar to that used by Read and Shockley[6] to deduce the corresponding result for grain boundary energies, and it will be sketched only briefly here. We assume that when the Miller indices are rational, the surface structure of lowest energy will consist of atomic steps arranged in some sort of two-dimensional lattice structure. If the unit normal describing the orientation of the surface is changed infinitesimally, say from $\mathbf{n}$ to $(\mathbf{n}+\delta\mathbf{n})$, the arrangement of minimum energy will be the same two-dimensional lattice of steps as before, but with widely spaced lines along which the interval between steps is slightly greater or slightly less than in the original lattice. The density of these lines will be proportional to $\delta\mathbf{n}$; and when this density is low, the modification of the energy will be proportional to the density of lines, hence to $\delta\mathbf{n}$. A similar proportionality to $\delta\mathbf{n}$ will hold for the energy change when the normal is changed to $(\mathbf{n}-\delta\mathbf{n})$; but the coefficient will, in general, be different. The average of the specific surface energies for $(\mathbf{n}+\delta\mathbf{n})$ and $(\mathbf{n}-\delta\mathbf{n})$ will thus, in general, differ from that for $\mathbf{n}$ by an amount of order $\delta\mathbf{n}$, so that the γ-plot has a cusp for orientation $\mathbf{n}$. This cusp must point toward rather than away from the origin, since otherwise the step array assumed for orientation $\mathbf{n}$ would not be the arrangement of minimum energy.

This conclusion needs to be modified somewhat at the high temperatures at which most of the phenomena involving surface tension of crystals occur. For when the spacing between steps is large, as for say a (20, 1, 0) surface of a cubic crystal, thermal fluctuations in the positions of the steps may be sufficient to prevent their having any long-range order; in other words, the two-dimensional lattice of steps may "melt."[7] When this occurs, no cusp in the γ-plot is to be expected. When the spacing of steps is small—for example, a (210) surface—they may be expected to have a long-range order, and the considerations of the preceding paragraph should apply. The most reasonable form to assume for the γ-plot of a crystal at elevated temperature is, therefore, a plot which is smooth except in directions in which two or all of the Miller indices have the ratio of sufficiently small integers; in these directions cusps of the type mentioned in the preceding paragraph should occur.

Assuming the γ-plots of crystals to be of this form, we may use the italicized results above to classify the possibilities for crystals as follows:

(c) The equilibrium shape consists of a number of flat surfaces joined by rounded regions, with no sharp edges or corners. This will occur if the cusps are so mild that none of the tangent spheres passes outside the γ-plot.

(d) The equilibrium shape consists of flat surfaces and curved regions, with sharp edges.

(e) The equilibrium shape is a polyhedron. This will occur if the cusps are so pronounced that no tangent sphere can be drawn inside all the cusps.

Of the five cases we have enumerated, all except case (e) have been practically ignored in the literature.

IV. SPECIAL CASES WHICH LEAD TO A γ-PLOT COMPOUNDED OF PORTIONS OF SPHERES

It is clear from the results of the preceding section that a cusped γ-plot whose smooth regions are portions of spheres through the origin represents a transitional case

[6] H. Zocher, Z. anorg. u. allgem. Chem. **147**, 91 (1925); J. Jochims, Kolloid-Z. **41**, 215 (1927); H. Zocher and K. Jacobsohn, Kolloid-Z. **41**, 220 (1927), Kolloid-Beihefte **28**, 167 (1929); W. Heller and W. Wojtewicz, Phys. Rev. (A) **75**, 343 (1949).

[6] W. T. Read and W. Shockley, Phys. Rev. **78**, 275 (1950).

[7] This "melting" is closely related to the existence of a critical temperature for surface fluctuations, a phenomenon which has been studied quantitatively by W. K. Burton and N. Cabrera, Disc. Faraday Soc. **5**, 33 (1949).

between case (e) (polyhedral equilibrium shape) and case (c) (smooth shape). For such a γ-plot all of the perpendicular planes erected on radius vectors of any one of the spherical regions pass through a common point. The principal object of this Section is to prove that a theoretical γ-plot of this sort is predicted by any model of a crystal based on the assumptions that the atoms interact attractively in pairs by means of forces of finite range and that the surface and interior lattice spacings are the same.

Let us assume the energy of a crystal relative to separated atoms to be

$$E=-\tfrac{1}{2}\sum_{i\neq j}\epsilon_{ij}=-\sum_{\mathbf{b}}\nu_{\mathbf{b}}\epsilon_{\mathbf{b}}, \tag{6}$$

where $\epsilon_{ij}=\epsilon_{\mathbf{b}}$ is the negative interaction energy of atoms i and j, a function of the vector $\mathbf{b}$ connecting them, and $\nu_{\mathbf{b}}$ is the number of pairs of atoms separated by the vector $\mathbf{b}$. For simplicity we assume, in the present treatment, that all atoms are alike; however, the analysis can be generalized to include at least some types of non-monatomic crystals. If the surface and interior lattice spacings are assumed to be the same, an ideal surface of the crystal normal to any unit vector $\mathbf{n}$ will have the same atomic arrangement as if one passed a plane normal to $\mathbf{n}$ through the middle of the lattice and removed the material on one side. If $f_{\mathbf{b}}$ is the number of interatomic vectors of type $\mathbf{b}$ per unit area of a plane normal to $\mathbf{b}$, the surface energy, as determined from the number of bonds cut, is

$$\gamma_{\mathbf{n}}=\Sigma_{\mathbf{b}}\,\epsilon_{\mathbf{b}}f_{\mathbf{b}}|\,\mathbf{n}\cdot\mathbf{b}\,|/b. \tag{7}$$

If the interatomic forces have finite range, there will be a only finite number of $\mathbf{b}$'s for which $\epsilon_{\mathbf{b}}\neq 0$, and the possible directions for $\mathbf{n}$ can be divided into pyramids within each of which none of the quantities $\mathbf{n}\cdot\mathbf{b}$ changes sign. Within any such pyramid p, therefore,

$$\gamma_{\mathbf{n}}=\mathbf{n}\cdot\mathbf{s}_p, \tag{8}$$

the vector $\mathbf{s}_p$ changing as we go from one pyramid to another. Thus, under the assumptions used, the locus of the end of the vector $\gamma_{\mathbf{n}}\mathbf{n}$ is, within each pyramid, the surface of a sphere passing through the origin; the spheres change as we go from one pyramid to another.

Consider now a path on the surface of the γ-plot, passing from one of the pyramidal regions of solid angle, say p_1, to another p_2. As we follow this path, either the sphere going with p_2 will cut inside that going with p_1, as in (a) of Fig. 3, or it will cut outside as in (b). The former is impossible if all the $\epsilon_{\mathbf{b}}$ are of the same sign (>0). For then all the terms in Eq. (7) are positive, so that the $\mathbf{s}_p$ in whose pyramid $\mathbf{n}$ lies gives a larger value of $\mathbf{n}\cdot\mathbf{s}_p$ than any other pyramid p'. Since for case (a) of Fig. 3 a vector $\mathbf{n}$ lying in p_1 has $\mathbf{n}\cdot\mathbf{s}_1<\mathbf{n}\cdot\mathbf{s}_2$, only cusps of the type shown in (b) can occur when all $\epsilon_{\mathbf{b}}$ are >0. When some of the $\epsilon_{\mathbf{b}}$ are <0, as for an ionic crystal, Eq. (8) may lead either to case (a) or to case (b). If it leads to case (a), the ideal crystal surface formed by cutting through the volume of the crystal along a plane cannot be stable, since, as was shown in the preceding section, the γ-plot cannot have outward-pointing cusps.

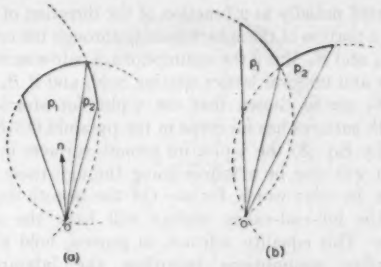

FIG. 3. Portions of the polar plot of the surface energy of an ideal crystal plane for a crystal model obeying Eq. (6). The heavy curves are portions of the polar plot, while the dashed curves are the continuations of the circles to which they belong.

The results just proved can be generalized a little. Consider a surface whose orientation differs from that of one of the simple crystallographic planes (hkl) by a fairly small angle θ, so that fairly widely spaced steps result. Instead of assuming that the atoms interact in pairs, we may assume merely that the energy of the surface in question is proportional to the projection of its area onto (hkl) plus a term proportional to the density of steps, i.e., that steps whose spacing exceeds a certain distance do not interact. This assumption, as is easily seen, leads to the prediction of the spherical form of Fig. 3 (b) for the γ-plot over the range of orientations to which the assumption applies.

Stranski and his collaborators[8,9] have carried out extensive investigations on the dependence of equilibrium forms and other properties of crystals on the range of the interatomic forces, using the assumption of attractive pair-wise interactions. From what has been said earlier in this Section, it is clear that this model, though useful as an aid in visualizing the physical mechanisms responsible for the surface structures of crystals, has rather special properties which real crystals, especially metallic ones, will not, in general, possess. One illustration of this fact is provided by the comparison of the energies of an atomically smooth surface and a hill-and-valley surface, the problem we have treated for the general case in Sec. II. Our Eq. (5), which has the same form as Eq. (8), implies that if a surface with macroscopic normal OA (Fig. 1) is made up of hills with sides normal to vectors OB_1, OB_2, OB_3 of the γ-plot, the macroscopic surface tension $\gamma_{\mathbf{n}}$ will,

[8] This work has been published in a large number of papers of which we shall cite only a few: I. N. Stranski, Z. physik. Chem. **B11**, 342 (1931); I. N. Stranski and R. Kaischew, Z. Krist. **78**, 373 (1931), Z. physik. Chem. **B26**, 312 (1934); Ann. Physik **23**, 330 (1935); I. N. Stranski, Z. physik. Chem. **B38**, 451 (1938); I. N. Stranski and R. Suhrmann, Z. Krist. **105**, 481 (1944), Ann. Physik **1**, 153 (1947); I. N. Stranski, Disc. Faraday Soc. **5**, 13 (1949). See also the brief summary in reference 9.

[9] I. N. Stranski, Ber. deut. chem. Ges. **A72**, 141 (1939).

if plotted radially as a function of the direction of OA, lie on a portion of the sphere passing through the origin, B_1, B_2, and B_3. But if the assumptions of pair-wise interaction and uniform lattice spacing hold, and if B_1, B_2, and B_3 are so chosen that the γ-plot for atomically smooth surfaces has no cusps in the pyramid $OB_1B_2B_3$, then by Eq. (8) the γ-plot for smooth surfaces in this region will also be a sphere going through these four points. In other words, for any OA the smooth surface and the hill-and-valley surface will have the same energy. This equality will not, in general, hold if less restrictive assumptions regarding the interatomic forces are used. In the next Section, we shall discuss another problem with respect to which this model likewise behaves in an exceptional manner.

V. APPLICATION TO THE ROUNDING OF EDGES

In this Section, we shall consider the question of the sharpness of the edges and corners of an equilibrium polyhedron, or of a hill-and-valley surface formed by thermal etching. The present discussion will be limited to cases in which the Wulff construction predicts ideally sharp edges, i.e., cases (b), (d), and (e) of Sec. III. Moreover, since this paper is concerned with the phenomenological rather than the atomistic approach to crystal surfaces, we shall be able to treat only those cases (if such exist) in which the radius of curvature of the edges and corners is fairly large compared with atomic dimensions; these are, of course, the cases for which the departure from ideal sharpness is most likely to be detectable experimentally.

When the minimum radius of curvature is large, it is tempting to retain the expression (1) for the surface free energy of the crystal, taking account of the curved edges by allowing γ to depend on the radius of curvature ρ of the surface, e.g., by setting

$$\gamma(\mathbf{n},\rho)=\gamma_0(\mathbf{n})+[\gamma_1(\mathbf{n})/\rho]+[\gamma_2(\mathbf{n})/\rho^2]\cdots. \quad (9)$$

For simplicity we shall consider only an edge where the surface contour is cylindrical, so that only one radius of curvature need be considered. To make an equation of the form of Eq. (9) significant it is, of course, necessary that the position of the mathematical surface, by which the crystal surface is idealized, be defined accurately at each point. For a crystal a definition of sufficient accuracy is that of Gibbs,[10] which places the surface in such a position that, for any cylinder bounded by an element of the surface, the normals erected around its boundary, and a closing surface in the deep interior, the mass within the cylinder equals its volume times the interior density. This definition locates a plane surface precisely and locates a curved surface to within an uncertainty in the normal direction of the order of a^2/ρ, where a is the lattice constant; this accuracy is sufficient for our purpose.

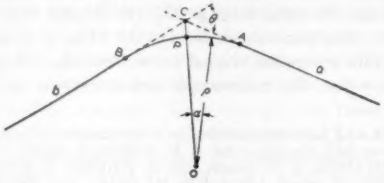

FIG. 4. Cross section of the surface of a crystal near where two flat faces a and b meet in a rounded edge.

[10] J. W. Gibbs, *Collected Works* (Longmans, Green, and Company, New York, 1928), p. 314.

Consider the rounded edge, shown in Fig. 4, connecting two flat surfaces a and b which make an angle θ with each other. Although this edge will not, in general, have a circular cross section, for simplicity we shall consider it constrained to be circular, so that ρ is constant over it. We wish to compare the free energies of the various possible surfaces of this form which one can obtain by choosing different values for ρ. When $\rho=0$, the surface is the sharp-edged one ACB which minimizes $\int\gamma_0 dS$ but makes the higher terms of Eq. (9) infinite; when ρ is very large, the higher terms of Eq. (9) are negligible and $\int\gamma_0 dS$ increases with increasing ρ. The explicit expression for $\int\gamma dS$ is easily written down if faces a and b have an extension $\gg\rho$, since, for this case, only a negligible outward displacement of faces a and b is required to keep the volume of the crystal constant when ρ is changed. Supposing planes a and b fixed, we have, for a length L normal to the plane of the figure,

$$(1/L)\int\gamma_0 dS = \text{const}-(\gamma_{0a}+\gamma_{0b})\rho\tan(\theta/2)+\langle\gamma_0\rangle_{Av}\rho\theta, \quad (10)$$

$$(1/L)\int[(\gamma_1/\rho)+(\gamma_2/\rho^2)]dS=\langle\gamma_1\rangle_{Av}\theta+\langle\gamma_2\rangle_{Av}\theta/\rho, \quad (11)$$

where $\langle\gamma_0\rangle_{Av}$, $\langle\gamma_1\rangle_{Av}$, $\langle\gamma_2\rangle_{Av}$ are averages over the range $-\theta/2$ to $\theta/2$ of the angle α of Fig. 4. The sum of Eqs. (10) and (11) is a minimum with respect to ρ when

$$\rho^2=\langle\gamma_2\rangle_{Av}\theta/[\langle\gamma_0\rangle_{Av}\theta-(\gamma_{0a}+\gamma_{0b})\tan(\theta/2)]. \quad (12)$$

Whenever this equation gives a $\rho\gg$ the lattice constant, it should describe fairly correctly the amount of rounding which an edge of the equilibrium shape will have.

The denominator of Eq. (12) has a simple geometrical interpretation in terms of the polar plot of surface free energy, an interpretation which, though valid for any γ_{0a} and γ_{0b}, is most easily demonstrated for the case where $\gamma_{0a}=\gamma_{0b}$. This denominator can be written

$$\int_{-\theta/2}^{\theta/2}[\gamma_0-\tfrac{1}{2}(\gamma_{0a}+\gamma_{0b})\sec(\theta/2)\cos\alpha]d\alpha. \quad (13)$$

When $\gamma_{0a}=\gamma_{0b}$, the coefficient of $\cos\alpha$ in the integrand is just the distance from the origin to the edge C of the Wulff construction in Fig. 5. The whole integrand is, therefore, the distance NM, where $ON=\gamma_0(\alpha)$, and M

is the intersection of ON with the sphere having OC as a diameter. The integral Eq. (13), which is the denominator of Eq. (12), is, therefore, essentially proportional to the area of the shaded region, being an integral over this region in which each element of area is given a weight inversely proportional to its distance from the origin. Thus, the more nearly this portion of the γ-plot approaches the dotted sphere, the larger will be the equilibrium radius of curvature ρ of the edge of the crystal. The theoretical model considered in the preceding Section, which assumes pair-wise attractive interactions and uniform lattice spacing, therefore predicts a very large value of ρ for the edges of the equilibrium form, this value being limited only by the fact that the size of the specimen is finite rather than infinite as we have assumed in deriving Eq. (12). Stranski,[9] using an atomistic argument based on this model, has already pointed out that ρ becomes infinite as the size of the specimen is increased; the new feature of the calculation of Eq. (12) is that it allows us to estimate ρ when the assumptions of this model are not fulfilled.

At the present time, numerical estimates must, of course, be very crude, since we can only guess at $\langle\gamma_2\rangle_{Av}$. A reasonable guess would be $\langle\gamma_2\rangle_{Av}\sim f\langle\gamma_0\rangle_{Av}a^2$, where a is the lattice constant, and f is a quantity of the order of a fraction of unity. Equation (12) then gives

$$\rho/a\sim(2fA/\Delta A)^{\frac{1}{2}}, \tag{14}$$

where A is the area of the section of the γ-plot of Fig. 5 between the normals to a and b, and ΔA is the shaded area. It is clear from this that the γ-plot must be very close indeed to the sphere before ρ becomes larger than 10 or 20 atom spacings. It does not seem likely that the special models, referred to in the preceding paragraph and in Sec. IV, can be sufficiently nearly valid for any metals for this to occur; and we accordingly conclude that, for metals for which case (e) of Sec. III holds, the edges and corners of the equilibrium shape will be sharp to within at most a few tens of atom spacings. When case (d) or case (c) obtains, part or all of the equilibrium shape will be smoothly rounded, and reasoning similar to that just given suggests that for specimens of observable size the amount of rounding will correspond

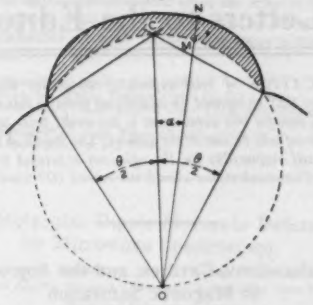

FIG. 5. Geometrical significance of the denominator of Eq. (12). The heavy curve is the polar plot of surface free energy with origin at O, and the dashed curve is a section of a sphere.

fairly closely to that demanded by the Wulff construction without any further refinements.

An example to which these conclusions can be applied is provided by the sharp points of tungsten and other metals which have been used in field emission studies.[11] These points, of the order of a micron or less in diameter, appear to revert to a particular standard shape when heated to temperatures of the order of half the melting temperature, this shape being a smoothly rounded one with, perhaps, a few flat regions in the crystallographically simplest directions. For tungsten, at least, there is other evidence, summarized in reference 1, which suggests that the equilibrium shape for a larger specimen is polyhedral or almost so. Since the arguments just given are unfavorable to the hypothesis that the observed rounding is due to the dependence of surface tension on curvature, we must conclude either that the equilibrium shape determined by the Wulff construction is not polyhedral after all but of the smoothly rounded type (c), or else that the standard shape of the field emission points is not an equilibrium shape but a quasi-steady configuration determined by some continuing transport process.

[11] A review has been given by R. O. Jenkins, Repts. Prog. Phys. 9, 177 (1943). See also E. W. Müller, Z. Physik 120, 270 (1943); 126, 642 (1949).

Letters to the Editor

PUBLICATION of brief reports of important discoveries in physics may be secured by addressing them to this department. The closing date for this department is five weeks prior to the date of issue. No proof will be sent to the authors. The Board of Editors does not hold itself responsible for the opinions expressed by the correspondents. Communications should not exceed 600 words in length.

Dislocations, Cavities, and the Approach to Magnetic Saturation

WILLIAM FULLER BROWN, JR.
Sun Physical Laboratory, Newtown Square, Pennsylvania
(Received January 22, 1951)

IN discussing the approach to magnetic saturation, Stoner[1] writes: "In a related paper dealing with the a/H term, and also describing work virtually completed in 1945, Néel (1948a) points out that no mechanism involving perturbing forces can give rise to a rigorous law of this type, which implies an indefinitely large work of magnetization. This rules out most of the suggestions that have been made, including those of Brown (1940b, 1941), whose study of the effect of point, line, and plane concentrations of force, or, less formally, of dislocations, is none the less of great interest."

Apparently Néel[2] misunderstood my dislocation formulas,[3] and Stoner accepted his interpretation. Any result obtained by integrating the formulas to $H=\infty$ is meaningless, because they are based on approximations that break down at very high field intensities. This fact does not impair the validity of the formulas over the range in which they were intended to be applied; nor can it discredit the physical hypothesis on which the calculation was based.

Throughout, the dislocation radius was treated as vanishingly small. This approximation is permissible if the magnetic decay distance (proportional to $H^{-\frac{1}{2}}$) is large in comparison with the dislocation radius, i.e., with the lattice spacing. At the highest field intensity considered, 6000 oersteds, the decay distance is about 2×10^{-6} cm—still 100 times the lattice spacing.

Formulas (25) and (45) of reference 3, based on the "doublet" approximation, are applicable to actual dislocation pairs only if the decay distance is large in comparison with the separation distance. Because of this restriction, the doublet formulas were used only as a basis for qualitative discussion; in particular, for estimating the importance of magnetic interactions, which could be taken into account more easily in the doublet calculation than in the main calculation.

The numerical calculations were based, not on the doublet formulas, but on the formulas of Sec. 3. In the working formula (41), the resolution into terms a/H, b/H^2, and $\chi(H)$ depends on a classification of the separation distances into three groups, explicitly defined (p. 144, column 2, lines 5–15) with reference to "the range of fields under investigation." If the range is shifted upward, the number of dislocation pairs in the a/H group will decrease and the number in the b/H^2 group will increase. There is therefore no question of a rigorous a/H law or of an infinite magnetization work. (The more general formulas (28)–(32) would give a finite magnetization work, but it would be incorrect because of the approximation in regard to dislocation radius.)

When my approximations are permissible, the integration over a stress singularity—to which Néel objected—is also permissible. What makes it so is the term $\nabla^2\alpha$ in Eq. (17). Néel's omission of this term in his cavity calculation is equivalent to setting the decay distance equal to zero. His formula therefore holds only if the decay distance is small in comparison with the cavity dimensions.

That the coefficient a increases with plastic flow is an experimental fact, independent of any theoretical calculation. It is this experimental fact that I interpreted by use of dislocation theory. Plastic flow is a shear process, not explicable in terms of cavities. Néel's cavity formula no doubt describes correctly the behavior of his samples of porous iron; but they were specially designed to exhibit the behavior described by the formula. His theory does not explain the effects of plastic flow, and it therefore affords no all-inclusive explanation of the origin of the a/H term in an arbitrary specimen.

[1] Edmund C. Stoner, *Reports on Progress in Physics* (The Physical Society, London, 1950), Vol. 13, pp. 83–183. See especially pp. 142–143.
[2] L. Néel, J. de phys. 9, 184 (1948).
[3] William Fuller Brown, Jr., Phys. Rev. 60, 139 (1941).

Notes on the Electrical and Thermal Conductivities of Graphite and Amorphous Carbon

SANCHI MIZUSHIMA AND JUN OKADA
Research Laboratory, Tohoi Electrode Company, Fujisawa, Japan
(Received October 16, 1950)

ACCORDING to the theory proposed by Wallace,[1] the electrical conductivity σ in the direction parallel to the basal plane of a graphite crystal is given by the following expression

$$\sigma=(16\pi e^2\tau/h^3c)kT\log 2,$$

where τ = relaxation time of the conduction electrons, c = lattice constant in the direction normal to the basal plane, T = temperature, and other notations have their usual meanings. The conductivity in the direction normal to the basal plane is far smaller than the former, so that the apparent conductivity of a polycrystalline material will be determined almost solely by σ. Hence, specific resistance times temperature will be proportional to $1/\tau$. The resistivity of artificial graphite is known to decrease with the graphitization temperature. This relation has been made clear by the experiments of Nishiyama[2] on the graphitization of carbon filaments in connection with the temperature dependence of the resistivity. From his data, values of ρT were calculated. These are plotted in Fig. 1 against temperature. These curves corresponding to different heat treatments are nearly parallel to each other, which indicates that the relation $1/\tau=(1/\tau_0)+1/\tau'$ holds fairly well for each curve, where the first term on the right-hand side represents the reciprocal of the relaxation time for pure graphite, and the second term depends on the temperature at which the heat treatment was carried out. This situation is analogous to that of common metals containing impurities. Hence, the second term bears a closer resemblance to the residual resistance of metals than to the temperature dependent resistivity of semiconductors

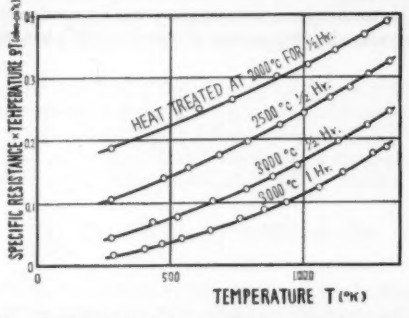

FIG. 1. Temperature dependence of ρT; i.e., the resistivity of carbon filaments graphitized at different temperatures times absolute temperature. ρT is inversely proportional to the relaxation time of the conduction electrons.

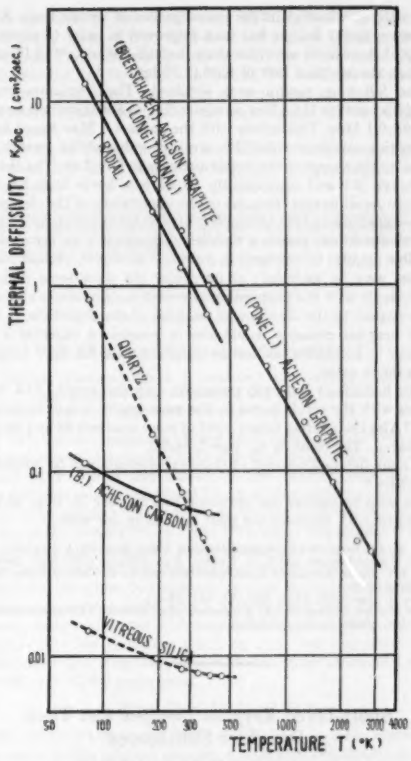

FIG. 2. Variation with temperature of the thermal diffusivities of carbon and silica.

for the impurity scattering. This result may be attributed to the dependence of the energy on the wave number vector, which is linear near the Fermi surface, and to the proportionality of the effective mass to temperature. On the other hand, the electrical conductivity of amorphous carbon, such as pitch coke which has been heated at low temperatures, was found to be expressed approximately by $\sigma = A \exp(-E/kT)$, where A is a constant. The activation energy E varied from about 0.10 ev to 0.03 ev for specimens heated between 520°C and 715°C. Films of organic substance remaining at the crystallite boundaries are probably playing an important role in these cases.

It has been noted that there is a remarkable difference between the thermal conductivity of graphite and that of amorphous carbon. This can be explained by the difference of the mean free paths of thermal elastic waves in the two media. The thermal conductivity K is expressed in terms of the propagation velocity u and the mean free path l as $K/DC = lu/3$, where D is the density and C is the specific heat. Values of the thermal diffusivity are plotted in Fig. 2 against temperature for artificial graphite and amorphous carbon using the experimental data obtained by several investigators.[2,4] For comparison, curves for quartz and vitreous silica are included there also. It is evident from this figure that there is a close resemblance between these two sets of curves. Therefore, the mean free path is considered to be determined by mutual collisions in the case of graphite and by the crystallite boundaries in the case of amorphous carbon, just as for the two allotropic forms of silica.[5] In fact, the mean free path in amorphous carbon was estimated to be the order of 50A, which may be compared with the crystallite size of several tens of angstroms measured by x-ray methods for many kinds of amorphous carbon.

[1] D. P. Wallace, Phys. Rev. 71, 622 (1947).
[2] Y. Nishiyama, Sci. Repts. Tohoku Univ. 21, 171 (1932).
[3] R. W. Powell and F. H. Schofield, Proc. Phys. Soc. (London) 51, 153 (1939).
[4] R. A. Buerschaper, J. Appl. Phys. 15, 452 (1944).
[5] C. Kittel, Phys. Rev. 75, 972 (1949).

Some Molecular Dipole Moments Determined by Microwave Spectroscopy

JAMES N. SHOOLERY* AND A. HARRY SHARBAUGH
General Electric Research Laboratory, Schenectady, New York

(Received February 9, 1951)

A STARK modulation type absorption cell has been constructed in which the electrode spacing is known to ±0.2 percent. The dipole moments of several compounds have been measured and these are listed in Table I.

TABLE I. Dipole moments from Stark effect measurements.

Formula	Compound	$\mu \times 10^{18}$ (esu)	Transition observed
OCS	Carbonyl sulfide	0.712 ± 0.004	$J_{1\to 2}$
HNCO	Isocyanic acid	1.592 ± 0.010	$0_{0,0}\to 1_{0,1}$
H_2CO	Formaldehyde	2.339 ± 0.013[a]	$9_{0,9}\to 9_{0,7}$
		2.340 ± 0.019	$3_{1,3}\to 3_{1,2}$
CHF_3	Fluoroform	1.645 ± 0.009	$J_{0\to 1}$

[a] The absolute accuracy of the value 2.17 ± 0.02 Debye units, reported by J. K. Bragg and A. H. Sharbaugh [Phys. Rev. 75, 1774 (1949)], was in error because of an irregularly spaced Stark electrode. Use of the new precision cell precludes this possibility in the present work.

The experimental error quoted is the sum of the precision error of the particular measurement and the systematic errors. These are: (1) Electrode spacing, ±0.2 percent. (2) Voltage divider, ±0.06 percent, and (3) Error in the measurement of the displacement of the absorption line, under the applied field, ±0.1 percent, due to uncertainty in the frequency of the undisplaced line. This error can be neglected in the measurements for OCS, since the dipole moment was calculated from Stark components which moved to higher and lower frequencies.

A reduction of 0.7 percent has been applied to the calculated dipole moments to account for field inhomogeneities and the fact that the average of the displacements caused by the top and bottom of the square wave does not yield the displacement corresponding to the applied dc voltage.

Shulman and Townes[1] have recently reported a value of 0.7085 ±0.004 Debye units for the dipole moment of OCS. Our measurements agree with this figure within experimental error. Carbonyl sulfide should prove to be a convenient compound for calibrating a microwave spectroscope in which the systematic errors have not been accurately determined by direct measurement.

* General Electric Swope Fellow, 1950–1951. Present address: California Institute of Technology, Pasadena, California.
[1] R. G. Shulman and C. H. Townes, Phys. Rev. 77, 500 (1950).

Microwave Spectrum of Methyl Mercaptan

F. KENNETH HURD* AND W. D. HERSHBERGER†
University of California, Los Angeles, California

(Received February 9, 1951)

THE study of the K-Band microwave spectrum of CH_3SH is currently in progress. In the spectroscope, a 48-foot absorption cell is used with a double modulation method which employs both wide range saw-tooth 60 cycle/sec modulation and narrow range sinusoidal 87 kc/sec modulation. This technique in

conjunction with a low noise input circuit described by Good[1] for the 87 kc/sec amplifier and a low pass filter gives a sensitivity of 1×10^{-7} nepers/cm as judged by the ability to detect all of the weak $N^{15}H_3$ lines tabulated by Kisliuk and Townes.[2]

The observed spectrum consists of some 55 lines extending from 19,940 Mc/sec to 25,656 Mc/sec with only a few scattered lines between 23,790 Mc/sec and 24,980 Mc/sec suggesting two groupings of lines. The region from 25,656 Mc/sec to 25,920 Mc/sec which is the present upper limit of our equipment is void of lines. The complete tabulation of lines is shown in Table I, where the

TABLE I. Methyl mercaptan microwave spectra. Frequencies are known to an estimated 5 Mc/sec.

Frequency (Mc/sec)	Frequency (Mc/sec)	Frequency (Mc/sec)
19,909	22,414	24,485
19,996	22,558.0	24,995
20,052	22,561.2[a]	25,015
20,136	22,663	25,125
20,163	22,830	25,145.0
20,380	23,071.5	25,147.0[a]
20,645	23,075.0[a]	25,150.5
20,712.5	23,233[b]	25,152.0[a]
20,714.0[a]	23,260	25,210
21,058	23,340	25,225
21,522	23,500	25,290.0
21,735	23,525.0	25,290.4[a]
21,770	23,532.3[a]	25,565
21,866	23,565	25,660
21,878	23,622	
21,903	23,780	
21,945	23,805	
21,976	23,995	
22,270	24,072	
22,333	24,420	
	24,455	

[a] For each pair of lines so marked the separation of the two lines of the pair is known to an estimated 20 percent and the mean frequency of the pair to 5 Mc/sec.
[b] The accuracy of this frequency assignment is considered to be good to 0.5 Mc/sec. This is known by reference to an ammonia line at 23,232.20 Mc/sec.

frequencies are given to an estimated 5 Mc/sec as measured by a wavemeter calibrated against the known frequencies of the NH_3 lines.[2]

The interpretation of this spectrum has not yet been achieved. The CH_3SH molecule is a slightly asymmetric rotator with moments of inertia for the S^{32} isotope[2] consistent with a pure rotational transition $J_0=0\rightarrow J_0=1$ at approximately 24,600 Mc/sec. Because of the small Boltzmann factor for all vibrational levels other than $v_i=0$ this transition would be expected to yield a single strong line accompanied by a large number of extremely weak lines due to the excited vibrational levels. The 4.18 percent naturally occurring S^{34} would give a similar spectrum of intensity ratio 1 to 24 with respect to that of S^{32}. The observed spectrum does not fit this scheme. There exists, however, the splitting of the torsional vibration $v=0$ level into three levels as a result of hindered internal rotation. This splitting depends upon the quantum number K in a complex manner.[4] Transitions between these levels could easily yield the large number of lines observed.

* Physics Department.
† College of Engineering.
[1] W. E. Good, Westinghouse Research Paper 1538.
[2] P. Kisliuk and C. H. Townes, J. Research Natl. Bur. Standards **44**, 611 (1950).
[3] Russel, Osborne, and Yost, J. Am. Chem. Soc. **64**, 165 (1942).
[4] Koehler and Dennison, Phys. Rev. **57**, 1006 (1940).

β-Recoil Experiments with Kr^{89}

O. KOFOED-HANSEN AND P. KRISTENSEN
Institute for Theoretical Physics, University of Copenhagen, Copenhagen, Denmark
(Received February 9, 1951)

THE maximum energy and the average value of the energy divided by the charge of the recoil from the β-decay of Kr^{89} have been measured. The experimental method is similar to that used previously[1] in the investigation of recoils from Kr^{96}. However, the technique has been improved in order to permit a study of short-lived activities since the half-life of Kr^{89} (3.18 min) is much shorter than that of Kr^{88} (2.77 hr).

The following results were obtained. The maximum recoil energy is equal to 115±5 ev corresponding to a maximum β-energy of 3.9±0.1 Mev. This agrees with the value 4.0 Mev found from absorption measurements.[2] The average value of the energy divided by the charge of the recoils amounts to 58±2 ev. The charge is always $\geqslant 1$ and consequently 58 ev is a lower limit for the average recoil energy. Because of the uncertainty of the charge of the recoil atoms and the incomplete knowledge of the decay scheme the results do not permit a detailed comparison with the various possible angular correlations in β-decay.[3] However, certain possibilities may be excluded; in particular the data seem difficult to reconcile with the assumption of a backward neutrino emission with respect to the direction of emission of the β-particle. A forward neutrino emission would also in general be expected if the β-decay is forbidden, as seems to be the case for Kr^{89} judging from the ft value.

The half-life of Kr^{89} was measured, and the result, 3.14 min, agrees with the result found in the mass spectroscopic investigation.[3] Also the relative fission yield of mass numbers 88 and 89 was estimated. The result is $y_{89}/y_{88}=1.5\pm0.2$.

A more detailed account of these experiments will be published elsewhere.[4]

We wish to express our gratitude to Professor N. Bohr and to Professor J. C. Jacobsen for their interest in our work.

[1] J. C. Jacobsen and O. Kofoed-Hansen, Phys. Rev. **73**, 675 (1948).
[2] O. Kofoed-Hansen and K. O. Nielsen, Kgl. Danske Videnskab. Selskab Mat.-fys. Medd. See also O. Kofoed-Hansen and K. O. Nielsen, Phys. Rev., following letter.
[3] D. R. Hamilton, Phys. Rev. **71**, 457 (1947).
[4] O. Kofoed-Hansen and P. Kristensen, Kgl. Danske Videnskab. Selskab Mat.-fys. Medd. (to be published).

Short-Lived Krypton Isotopes and Their Daughter Substances

O. KOFOED-HANSEN AND K. O. NIELSEN
Institute for Theoretical Physics, University of Copenhagen, Copenhagen, Denmark
(Received February 9, 1951)

THE isotopes Kr^{89}, Kr^{90}, Kr^{91}, and their daughter substances have been investigated. Krypton formed in fission of uranium was pumped through a 10-m long tube directly from the cyclotron into the ion source of the isotope separator. The cyclotron and the isotope separator were operated simultaneously, and the counting could begin immediately after the interruption of the separation. The rubidium and strontium daughter substances were separated chemically; strontium was precipitated as carbonate. Half-lives were measured and an absorption analysis of the radiations was carried out. The results are given in Table I.

TABLE I. Observed radiations.

Isotope	Half-life	Radiation	E_β^{max}	Spectrum
Kr^{89}	3.18 min (2.6)	β^-, γ	4.0 Mev	Complex
Kr^{90}	33 sec (33)	β^-, γ	3.2 Mev	Complex
Rb^{90}	2.74 min	β^-, γ	5.7 Mev	Complex
Kr^{91}	10 sec (9.8)	β^-, γ probable	~3.6 Mev	Complex
Rb^{91}	100 sec	β^-, γ	4.6 Mev	Complex
Rb^{91}	14 min	β^-, γ	3.0 Mev	Complex

Previous data (see N.B.S. Circular 499: Nuclear Data) are given in parentheses.

It was found that at least 35 percent of the decays of Kr^{89} lead to an excited state of Rb^{89} which lies ~2 Mev above the ground state. This result is of importance for the interpretation of the β-recoil experiments with this krypton isotope.[1]

Furthermore it was found that Rb^{86} has an isomeric state. Both these states of Rb^{91} (half-lives 100 sec and 14 min, respectively) decay to the well-known Sr^{91} 9.7 hr which again decays to the 60-day and the 50-min isomers of Y^{91}. All these radioactivities were found in the samples of mass number 91.

A more detailed account of the experiments will be published elsewhere.[2]

We wish to thank Professor N. Bohr for his interest taken in our work and Dr. J. Koch for help and advice during this investigation.

[1] O. Kofoed-Hansen and P. Kristensen, Kgl. Danske Videnskab. Selskab Mat.-fys. Medd. (to be published); see also Phys. Rev., preceding letter.
[2] O. Kofoed-Hansen and K. O. Nielsen Kgl. Danske Videnskab. Selskab Mat.-fys. Medd. (to be published).

The Nuclear Magnetic Moment of I^{129}

HAROLD WALCHLI,* RALPH LIVINGSTON,† AND GORDON HEBERT†
Oak Ridge National Laboratory,‡ Oak Ridge, Tennessee
(Received February 9, 1951)

THE nuclear resonance of long-lived radioactive I^{129} has been observed in a nuclear induction apparatus of the type originated by F. Bloch and similar to that recently described by Proctor.[1] The sample contained 33 mg of total iodine, as iodide, in a hydrazine solution. The iodine was isolated from fission products by one of the authors (G. H.). The I^{129} content was estimated to be 80 percent, the remainder being stable I^{127}. Heavy water was added to the solution, and all frequency ratio measurements were relative to deuterium. No magnetic catalyst was added. Frequency measurements were made with a Signal Corps type BC-221 frequency meter calibrated with harmonics from an external 100 kc, crystal-controlled oscillator which in turn was compared with WWV at 10 Mc. Frequency measurements made at nominal fields of 9500 and 12,200 gauss gave

$$\nu(I^{129})/\nu(D)=0.86744\pm0.0001.$$

Measurements were also made on I^{127}, but, since the resonance was weak in the original sample, a separate, chemically similar solution was used with a larger amount of I^{127} added. Measurements at nominal fields of 7500 and 9300 gauss gave

$$\nu(I^{127})/\nu(D)=1.30337\pm0.0002.$$

Measurements on I^{127} were also made in a sodium iodide solution and were not significantly different from the above.

Using Levinthal's[2] deuteron-to-proton frequency ratio of 0.1535059, the above ratios yield the following frequency ratios relative to the proton:

$$\nu(I^{129})/\nu(H)=0.13316$$
$$\nu(I^{127})/\nu(H)=0.20007_4.$$

With an iodine diamagnetic correction of 0.545 percent,[3] a spin of 7/2 for I^{129} [4] and 5/2 for I^{127},[5] and a value of 2.79268 nuclear magnetons[6] for the proton moment, these ratios give the following values of nuclear magnetic moments, in units of the nuclear magneton

$$\mu(I^{129})=+2.6173\pm0.0003$$
$$\mu(I^{127})=+2.8090\pm0.0004$$
$$\mu(I^{127})/\mu(I^{129})=1.0732.$$

The indicated estimated accuracy of the above values does not include the uncertainty in the diamagnetic correction. The sign of the I^{129} magnetic moment was obtained by comparison with I^{127} and D which are known to be positive.[1]

A previous measurement[7] of the nuclear magnetic moment of I^{129} made by microwave spectroscopy gave 2.74±0.14 nuclear magnetons, which is consistent with the above value. The I^{127} results can conveniently be compared with published data in terms of the ratio of the I^{127} frequency to the proton frequency. Pound's[8] ratio for I^{127} relative to Na^{23}, 0.75664±0.0002, has been converted to the ratio relative to the proton by using Bitter's[9] Na^{23}-to-proton ratio of 0.26450±0.000026. This ratio and the ratio relative to the proton determined by Zimmerman and Williams[10] are compared below with the ratio obtained in this work.

$\nu(I^{127})/\nu(H)$	
0.20013 ±0.00005	Pound
0.20003 ±0.00007	Zimmerman and Williams
0.20007_4±0.00003	This work.

* Isotope Research and Production Division, Y-12.
† Chemistry Division, X-10.
‡ Work performed under contract with the AEC.
[1] W. G. Proctor, Phys. Rev. **79**, 35 (1950).
[2] E. C. Levinthal, Phys. Rev. **78**, 204 (1950).
[3] W. C. Dickinson, Phys. Rev. **80**, 563 (1950).
[4] Livingston, Gilliam, and Gordy, Phys. Rev. **76**, 149 (1949).
[5] S. Tolansky, Proc. Roy. Soc. (London) **A-170**, 205 (1939).
[6] Sommer, Thomas, and Hipple, Phys. Rev. **80**, 487 (1950).
[7] Gordy, Gilliam, and Livingston, Phys. Rev. **76**, 443 (1949).
[8] R. V. Pound, Phys. Rev. **73**, 1112 (1948).
[9] F. Bitter, Phys. Rev. **75**, 1326 (1949).
[10] J. R. Zimmerman and D. Williams, Phys. Rev. **76**, 350 (1949).

Evidence Concerning the Reaction $p+p\rightarrow\pi^++d^*$

FRANK S. CRAWFORD, JR., KENNETH M. CROWE, AND M. LYNN STEVENSON
Radiation Laboratory, Department of Physics, University of California, Berkeley, California
(Received February 9, 1951)

THE mesons produced by protons on protons have been reported[1,2] by various observers. The strong forward high energy peak in the cross section found in the early work indicated that a deuteron may be produced in the reaction. The shape of the peak and the energetics of the reaction have given further evidence that this is the case.[3,4]

We have observed the reaction $p+p\rightarrow\pi^++d$ by coincidence counting technique. By using a magnetic field to determine the momentum of the particles and finding the range of both in aluminum, we have essentially identified the reaction products by measuring the masses of both the meson and deuteron.

The arrangement is shown in Fig. 1. The 340-Mev external proton beam of the Berkeley cyclotron strikes a 1-inch thick polyethylene target. Typical trajectories are shown for the meson and deuteron in the forward direction. The orbits were located by using a wire with known current and tension. Each counter

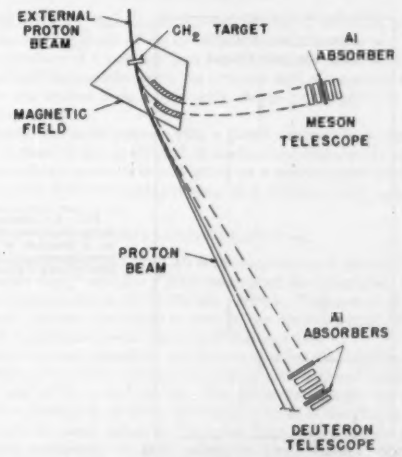

FIG. 1. The geometry of the experiment.

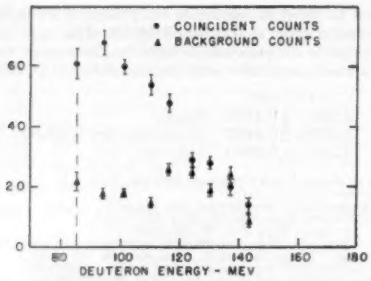

FIG. 2. The integral range spectrum of meson-deuteron coincidence counts as a function of deuteron energy. Probable errors are shown.

telescope consists of four liquid scintillators, $4\times5\times\frac{1}{2}$ inches in size, viewed by photo-multipliers. The outputs were mixed, using conventional electronics. The events recorded require both particles to have range large enough to enter the third counter of each telescope but to stop before the fourth. Range was varied with absorbers in the position shown. The integral range spectrum for the coincident events is shown as a function of range in the deuteron telescope in Fig. 2. The slope of the spectrum between 110 and 130 Mev corresponds to the variation of measured deuteron energy for production at various target depths owing to its energy loss in passing through the rest of the target. Protons from the reaction $p+p\rightarrow\pi^{+}+n+p$ of approximately the same velocity as the deuteron would not appear at ranges greater than the deuteron range of 90 Mev. The lowest energy point on Fig. 2 corresponds to zero absorber.

The momentum of the deuteron was measured by shifting the position of the deuteron telescope (see Fig. 3). Deuterons produced at the front and back of the target are expected to have momenta 630 and 710 Mev/c, respectively. The cone of the coincident deuterons was defined by the meson telescope to be $\sim2\frac{1}{2}$ inches in diameter. Protons from the reaction $p+p\rightarrow\pi^{+}+p+n$, for which we would have detected the meson, would appear at a maximum momentum of about 450 Mev/c ($\sim$12 inches from the center of the deuteron telescope). The main proton beam appears at 855 Mev/c (8.5 inches from the deuteron telescope). The deuteron mass calculated from these data is $2.2^{+0.6}_{-0.4}$ proton masses. The meson mass was obtained by varying the magnetic field and measuring the range spectrum in the meson telescope. We obtain 270^{+80}_{-90} electron masses. The errors in the masses correspond to the limits of uncertainties in the momentum and range resolution of the deuteron and meson telescopes.

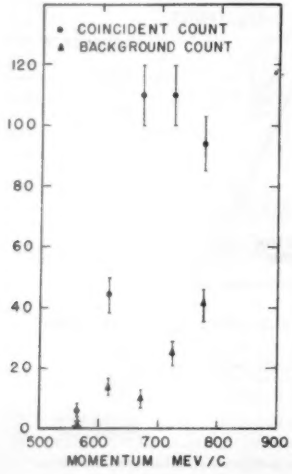

FIG. 3. Meson-deuteron coincidence counts as a function of deuteron momentum. Probable errors are shown.

TABLE I. Typical data taken with same geometry and beam intensity for equivalent number of protons. Probable errors are given.

Target	Meson counts	Coincidence counts	Background	Difference	Meson deuteron coincidences: Meson counts
Polyethylene	1085±18	144±7	46±4	98±8	—
Carbon	288±11	3±1	6±2	−3±2	−0.010±0.007
Hydrogen (Equivalent)	707±31	141±7	40±4	101±8	+0.127±0.010

Mesons produced by 340-Mev protons on carbon in the same solid angle do not appear to be accompanied by correlated deuterons (see Table I). The meson telescope counts are approximately 90 percent mesons, and our high background appears to be accidental coincidences between the meson-deuteron events and the excessive singles rates of the final deuteron telescope counters.

Measurements of the absolute cross section are in progress.

We wish to thank Professor W. K. H. Panofsky for encouragement and generous assistance throughout the measurements, Dr. E. Martinelli and Mr. L. Neher for their discussions and assistance, Mr. R. Hildebrand for loan of the counters used, Mr. A. J. Stripeika and the electronics group for maintenance of the electronics, and Mr. J. Vale and the crew for the proton bombardments.

* This work was performed under the auspices of the AEC.

[1] Cartwright, Richman, Whitehead, and Wilcox, Phys. Rev. **78**, 823 (1950).
[2] V. Z. Peterson, Phys. Rev. **79**, 407 (1950).
[3] Cartwright, Richman, Whitehead, and Wilcox, Phys. Rev. **81**, 652 (1951).
[4] Peterson, Iloff, and Sherman, Phys. Rev. **81**, 647 (1951).

On the $\gamma-\gamma$-Correlation with Higher Multipoles

DAVID L. FALKOFF
Brookhaven National Laboratory, Upton, Long Island, New York, and University of Notre Dame, Notre Dame, Indiana*

(Received January 24, 1951)

RECENT experiments on $\gamma-\gamma$-angular correlations,[1] in particular the observed correlation[2] in the long-lived isomer Pb^{204}, have emphasized the need to extend the angular correlation calculations to higher multipoles. Thus far the only published tables of $\gamma-\gamma$-correlations are those of Hamilton,[3] but these are applicable only to successive nuclear transitions in which the γ-rays are either dipole or quadrupole. The extension of these tables using the method of Hamilton, although straightforward in principle, has thus far not been attempted because the amount of calculation required increases rapidly with the higher multipoles.

In this note we remark on several alternative methods of calculation which considerably simplify the problem of obtaining $W(\vartheta)$ for higher angular momenta. We first give specific results for some of the simpler cases of interest, and then indicate a general method for obtaining more complete tabulations:

(i) Instead of calculating $W(\vartheta)$ for all possible transitions consistent with the angular momentum selection rules for *fixed* multipole orders of the γ-rays, as Hamilton[3] has done, one can fix the multipole order of one of the γ-rays, say, the second, and the spins of the intermediate and final nuclear states, and vary the multipole order and spin of the initial state. This method is particularly simple when the final state has spin zero. For example, for transitions of the type:

$$\text{IA}: \quad L+1 \xrightarrow{2^{L}} 1 \xrightarrow{2^{1}} 0$$

(here the multipole order of the γ-ray is indicated above the arrow), one obtains

$$W(\vartheta)=1+a_2\cos^2\vartheta$$

with

$$a_2=\frac{-(L^2+L-3)}{3L^2+7L+3}.$$

Since most of the nuclei in which $\gamma-\gamma$-correlations have been measured[1,2] are presumed to have spin zero ground states, we have similarly calculated the coefficients a_{2i} in $W(\vartheta)=1+\Sigma a_{2i}\cos^{2i}\vartheta$ as functions of L for correlations of type:

$$\text{IB: } L \xrightarrow{2^L} 1 \xrightarrow{2^1} 0$$

$$\text{IIA: } L+2 \xrightarrow{2^L} 2 \xrightarrow{2^2} 0$$

$$\text{IIB: } L+1 \xrightarrow{2^L} 2 \xrightarrow{2^2} 0$$

$$\text{IIIA: } L+3 \xrightarrow{2^L} 3 \xrightarrow{2^3} 0$$

$$\text{IIIB: } L+2 \xrightarrow{2^L} 3 \xrightarrow{2^3} 0.$$

The results are given in Tables I, II, and III. In all of the above

TABLE I. a_2 in $W(\vartheta)=1+a_2\cos^2\vartheta$ for $\gamma-\gamma$-correlations of types IA and IB.

L	IA a_2	IB a_2
1	+0.076	−0.333
2	−0.103	+0.429
3	−0.176	0.692
4	−0.215	0.810
5	−0.239	0.871
6	−0.255	0.907
7	−0.266	0.930
8	−0.275	0.945

TABLE II. a_2 and a_4 in $W(\vartheta)=1+a_2\cos^2\vartheta+a_4\cos^4\vartheta$ for $\gamma-\gamma$-correlations of types IIA and IIB.

L	IIA a_2	IIA a_4	IIB a_2	IIB a_4
1	−0.104	0	+0.428	0
2	+0.125	+0.042	0	−0.333
3	0.313	−0.021	−0.455	+0.121
4	0.452	−0.089	−0.721	0.433
5	0.556	−0.149	−0.888	0.640
6	0.635	−0.197	−1.000	0.784
7	0.698	−0.237	−1.079	0.889
8	0.749	−0.271	−1.138	0.969

TABLE III. a_2, a_4, a_6 in $W(\vartheta)$ for $\gamma-\gamma$-correlations of types IIIA and IIIB.

L	IIIA a_2	IIIA a_4	IIIA a_6	IIIB a_2	IIIB a_4	IIIB a_6
1	−0.176	0	0	+0.692	0	0
2	+0.313	−0.024	0	−0.439	0.156	0
3	0.554	−0.014	0.018	−0.441	0.176	−0.161
4	0.676	+0.045	0.001	−0.258	−0.129	−0.023
5	0.742	0.118	−0.030	−0.053	−0.522	+0.206
6	0.779	0.195	−0.067	0.135	−0.908	0.447
7	0.801	0.264	−0.102	0.302	−1.260	0.675

cases the second multipole is the only one allowed by the angular momentum selection rule while the first multipole is taken to be either the maximum allowed (IA, IIA, IIIA) or the next allowed (IB, IIB, IIIB), to cover the case when the former is forbidden by parity.

These tables confirm the expectation that $W(\vartheta)$ should become increasingly anisotropic with higher multipole γ-rays. It is noteworthy that none of these correlation functions can explain the "anomalous"[4] measured correlation in Rh^{105}.

(ii) The most extensive tabulation of angular correlation functions which has appeared so far is that of Gardner,[5] who treated $\sigma^-\sigma^-$ correlations. Tables of equal completeness, i.e., applicable to transitions of any multipole orders, can also be gotten for the $\gamma-\gamma$-correlation. Indeed, one can also use the same methods of Racah,[6] which Gardner used, to obtain directly the $\gamma-\gamma$-correlation functions. However, this method, though very elegant and more wieldy than Hamilton's, would involve an unnecessary duplication of effort. For it has been shown[7] that once correlation functions have been tabulated for *any* successive particle emissions, these same tables may be used to obtain $W(\vartheta)$ for other particles. This theorem was applied in detail in reference 7, where Hamilton's $\gamma-\gamma$-tables were adapted to other correlation processes (such as $\beta-\gamma$, internal conversion$-\gamma$, $\alpha-\gamma$, etc.) which involved the same angular momenta. It thus appears that the most economical procedure for systematically obtaining $W(\vartheta)$ for higher angular momenta is to apply similarly the theorems of reference 7 to the tables already worked out by Gardner.

I should like to thank Miss Theresa Danielson, of the computing group at Brookhaven National Laboratory, for doing the numerical work.

* Research supported by the AEC at Brookhaven National Laboratory.

[1] E. L. Brady and M. Deutsch, Phys. Rev. **78**, 558 (1950).
[2] Sunyar, Alburger, Friedlander, Goldhaber, and Scharff-Goldhaber, Phys. Rev. **79**, 181 (1950).
[3] D. R. Hamilton, Phys. Rev. **58**, 122 (1940).
[4] Brady and Deutsch, reference 1. It should be remarked that excellent agreement of the correlation theory with the measurements on both directional correlation and direction-polarization correlation in Rh^{105} can be had, provided one assigns to the nuclear states the angular momenta 1, 2, 1, respectively, and takes both multipoles as electric quadrupole. However, this entails new difficulties, in that an even-even nucleus is then assigned a non-zero spin, and some additional selection rule is then needed to account for the absence of the expected cross-over γ-ray. (See Alburger, der Mateosian, Goldhaber, and Katcoff, Bull. Am. Phys. Soc. **26**, No. 1, 45 (1951).)
[5] J. W. Gardner, Proc. Phys. Soc. London **62**, 763 (1949).
[6] G. Racah, Phys. Rev. **62**, 438 (1942) and Bull. Am. Phys. Soc. **26**, No. 1, 22 (1951).
[7] D. L. Falkoff and G. E. Uhlenbeck, Phys. Rev. **79**, 323 (1950).

On the Decay of μ-Mesons

V. VOTRUBA
Institute for Theoretical Physics, Charles University, Prague, Czechoslovakia
AND
Č. MUZIKÁŘ
Central Institute for Physics, Prague, Czechoslovakia
(Received February 9, 1951)

RECENTLY Ogawa and Kamefuchi[1] called attention to an interesting mode of decay of μ-mesons in matter, *viz.*, the transmutation of a μ-meson into one electron (or positron) only. This should be possible e.g. in the coulomb field of a nucleus if we adopt the scheme $\mu\to e+\nu+\nu^\dagger$ with charge exchange[1,2] for the ordinary decay.

Clearly, the same process, with a closed neutrino loop, should then be possible also in the field of an electron.[3] But also the spontaneous decay $\mu\to e+\gamma$ should occur as a second-order process. With scalar or pseudoscalar coupling its probability w for a meson at rest turns out to be

$$w=(48/\pi)\cdot(\ell^6/\hbar c)\cdot(\Lambda/\mu^3c^3)^2\cdot w_0,$$

where $w_0=(g^2/48\pi^3)(\mu/2)^5(c^4/\hbar^7)$ is the probability of the ordinary first-order decay[4] and $A=\int\bar p^2d\bar p$ comes from the integration over the momentum space of the virtual neutrino. The mass m of the electron has been put equal to zero in the approximation. With cut-off momentum $\bar p=\mu c$ the ratio $R=w/w_0=0.01$.

For μ^+-mesons, especially, we have in addition the annihilation processes $\mu^++e^-\to 2\gamma$ (third-order process with a closed neutrino loop) and $\mu^++e^-\to\nu+\nu^\dagger$ (or 2ν). The latter process (of the first order) is possible in all three of Wheeler's cases of the theory. As just such an event seems to be rather frequent in the electron sensitive emulsions,[5] we have calculated its probability, w', and the ratio, R', of w' to the corresponding probability of the ordi-

nary spontaneous decay, with all five types of the coupling in each case.

For very slow mesons w' vanishes in the case of charge retention with scalar or pseudovector coupling in the approximation $m=0$. The optimum numerical value of R', for slow mesons, is provided by the theory of charge retention with pseudoscalar coupling and turns out to be (with $m=0$):

$$R'=192\pi^2(\hbar/\mu c)^3N.$$

Here N is the number of electrons per cm³ of the medium. For $N\sim10^{24}$/cm³ the ratio R' is only of the order of magnitude 10^{-11}. Neither can the preparatory formation of the mesotronium yield significantly larger values for R'. The absence of the positron track at the end of some μ^+-meson tracks must therefore be accounted for in another way.[5]

[1] S. Ogawa and S. Kamefuchi, Prog. Theor. Phys. **5**, 311 (1950).
[2] J. Tiomno and J. A. Wheeler, Revs. Modern Phys. **21**, 144 (1949).
[3] This second event might also be observable (in spite of having presumably smaller probability than the first one) because it may be technically easier to detect in the photographic emulsion a splitting of the μ-meson track into two electron tracks than to find an unusually fast decay electron.
[4] The value w_0 given by Ogawa and Kamefuchi, reference 1, is too large by a factor of 2.
[5] C. Franzinetti, Phil. Mag. **41**, 86 (1950); see especially p. 101. Further, C. F. Powell, *Cosmic Radiation* (Colston Papers, 1949), Vol. I, p. 85.

A Note on Time Reversal and the Dirac Equation*

L. Biedenharn
Oak Ridge National Laboratories, Oak Ridge, Tennessee
(Received December 18, 1950)

It has been known for some time that in the customary formulation of the one-particle Dirac theory the bilinear form $\psi^\dagger\psi(\psi^\dagger=i\gamma_4\psi^*)$ is invariant under continuous Lorentz transformations and space inversion but not under time reflection.[1] For a properly quantized field theory, however, $\psi^\dagger\psi$ can be made invariant to time reflection.[2] This behavior causes no difficulty in the one electron theory [it is necessary, in fact, in order that the normalization integral $\int(\psi^\dagger\gamma_4\psi)dx^1dx^2dx^3$ be a scalar under the extended group]. It might be of consequence, however, for interaction with other spin $\frac{1}{2}$ particles (e.g., β-decay).

If the invariance of $\psi^\dagger\psi$ to the extended group is postulated in addition to the usual postulates of the Dirac theory, some generalization must be made. A possible generalization is to consider equations with all real elements in which ψ is an 8-rowed column vector, and the matrices 8×8. Motivation for this is the observation that the nonlinear operation[3] of complex conjugation, K_0, is adjointed to the Dirac matrix operations and plays an intimate role in the usual theory. By adjoining to the 4×4 Dirac matrices (multiplied by i if imaginary) the four matrices

$$I=\begin{pmatrix}1&0\\0&1\end{pmatrix},\quad K_0=\begin{pmatrix}1&0\\0&-1\end{pmatrix},\quad K_1=\begin{pmatrix}0&-1\\1&0\end{pmatrix},\quad K_2=\begin{pmatrix}0&1\\1&0\end{pmatrix},$$

we linearize all matrix operations. The algebra generated by this process has 64 elements, is irreducible, and is quite similar to the usual Dirac algebra. It is generated by the commutation relation:

$$\Gamma^\mu\Gamma^\nu+\Gamma^\nu\Gamma^\mu=2g^{\mu\nu}(\mu,\nu=0\cdots5);\quad g^{\mu\nu}=\pm\delta^{\mu\nu},$$
$$-\text{ for }\mu=0,4,5;\quad+\text{ for }\mu=1,2,3).$$

It is found possible to maintain all the postulates leading to the Dirac theory plus the additional requirement of the invariance of $\psi^\dagger\psi$. The wave equation is

$$(\Gamma^\lambda\partial_\lambda+\kappa)\psi=0(\lambda=0\cdots3;\quad\partial_\lambda=\partial/\partial x^\lambda;\quad x^0=t;\quad\hbar=c=1);$$

the adjoint equation is $\psi^\dagger(\Gamma^\lambda\partial_\lambda-\kappa)=0$ with the adjoint uniquely determined to be $\psi^\dagger=$transpose $(\Gamma^0\Gamma^4\Gamma^5\psi)$. To every wave function ψ there correspond three "conjugate" functions generated by the operators $\Gamma^4\Gamma^5$, $\Gamma^4\Gamma^0$, and $\Gamma^4\Gamma^5(\Gamma^5=\Gamma^0\Gamma^1\Gamma^2\Gamma^3\Gamma^4\Gamma^5)$. These conjugates are analogous to the usual charge conjugate solution; interactions with external fields distinguish among them. Three anti-commuting operators are available for interactions $\Gamma^4\Gamma^5$, Γ^4, Γ^5. The proper operator for vector interactions is $\Gamma^4\Gamma^5$, and with this we get gauge invariance and a continuity equation. Gauge invariance (of the first kind) is lost, however, if the operators Γ^4 and/or Γ^5 appear in the wave equation with nonzero mass. The spin of the particles is readily shown to be $\frac{1}{2}$.

The time reversal operator in this formulation is $\Gamma^0\Gamma^4$ (or $\Gamma^0\Gamma^5$ equivalently). In the representation where $\Gamma^4\Gamma^5$ corresponds to i (the usual Dirac formalism), the time reversal operator becomes $i\sigma_yK_0$.[3-5] The reversal in sign of $\psi^\dagger\psi$ under time reflection in the Dirac theory is therefore due to the incorrect identification of $\gamma^1\gamma^2\gamma^3$ as the time reversal operator.

Because transpose $(\psi^\dagger O\psi)=\psi^\dagger O\psi$, the expectation value of many operators is identically zero. In particular, we may have only the S, A, P covariants[5] with I (the identity); V, T with $\Gamma^4\Gamma^5$; and T, A with Γ^4 and Γ^5. As a result, the only nonvanishing vector is $j^\mu=\psi^\dagger\Gamma^4\Gamma^5\Gamma^\mu\psi(\mu=0\cdots3)$. Since $\Gamma^4\Gamma^5$ is a scalar to all Lorentz transformations except time reversal, where it changes sign, the proper behavior for j^0 is obtained. Considering $\Gamma^4\Gamma^5$ as the charge operator, one is led to the conclusion that changing sign under time reversal is a basic property of charge.

Besides the Dirac equation the proposed generalization includes other equations describing spin $\frac{1}{2}$ particles, the significance of which is yet to be explored.

The writer wishes to thank Dr. M. E. Rose and Professor E. P. Wigner for helpful discussions.

* This document is based on work performed for the Atomic Energy Project at Oak Ridge.
[1] W. Pauli, Revs. Modern Phys. **13**, 203 (1941).
[2] J. Schwinger, Lectures on field theory, Harvard, 1948.
[3] E. Wigner, *Göttinger Nachrichten* (1932), p. 546.
[4] T. D. Newton and E. Wigner, Revs. Modern Phys. **21**, 400 (1949).
[5] C. L. Critchfield, Phys. Rev. **63**, 417 (1943).

Neutron Yield for the Li+T Reactions*

R. W. Crews
University of California, Los Alamos Scientific Laboratory, Los Alamos, New Mexico
(Received January 17, 1951)

A PRELIMINARY investigation of neutron production from bombardment of natural metallic lithium by tritons with energies between 0.25 and 2.10 Mev has been made using the Los Alamos 2.5-Mev electrostatic accelerator.

Targets were made by evaporating lithium on thin aluminum or tungsten disks which could be attached to the target end of the accelerating tube. Thicknesses of the lithium films were obtained by measuring the neutron yields from $Li^7(p,n)Be^7$ for 2-Mev protons and using a value[1] of 0.025 barn for the differential cross section at 0°. Targets were about ~50 kev thick for 2-Mev protons.

Neutron yields were measured with a BF_3 "long counter"[2] placed about one meter from the target and at angles of 0° to 135°

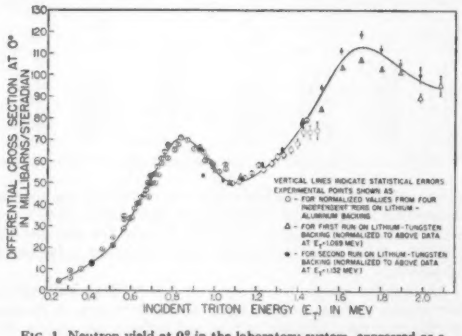
DIFFERENTIAL CROSS SECTION AT 0° IN MILLIBARNS/STERADIAN
INCIDENT TRITON ENERGY (E_T) IN MEV
VERTICAL LINES INDICATE STATISTICAL ERRORS
EXPERIMENTAL POINTS SHOWN AS
○ - FOR NORMALIZED VALUES FROM FOUR INDEPENDENT RUNS ON LITHIUM - ALUMINUM BACKING
△ - FOR FIRST RUN ON LITHIUM-TUNGSTEN BACKING (NORMALIZED TO ABOVE DATA AT E_T=1.059 MEV)
● - FOR SECOND RUN ON LITHIUM-TUNGSTEN BACKING (NORMALIZED TO ABOVE DATA AT E_T=1.52 MEV)

FIG. 1. Neutron yield at 0° in the laboratory system, expressed as a cross section, for the Li+T reactions.

with respect to the triton beam. The efficiency of the counter was obtained by measuring the yield from a standard RaBe source placed at the target. Errors up to 20 percent in total yield measurements may arise from a difference in sensitivity of the counter to neutrons from Li+T and from the RaBe source. The neutron energy-spectrum from Li+T is not known.

Data were obtained in a series of eight runs using beams of mass 6 (TT^+), mass 4 (HT^+), and mass 3 (principally T^+), which covered a triton energy range from 0.258 to 2.080 Mev. One of each of the following targets was used: lithium on aluminum, lithium on tungsten, aluminum blank, tungsten blank.

Background measurements were obtained from runs on the metal blanks. For triton energies below 1.0 Mev, backgrounds were negligible. Above 1.5 Mev, tritons on aluminum produced backgrounds which were twice as large as those for tritons on tungsten. At angles greater than 90°, backgrounds were at least twice as large as those at 0°.

For the machine energies available, probable neutron-producing reactions are:

$$Li^6+T\rightarrow 2He^4+n+16.02 \text{ Mev}, \quad (1)$$
$$Li^6+T\rightarrow Be^8+n+15.97 \text{ Mev}, \quad (2)$$
$$Li^7+T\rightarrow Be^9+n+10.52 \text{ Mev}, \quad (3)$$
$$Li^7+T\rightarrow 2He^4+2n+8.88 \text{ Mev}, \quad (4)$$
$$Li^7+T\rightarrow Be^8+2n+8.83 \text{ Mev, and} \quad (5)$$
$$Li^7+T\rightarrow He^5+He^4+n+8.08 \text{ Mev}. \quad (6)$$

The compound nucleus from Li^7+T is Be^{10} with an excitation energy of 17.324 Mev. Contributions from the 7.4 percent Li^6 present in the targets are assumed to be small.

The neutron yield at 0°, expressed as a cross section, is shown in Fig. 1. Apparent resonances occur at triton energies of 0.84 and 1.70 Mev. One may assume these peaks to indicate virtual states in Be^{10} of 17.91 Mev and 18.51 Mev.

Figure 2 shows two angular distributions of neutron yields, expressed in terms of differential cross sections. Numerical integration of the data at 0.728 Mev gives a total cross section of

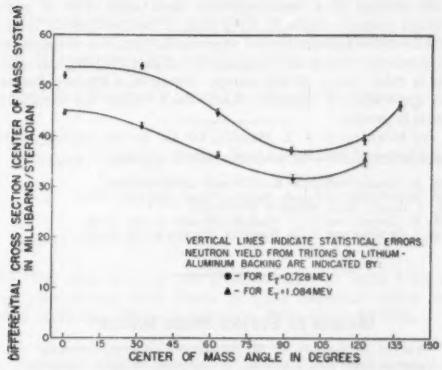
DIFFERENTIAL CROSS SECTION (CENTER OF MASS SYSTEM) IN MILLIBARNS/STERADIAN
CENTER OF MASS ANGLE IN DEGREES
VERTICAL LINES INDICATE STATISTICAL ERRORS
NEUTRON YIELD FROM TRITONS ON LITHIUM-ALUMINUM BACKING ARE INDICATED BY
● - FOR E_T=0.728 MEV
▲ - FOR E_T=1.084 MEV

FIG. 2. Angular distribution of neutron yields in the center-of-mass system, expressed as cross section values, for the Li+T reactions.

approximately 0.5 barn. An average total cross section ~0.7 barn is obtained for a triton energy range of 0.25 to 2.0 Mev. Almqvist[3] reports an average total cross section of 1.5 barns for a thick target and a maximum triton energy of 2.6 Mev.

The author is indebted to the other members of the Los Alamos electrostatic accelerator group for their assistance during the experiment.

* Work done under the auspices of the AEC.

[1] R. Taschek and A. Hemmendinger, Phys. Rev. **74**, 373 (1948).
[2] A. O. Hanson and J. L. McKibben, Phys. Rev. **72**, 673 (1947).
[3] E. Almqvist, Can. J. Research **28A**, 433 (1950).

On the Spin of the Nuclear Ground State in the *jj*-Coupling Scheme

IGAL TALMI*
Physikalisches Institut der Eidgenössischen Technischen Hochschule, Zürich, Switzerland
(Received February 13, 1951)

RECENTLY, some interest has arisen in the problem concerning the spin of the ground state of the j^n configuration predicted for Majorana forces in the *jj*-coupling scheme.

Racah[1] showed, on the basis of the "long range" approximation, in which one assumes that the potential between a pair of nucleons can be approximated by a square well in the region where the amplitudes of the wave functions are important, that the ground state has the minimum value of spin J allowed by the Pauli principle. On the other hand, results of Mayer[2] show that in the case of δ-type interaction between the nucleons, the spin of the ground state is j if n is odd and 0 if n is even. This case should be referred to as the "short range" approximation, because here one considers an interaction potential which differs from zero only in a region so small that the change of the wave function in it is small compared to the wave function itself.

In order to see how these results depend on the approximations used, it is useful to develop the interaction potential in a series of Legendre polynomials.[3]

$$V(|r_1-r_2|)=\sum_{k=0}^{\infty} f_k(r_1,r_2)P_k(\cos\omega).$$

The energy levels are then given as finite sums of the radial integrals

$$F^k=\int_0^\infty\int_0^\infty R_j^2(r_1)R_j^2(r_2)f_k(r_1,r_2)dr_1dr_2,$$

the coefficients of which are integrals of products of spherical harmonics. The term values of the Majorana interaction for the levels in the *jj*-coupling are easily found by the method of sums in a way similar to that used for ordinary forces,[4] and the relative order can be determined as a function of the parameters F^k.

It is easy to see that in the "long range" limit

$$f_k(r_1,r_2)=\frac{2k+1}{2}\int_{-1}^{+1}V(|r_1-r_2|)P_k(\cos\omega)d\cos\omega$$
$$=\frac{2k+1}{2}V\int_{-1}^{+1}P_k(\cos\omega)d\cos\omega,$$

where V is the (fixed) depth of the potential well; therefore, only F^0 does not vanish. This approximation is accomplished by setting

$$F^k\ll F^0 \quad k\geq 1.$$

In the approximation of Mayer we simply have the expansion of the δ-function in a series of orthogonal functions

$$\delta(\cos\omega-1)=\sum_{k=0}^{\infty}\Theta_{k0}(\cos\omega)\Theta_{k0}(1)=\tfrac{1}{2}\sum_{k=0}^{\infty}(2k+1)P_k(\cos\omega),$$

and the limit is reached by putting

$$F^k=(2k+1)F^0.$$

The simplest configuration in which the two approximations give different order of levels is $(d_{5/2})^3$, where we obtain

$$E_{5/2}=4/5F^0-(56/245)F^2-(217/735)F^4,$$
$$E_{3/2}=3/5F^0+(12/245)F^2-(209/735)F^4.$$

Assuming a special form of potential and of wave functions, one is able to calculate the F^k. Kurath[5] took a gaussian potential and harmonic oscillator wave functions without nodes and obtained the result that a "cross-over" of these levels occurred at a value of r_1, which lies in a region of physical interest. The gaussian potential yields the two extreme limits: if r_0 tends to infinity, the potential approximates a square well; and if r_0 tends to zero and V is appropriately increased (for the well to have a fixed volume), the δ-potential is obtained.

The case of the Yukawa potential

$$V(|r_1-r_2|)=V(r_{12})=\exp(-r_{12}/r_0)/(r_{12}/r_0),$$

is different. For a vanishing r_0 (and appropriately increased V) it gives the Mayer limit; but if r_0 tends to infinity, not a square well but the coulomb potential is obtained, in which case the values of the F^k (for $k \gtrsim 1$), while being smaller than that of F^0, are not negligible compared to it.

For the Yukawa potential, it is possible to calculate the F^k by elementary integrations, taking the coulomb-field wave functions without nodes

$$R_l(r)=N_l\, r^{l+1}\exp(-r/r_l),$$

with the aid of the addition theorem

$$\exp\left(-\frac{(r_1^2+r_2^2-2r_1r_2\cos\omega)^{\frac{1}{2}}}{r_0}\right)\Big/\frac{(r_1^2+r_2^2-2r_1r_2\cos\omega)^{\frac{1}{2}}}{r_0}$$
$$=\sum_{k=0}^{\infty}(2k+1)\frac{K_{k+\frac{1}{2}}(r_1/r_0)I_{k+\frac{1}{2}}(r_2/r_0)}{(r_1/r_0)^{\frac{1}{2}}(r_2/r_0)^{\frac{1}{2}}}\quad r_1\gtrsim r_2.$$

The result, however elementary, is complicated: all the F^k are expressed as the quotient of two polynomials in the ratio $\lambda=r_0/r_1$. The numerator is a polynomial of the degree $4l+2$ (with coefficients that are complicated functions of k and l) multiplied by λ^k, and the denominator is $(1+2\lambda)^{4l+4}$.

Returning to the configuration $(d_{3/2})^3$, we find that the cross-over occurs at a value $\lambda=10$. We compute r_l in terms of the nuclear radius R by the relationship $R=\frac{1}{2}r_l[(4l+4)(4l+3)]^{\frac{1}{2}}$, which gives for d-nucleons $r_l=R/3.74$ and determines that the cross-over occurs at $R=r_0\times 3.74/10=\frac{1}{3}r_0$.

Taking for r_0 the value 1.4×10^{-13} cm, we see that the $J=5/2$ level is lower than the $J=3/2$ level for all nuclei having $R>0.53\times10^{-13}$ cm which, in fact, applies to all cases where this configuration appears.

In order to compare this result with that cited above we must choose the wave functions so that they will give equal nuclear radii. For the oscillator wave functions, $R=\frac{1}{2}r_l(2l+3)^{\frac{1}{2}}$, and in this case $r_l=R/1.3$. The cross-over occurs at $\lambda=1.32$, or at $R\sim r_0$. The difference in the results can be attributed to the singularity of the Yukawa potential at the origin.

The above calculations support the assumption that the Mayer approximation is more reasonable than the "long range" one for the physically interesting cases.

I want to express my thanks to Professor W. Pauli for his stimulating interest and to Professor G. Racah for suggestions and helpful discussions.

* Hebrew University, Jerusalem, Israel.

[1] G. Racah, Phys. Rev. **78**, 622 (1950).
[2] M. G. Mayer, Phys. Rev. **78**, 22 (1950).
[3] Condon and Shortley, *Theory of Atomic Spectra* (Cambridge University Press, London, England), p. 174.
[4] R. D. Inglis, Phys. Rev. **38**, 862 (1931).
[5] D. Kurath, Phys. Rev. **80**, 98 (1950).

Adiabatic Magnetization of a Superconductor

R. L. Dolecek
Naval Research Laboratory, Washington, D. C.
(Received February 9, 1951)

It has been demonstrated[1,2] that the suppression of superconductivity by a magnetic field is accompanied by the absorption of energy. However, knowledge of possible changes in entropy upon application of subthreshold magnetic fields is necessary for thermodynamic treatment of this phenomenon.[3]

In initiating a study of the adiabatic magnetization of a superconductor, an upper limit of possible entropy change upon application of subthreshold magnetic fields has been established. This was done by measuring the temperature change accompanying the adiabatic magnetization of a superconducting polycrystalline tin sphere by subthreshold fields. For this geometry the transition from the superconducting to the intermediate state should be quite well defined at a threshold field equal to two-thirds the critical field for bulk material, and the application of a magnetic field smaller than this threshold value should not convert any portion of the sample to the intermediate state. A carbon thermometer was employed for the measurement of temperatures. Lack of complete thermal insulation of the sample, and small induction effects upon the application of the magnetic fields, limited the accuracy of measurement of temperature changes to approximately 10^{-4} degree K. To this accuracy, no measurable changes were observed upon the application of subthreshold magnetic fields. The result is in agreement with the observations of Keesom and Kok.[1] Sample data are given in Table I. For analysis, the

Table I. Upper limit of entropy change produced by the application of subthreshold magnetic fields to a superconducting tin sphere.

Reduced temperature of sample T/T_c	Magnetic field applied H/H_T	Upper limit percent entropy change $100\times\Delta S/\Delta S'$
0.65	0.76	0.038
0.73	0.92	0.053
0.76	0.72	0.031
0.80	0.85	0.040
0.86	0.96	0.14
0.91	0.43	0.29

temperature (T) at which the field was applied is expressed in terms of the transition temperature (T_c) of the sample, the upper limit of possible entropy change (ΔS) is expressed in percent of the theoretical entropy change ($\Delta S'$) that would be expected to accompany the complete suppression of superconductivity,[4] and the magnetic field applied (H) is expressed in terms of the threshold field (H_T) at the temperature (T). The data of de Haas and Engelkes[5] were used in calculating the critical fields. As evidenced by measurable entropy changes, the transition temperature and threshold fields for the sample used were in good agreement with these data.

Data obtained in this investigation indicate little if any change in the entropy of a superconductor upon application of subthreshold magnetic fields. It is felt that, in thermodynamic treatments of the magnetization of superconductors, the assumption of zero entropy change upon application of subthreshold magnetic fields is valid. Study of the entropy change of a superconductor upon application of magnetic fields which exceed the threshold value is in process.

I am indebted to J. J. Madden for aid in the assembly and manipulation of the experimental equipment used.

[1] W. H. Keesom and J. A. Kok, Physica **1**, 595 (1934).
[2] K. Mendelssohn and J. R. Moore, Nature **133**, 413 (1934).
[3] C. J. Gorter, Arch. Teyler **7**, 378 (1933).
[4] W. H. Keesom and P. H. VanLaer, Physica **5**, 193 (1938).
[5] W. J. de Haas and A. D. Engelkes, Physica **4**, 325 (1937).

Meson to Proton Mass Ratios*

Walter H. Barkas, F. M. Smith, and Eugene Gardner†
Radiation Laboratory, University of California, Berkeley, California
(Received February 9, 1951)

An extended series of measurements has been made on the ratios of meson masses to the mass of the proton. As in our previous work,[1] momenta and ranges of the mesons were measured, but a number of improvements over our earlier procedures have been devised to reduce systematic errors. Using prior knowledge of the approximate mass ratios, protons and mesons from separate targets in the 184-in. cyclotron were magnetically selected so as to lie in the same 5 percent velocity interval. The particles were stopped in the same nuclear emulsion, which they entered at a small angle to the surface. Relative momenta were calculated with errors of less than one part per thousand for the orbits,[2] which are approximately semi-circular. The rectified ranges in emulsion of

the particles were carefully measured. For a small interval, the range-momentum relation is well represented by a power law: $R/m=c(p/m)^q$, where R is the range, m the particle mass, p the momentum, and c a constant of the emulsion. We have used the exponent $q=3.50$ derived from the range-energy relation[2]; the results, however, are insensitive to the value of q chosen. The utilization of protons with velocities distributed about the average meson velocity enabled us to evaluate c, and only momentum and range ratios entered into the determination of the mass ratios. Since all the particles are stopped in the same body of nuclear emulsion, the stopping power of the emulsion is eliminated. The momentum ratios are independent of the absolute value of the magnetic field intensity.

Other statistical errors are small in comparison to the range-straggling error of an individual observation. We have observed that for monoenergetic (π-μ-decay) particles the straggling of ranges has closely a normal distribution. The most probable mass is therefore obtained by averaging the individual observations of that function of the mass in which the range occurs linearly (i.e., $R/p^{3.5}$).

We find the following mass ratios:

$$(\pi^+/\text{proton})=0.1511\pm0.0006,$$
$$(\pi^-/\text{proton})=0.1504\pm0.0007.$$

If the proton to electron mass ratio is 1836.1, these figures correspond to 277.4 ± 1.1 and 276.1 ± 1.3, respectively, in units of the electron mass.

Particles[4] which were presumed to be μ^+ mesons originating from the decay of π^+ mesons stopping in the target were measured in the same experiment. The dispersion of apparent masses in this case, however, exceeds that to be expected if the particles were representatives of a single mass group, all of which comes from the target. μ^+ mesons which arise from decay of π^+ mesons in flight doubtlessly contribute to the distribution found, and we therefore must defer quoting a new μ^+ mass measurement until a better separation of the groups is obtained.

We wish to acknowledge the assistance we have received from numerous individuals of the Radiation Laboratory staff.

* This work was supported by the AEC.

† Dr. Gardner died on November 26, 1950, as a result of beryllium poisoning contracted while working on the Manhattan Project in 1942.

[1] F. M. Smith, *et al.*, Phys. Rev. **78**, 86 (1950).
[2] W. H. Barkas, Phys. Rev. **78**, 90 (1950).
[3] H. Bradner, *et al.*, Phys. Rev. **77**, 462 (1950).
[4] Burfening, Gardner, and Lattes, Phys. Rev. **75**, 382 (1949).

Erratum: Energy Dependence of Proton-Proton Scattering, 18.8 to 31.8 Mev

[Phys. Rev. **80**, 321 (1950)]

BRUCE CORK
Radiation Laboratory, Department of Physics, University of California, Berkeley, California

THE value given in row 8 of column 5 of Table I for the normalized triple should be 14.45 millibarns rather than 25.45 millibarns. The values given in Table IV are correct.

Recombination and the Helium Afterglow Spectrum

D. R. BATES
Department of Physics, University College, London, England
(Received December 26, 1950)

JOHNSON, McClure, and Holt[1] have recently made some important observations on the spectrum of a helium afterglow. They find that it consists of He_2 bands and that it does not contain He lines; they find also that the intensity of the luminosity is high, and over a considerable period is proportional to $[n(e)]^2$, the square of the electron concentration. These results might seem to be contradictory to the view[2] that electrons in such an afterglow disappear by dissociative recombination,

$$He_2^+ + e \rightarrow 2He. \quad (1)$$

However, in fact this is not necessarily the case. The absence of lines is to be expected: For the energy available from (1) is only about 21.4 ev, so that the atoms formed are limited to the 1^1S, 2^1S, 2^1P, 2^3S, 2^3P levels and in consequence do not radiate in the λ2000–8000A region studied.[3] Collisions involving them might, however, give rise to excited helium molecules and hence to band emission. Their rate of formation through (1) is proportional to $[n(e)]^2$ during the period in which He_2^+ is the principal ion, and, therefore, the intensity also follows this law. It is only necessary that their removal should be mainly due to the process suggested in order that a high photon yield should ensue. Phelps[4] finds that the rate of destruction of helium metastable atoms is proportional to the square of the gas pressure. The natural inference is that three-body collisions are the predominant cause of the destruction. These are likely to result in the production of molecules; it is not known whether they lead to the required excitation.

[1] Johnson, McClure, and Holt, Phys. Rev. **80**, 376 (1950).
[2] D. R. Bates, Phys. Rev. **77**, 718 (1950); **78**, 492 (1950).
[3] Although all the levels listed can be reached energetically, this does not mean that all are necessarily populated since other factors besides energy considerations enter. It would be of value to determine whether λ10,830A (2^3P-2^3S) is emitted.
[4] A. V. Phelps, *Conference on Gaseous Electronics* (American Physical Society, Division of Electron Physics, New York, October, 1950). Unfortunately the abstract of the paper read at the conference does not give the pressure range covered.

The Disintegration Scheme of I^{131}

P. R. BELL, JUDITH M. CASSIDY, AND G. G. KELLEY
*Oak Ridge National Laboratory, Oak Ridge, Tennessee**
(Received January 27, 1951)

COINCIDENT scintillation spectrometers have been applied to the study of 8-day I^{131}. Gamma-gamma and beta-gamma-coincidence spectra show that a consistent decay scheme can be made including the 720-kev gamma-ray recently found by Zeldes, Brosi, and Ketelle.[1]

The gamma-gamma-coincidence spectra were obtained using NaI-Tl phosphors and 5819 photo-multipliers. A thin sample was placed in a central hole in a 3-mm lead diaphragm between the two crystals, as shown, approximately to scale, in Fig. 1A. The lead absorber reduces the back scattering of photons by the Compton process from crystal to crystal. Curve A, Fig. 2 shows the gross gamma-ray spectrum. The positions of the six known gamma-rays[1,2] are indicated by arrows.

The spectrum of pulses that have a coincident pulse of any energy in the other spectrometer is shown in Fig. 2, curve B. This curve has been corrected for random coincidences which are shown in curve C. The random coincidences were measured by delaying one spectrometer pulse with respect to the other until immediate coincidences were impossible. The peak due to the 364-kev gamma-ray, as well as the bulge due to the 720-kev transition, is absent from the coincidence spectrum. The x-rays, the 80-kev, 284-kev, and 638-kev gamma-rays remain, showing that each is in coincidence with at least one other.

When the second spectrometer is set to count only pulses representing 525-kev energy or greater, the coincidence spectrum is that shown in Fig. 2D. The peak due to the 284-kev gamma-ray and, of course, the 638-kev peak are now absent. This result shows that the 284-kev transition is not in cascade with the 638-kev transition, and since it does appear in the total coincidence curve, it must be in cascade with that of 80 kev. The presence of the 80-kev peak (and the x-rays) in Fig. 2D shows that the 638-kev transition is in cascade with the 80-kev transition. The coincidence count at two points, with the second spectrometer set to count 675 kev and over, are shown at the bottom of Fig. 2 without subtracting the accidentals, together with the accidentals corresponding, showing that only a few x-ray coincidences remain.

These coincidence results lead to the decay scheme shown in Fig. 3. This is essentially that of Kern, Mitchell, and Zaffarano,[2] except for the 720-kev transition, which they did not see.

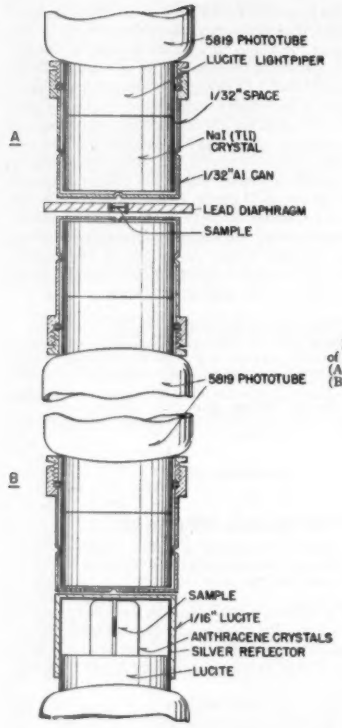

FIG. 1. Arrangement of source and detectors. (A) $\gamma-\gamma$ coincidence. (B) $\beta-\gamma$ coincidence.

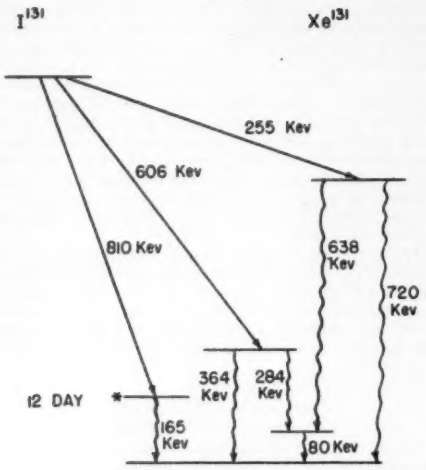

FIG. 3. Decay scheme of I^{131}.

Since the energy generally reported for the lower beta-ray[2] would not fit this decay scheme, a redetermination of this beta-ray was made. A split crystal spectrometer[4] using anthracene was placed in coincidence with a NaI-Tl gamma-spectrometer (Fig. 1B to scale). A thin source on 0.1 mg/cm² formvar was used inside the split crystal. The beta-spectrum in coincidence with all pulses in the gamma-spectrometer representing 525 kev or greater gives the Fermi-Kurie plot of Fig. 4A. This plot is quite distorted and gives an end point which is 80 kev higher than the expected beta-ray, since all electrons emitted by the source are absorbed by the anthracene.

This effect is caused by the 80-kev transition, which is coincident with the beta-ray and the 638-kev gamma-ray. The 80-kev

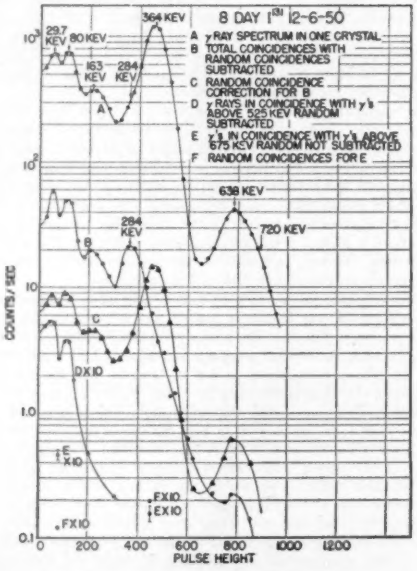

FIG. 2. γ-ray gross spectrum and coincidence spectra.

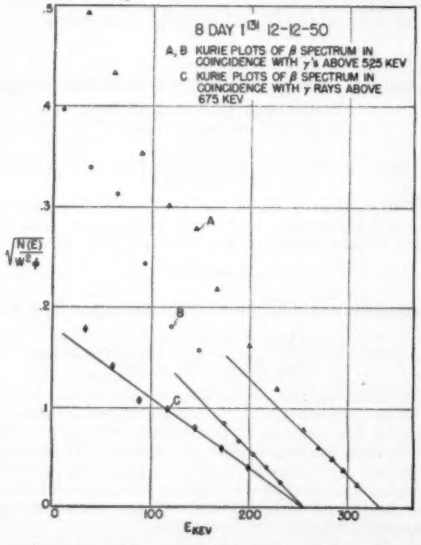
8 DAY I131 12-12-50
A, B KURIE PLOTS OF β SPECTRUM IN COINCIDENCE WITH γ's ABOVE 525 KEV
C KURIE PLOTS OF β SPECTRUM IN COINCIDENCE WITH γ RAYS ABOVE 675 KEV
EKEV

FIG. 4. Kurie plots of β-spectra in coincidence with higher energy γ-rays.

gamma-ray is strongly internally converted, and the conversion electron and following x-ray or Auger electrons are detected, simultaneously, with the beta-ray, and produce a pulse 80 kev larger than the beta-ray. If 80 kev is subtracted from the apparent energy of the spectrum points, and a new Kurie plot is made, curve B results with an end point at 255±10 kev. For confirmation, the gamma-spectrometer was set to 675 kev and the beta-coincidence spectrum run. The remaining number of counts was small, but the Fermi-Kurie plot of the results is shown in curve C. The endpoint is 255±15 kev. This seems to confirm the lower beta-ray energy and establishes the position of the 720-kev transition in the decay scheme.

* Work performed for the Atomic Energy Project at Oak Ridge National Laboratory.
[1] Zeldes, Brosi, and Ketelle, Phys. Rev. 81, 642 (1951).
[2] K. Way *et al.*, Nuclear Data, Nat. Bur. Standards (U. S.), Circ. 499 (1950).
[3] Kern, Mitchell, and Zaffarano, Phys. Rev. 76, 94 (1949).
[4] B. H. Ketelle, Phys. Rev. 80, 758 (1950).

On the Magnetic Moments of Mg^{25}, Re^{185}, Re^{187}, and Be^{9}

F. Alder* and F. C. Yu
Department of Physics, Stanford University, Stanford, California†
(Received February 8, 1951)

USING the nuclear induction spectrometer,[1] the magnetic moments of Mg^{25}, Re^{185}, and Re^{187} have been determined. The values of the magnetic moments listed in Table I were computed directly from the measured frequency ratios, and the values of the magnetic moments of N^{14} and Na^{23} were used for the comparison without corrections of any kind.

Table I. Magnetic moments.

Nucleus	Magnetic moment in nuclear magnetons
Mg^{25}	−0.85466 ±0.00015
Re^{185}	3.1433 ±0.0006
Re^{187}	3.1755 ±0.0006

$\mu(Re^{187})/\mu(Re^{185}) = 1.01026 \pm 0.00008$

From the optical hfs method the nucleus Mg^{25} was known to have a spin value 5/2 and its magnetic moment was determined to be[2] −0.96±0.07 nm. Using a magnetic field of 11,000 gauss and a sample of 4.6-molar solution of $MgCl_2$ in water, the resonance of Mg^{25} was located near a frequency of 3.9 Mc. Comparing the resonance frequency of Mg^{25} with that of N^{14} from a sample of concentrated HNO_3, we found

$$\nu(Mg^{25})/\nu(N^{14}) = 0.84714 \pm 0.00008. \quad (1)$$

The sign was verified to be negative. Taking the value 5/2 for the spin of Mg^{25}, the frequency ratio (1) leads to

$$\mu(Mg^{25}) = -0.85446 \pm 0.00015 \text{ nm} \quad (2)$$

for the magnetic moment of Mg^{25} which is in good agreement with the spectroscopically determined value. In computing the value (2), we have made use of the value 0.40355±0.00005 nm for the magnetic moment of N^{14}, which is different from the value 0.40369±0.00006 nm reported by Proctor and Yu.[2] This is due to the fact that the newly determined value[4]

$$\mu(P) = 2.79245 \pm 0.00020 \text{ nm} \quad (3)$$

for the proton moment was used instead of the value 2.79348 ±0.00034 nm obtained by Taub and Kusch.[5]

The two isotopes Re^{185} and Re^{187} of rhenium were investigated by Schüler and Korsching.[6] From the hfs of the line λ4889 in the ReI spectrum, they obtained the ratio

$$\mu(Re^{187})/\mu(Re^{185}) = 1.02069 \pm 0.00043 \quad (4)$$

for the magnetic moments of Re^{185} and Re^{187}. In the present investigation, we have used a sample of an aqueous solution of the compound $NaReO_4$. As in the case of MnO_4^-, the ReO_4^- ion was presumed to be only feebly paramagnetic. The perturbation caused by a strong magnetic field at the position of the rhenium nucleus due to strong paramagnetism could thus be avoided. On the other hand, no resonance could be found with a water solution of the paramagnetic compound K_2ReCl_6. The two resonances of Re^{185} and Re^{187} were located near a frequency of 6.4 Mc in an external field of 6700 gauss. Their resonance frequencies were compared with that of Na^{23} from a 0.25-molar aqueous solution of NaCl with 1 molar of $MnSO_4$. We obtained

$$\nu(Re^{187})/\nu(Na^{23}) = 0.85987 \pm 0.00009, \quad (5a)$$
$$\nu(Re^{185})/\nu(Na^{23}) = 0.85114 \pm 0.00009, \quad (5b)$$
$$\nu(Re^{187})/\nu(Re^{185}) = 1.01026 \pm 0.00008. \quad (5c)$$

The sign of the magnetic moment was verified to be positive for both isotopes. Since both Re^{185} and Re^{187} are known[7] to have a spin 5/2, the ratio (5c) is equal to the ratio of their magnetic moments, which agrees very well with the hfs value (4). Taking the spin value 5/2 and the value 2.2158±0.0003 nm for the magnetic moment of Na^{23}, we obtained the values of the two magnetic moments of rhenium listed in Table I. The value of the magnetic moment of Na^{23} was computed from the proton moment (3) and the frequency ratio $\nu(Na^{23})/\nu(P)$ given by Bitter.[8] Both rhenium isotopes possess a large quadrupole moment. The interaction of this quadrupole moment with the molecular electric fields gave a line width of about 10 gauss for both rhenium signals. The magnitude of these signals was very much enhanced by using an rf field of about 3 gauss.

In the course of these measurements, we have also investigated the sign of the magnetic moment of Be^{9} with the use of an aqueous solution of $Be(NO_3)_2$. An earlier and, as it seems to us, unambiguous determination by Rabi and his co-workers[9] gave the sign to be negative; nevertheless, it is listed in the table compiled by Mack[10] with a question mark. Our result fully confirms the correctness of the above-mentioned earlier assignment.

We would like to thank Professor F. Bloch for his constant interest in this work.

* Brown Boveri Company Fellow at the University of Basel, Switzerland.
† Assisted by the joint program of the AEC and ONR.
[1] W. G. Proctor, Phys. Rev. 79, 35 (1950).
[2] Crawford, Kelly, Schawlow, and Gray, Phys. Rev. 76, 1527 (1949).
[3] W. G. Proctor and F. C. Yu, Phys. Rev. 81, 20 (1951).
[4] F. Bloch and C. D. Jeffries, Phys. Rev. 80, 305 (1950).
[5] H. Taub and P. Kusch, Phys. Rev. 75, 1481 (1949).
[6] H. Schüler and H. Korsching, Z. Physik 105, 168 (1937).
[7] Zeeman, Glaolf, and de Bruin, Nature 128, 637 (1931).
[8] F. Bitter, Phys. Rev. 75, 1326 (1949).
[9] Kusch, Millman, and Rabi, Phys. Rev. 55, 666 (1939).
[10] J. E. Mack, Revs. Modern Phys. 22, 64 (1950).

On the Nuclear Interaction of π^- Mesons in Nuclear Emulsions*

G. Bernardini, E. T. Booth, L. Lederman, and J. Tinlot†
Department of Physics, Columbia University, New York, New York
(Received February 9, 1951)

THE preliminary analysis of the nuclear interactions produced by π^- mesons in nuclear emulsions has been extended to the kinetic energy range of 70–90 Mev. Results are here presented on the nuclear stars, scatterings, and stoppings in flight observed in this energy range.

The experimental arrangement was similar to that already used for mesons of kinetic energy of 30–50 Mev.[1] The G-5 plates were exposed directly to the external meson beam (KE=95±5 Mev) of the Nevis cyclotron. Because of ionization losses suffered in traversing the glass and emulsion, the corresponding energies of mesons studied ranged between 70 and 90 Mev. Only those tracks entering the emulsion from the proper direction and longer than 500 microns were accepted in the analysis. The average grain density of the allowed tracks as compared to the minimum was found to be 1.18±0.07, in agreement with that expected for

mesons of this energy. The minimum grain density was assumed to be that observed in cosmic-ray tracks crossing the emulsion in a direction perpendicular to the meson beam, and showing an average multiple scattering of less than 0.1° per 100 microns.

Two methods of scanning were used, and the results are presented separately. The first method consisted in scanning "along the tracks." In this study, individual tracks were followed, and all stars, stoppings, and scatterings by more than 20 degrees noted. The second method of "area" scanning was found to be reliable in detecting stars and inelastic scatterings, and in this way a larger number of these events was catalogued. As a check, all stars and inelastic scatterings, except one, found by "along the track" scanning were also found by "area" scanning.

The results are given in four tables. In Table I is given the frequency of stars *versus* number of prongs as found in "area" scanning. A "star" is defined as any event in which the prongs are only nucleons or groups of nucleons. In the second line are given the relative frequencies of all the stars; in the third line are those of stars emitting at least one lightly ionizing particle greater than 30 Mev. In all but four cases, these particles were identified as energetic protons. These protons were found to have an average energy, as determined from grain density measurements, of 55±8 Mev.[1] Table II gives the frequency of "inelastic" scatterings as found in the "area" scanning. These are here defined as events either (a) associated with an outgoing meson having a grain density greater than three times that of the incoming particle or (b) having one or more nucleonic prongs at the scattering vertex. For these scatterings, a large change in meson energy was evident. The average energy loss of the meson found for this group was about 60 Mev. In the first line of Table II, the number of prongs (usually protons) associated with the scattering is given.

TABLE I. Star-prong distribution ("area" scanning).

No. of prongs	1	2	3	4	5	Totals
No. of stars	17	40	22	11	3	93
No. of stars with a fast proton	6	13	8	3	1	31

TABLE II. Inelastic scatterings ("area" scanning).

No. of recoil prongs	0	1	2	3	4	Totals
No. of scatterings	3	16	2	1	2	24

Results from "along the track" scanning are given in Tables III and IV. Table III summarizes the frequencies of "elastic" scatterings as a function of angles of mesons deflected by more than 20 degrees. These events are not associated with any prongs, although in many cases a heavy cluster of grains is seen at the scattering vertex. The energy change of the elastic scatterings, if any, is less than 30 Mev. In Table IV are summarized all events found in "along the track" scanning. In this table are listed four disappearances-in-flight. These disappearances-in-flight took place in sensitive portions of the emulsion, and the incoming particle was identified as a meson in each case by grain count and multiple scattering measurements.

TABLE III. Elastic scatterings ("along the track scanning").

Scattering angle	20°–45°	45°–90°	90°–135°	135°–180°
No. of scatterings	6	0	0	5

TABLE IV. Summary of results ("along the track scanning").

Stars	Inelastic scatterings	Elastic scatterings	Stoppings
20	6	11	4

In computing the absolute and relative cross sections for the interactions of π^- mesons in emulsion, only the data obtained by scanning along the track were used. In all, 1150±50 cm of track were scanned by this procedure. An analysis of the proportion of μ^- mesons and fast electrons in the flux yielded 30±10 percent. Thus, only 70±10 percent of the accepted tracks were actually due to π^- mesons. Furthermore, the scatterings which occur for projected angles larger than 160° and without sensible change in grain density have almost twice the probability of being counted. A crude correction for this phenomenon was made by ignoring two of the five cases of 135°–180° scatterings. The average length of meson track in the emulsion was 4000 microns. Because events associated with track lengths of less than 500 microns were excluded, a further correction of 0.87 was applied to the flux in computing the mean free path. With these corrections, the mean free path of 75-Mev π^- mesons for the productions of scatterings (excluding the elastic scatterings for angles less than 20°), stars, and stoppings, in emulsion is:

$$[(1150\pm50)(0.70\pm0.10)\times0.87]/(39\pm7)=18\pm4 \text{ cm}.$$

If allowance is made for the finite size of the nucleus, very few, if any, elastic scatterings greater than 20 degrees can be ascribed to coulomb scattering by silver or bromine. With a cut-off angle of 20°, however, a significant fraction of the diffraction scattering expected for mesons of this energy should be included in our results. Most of the observed elastic scatterings in the 20–45 degree interval listed in Table III may be attributed to the diffraction expected on the basis of the observed catastrophic (stars plus inelastic scatterings plus stoppings) interactions.

* This research was jointly supported by the ONR and AEC.
† Now at the University of Rochester, Rochester, New York.
[1] Bernardini, Booth, Lederman, and Tinlot, Phys. Rev. **80**, 924 (1950).
[2] In 11 cases, the energy values were checked by the multiple scattering method and were found to be 70 Mev.

Ferromagnetic Domains in Bicrystals of Nickel

URSULA M. MARTIUS, KENELM V. GOW, AND BRUCE CHALMERS
Department of Metallurgical Engineering, University of Toronto, Toronto, Canada
(Received January 24, 1951)

THE method of growing bicrystals of predetermined orientation developed by Chalmers[1] has been adapted for metals of high melting points.[2] In the course of these investigations, bicrystals of Mond nickel (99.92 percent Ni) were produced. Figure 1 shows the top surface of such a specimen. The orientations of the individual crystals are indicated.

The preparation of bicrystals of nickel was undertaken in order to observe the influence of grain boundaries on ferromagnetic domain patterns. Up to now, no distinct domain pattern has been

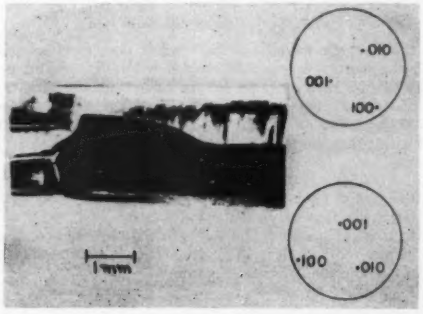

FIG. 1. Bicrystal of nickel and the orientations of the individual crystals.

observed for nickel. The low anisotropy energy has been regarded as the reason for the failure to observe the domains. Bozorth and Walker[3] reported recently a pattern on a crystal of a cobalt-nickel alloy (40 percent Ni; 60 percent Co). This alloy was chosen because it has a higher anisotropy energy than nickel but the same direction of easiest magnetization.

Previous considerations of the effects of grain boundaries on ferromagnetic properties[4] led to the prediction that a domain structure should be observable in nickel bicrystals of suitable orientations. This has been confirmed by using ferromagnetic powder technique.[5] The experiments showed simple domain structures on the electropolished crystal surface. A typical pattern, obtained in the absence of an external field, is shown in Fig. 2,

FIG. 2. Powder pattern on the surface of the bicrystal. AB is the grain boundary.

in which AB is the grain boundary. Patterns formed in external magnetic fields were also studied. All observed patterns are consistent with domain structures to be expected in nickel. They contain basic domains and "tree pattern" with the walls of the basic domains as "trunks." In the immediate neighborhood of the grain boundary, however, the boundary itself forms the "trunk." Effects of the grain boundary can be observed on all patterns.

The study of ferromagnetic domain structures in their relationship to grain boundaries may provide additional information about the properties and structure of crystal boundaries.

[1] B. Chalmers, Proc. Roy. Soc. (London) **A175**, 100 (1940).
[2] K. V. Gow and B. Chalmers, to be published.
[3] R. M. Bozorth and T. G. Walker, Phys. Rev. **79**, 888 (1950).
[4] U. M. Martius, Can. J. Phys. **1** (1951).
[5] Williams, Bozorth, and Shockley, Phys. Rev. **75**, 155 (1949).

Does Diffusive Separation Exist in the Atmosphere below 55 Kilometers?*

D. W. HAGELBARGER, LESLIE T. LOH, H. W. NEILL, M. H. NICHOLS, AND E. A. WENZEL
Department of Aeronautical Engineering, University of Michigan, Ann Arbor, Michigan
(Received February 9, 1951)

IN a recent letter,[1] McQueen infers that above 40 km diffusive separation increases the proportion of $N^{14}N^{14}$ molecules as compared to the $N^{14}N^{15}$ molecules. This inference rests on mass spectrographic analyses of six air samples obtained by rockets under an U. S. Army Signal Corps contract with the University of Michigan. For purposes of discussion (and also inasmuch as there are errors in the dates and altitudes of several of the samples), McQueen's table of results is reproduced here with the correct dates and with certain results obtained at the University of Durham and at the University of Michigan, which will be discussed in a later paragraph.

Suppose that in a particular layer of the atmosphere there is no mixing at all. Then, for any constituent of molecular weight M, the height distribution in terms of the number of molecules, n, per unit volume is given by

$$n = n_0 e^{-h/H}, \tag{1}$$

where n_0 = number of molecules per unit volume at the base of the layer, h = height above the base of the layer, and, if it is assumed that the temperature T is essentially constant throughout the layer, $H = RT/Mg$ where R is the molar gas constant. Now consider the relative concentration, $\rho = n'/n$, of two gases of molecular weights M and M'. From Eq. (1)

$$\rho = \rho_0 e^{-(h/H'-h/H)} = \rho_0 e^{-h/H_1}, \tag{2}$$

where $H_1 = RT/(M'-M)g$ and ρ_0 is the ratio at the base of the layer. The percent change, P, in ρ relative to ρ_0 is, from Eq. (2),

$$P = -100(1-e^{-h/H_1}). \tag{3}$$

McQueen's results imply that there is no diffusive separation up to about 47 km but that there is about a 3 percent separation at about 55 km, implying a cessation or reduction of mixing over the 8.4 km between mean levels of the two groups of samples. (The time interval between the two groups is only a few months, and in this region diffusion is too slow for any appreciable change in P between the two levels to occur during this interval.) If it is assumed that no mixing occurs over the 8.4-km range and if T is taken as 280°K,[2,3] then for the $N^{14}N^{14}/N^{14}N^{15}$ ratio, for which $M'-M=-1$, Eq. (3) gives $P=3.5$ percent so that McQueen's results are not inconsistent in this respect. On the other hand, for the $He/(N_2+A)$ ratio ($M'=4$, $M=28$), Eq. (3) gives $P=134$ percent under the same conditions; and for Ne/A, $P=107$ percent.

Other portions of the samples analyzed by McQueen have also been analyzed by the charcoal absorption method at the University of Durham by Paneth and co-workers[4] for He, Ne, A, and N_2, and by the present writers for He, Ne, and (N_2+A). In these samples and in six others, the relative concentrations of the gases did not vary more than several percent from the corresponding values at the surface of the earth. At this time, analyses by the charcoal method have been made for only three of the six samples reported by McQueen (results on the three other samples will be reported later); results from these three samples are given in Table I in terms of percentage deviation of the relative helium (to nitrogen plus argon) concentration in the sample from the corresponding concentration at the surface of the earth, and in terms of the percentage deviation of the neon to argon ratio from the corresponding surface value.

The small concentration of helium in the earth's atmosphere implies escape of helium from upper atmospheric levels. This

TABLE I.[a] Comparison of McQueen's results (reference 1) with those of Paneth and co-workers (reference 4) and with those obtained at the University of Michigan. The percent deviation is from the corresponding ratios at the earth's surface—i.e., the quantity P in Eq. (3). The mean deviations are given.

	Height	Date	Separation (%) $N^{14}N^{14}/N^{14}N^{15}$ McQueen (reference 1)	Separation (%) Paneth and co-workers (reference 4) $He/(N_2+A)$	Separation (%) Paneth and co-workers (reference 4) Ne/A	Separation (%) $He/(N_2+A)$ (Univ. of Mich.)
(19B)	54.7–56.3	7–21–49	3.9±0.4			
(15C)	53.6–57.7	9– 2–49	2.7±0.2	0.3±0.3	−1.3±0.8	−3[b]
(5B)	49.0–50.8	7–26–48	2.7±0.5			0[c]
(25B)	50.4–53.3	12– 6–49	0.4±0.3			
(20B)	45.0–47.8	9–20–49	0.8±0.3			
(28B)	41.4–44.9	12– 6–49	less than 0.3			−0.3±0.3[d]

[a] The samples are labeled by a number and a letter. The number refers to the original sample and the letter to the subdivision. The particular letters given in this table refer to the subdivisions sent to McQueen.
[b] Only one valid run was made on this subdivision of sample 15 so that a mean deviation cannot be deduced. This run was made early in the analysis program, and it is estimated that the mean deviation is not greater than 3 percent.
[c] This is the average of two runs which were made early in the analysis program, and it is estimated that the mean deviation is not greater than 3 percent.
[d] This is the average of four runs.

effect would increase the absolute value of the density gradient of helium over that computed on the basis of Eq. (1).[5] However, the neon to argon ratio is not subject to this effect, since it is believed that these gases do not escape from the atmosphere.

Hence, it seems that mixing must prevail at least up to about 60 km and that McQueen's results must be interpreted in some other way than by diffusive separation in the atmosphere.

Details of the sampling procedure, etc., used by the writers will be published elsewhere. We are indebted to Professor Sydney Chapman for discussions in connection with our results.

* This work is sponsored by a contract with the Meteorological Branch of the U. S. Army Signal Corps.

[1] J. H. McQueen, Phys. Rev. **80**, 100 (1950).
[2] Havens, Koll, and Lagow, "Pressures and temperatures in the earth's upper atmosphere," Naval Research Laboratory Report, March, 1950.
[3] Bartman, Liu, and Schaefer, "An aerodynamic method of measuring ambient temperature of air at high altitudes," Engineering Research Institute, University of Michigan Report (U. S. Army Signal Corps Coatract), July, 1950.
[4] Chackett, Paneth, and Wilson, J. Atmos. Terr. Phys. **1**, 49 (1950).
[5] S. K. Mitra, *The Upper Atmosphere* (Royal Asiatic Society of Bengal, Calcutta, 1947), p. 21.

An Empirical Formula for the Microwave Spectrum of Ammonia

C. C. COSTAIN
Randall Laboratory of Physics, University of Michigan, Ann Arbor, Michigan
(Received February 13, 1951)

THE inversion splitting for a double minimum potential was obtained by Dennison and Uhlenbeck[1] using the W–K–B approximation. They found

$$\Delta = 2h\nu \exp\left[(-2/\hbar)\int_0^{y_1}[2\mu(V-E)]^{\frac{1}{2}}dy\right]. \quad (1)$$

If this expression is a good approximation for the region, the microwave inversion spectrum might be more accurately represented by a formula

$$\nu = \nu_0 \exp[AJ(J+1)+BK^2+CJ^2(J+1)^2+DJ(J+1)K^2+EK^4] \quad (2)$$

than by the usual expression

$$\nu = \nu_0+A'J(J+1)+B'K^2+C'J^2(J+1)^2+D'J(J+1)K^2+E'K^4. \quad (3)$$

TABLE I. Frequency of NH_3 lines.

J	K	Freq.	Error	Ref.	J	K	Freq.	Error	Ref.
1	1	23,694.49	0	2	9	9	27,478.00	−0.08	3
2	2	23,722.63	−0.01	2	9	8	23,657.48	−0.08	2
2	1	23,098.79	−0.07	2	9	7	20,735.44	+0.01	2
3	3	23,870.13	(−0.21)	2	9	6	18,499.5	−0.62	4
3	2	22,834.17	−0.05	2	9	5	16,798.3	−2.04	4
3	1	22,234.53	0	2	10	10	28,604.73	−0.18	3
4	4	24,139.41	+0.07	2	10	9	24,205.29	−0.10	2
4	3	22,688.29	(+1.76)	2	10	8	20,852.51	−0.04	2
4	2	21,703.36	+0.03	2	10	7	18,285.6	−1.08	4
4	1	21,134.29	+0.04	2	11	11	29,914.66	+0.12	3
5	5	24,532.98	+0.07	2	11	10	24,881.90	−0.01	2
5	4	22,653.00	−0.01	2	11	9	21,070.70	−0.01	2
5	3	21,985.27	(−7.03)	2	11	8	18,162.6	−1.59	4
5	2	20,371.46	+0.11	2	12	12	31,424.97	+0.51	3
5	1	19,838.4	+0.14	4	12	11	25,695.23	+0.36	2
6	6	25,056.02	+0.05	2	12	10	21,391.55	+0.19	3
6	5	22,732.43	+0.02	2	12	9	18,127.2	−2.36	4
6	4	20,994.61	+0.09	2	13	13	33,156.95	+1.22	3
6	3	19,757.57	(+21.18)	2	13	12	26,655.00	+1.27	3
6	2	18,884.9	+0.14	4	13	11	21,818.1	+0.93	4
6	1	18,391.6	−0.15	4	13	10	18,178.0	−2.82	4
7	7	25,715.17	−0.01	2	14	14	35,134.44	+3.38	3
7	6	22,924.94	−0.01	2	14	13	27,772.52	+2.79	3
7	5	20,804.83	+0.10	2	14	11	18,313.9	−3.16	4
7	4	19,218.52	0	2	15	15	37,385.18	+6.74	3
7	3	18,017.6	(−52.39)	4	15	14	29,061.14	+5.05	3
7	2	17,291.6	−0.82	4	15	12	18,535.1	−3.26	4
7	1	16,841.3	−0.95	4	16	16	39,941.54	+12.61	3
8	8	26,518.91	−0.13	3	16	14	23,777.4	+6.52	4
8	7	23,232.24	−0.04	2	16	13	18,842.9	−2.64	4
8	6	20,719.21	+0.06	2	17	15	24,680.1	+12.27	4
8	5	18,808.7	−0.09	4					
8	4	17,378.1	−1.18	4					

Formula (2) was fitted to 64 lines, as published[2–4] to date. The six constants were obtained graphically using the differences of the logarithms of the frequencies, and were not adjusted to obtain a better fit for high J values. The equation obtained is

$$\nu = 23{,}785.88 \exp[-6.36996\times10^{-3}J(J+1)+8.88986\times10^{-3}K^2 +8.6922\times10^{-7}J^2(J+1)^2-1.7845\times10^{-4}J(J+1)K^2 +5.3075\times10^{-7}K^4]. \quad (4)$$

The experimental frequencies are listed in Table I, together with the errors obtained by subtracting the calculated from the experimental frequencies.

The rms error (omitting $K=3$ lines) in fitting Eq. (4) to 60 lines is 2.9 Mc/sec and the average error 1.3 Mc/sec. The best fit so far obtained with a power series,[3] such as Eq. (3), gives an average deviation of 26 Mc/sec, while a partially exponential equation[5] gives 46 Mc/sec. With a power series employing sixth-power terms in J and K and ten constants,[4] the average deviation is 7 Mc/sec, compared to 1.3 Mc/sec obtained with six constants above. The accuracy of Eq. (4) is best demonstrated by using only lines measured by Good and Coles.[2] Leaving out $J=12$, $K=11$, the rms error is then 0.05 Mc/sec.

The anomalous deviations of the 3,3; 4,3; 5,3; 6,3; 7,3 lines are −0.21; +1.76; −7.03; +21.18; −52.39 Mc/sec, respectively. Nielsen and Dennison[6] have shown that the deviation to be expected theoretically is of the form

$$\Delta\nu = AF(J). \quad (5)$$

They calculated $A=0.258\pm10$ percent from molecular constants, and $F(J)=-1$, 7, −28, 84, −210, for $J=3$ to 7, inclusive. If $A=0.252$, the deviations given by Eq. (5) are −0.25, +1.76, −7.06, +21.18, −52.9, for $J=3$ to 7, respectively.

The agreement obtained indicates that the functional form of Eq. (4) is correct. Further, the second-order coefficients are about 10^{-4} of the first-order terms, a more reasonable value than 10^{-2} of the first-order in the power series expressions. The third-order terms necessary for a more accurate fit of high J values were not calculated accurately but are reduced by a further factor of 10^{-4}. Examination of the deviations calculated with Eq. (4) indicates that some of the frequencies given in reference 4 may be in error by about 1 Mc/sec.

[1] Dennison and Uhlenbeck, Phys. Rev. **41**, 313 (1932).
[2] Good and Coles, Phys. Rev. **71**, 383 (1947).
[3] Simmons and Gordy, Phys. Rev. **73**, 713 (1948).
[4] Sharbaugh, Madison, and Bragg, Phys. Rev. **76**, 1529 (1949).
[5] Strandberg, Kyhl, Wentink, and Hilliger, Phys. Rev. **71**, 326 (1947).
[6] Nielsen and Dennison, Phys. Rev. **72**, 1101 (1947).

New Ferroelectric Tartrates

B. T. MATTHIAS* AND J. K. HULM
Institute for the Study of Metals, University of Chicago, Chicago, Illinois
(Received February 8, 1951)

ALTHOUGH several groups of ferroelectric crystals have been discovered in the thirty years since Valasek[1] first observed the phenomenon of ferroelectricity in Rochelle salt, the latter substance has so far occupied a special position among ferroelectric materials because of two distinctive features of its behavior: first, the existence of both a lower and an upper Curie point, and second, the fact that the only known ferroelectric crystals isomorphous with Rochelle salt were mixtures of this substance with other tartrates,[2] no other tartrate being known to be ferroelectric by itself. In reviewing this subject we have recently noticed that Scholz[3] measurements on $LiNH_4C_4H_4O_6\cdot H_2O$ at temperatures above 125°K show a steep rise in certain piezoelectric moduli for this crystal with decreasing temperature, a reasonable extrapolation indicating that the piezo-moduli become infinitely large in the neighborhood of 100°K. This behavior led us to expect the occurrence of ferroelectricity in lithium ammonium tartrate at low temperatures, a hypothesis which has now been confirmed by experiment.

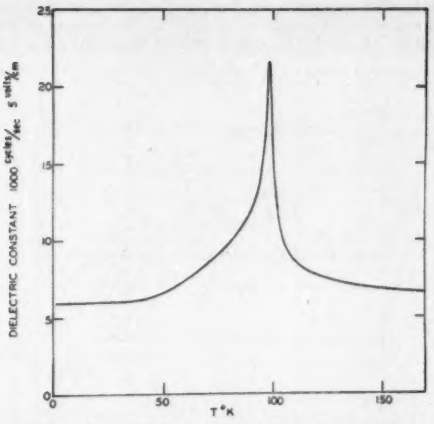

FIG. 1. Temperature variation of ϵ_b, $LiNH_4C_4H_4O_6 \cdot H_2O$.

Figure 1 shows the temperature variation of ϵ_b, the dielectric constant, of a typical $LiNH_4C_4H_4O_6 \cdot H_2O$ crystal plate with the electric field parallel to the b axis of the crystal. The sharp peak at 98.5°K marks an upper Curie point below which the crystal exhibits a well-defined ferroelectric hysteresis loop at high field strength (~10,000 volts/cm), with a spontaneous polarization 0.22×10^{-8} coulomb per cm² in the b direction at 78°K. Other striking features of Fig. 1 are, firstly, the low average value of the dielectric constant compared with average values for other ferroelectric crystals, including Rochelle salt; and, secondly, the absence of a lower Curie point, which may be inferred from the monotonic variation of ϵ_b from the upper Curie point down to 1.3°K, the lowest temperature of measurement.

The above discovery immediately raised the question as to whether a similar type of ferroelectric behavior might occur in other isomorphous crystals, or whether lithium ammonium tartrate would turn out to be another singular case. Although the only other isomorphous crystal studied by Scholz,[3] $LiKC_4H_4O_6 \cdot H_2O$, gave no marked variation of piezo-moduli with temperature, this did not seem unreasonable in view of the difference between the K^+ and NH_4^+ ions. It appeared that ferroelectricity would be less disturbed in the replacement of NH_4^+ by the more nearly isosteric Rb^+ and Tl^+ ions; and, since no electrical data were available for either of the resulting crystals, we undertook a study of both.

Figure 2 shows the temperature variation of the dielectric constant, ϵ_a, of a crystal of $LiTlC_4H_4O_6 \cdot H_2O$ with the electric field applied parallel to the a axis. With decreasing temperature, ϵ_a showed an unusually rapid rise between liquid hydrogen and liquid helium temperatures, but for a given field strength, it eventually passed through a very flat maximum and tended to a steady value as the absolute zero was approached. At liquid helium temperature, however, ϵ_a was extremely sensitive to small changes in field strength owing to the fact that below 10 (±1)°K the crystal exhibited a ferroelectric hysteresis loop, the coercive field strength being only 120 volts per cm for an applied field of 3000 volts per cm. In this field at 1.3°K, the crystal showed a reversible spontaneous polarization of about 0.14×10^{-8} coulomb per cm² (which is probably close to the saturation value), superimposed on an induced polarization of the same order of magnitude associated with the high initial dielectric constant. The existence of an upper Curie point at about 10°K was evident from the disappearance of hysteresis and field dependence of ϵ_a on heating through this temperature, and also from application of a Curie-Weiss formula to the steeply falling dielectric constant at higher temperatures. No lower Curie point was observed down to 1.3°K.

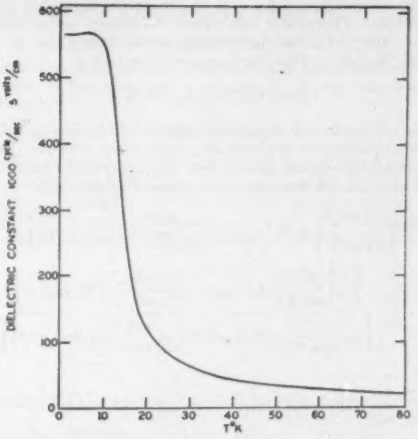

FIG. 2. Temperature variation of ϵ_a, $LiTlC_4H_4O_6 \cdot H_2O$.

In comparing the new ferroelectric crystals with Rochelle salt, it has to be borne in mind that although the crystal symmetry is the same in each case, the axial ratios are quite different, while in addition, Rochelle salt has four molecules of water of crystallization compared with one molecule in both of the new crystals. In view of this fact, it is somewhat surprising that practically the same value of spontaneous polarization is observed for each crystal, which may indicate that the water molecules play a relatively unimportant role in the ferroelectric behavior. The low value of dielectric constant and unusual (b) direction of ferroelectric behavior in lithium ammonium tartrate is possibly the result of an interaction between ammonium ions of the type observed in $NH_4H_2PO_4$.[4] The new results strengthen the assumption that the lower Curie point in Rochelle salt is somewhat accidental. A comparison of the lithium thallium tartrate data with those for potassium tantalate[5] seems to indicate that sharp dielectric constant peaks do not occur near the absolute zero. Finally, we draw attention to the positive birefringence of all three known ferroelectric tartrates, a property which is rather uncommon among other orthorhombic tartrates.

A more detailed paper, with data on lithium rubidium tartrate, will be published later.

* On leave of absence from the Bell Telephone Laboratories, Murray Hill, New Jersey.

[1] J. Valasek, Phys. Rev. 19, 478 (1921).
[2] I. V. Kurchatov, *Seignettelectricity* (Moscow, 1933).
[3] H. Scholz, Dissertation (Gottingen, 1940).
[4] B. T. Matthias and W. Merz, Helv. Phys. Acta 20, 274 (1947).
[5] Hulm, Matthias, and Long, Phys. Rev. 79, 885 (1950).

Resistivity and Hall Constant of Semiconductors

CARL N. KLAHR
Westinghouse Research Laboratories, East Pittsburgh, Pennsylvania
(Received January 26, 1951)

IN a recent letter Jones[1] has pointed out that the contributions to the resistivity of semiconductors caused by lattice scattering and by ionized impurity scattering are not simply additive. It is necessary to consider an energy average of these contributions; and, when this is done, new expressions for the Hall constant and the resistivity result.

There have been calculations paralleling those of Jones carried out at this laboratory, but in a more general representation. One considers mean free paths l_L, due to lattice scattering, l_{II}, due to

ionized impurities, and l_{NI}, due to non-ionized impurities. l_L is independent of electron or hole energy;[2] l_{II} depends on the square of the energy,[3] $l_{II}=a\epsilon^2$; l_{NI} depends on the square root of the energy,[4] $l_{NI}=b\sqrt{\epsilon}$. Then the total mean free path is

$$1/l_T=(1/l_L)+(1/l_{II})+1/l_{NI}. \tag{1}$$

One can obtain the energy distributions by considering Boltzmann's equations for electrons and holes. Using these and (1) in calculating the electric current flow, one may readily derive the resistivity and the Hall constant for weak magnetic fields.

$$\frac{1}{\rho}=\frac{4}{3}e^2\left[\frac{a_eK^2T^2}{(2\pi m_eKT)^{\frac{1}{2}}}\Phi_2(\gamma_e,\alpha_e)n_e+\frac{a_HK^2T^2}{(2\pi m_HKT)^{\frac{1}{2}}}\Phi_2(\gamma_H,\alpha_H)n_H\right], \tag{2}$$

$$R=-\frac{3\pi^{\frac{1}{2}}}{4ec}\frac{\left[n_e\frac{(a_eK^2T^2)^2}{2\pi m_eKT}\Phi_1(\gamma_e,\alpha_e)-n_H\frac{(a_HK^2T^2)^2}{2\pi m_HKT}\Phi_1(\gamma_H,\alpha_H)\right]}{\left[n_e\frac{a_eK^2T^2}{(2\pi m_eKT)^{\frac{1}{2}}}\Phi_2(\gamma_e,\alpha_e)+n_H\frac{a_HK^2T^2}{(2\pi m_HKT)^{\frac{1}{2}}}\Phi_2(\gamma_H,\alpha_H)\right]^2}, \tag{3}$$

where the subscripts e and H denote electrons and holes, respectively, and

$$\Phi_1(\gamma,\alpha)=\int_0^\infty\frac{\epsilon^{-x}x^{3/2}dx}{[1+\gamma x^{3/2}(1+\alpha x^{\frac{1}{2}})]^2}, \tag{4}$$

$$\Phi_2(\gamma,\alpha)=\int_0^\infty\frac{\epsilon^{-x}x^2dx}{[1+\gamma x^{3/2}(1+\alpha x^{\frac{1}{2}})]^2}, \tag{5}$$

$$\gamma=\frac{aK^2T^2}{b(KT)^{\frac{1}{2}}}=\frac{\text{average ionized impurity mean free path}}{\text{average non-ionized impurity mean free path}},$$

and

$$\alpha=\frac{b(KT)^{\frac{1}{2}}}{l_L}=\frac{\text{average non-ionized impurity mean free path}}{\text{lattice scattering mean free path}}.$$

γ varies as $(T^3/N_I)/(T^{\frac{1}{2}}/N_n)$, and α varies as $(T^{\frac{1}{2}}/N_n)/(1/T)$, where N_I and N_n are, respectively, the concentrations of ionized and non-ionized impurities. The product $\gamma\alpha$ will be called ϵ.

In the exhaustion range $\gamma\to0$ and $\alpha\to\infty$, while ϵ is finite. $\Phi_1(\gamma,\alpha)$ goes over into $F_1(\epsilon)$ and $\Phi_2(\gamma,\alpha)$ goes over into $F_2(\epsilon)$, where

$$F_1(\epsilon)=\int_0^\infty\frac{\epsilon^{-x}x^{3/2}dx}{(1+\epsilon x^2)^2}, \tag{6}$$

$$F_2(\epsilon)=\int_0^\infty\frac{\epsilon^{-x}x^2dx}{(1+\epsilon x^2)^2}. \tag{7}$$

In the low temperature range $\alpha\to0$, and $\Phi_1(\gamma,0)=f_1(\gamma)$ and $\Phi_2(\gamma,0)=f_2(\gamma)$ become the pertinent functions. Plots of $F_1(\epsilon)$, $F_2(\epsilon)$, $f_1(\gamma)$, and $f_2(\gamma)$ are shown in Fig. 1. The relation of γ to impurity concentration is discussed in a previous letter by the author.[5]

When $n_H=0$ the mobility μ_e becomes

$$\mu_e=-\frac{e}{c}\frac{a_eK^2T^2}{(2\pi m_eKT)^{\frac{1}{2}}}\frac{\Phi_1(\gamma_e,\alpha_e)}{\Phi_2(\gamma_e,\alpha_e)}, \tag{8}$$

and when $n_e=0$,

$$\mu_n=\frac{e}{c}\frac{a_HK^2T^2}{(2\pi m_HKT)^{\frac{1}{2}}}\frac{\Phi_1(\gamma_H,\alpha_H)}{\Phi_2(\gamma_H,\alpha_H)}. \tag{9}$$

Only in the approximation in which $\gamma_e=\gamma_H$ and $\alpha_e=\alpha_H$ can one substitute (8) and (9) into (3) to obtain

$$R=-\frac{3\pi}{8}\frac{1}{ec}\frac{n_e\mu_e^2-n_H\mu_H^2}{[n_e\mu_e+n_H\mu_H]^2}. \tag{10}$$

The familiar expressions for Hall constant and resistivity are obtained as limiting cases of (2) and (3). For instance, if one tabulates $-R\cdot n_ec$ for the case of electron conduction alone, one

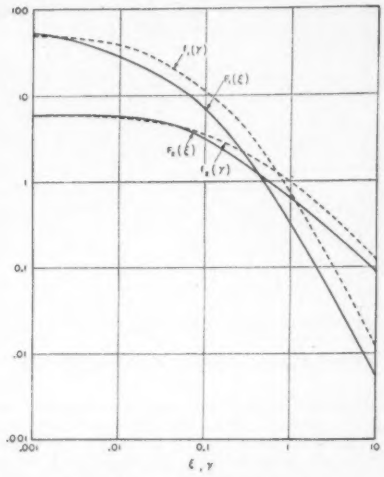

FIG. 1. Functions related to Hall constant.

obtains for $\epsilon=\infty$, $3\pi/8$; for $\epsilon=0$, 315/512; for $\gamma=0$, 315/512; for $\gamma=\infty$, $8/\sqrt{\pi}$. Limiting results for the exhaustion range when the Φ's are replaced by the $F(\epsilon)$'s are shown in the figure of reference 1. From Eqs. (2) and (3) it can be seen that the presence of holes and non-ionized impurities tend to lower the previously published values of $-R\cdot n_ec$.

[1] H. Jones, Phys. Rev. **81**, 149 (1951).
[2] A. H. Wilson, *The Theory of Metals* (Cambridge University Press, London, 1936), Chapter VI.
[3] E. Conwell and V. F. Weisskopf, Phys. Rev. **77**, 388 (1950).
[4] Cavid Erginsoy, Phys. Rev. **79**, 1013 (1950).
[5] C. N. Klahr and L. P. Hunter, Phys. Rev. **81**, 1058 (1951).

Fluctuations in the Refractive Index of the Atmosphere at Microwave Frequencies

GEORGE BIRNBAUM
National Bureau of Standards, Washington, D. C.
(Received January 27, 1951)

FLUCTUATIONS in atmospheric refractive index are being measured with a recording microwave refractometer, described in a previous paper.[1] The instrument employs a frequency modulation technique to measure small changes in frequency difference between two cavity resonators which, in the present work, are of the cylindrical TE_{011} type and made of Invar. About 30 percent of the area of each end plate was removed to permit the flow of atmosphere through the cavity. Because the openings were located at the center and along the circumference of the end plates, the reduction in cavity Q was not serious. Variations in the output current of the refractometer were amplified by a dc amplifier and measured by a recording milliammeter; the meter limited the response time of the equipment to about 0.5 sec.

Preliminary observations have been obtained with this apparatus installed on top of a building at the National Bureau of Standards. In view of the well-known turbulent aspect of the atmosphere, it was not surprising to find that the instantaneous

refractive index varies rapidly and in an irregular fashion about a mean value. A typical record of these fluctuations, obtained with one cavity open to the atmosphere and the other closed, is shown in Fig. 1b.[2] For comparison, Fig. 1a shows a record of the

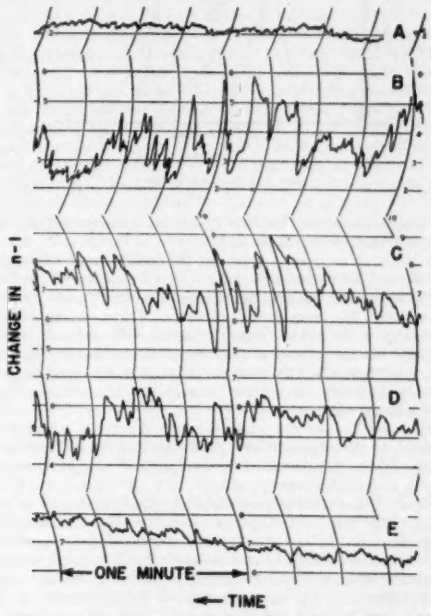

FIG. 1. The measurement of fluctuations in atmospheric refractive index with two cavity resonators: (a) both closed; (b) one open, the other closed; (c) both open, separated 1.8 m; (d) both open, separated 0.61 m; (e) both open, separated 7.6 cm. (Data taken on November 7, 1950; average wind speed was roughly 0.5 m/sec.)

stability of the instrument when both cavities were closed. In Fig. 1, ten small divisions are equal to nearly 0.8×10^{-6} in $n-1$.

Starting with an empirical expression for the radio (or microwave) refractive index of moist air,[3] and inserting mean values of temperature ($T=19.2$°C), water vapor pressure ($e=7.4$ millibars), and total pressure ($p=1011$ millibars) appropriate for the data of Fig. 1, the change in index Δn is found to be

$$10^6\Delta n=-1.1\Delta T+4.4\Delta e+0.27\Delta p. \quad (1)$$

The Δp term is unimportant, since fluctuations in pressure[4] are too small to have any significant effect on Δn. Thus, a simultaneous measurement of Δn and ΔT could determine Δe. It is sufficient to note here that an examination of a few records of simultaneous temperature and refractive index fluctuations did not reveal, in general, any marked correlation between these factors.

Some indication of a size for the random refractive index inhomogeneities[5] was obtained by observing the instantaneous difference in refractive index between two open cavities as their distance of separation was varied. Typical of several trials are the records shown in Fig. 1. When the cavity separation was less than 10 cm, fluctuations at one cavity were closely correlated with fluctuations at the other (Fig. 1e). For larger separations, the correlation began to disappear, as suggested by Figs. 1c and 1d.

To obtain a quantitative estimate of inhomogeneity size, a correlation coefficient ρ is defined as the correlation between simultaneous values of Δn and $\Delta n'$ distant x apart, thus

$$\rho=\langle(\Delta n)(\Delta n')\rangle_{Av}[\langle(\Delta n)^2\rangle_{Av}\langle(\Delta n')^2\rangle_{Av}]^{-\frac{1}{2}}. \quad (2)$$

If the inhomogeneities are isotropic, ρ may be regarded as independent of direction, and a measure of average size may be defined by[6]

$$L=\int_0^\infty \rho dx. \quad (3)$$

In the present instance, the quantities on the right side of Eq. (2) were determined from a periodic sampling of the recorded data, part of which are shown in Fig. 1. All the records were obtained within 50 minutes, during which time the weather remained practically unchanged. Figure 2 shows ρ fitted by the equation

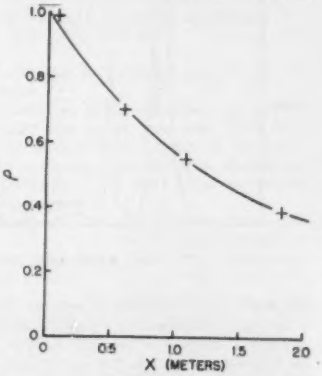

FIG. 2. Correlation coefficient, ρ, of refractive index fluctuation as a function of distance, x.

$\rho=\exp(-x/1.9)$; inserting this in Eq. (3) gives a size of 1.9 m. The root-mean-square deviation of refractive index $\langle(\Delta n)^2\rangle_{Av}^{\frac{1}{2}}$ was nearly 0.3×10^{-6}. These results apply, of course, for a particular site and state of the atmosphere. Further investigations along these lines are now in progress.

The author wishes to thank Mr. S. J. Kryder and Mr. R. R. Larson for assistance with the experiments.

[1] G. Birnbaum, Rev. Sci. Instr. **21**, 169 (1950).
[2] Similar observations are described by C. M. Crain and J. R. Gerhardt, Bull. Am. Meteorol. Soc. **31**, 330 (1950).
[3] *Meteorological Factors in Radio-Wave Propagation*, The Physical Society, London, 1947), foreword.
[4] R. D. M. Clark, J. Meteorol. **7**, 70 (1950).
[5] A theory of radio scattering in the troposphere from such inhomogeneities is described by H. G. Booker and W. E. Gordon, Proc. Inst. Radio Engrs. **38**, 401 (1950).
[6] A scale of turbulence is similarly defined. See, for example, O. G. Sutton, *Atmospheric Turbulence* (Methuen and Company, Ltd., London, 1949), pp. 62–65.

On the Decay of $Xe^{125}\rightarrow I^{125}\rightarrow Te^{125}$

INGMAR BERGSTRÖM
Nobel Institute of Physics, Stockholm, Sweden
(Received February 9, 1951)

RECENTLY, Anderson and Pool[1] reported a new isotope, Xe^{125}, with the half-life of 20 hr, produced in a $Te(\alpha, n)$ reaction. K x-rays of I and a weak γ-ray of the energy ~0.6 Mev were reported.

We have produced Xe^{125} by neutron irradiation of Xe in the Harwell pile. After electromagnetic separation, a gas activity of the half-life 18±0.5 hr appeared on the collector foil (0.15 mg Al/cm²) at mass number 125, confirming the existence of Xe^{125}. All odd mass numbers between 135 and 125 showed activities strong enough for β-spectrometer investigations. The activities at the mass numbers 133, 131, 129 (a new 9-day isomer, $E_\gamma=195$

kev), and 127 were investigated in a sample from an earlier irradiation.[3]

Figure 1 shows the β-spectrum of Xe^{125}. In Table I we have summarized the results obtained with the β-spectrometer and the NaI scintillation spectrometer. As can be seen from Fig. 1, the first K conversion line K_1 is overlapped by the Auger-line (A_1 in Fig. 1) $K-2L$. Knowing the intensity ratio $NA_1/NA_2=2$ from measurements on Xe^{121m}, it has been possible to give the intensity of the K_1 line in Table I. In Fig. 1 the half-width of the K_2+K_3

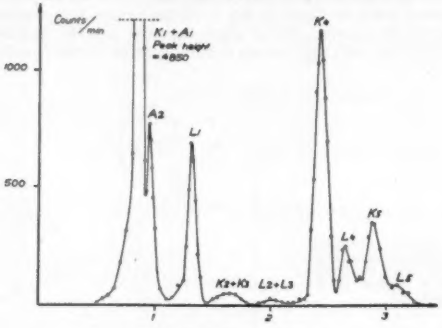

FIG. 1. β-spectrum of Xe^{125}.

line shows that it is double. A separate investigation, not shown in the figure, indicates two conversion lines of the energies given in Table I. Because of intensity reasons it was not possible to get accurate information of these two lines.

It should be noticed that the 54-kev and the 187-kev γ-rays sum up to give the same energy as the 243-kev γ-ray. From intensity considerations it is also probable that the 54- and 187-kev γ-rays are emitted in cascade. Within the limits of error, the sum of the energies of the 96-, 106-, and 243-kev γ-rays are equal to the energy of the 460-kev γ-ray. The suggested level scheme must be considered as tentative, and coincidence measurements have to be performed before an unambiguous level scheme can be given.

No positrons or electrons in addition to the conversion electrons were found. In most cases the Auger-lines are not overlapped by conversion lines, and it is possible to find the Z-value to which a certain decay takes place from the energy of the Auger-lines. Knowing the x-ray fluorescence yield, it is also possible to prove K-capture from comparison of the intensities of the Auger-lines and the conversion lines. In this case

$$(NA_1+NA_2)/(NK_1+NK_2+NK_3+NK_4+NK_5)=0.44.$$

If no K-capture were present, this ratio would have been ~ 0.11.[3]

TABLE I. Summary of results.

Energy of the electron line (kev)	Interpretation	Corresponding γ-ray energy (kev)	Relative intensity
20.7	K_1+A_1		100
26.2	A_2		16
	A_1		32
	K_1	54.0	68
49.5	L_1	54.7	16
63	K_2	96	1
73	K_3	106	1
107	L_2+L_3		0.4
153	K_4	187	24
183	L_4	188	5.2
208	K_5	243	7.2
238	L_5	243	
	Scintillation spectrometer	460	Weak

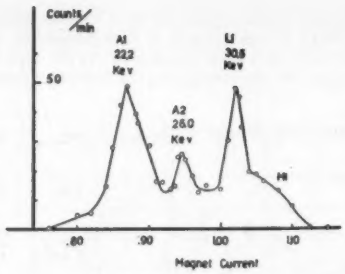

FIG. 2. β-spectrum of I^{125}.

We therefore conclude that Xe^{125} decays predominantly by K-capture to several excited states in I^{125}.

It is also of interest to point out the similarities in the decay of Xe^{125} and Xe^{127}. Earlier we have reported[2] that Xe^{127} decays by K-capture to I^{127}. γ-rays of the energies 57, 145, 170, and 200 kev are emitted. The energies of the first two γ-rays sum up to give the energy of the 200-kev γ-ray. Using the NaI scintillation spectrometer we later found a weak γ-ray of the energy 365 kev, indicating that the 170- and the 200-kev γ-rays probably are emitted in cascade, since their γ-energy sum is the same as the energy of the 365-kev γ-ray.

Reid and Keston[4] discovered a 56-day I activity which they assigned to the mass number 125. X-rays and weak electrons of energy 100 kev were observed. In our aged Xe^{125} sample we should be able to find this activity.

Figure 2 shows the β-spectrum of the Xe^{125} sample about one month after the electromagnetic separation. In addition to the Auger-lines $K-2L$ and $K-L-M$ characteristic for Te, we observe two conversion lines of energies 30.5 and 34 kev, which are consistent with the L and M conversion lines of a 35.5-kev γ-ray. G. Friedlander *et al.*[5] have investigated the Te fraction of the sample used by Reid and Keston and found weak electrons of the energy $\sim$120 kev. In investigations by K. Siegbahn and W. Forsling[6] and R. D. Hill,[7] it is definitely concluded that Te^{125m} decays by emission of two γ-rays in cascade (35 and 109 kev). The low energy γ-rays found by these investigators and that found by us are certainly emitted from the same level in Te^{125}.

This fact and the results of Friedlander *et al.* support the assumption that I^{125} decays by K-capture to both the levels in Te^{125}. The branching ratio, however, would then be small, since we have not found the conversion lines of the 109-kev γ-ray. The spin of I^{127} is 5/2, and the nuclear shell theories suggest 5/2 also for I^{125}. The spins 3/2 and 11/2 for the excited states in Te^{125} are consistent with the measurements.[7] K-capture to the upper level of Te^{125} would then be more forbidden than to the lower level in agreement with the measurements.

[1] D. L. Anderson and M. L. Pool, Phys. Rev. **77**, 142 (1950).
[2] I. Bergström, Nature (to be published).
[3] I. Bergström and S. Thulin, Phys. Rev. **79**, 338 (1950).
[4] A. F. Reid and A. S. Keston, Phys. Rev. **70**, 987 (1946).
[5] Friedlander, Goldhaber, and Scharff-Goldhaber, Phys. Rev. **74**, 981 (1948).
[6] K. Siegbahn and W. Forsling, Arkiv Fysik, Bd 1, No. 24, 505 (1949).
[7] R. D. Hill, Phys. Rev. **76**, 333 (1949).

β-Spectrometer Investigations on Electromagnetically Separated Xe^{125} and Kr^{79}

INGMAR BERGSTRÖM
Nobel Institute of Physics, Stockholm, Sweden
(Received February 9, 1951)

Xe^{125}.—Xe^{125} has been investigated in the β-spectrometer by Peacock *et al.*,[1] who report a β-spectrum of the upper limit 0.93 Mev and a 0.247-Mev γ-ray. In an investigation on Xe^{125m} [2]

produced in fission we also obtained a strong Xe^{135} activity after electromagnetic separation of the fission gas. Because of the ideal character of the β-spectrometer samples obtained by electromagnetic separation of the radioactive isotopes, it will be of interest to report our results on Xe^{135}.

The activity at mass number 135 was collected on thin commercial Al foils (0.15 mg/cm²). These foils perhaps seem to be too thick for measurements of the β-spectrum in the low energy region. Nevertheless, it is a fact that the Fermi plot of Xe^{135} is a straight line from the upper limit 905±10 kev down to 50 kev (Fig. 1). In the case of the 4.4-hr Kr^{85} β-spectrum[2] when the same weight of Al foil was used as a backing, the Fermi plot was straight from the end point 817 down to 35 kev. In both these cases the β-spectra belong to the allowed group, and the deviations from the straight line of the Fermi plot does not set in before $E<0.05\cdot E$ max. Because of the quite negligible thickness of our carrier-free electromagnetically separated samples, we conclude that the thickness of the sample is relatively more critical than the sample backing when investigating the low energy region of β-spectra.

Thus, the β-spectrum of Xe^{135} is simple and has an allowed form. We also obtain $ft=3\cdot10^6$, classifying the β-spectrum in the allowed group.

The K and L conversion lines corresponding to a γ-ray energy of 248±2 kev were found, which is in good agreement with the results of Peacock *et al.* $e^- - \beta^-$ coincidence measurements in the β-spectrometer showed a strong coincidence effect. The mass difference between Xe^{135} and Cs^{135} would then correspond to 1.15 Mev.

Kr^{79}.—Absorption measurements[4] have shown that Kr^{79} decays by K-capture and positron emission with a half-life of 34.5 hr. A γ-ray of the energy 0.2 Mev has also been reported.[4]

In order to get more detailed information on Kr^{79}, Kr was irradiated in the Harwell pile and then electromagnetically separated for a β-spectrometer investigation. Two activities at mass numbers 79 and 85, with the half-lives 34±4 hr and ~4 hr, were the only ones present when the β-spectrometer investigations started. Figure 2 shows the β-spectrum of Kr^{79}. The decay of this

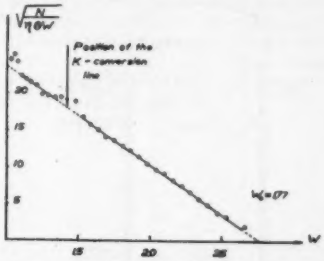

FIG. 1. Fermi plot of Xe^{135}.

isotope is associated with a very strong K-capture, as can be seen from the large intensity of the Auger lines $K-2L$ ($A1$ in Fig. 2) and $K-L-M$ ($A2$ in Fig. 2), characteristic of Br as compared with the β-spectrum. In a separate investigation the β-particles were identified as positrons by the use of helical baffles in the lens spectrometer. No negatrons in addition to conversion and Auger electrons were found. We estimate the ratio of the intensity of K-capture to positron emission to be about 10. This value is somewhat uncertain because of G-M window (cut-off ~6 kev) absorption correction for the Auger lines, but it is definitely lower than the value 50 reported by Woodword *et al.*[5]

The Fermi plot of the β-spectrum of Kr^{79} is a straight line from the upper limit, 595 kev, down to 110 kev. The same weight of Al foil as in the case of Kr^{85} and Xe^{135} was used as collector foil, and we notice that the low energy deviation starts earlier than expected if the positron spectrum is simple and has the allowed form.

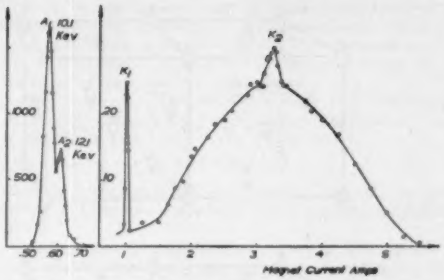

FIG. 2. β-spectrum of Kr^{79}. To the left, the low energy region in a magnified scale.

Because of the rather weak sample, we cannot come to any conclusion about this deviation.

Except for the uncertain low energy deviation, the positron spectrum is simple and the high energy component (0.9–1 Mev) reported by other investigators[4,6] must be due to impurities. Using the approximate branching ratio 10 for K-capture and positron emission, we obtain $ft=2\cdot10^6$, which places the positron spectrum in the allowed group.

Two conversion lines (K_1 and K_2 in Fig. 2) having the energies 30.3 and 249 kev were found. These lines are most probably K lines corresponding to the γ-energies 44 and 263 kev, respectively. If the positron emission is followed by the 263-kev γ-ray, we obtain a rough value for the K conversion coefficient α_K of this γ-ray. α_K~0.016, and indicates that the γ-transition is to be associated with electric quadrupole or magnetic dipole radiation.

Feenberg and Trigg[6] have given the probability ratio for positron emission and K-capture to the same level. For the positron energy 595 kev, we obtain $f_K:f_+=10$ (from the curves of Feenberg and Trigg). This value is close to that obtained from our experiments, suggesting that the main part of the K-capture and the positron transitions lead to the same level, probably that from which the 263-kev γ-ray is emitted.

We wish to express our sincere thanks to Dr. W. T. Arrol at the Isotope Division, Harwell, for much good advice regarding the rare gas irradiations. Without the prompt service from Harwell, it would not have been possible to perform the measurements on Kr^{79} and Xe^{135}.

[1] Peacock, Brosi, and Bogard, reported by G. T. Seaborg and I. Perlman, Revs. Modern Phys. 20, 585 (1948).
[2] I. Bergström and S. Thulin, Phys. Rev. 79, 538 (1950).
[3] I. Bergström and S. Thulin, Phys. Rev. 79, 537 (1950).
[4] E. Hoagland and N. Sugarman, reported by G. T. Seaborg and I. Perlman, Revs. Modern Phys. 20, 585 (1948).
[5] Woodward, McCown, and Pool, Phys. Rev. 74, 761 (1948).
[6] E. Feenberg and G. Trigg, Revs. Modern Phys. 22, 399 (1950).

Crystal Structure Transitions in Antiferromagnetic Compounds at the Curie Temperature*

J. SAMUEL SMART AND SELMA GREENWALD
U. S. Naval Ordnance Laboratory, White Oak, Silver Spring, Maryland
(Received January 12, 1951)

THE antiferromagnetic compounds MnO, FeO, CoO, and NiO undergo crystal structure transitions near their Curie temperatures.[1–3] Above their Curie temperatures all four compounds have the NaCl structure with the metal atoms alone forming a face-centered cube. Below the Curie temperature, the crystal structure of CoO is deformed to tetragonal symmetry, while the structures of the other three compounds are deformed to rhombohedral symmetry. The authors[3] have suggested that these transitions are due to the fact that the magnetic atoms can increase their exchange interaction energy by shifting their positions. The purpose of this letter is to point out that the crystal structure

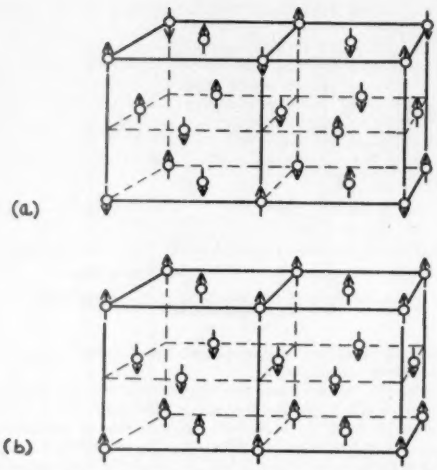

FIG. 1. Possible magnetic structures for a face-centered cubic lattice. (a) Antiferromagnetic next-nearest-neighbor ordering. (b) Antiferromagnetic nearest-neighbor ordering.

transitions can be correlated with the magnetic structures of these compounds.

Figure 1 shows two possible magnetic structures for a face-centered lattice. Case (a) illustrates the arrangement of lowest energy when the most important exchange interactions are antiferromagnetic interactions between next nearest neighbors. This magnetic structure is the one discovered by Shull[4] in his neutron diffraction experiments on the four compounds listed above. This configuration consists of four interpenetrating simple cubic lattices, each arranged antiferromagnetically within itself. Actually the neutron diffraction data does not distinguish between the magnetic structure of case (a) and one in which there is no correlation of spin directions between different sublattices. As indicated below, the x-ray diffraction data seem to favor the first arrangement.

Case (b) is a possible structure when antiferromagnetic nearest neighbor interactions are most important, and is especially favorable if there are also ferromagnetic next nearest neighbor interactions.[5] So far, this structure has not been observed experimentally.

In case (a) there is a set of (111) planes and in case (b) a set of (100) planes in which all spins in a given plane are parallel but the spins in neighboring planes are antiparallel. If our argument concerning the crystal structure transitions[3] is correct, and if we assume the existence of nearest-neighbor interactions, we should expect that at the Curie temperature the crystal would expand or contract along a direction perpendicular to these planes. Therefore, structure transitions to rhombohedral and tetragonal symmetry should occur for cases (a) and (b), respectively.

As predicted by our arguments, MnO, FeO, and NiO, which have the magnetic structure of case (a), undergo transitions to rhombohedral symmetry at the Curie temperature. Rooksby and Tombs[6] have reported that MnS undergoes a transition to rhombohedral symmetry near its Curie temperature, indicating that its magnetic structure is the same as that of the oxides. Finally, Greenwald[7] has determined that Cr_2O_3, which has the corundum structure, contracts along a [111] direction at the Curie temperature. This result suggests that its magnetic structure is the one proposed by Néel[8] in which there is a set of (111) planes with alternating spin directions.

In the case of CoO, the interpretation of the crystal structure data apparently does not agree with the observed magnetic structure. The tetragonal deformation at the Curie temperature suggests that its magnetic structure is that of case (b) with nearest-neighbor ordering, but the reported neutron diffraction work[4] indicates that the magnetic structure is actually that of case (a). We have no explanation for this discrepancy.

In order-disorder transitions in 50-50 face-centered alloys, deformations to rhombohedral and tetragonal symmetry are observed for ordering of types (a) and (b), respectively.[9] These deformations may be due to variation of ordering energy with distance, in analogy with the antiferromagnetic case.

* This work was supported in part by the ONR.

[1] H. P. Rooksby, Acta Cryst. 1, 226 (1948).
[2] N. C. Tombs and H. P. Rooksby, Nature 165, 442 (1950).
[3] S. Greenwald and J. S. Smart, Nature 166, 523 (1950).
[4] C. G. Shull and J. S. Smart, Phys. Rev. 76, 1256 (1949), and report by J. H. Van Vleck at Grenoble Conference, 1950.
[5] P. W. Anderson [Phys. Rev. 79, 705 (1950)] has suggested a third structure, which we have not shown, which is best for nearest-neighbor ordering with additional antiferromagnetic next-nearest-neighbor interactions.
[6] H. P. Rooksby and N. C. Tombs, private communication.
[7] S. Greenwald, Acta Cryst. (to be published).
[8] L. Néel, Ann. Phys. 3, 137 (1948).
[9] C. H. Johannson and J. O. Linde, Ann. Physik 82, 449 (1927).

Evidence of Long-Range Secondary Electrons Accompanying Cosmic Rays in a Proportional Counter

S. D. CHATTERJEE*
Division of Physics, National Research Council of Canada, Ottawa, Canada
(Received January 24, 1951)

THE measurement of the ionizing power of individual cosmic-ray particles has usually been undertaken with one or two proportional counters connected in coincidence with Geiger

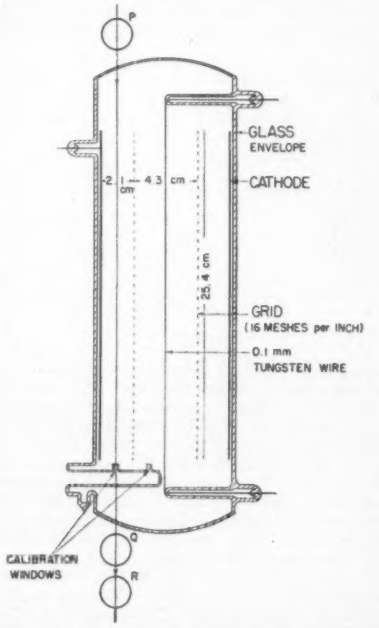

FIG. 1. The arrangement of the proportional counter.

counter telescopes.[1,2] It has, however, been found by Weisz and Swann that a cosmic ray traversing similar path lengths in two proportional counters gives pulses A and B which are unequal, A being sometimes less than and sometimes greater than B. Swann[3] has suggested, on theoretical grounds, a probable explanation for this discrepancy as being due to the statistical fluctuation in the number of high energy secondary electrons emitted within the gaseous volume of the proportional counter.

In order to test the validity of this hypothesis an experimental arrangement, schematically depicted in Fig. 1, was set up. The path of the cosmic ray was defined by three small Geiger counters P, Q, and R, using the usual coincidence circuit method and kept confined between grid and cathode of the proportional counter. The grid was maintained at a negative potential (approximately 90 volts) relative to the cathode, so that no negative ions produced in the region between grid and cathode could get to the wire. However, long-range secondary electrons emitted by the primary can pass through the grid and produce avalanches near the wire by an appropriate adjustment of the potential difference between grid and wire.

The pulse from the proportional counter was fed to a two-stage linear amplifier followed by a biased multivibrator and a Rossi tube. The latter was connected in coincidence with another similar circuit which was fed by the triple coincidence pulse from the Geiger counters after suitable modification. The triple and quadruple coincidences were recorded separately by an Esterline Angus pen-recorder.

Figure 2 shows two typical curves, obtained at two different sensitivities of the multivibrator, where the ratio of the quadruple to triple coincidences in percent has been plotted as a function of the voltage on the proportional counter. The nature of the curves most probably results from a combination of two phenomena:

(a) The increase to a maximum in the primary phenomenon under investigation, *viz*, the detection of the secondary electron, and

(b) superposition of the phenomenon resulting from the sucking of ions through the screen from the region outside, which would presumably mount at increasing rate with increase of "sucking-in" field. It is proposed to investigate more fully the phenomenon of leakage of ions by utilizing a grid having a smaller mesh of thinner wires and also by adopting two grids instead of one, the potentials being suitably adjusted.

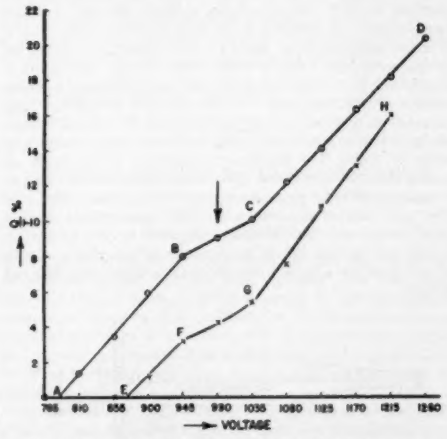

FIG. 2. The ratio of quadruple to triple coincidences in percent *vs* voltage on the proportional counter.

It may be seen, however, that the curve $ABCD$, obtained with the multivibrator operating at its maximum sensitivity, shows a point of inflection at about 9 percent. This represents probably the most acceptable value of the percentage of secondaries obtained under these experimental conditions.

It is interesting to compare this value with that deduced theoretically according to Swann's[3] method. The fraction P of the N secondaries, with energy $Q>Q_0$ is given by

$$P=Q_m/Q_0, \tag{1}$$

where Q_m is the lowest limit of Q ($\sim$10 ev), and Q_0 is the lowest energy of a secondary detectable under our experimental conditions.

Assuming that the secondaries are ejected at right angles to the path of the cosmic ray, like delta-rays accompanying swift β-particles,[4] it may be seen that the secondaries have to traverse an average length of approximately 1 cm in the gaseous mixture (5 cm of argon+15 cm of methane) before entering the sensitive volume of the proportional counter. This path length is equivalent to a range of approximately 0.2 cm in air at N.T.P. and necessitates a dissipation of approximately 3 kev on the part of the electron.[5] Moreover, the path length of 25.4 cm traversed by the primary through the gaseous volume of the counter gives about 130 primary ionizing events (N).

Therefore, the average number of cases where $Q>Q_0$ in the passage of a primary through the counter along the path designated is

$$PN=130\times3.3\times10^{-3}=0.43.$$

Now if, as a first approximation, we assume that the number of secondaries for $Q>Q_0$ shows fluctuations in accordance with Poisson's law, the fraction F of the primary rays which give n secondaries is represented by

$$F=x^n e^{-x}/n! \tag{2}$$

In this case x, the average number of secondaries per particle, is 0.43. The values of F for $n=0$, 1, 2, respectively, are 0.65, 0.28, 0.06. Thus, in only 34 percent of the cases, the primary ray is accompanied by secondaries above 3 kev, which are ejected in all directions perpendicular to the path of the former. On account of the geometry and dimensions of the cathode and grid, however, it can be shown that only 33 percent of these secondaries can penetrate through the grid into the active volume of the proportional counter. Therefore, the calculated percentage of long-range secondaries which can be detected in the present set up is about eleven, which compares favorably with our experimental finding.

The author is indebted to Dr. W. F. G. Swann for invaluable suggestions and to Dr. D. C. Rose for generous help.

* National Research Laboratories Post-Doctorate Fellow.
[1] P. Weisz and W. E. Ramsey, Rev. Sci. Instr. **13**, 258 (1942).
[2] Alichanian, Alichanow, and Nikitin, J. Phys. U.S.S.R. **9**, 167 (1945).
[3] W. F. G. Swann, J. Franklin Inst. **249**, 133 (1950).
[4] Rutherford, Chadwick, and Ellis, *Radiations from Radioactive Substances* (Cambridge University Press, London, 1930), p. 152.
[5] C. T. R. Wilson, Proc. Roy. Soc. (London) **A104**, 199 (1923).

Measurement of Isomeric Transition Energies with a Scintillation Spectrometer

E. DER MATEOSIAN AND M. GOLDHABER
Brookhaven National Laboratory, Upton, Long Island, New York*
(Received February 15, 1951)

AN accurate determination of isomeric transition energies is necessary for a comparison between theoretical and experimental gamma-ray lifetimes and plays, therefore, an important role in any systematic investigation of isomers. The gamma-ray scintillation spectrometer[1] is particularly suited for the determination of isomeric transition energies whenever one or more of the following conditions are fulfilled: the isomeric transition is not too highly converted, the specific activity is low, and the lifetime is short. Under such circumstances the use of the scintillation

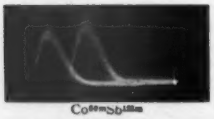

FIG. 1. Oscilloscope traces of Co^{60m} (10.7 min) (59 kev standard) and Sb^{120m} (5.5 min) indicating a γ-ray energy of 68 kev.

counter may yield results which are superior to absorption measurements and may compare in accuracy with those attainable with a beta-ray spectrometer. The scintillation counter shares with some other methods the disadvantage that the gamma-ray observed does not necessarily correspond to the isomeric transition. It may follow the isomeric transition or appear in a beta- or K branch. Subsidiary experiments may therefore be necessary in some cases.

We should like to report here on a series of measurements of isomeric transition energies which we have carried out with the help of a scintillation counter. We used NaI crystals activated with TlI. We found a comparatively small crystal ($\sim$2 cm^3 in area and 1 cm high) most useful for a determination of low energy gamma-rays. The crystal, covered with a layer of mineral oil, was fixed to a 5819 RCA photo-tube and backed by an aluminum foil reflector. The photo-tube was connected to a 204B Atomic

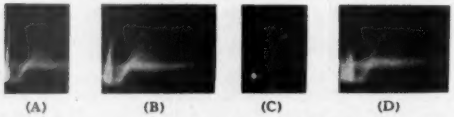

FIG. 2. Oscilloscope traces showing γ-ray continuum from Ir^{192m} (1.5 min). (A) 10-sec exposure, (B) 15-sec exposure, (C) shows, for comparison, an electronically produced pulse corresponding in height to the center of a 50-kev γ-line, and (D) shows the γ-ray of Rh^{104m} (4.7 min) indicating an energy of 52 kev.

Instrument Company linear amplifier and a DuMont 248 oscilloscope for display of the self-triggered pulses (sweep time $\sim$5μsec). The pulse distribution was photographed with the help of a polaroid camera. The linearity of our arrangement was checked with a number of well-known gamma-ray lines (Co^{60m} (59 kev), Te^{123m} (159 kev), Te^{121m} (213 kev), Cr^{51} (320 kev), Cs^{137} (661 kev)) and found to be satisfactory in this energy range. To obtain the metastable states which we investigated, suitable samples (metals or oxides) were exposed to slow neutrons in the Brookhaven reactor and then transferred rapidly to the scintillation counter. Typical oscilloscope traces are shown in Figs. 1 and 2. Table I summarizes our results. The apparent gamma-ray continuum previously found[3] for Ir^{192m} (1.5 min) in competition with the 57.4 kev internally converted transition,[3] yields a pulse distribution with an upper limit close to this energy but of very different appearance than that obtained for gamma-rays of other isomers of similar excitation energy. This spectrum is being investigated further.

Antimony was used in isotopically enriched form (97.7 percent Sb^{121}). Our energy values are estimated to be accurate to 10 percent. The only serious discrepancy between our values and earlier ones appears in the case of Hf^{179m} (19 sec), where Hole[4] had found a transition energy of 150 kev with a beta-ray spectrograph, and where our value is considerably higher (215 kev).[5] The possibility that we are dealing here with a two-step isomeric transition is being investigated.

We wish to thank Dr. C. E. Larson, Oak Ridge, for putting hafnium metal at our disposal and Dr. Keim's group for the isotopically enriched antimony sample. Thanks are also due to Mr. Jack Floyd for help in making the neutron exposures.

TABLE I. Isomeric transition energies.

Isomer	Present work: Half-life time	Present work: Energy of γ (kev)	Previous data: Energy of e^- (kev)	Previous data: Energy of γ (kev)	Transition energy (kev) as given by K. Way *et al.*[a]
Sc^{48m}	19.5 sec	135	165 (abs[b])	180 (abs)	150
Sc^{47m}	17.5 sec	150	150 (abs)	150 (abs)	150
Rh^{104m}	4.7 min	53	69.5 (spect[c])	50 (abs)	80; 50
Sb^{120m}	5.5 min	68	$\sim$110 (abs[d])		140
Hf^{179m} [e]	19 sec	215	86.1, 135.1 (spect[c])		150
			190 (abs[f])		190
Ir^{192m}	1.5 min	Continuum	44.1L_I, 46.0L_{III}	Continuum	57.4

[a] Previous data for which no explicit references are given are taken from K. Way *et al.*, Nuclear Data, Nat. Bur. Standards (U. S.), Circ. 499.
[b] M. Goldhaber and C. O. Muehlhause, Phys. Rev. 74, 1877 (1948).
[c] N. Hole, Arkiv. Mat. Astron. Fysik 34B, No. 5 (1947).
[d] der Mateosian, Goldhaber, Muehlhause, and McKeown, Phys. Rev. 72, 1271 (1947).
[e] Reference 4.
[f] A. Flammersfeld, Z. Naturforsch. 1, 190 (1946).
[g] This mass number was recently assigned by C. O. Muehlhause by bombarding enriched Hf isotopes with slow neutrons (private communication).

* Research carried out under contract with the AEC.
[1] R. Hofstadter and J. A. McIntyre, Phys. Rev. 80, 631 (1950); S. A. E. Johansson, Arkiv Fysik 18, 171 (1950); Pringle, Roulston, and Standil, Phys. Rev. 78, 627 (1950); P. R. Bell and J. M. Cassidy, Phys. Rev. 79, 173 (1950).
[2] Goldhaber, Muehlhause, and Turkel, Phys. Rev. 71, 372 (1947).
[3] R. L. Caldwell, Phys. Rev. 78, 407 (1950).
[4] N. Hole, Arkiv Mat. Astron. Fysik 36A, No. 9 (1948).
[5] Dr. E. C. Campbell of Oak Ridge informs us that he has also obtained a value of 215 kev for the Hf gamma-ray.

Quantum Effects in the Interaction between Free Electrons and Electromagnetic Fields

CARL SHULMAN
RCA Laboratories Division, Radio Corporation of America, Princeton, New Jersey, and Princeton University, Princeton, New Jersey
(Received January 22, 1951)

THE quantum nature of the exchange of energy between free electrons and electromagnetic fields implies a dispersion in energy exchange which the classical theory cannot predict. Smith[1] has treated the quantum mechanical description of this process in some detail, and he has calculated probabilities for the exchange process in a few simple cases. The standard deviation is shown to be proportional to the square root of the number of photons handled by an interacting electron, while the mean expected energy exchange is proportional to the total number handled. Hence, the transition to the classical description may be understood in terms of the vanishing of the ratio of the standard deviation to the mean expected exchange in the limit of large number of photons handled. This calculation suggests that the quantum dispersion might be observed in the presence of a strong electric field if the mean exchange could be made small. One could, for instance, use a high velocity beam whose energy distribution is characterized by a temperature T, sending it through a strong oscillating electric field such that the standard deviation arising from quantum processes is at least of the order kT, while the mean exchange is held to zero by adjusting the transit time to an integral number of cycles. The apparent temperature of the beam on emerging from the interaction space would be increased owing to the quantum effect by an amount proportional to the square root of the total number of photons handled during transit. Such a method circumvents the limitation suggested by Ward,[2] that in order to use electron beams to detect quantum effects of this kind, one must use a beam mono-energetic to within less than one quantum.

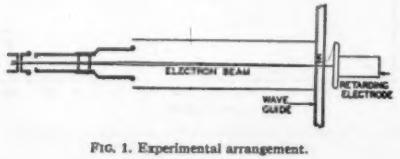

FIG. 1. Experimental arrangement.

We have detected this quantum dispersion with the arrangement shown in Fig. 1. A fine electron beam was shot through a longitudinal r-f field in the wave guide, as shown. The transit time in the guide was adjusted to an integral number of r-f cycles. After emergence from the interaction space, the energy distribution was measured by a retarding field method. This energy distribution has three main sources: (1) emission velocity distribution in the beam, (2) a classical energy exchange arising from a small functional dependence of transit time on the r-f field strength, and (3) the quantum effect sought. By using high beam voltage (10 kv), small beam angle (0.004 radian), and strong r-f field, the classical effect No. 2 was made small relative to effect No. 1, while the quantum effect No. 3 was made large.

The actual measurement was made in terms of the dependence of the current to the retarding electrode on the r-f field strength. Assuming a Maxwell-Boltzmann distribution in the beam, and applying the Smith treatment, one can calculate the current to the retarding electrode in terms of the three effects mentioned above. This current is given by the expression

$$\frac{I}{I_0}=J_0\left(i\frac{1}{4n\pi}\frac{eV^2}{V_0kT}\right)\exp\left(\frac{1}{\pi}\frac{eV}{kT}\frac{h\nu}{kT}\right),$$

where I is the current in the presence of r-f field; I_0 is the current in the absence of r-f field; V is the peak r-f voltage across wave guide; V_0 is the dc voltage at the wave guide; T is the beam temperature; and n is the number of r-f cycles of interaction time. The argument of the exponential term is a measure of the quantum dispersion in terms of the dispersion of the initial energy, while the argument of the Bessel term is a measure of the dispersion arising from the classical effect No. 2 in terms of the dispersion of initial energy.

The experiment was carried out at a free space wavelength of 1.25 cm with a pulsed magnetron oscillator as the source of r-f energy. From experimental plots of $-\ln[(I_0/I)J_0(ieV^2/4n\pi V_0kT)]$ *versus* V, one can decide whether or not he has observed the quantum effect by using the following argument: If the quantum dispersion were nonexistent, such plots would show no dependence on V. If, in addition, there occurs accidental asymmetry in the geometry of the interaction space, the plots would show quadratic dependence on V, representing a classical effect. If the quantum dispersion exists and if there is accidental asymmetry in the interaction space, the plots would again be quadratic. If the quantum effect is present and there is no asymmetry in the interaction space, the plots would show a linear relationship in V.

The experimental plots show a linear dependence of $-\ln[(I_0/I)\times J_0(ieV^2/4n\pi V_0kT)]$ on V and represent detection of the quantum effect. Computations of h from measurements of I/I_0, V, T, and V_0 give a spread of values whose average is 0.7 times the accepted value with a standard deviation of 0.2.

[1] L. P. Smith, Phys. Rev. **69**, 195 (1946).
[2] J. C. Ward, Phys. Rev. **80**, 119 (1950).

Disintegration of Neon by Fast Neutrons*

C. H. JOHNSON, C. K. BOCKELMAN,† AND H. H. BARSCHALL
University of Wisconsin, Madison, Wisconsin
(Received January 23, 1951)

IN a previous paper, measurements on the disintegration of nitrogen by fast neutrons were reported.[1] The same equipment was used to measure the cross section for the disintegration of neon by neutrons. For this purpose, the ionization chamber was filled with neon to a pressure of 30 atmospheres and operated as a proportional counter with a gas multiplication of about five. In order to obtain saturation at this pressure, the neon was purified by means of a calcium getter.

Fast neutrons of variable energy were obtained by bombarding a thin tritium target with protons from the electrostatic generator. The tritium was absorbed in an evaporated layer of zirconium having a stopping power of less than 15 kev for the protons used in the measurements. The energy spread of the neutrons entering the counter was caused primarily by the variation in energy of the neutrons as a function of angle of emission with respect to the incident protons. This energy spread could be varied by changing the distance of the counter from the target.

Figure 1 shows a pulse height distribution obtained with 2.45-Mev neutrons. Similar distribution curves were taken at intervals of about 0.2-Mev neutron energy. Only one group of disintegration pulses was found. In addition to the neon disintegrations, pulses from a Po α-particle source in the counter were registered at each neutron energy to fix the energy scale. In this way it was found that the disintegration pulses had an energy of 0.75 ± 0.05 Mev less than the incident neutrons. This value of the reaction energy is in fair agreement with values of -0.80 to -0.85 Mev as observed by Graves and Coon[2] for the Ne(n,α) reaction. Because of the uncertainty of the masses of O^{17} and Ne^{20}, the reaction energy can be obtained from the masses only to about ±150 kev, but it agrees within these limits of error with the value measured in the present experiment.

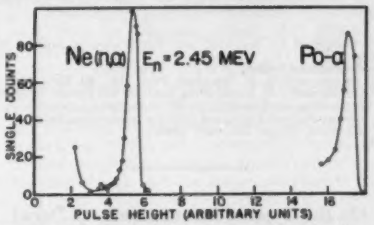

FIG. 1. Typical pulse height distribution curve obtained with fast neutrons incident on a neon-filled proportional counter. Po α-particles originate from a source mounted on the wall of the counter.

Figure 2 shows the disintegration cross section of neon as a function of neutron energy. The magnitude of the cross section at the three prominent resonance peaks excludes the possibility that the disintegrations could be caused in any but the most abundant isotope; consequently, the cross section was calculated under the assumption that Ne^{20} is responsible for the observed disintegrations. For the three large peaks, the neutron energy spread was somewhat less than the observed width of the resonance so that the cross section should reach nearly the true value.

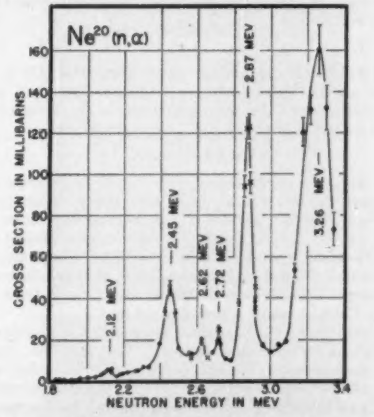

FIG. 2. Neon disintegration cross section. Circles indicate a neutron energy spread which increased from 40 kev at 1.8 Mev to 60 kev at 3.3 Mev. Crosses indicate an energy spread of 30 kev. Energies given at the resonance peaks have an uncertainty of less than 50 kev.

The cross section in the present experiment is larger than that given for 2.5-Mev neutrons in the preliminary report by Graves and Coon. If the present measurements are averaged over the larger energy spread used by these authors, a cross section of about 20 millibarns is obtained compared to 5 millibarns observed by Graves and Coon. The shape of the cross section curve given in Fig. 2 is in agreement with the yield curve published by Sikkema.[5]

* Work supported by the AEC and the Wisconsin Alumni Research Foundation.
† AEC Predoctoral Fellow.
[1] C. H. Johnson and H. H. Barschall, Phys. Rev. **80**, 818 (1950).
[2] E. R. Graves and J. H. Coon, Phys. Rev. **70**, 101 (1946). In more recent measurements, these authors find the above quoted reaction energy instead of −0.6 Mev as originally reported (private communication).
[5] C. P. Sikkema, Nature **165**, 1016 (1950).

On the Type of Interaction in β-Decay

STEVEN A. MOSZKOWSKI
Argonne National Laboratory, Chicago, Illinois
(Received February 8, 1951)

A KNOWLEDGE of the type of interaction responsible for β-decay would help in understanding the fundamental character of β-decay and its connection with other nuclear phenomena. According to Konopinski,[1] the β-decay interaction may be a linear combination of several types of interaction. These are the Fermi interactions (scalar and vector), the Gamow-Teller interactions (tensor and axial vector), and the pseudoscalar interaction. The possibility of the β-decay interaction including both scalar *and* vector or both tensor *and* axial vector interactions is ruled out by the observed shapes of allowed β-spectra.[2]

Let us assume that the type of interaction responsible for β-decay is the same for all transitions and that it is a linear combination of Fermi (scalar or vector), Gamow-Teller (tensor or axial vector), and pseudoscalar interactions.

The matrix elements squared for any β-transition can then be written as follows:[3]

$$|M|^2 = C_F^2|M_F|^2 + C_G^2|M_G|^2 + C_P^2|M_P|^2.$$

Here $|M|$ denotes the total matrix element, $|M_F|$, $|M_G|$, $|M_P|$ are the matrix elements of Fermi, Gamow-Teller, and pseudoscalar interactions. The relative amounts of the different interactions are indicated by C_F, C_G, C_P with the relation

$$C_F^2 + C_G^2 + C_P^2 = 1$$

For superallowed transitions, $|M_F|^2$ and $|M_G|^2$ are given by Konopinski on the basis of the Wigner supermultiplet model.[1,3] $|M_P|^2 = 0$; thus the amount of pseudoscalar interaction, given by C_P, cannot be ascertained by a study of superallowed transitions. However, a study of recent, accurate, measurements on superallowed β-decays makes it possible to draw conclusions as to the relative contributions of Fermi and Gamow-Teller interactions, C_F^2/C_G^2, which is here denoted by K.

A possible method of obtaining the value of K is to compare the β-transitions H^3-He^3 and He^6-Li^6. Wu[4] lists the results of latest measurements. For the decay of H^3, the value of ft is 1125 (±12 percent); for He^6, $ft = 584$ (±2 percent). According to the Wigner model, the above transitions may be represented as $S_{1/2}-S_{1/2}$ and S_0-S_1. The value of $|M|^2$ for the H^3-He^3 decay, in our notation, is $C_F^2+3C_G^2$; for the He^6-Li^6 decay, $|M|^2 = 6C_G^2$. Equating $|M|^2 ft$ for the two transitions,[1] and solving for K, it is found that $K = 0.11 \pm 0.45$.

Another method of estimating the value of K is the study of branching in the decay of Be^7 by orbital electron capture to the ground state or the excited state of Li^7. According to both the Wigner model and the Mayer shell model,[5] the ground states of Be^7 and Li^7 are $P_{3/2}$ states, while there is evidence that the excited state of Li^7, denoted here by Li^{7*}, has spin ½.[6] The energies of decay to ground and excited states are 0.88 and 0.40 Mev, respectively.[7] The fraction of all Be^7 decays going to Li^{7*} is 0.118 ± 0.01.[8] The Be^7-Li^7 and Be^7-Li^{7*} transitions may be represented as $P_{3/2}-P_{3/2}$ and $P_{3/2}-P_{1/2}$. The matrix elements have the following values:

$$|M|^2 \text{ for } Be^7-Li^7 = C_F^2 + 5/3C_G^2$$
$$|M|^2 \text{ for } Be^7-Li^{7*} = 4/3C_G^2.$$

The application of the Fermi β-decay theory to orbital electron capture[1] and the use of these matrix elements yields the result $K = 0.39 \pm 0.20$.

It appears from the previous argument that β-decay is primarily determined by a Gamow-Teller interaction, with an additional amount of Fermi interaction of relative magnitude $K = 0.2-0.4$, and an unknown amount of pseudoscalar interaction, provided the values of matrix elements given by the Wigner theory are correct. This excludes such interactions as the one proposed by Critchfield,[9] according to which $K = 1$.

It is expected that the Wigner model tends to break down for excited states, such as Li^{7*}, and for states involving more than one odd nucleon, such as Li^6. This would result in a reduction of the matrix elements for the He^6-Li^6 and the Be^7-Li^{7*} transitions, but not for the H^3-He^3 and the Be^7-Li^7 transitions. The result would be a reduction in the value of K. Perhaps K vanishes when the correct matrix elements are used. In this case the β-decay would be determined entirely by a Gamow-Teller interaction, plus an unknown amount of pseudoscalar interaction.

[1] E. J. Konopinski, Revs. Modern Phys. **15**, 209 (1943)
[2] S. R. de Groot and H. A. Tolhoek, Physica **16**, 456 (1950).
[3] E. P. Wigner, Phys. Rev. **56**, 519 (1939).
[4] C. S. Wu, Revs. Modern Phys. **22**, 386 (1950).
[5] M. G. Mayer, Phys. Rev. **78**, 16 (1950).
[6] D. R. Inglis, private communication, October, 1950.
[7] Hornyak, Lauritsen, Morrison, and Fowler, Revs. Modern Phys. **22**, 291 (1950).
[8] C. M. Turner, AECU-432 (1949) (unpublished).
[9] C. L. Critchfield, Phys. Rev. **63**, 417 (1943).

Variation of Dielectric Constants of Ionic Crystals with Pressure

D. A. A. S. NARAYANA RAO
Physics Department, Andhra University, Waltair, India
(Received October 2, 1950)

MAYBURG[1] determined the variation of dielectric constants of five ionic crystals with pressure and discussed the results on the basis of Mott and Littleton's theory of the static dielectric constants. But $\partial\gamma/\partial \ln\rho$ values calculated by the author on the same basis from the equation

$$(1-\gamma) = \frac{K+2}{K-1}\left\{1 \pm \left[\frac{K-1}{K+2}\,\frac{K_0+2}{K_0-1} - 1\right]^{\frac{1}{2}} \times \left[\frac{K-1}{K+2}\,\frac{9L^4(1-4\rho x/3)}{\pi(Ze)^2 x} - 1\right]^{\frac{1}{2}}\right\} \quad (1)$$

are at variance with those reported by Mayburg[1] in Table IV of his paper. In view of the importance of these values in supporting the theory, it is found necessary to report and discuss the recalculated values.

The variation of dielectric constants of ionic crystals with pressure may be discussed from a different point of view. Born and Mayer[2] gave the relation

$$K - K_0 = C_1\rho/\nu^2, \quad (2)$$

where K is the dielectric constant, K_0 the optical dielectric constant, C_1 a quantity independent of pressure, ρ the density, and ν the infrared absorption frequency. The variation of ν with pressure is not known, but it may be replaced by another quantity whose variation with pressure is known. For this purpose, the relations developed by Born and Brody[3] for ν and χ (compressibility) of ideally heteropolar solids are useful.

$$\nu^2 = \frac{1}{4\pi^2\mu}\,\frac{S_0(m)}{3}\,\frac{e^2}{L^3}\left\{\frac{(n-1)S_0'(n+2)}{S_0(n)} - \frac{(m-1)S_0'(m+2)}{S_0(m)}\right\}, \quad (3)$$

and

$$1/\chi = e^2 m S_0(m)(n-m)/18L^4. \quad (4)$$

The symbols have the usual significance, and of the right-hand side quantities, only L, the lattice distance, is dependent on pressure. On combining Eqs. (3) and (4) we get

$$v^2 = C_2/(\rho^{1/3}\chi), \quad (5)$$

where C_2 is a constant. Equation (5) is equivalent to the Madelung relation.[4] Equations (2) and (5), when combined, yield

$$K - K_0 = C\chi\rho^{4/3}, \quad (6)$$

where C is a constant, independent of pressure. Differentiating and rearranging,

$$\frac{1}{K}\left(\frac{\partial K}{\partial p}\right)_t = \frac{K-K_0}{K}\left[\frac{1}{\chi}\left(\frac{\partial \chi}{\partial p}\right)_t + \frac{4}{3}\chi\right] + 2K_0{}^{\frac{1}{2}}\chi\frac{\partial n}{\partial \ln\rho}, \quad (7)$$

since $\partial K_0/\partial p = (\partial n^2/\partial \ln\rho)(\partial \ln\rho/\partial p) = 2K_0{}^{\frac{1}{2}}\chi(\partial n/\partial \ln\rho)$, where n is the refractive index.

Values of $-(\partial \ln K/\partial p)_t$ are calculated for different substances from the data quoted by Mayburg[1] and are given in Table I.

TABLE I. Data used in calculations. (All pressure changes are in bars. For MgO, $\partial K_0/\partial p = \chi(K_0-1)$ is obtained from $(K_0-1)/\rho$ = constant. $(-\Delta V/V_i) = ap - bp^2$.)

Crystal	K	K_0	$a\times10^7$	$b\times10^{12}$	$\frac{\partial n}{\partial \ln\rho}$	$\frac{-\partial \ln K}{\partial p}\times10^6$ from (7)	$\frac{-\partial \ln K/\partial p}{\times10^6}$ observed[3]	$\partial\gamma/\partial \ln\rho$ from (1)
LiF	9.27	1.92	1.52	5.5	0.10	0.41	0.448±0.028	+2.8
NaCl	5.62	2.25	43.1	49.6	0.24	0.98	0.98 ±0.06	+2.6
KCl	4.68	2.13	56.8	72.4	0.23	0.90	1.05 ±0.08	−0.33
KBr	4.78	2.33	67.0	105.3	0.35	1.00	1.17 ±0.09	−0.16
MgO	9.8	2.95	5.95	1.0	—	0.17	0.320±0.019	—

Values of $\partial\gamma/\partial \ln\rho$ calculated by the author from Eq. (1) and data used by Mayburg are given in column 9 of the table.

The quantity γ, which is introduced in Mott and Littleton's theory to account for the effects of the overlap of ions, should decrease with increasing pressure and consequent increasing overlap. In contradiction to this expectation, γ must be taken to increase to a large extent in the cases of LiF and NaCl in order to justify the observed change of dielectric constant with pressure. Even in the cases of KCl and KBr, the sign of the variation $\partial\gamma/\partial \ln\rho$, which is small, will not be definite when the probable errors of the various experimental values are taken into consideration, as suggested by Mayburg. Thus, Mott and Littleton's theory leads to an anomalous position.

The explanation of the variation of dielectric constant on the basis of Eq. (6), which is a combination of the well-known Born and Madelung relations, is open to some criticism, as these relations are based upon ideal assumptions and hold good only approximately. Yet, it is interesting to note that the values of $\partial \ln K/\partial p$ calculated on the basis of that equation and the values observed by Mayburg are in good agreement in all cases except for MgO, which also shows abnormal behavior in other respects.

[1] S. Mayburg, Phys. Rev. **79**, 375 (1950).
[2] Born and Mayer, Handbuch der Phys. **24/2**, 647 (1933).
[3] Born and Brody, Z. Physik **11**, 327 (1922).
[4] Born and Mayer, Handbuch der Phys. **24/2**, 656 (1933).

Observation of Magnetic Domains by the Kerr Effect

H. J. WILLIAMS, F. G. FOSTER, AND E. A. WOOD
Bell Telephone Laboratories, Murray Hill, New Jersey
(Received January 18, 1951)

MAGNETIC domains have been observed by means of the Kerr magneto-optic effect on surfaces perpendicular and inclined to the c axis of hexagonal cobalt. The direction of easy magnetization in cobalt is along the c axis, so the domains are magnetized in either a positive or negative sense along this axis. When a surface cuts the c axis, each domain that extends to the surface forms either a north or south magnetic pole. Plane polarized light incident normal to the (0001) surface undergoes a rotation of approximately a quarter of a degree upon reflection, the rotation being positive or negative depending on the polarity of the reflecting region. With the use of a polarized light compensator[1] it is possible to make a set of domains of either polarity appear dark while the other set is light, thus permitting the observation of the domains.

The optical equipment used was a Bausch and Lomb Research Metallographic Microscope, inverted type, equipped with a polarized light compensator. The incident light is polarized by a Foster[2] type polarizing vertical illuminator prism which acts as polarizer for the incident beam and as permanently crossed analyzer for the reflected beam. After emerging from the prism, the polarized beam passes through a rotation compensator and an ellipticity compensator, both before and after reflection from the cobalt specimen, so that half of the compensation is accomplished on each traversal.

The compensator can be set so as to produce a rotation of the plane of polarization equal and opposite to that produced by reflection from the domains of a given polarity. The sense of the rotation of the light due to reflection depends on the polarity

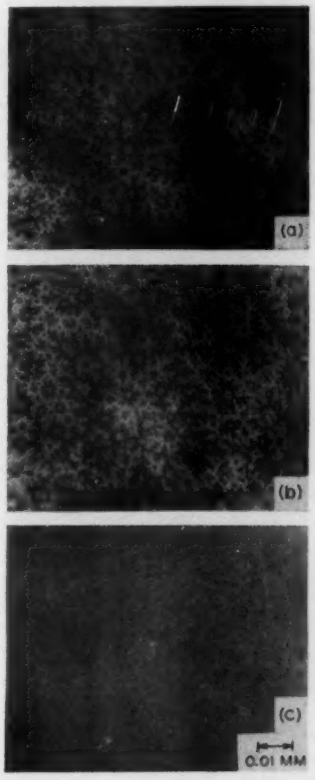

FIG. 1. Polarized light patterns showing dependence of rotation upon polarity of domains in cobalt single crystal. (Surface approximately normal to c axis.) (a) Rotation of $+\frac{1}{4}°$ optically compensated. (b) Rotation of $-\frac{1}{4}°$ optically compensated. (c) No rotational compensation.

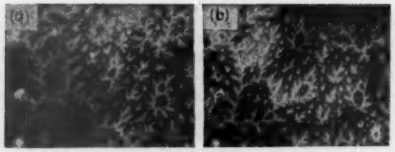

FIG. 2. Polarized light patterns showing change of domains in cobalt single crystal in response to a magnetic field. (a) Lower field. (b) Higher field.

of the magnetization at the reflecting surface. Thus, the rotation introduced by all the domains of like polarity can be compensated by a clockwise rotation of the compensator, for example, while those of the reverse polarity require a counter-clockwise rotation. Compare (a) and (b) in Fig. 1 of an electro-polished surface of a single cobalt crystal, approximately normal to the c axis. If the compensator is set to introduce no rotation, no distinction between the two sets of domains is observed [Fig. 1(c)], since the light intensity from each is dependent only on the amount of rotation of the plane of polarization and not on the sense of the rotation.

No magnetic field was applied when the pictures in Fig. 1(a), (b), and (c) were taken. However, when a magnetic field is applied, the patterns change with the field, as in Fig. 2(a) and (b), which were obtained for different values of a field applied normal to the surface. In Fig. 3, (a) and (b) show the effect of varying the applied field on a polycrystalline cobalt specimen which exhibits a different type of pattern. Figure 3(c) is a powder pattern[3] obtained with colloidal magnetite on the same surface at a later time. Slight changes in the domain structure may have occurred prior to this photograph.

A pattern like that shown in Fig. 1(a), though hardly visible, has also been observed by the authors with a Zeiss neophot type of metallographic microscope equipped with separate polarizer and analyzer. Photographs of the pattern were obtained with this equipment in collaboration with E. E. Thomas.

It should be mentioned that although it is comparatively easy to obtain photographs of polarized light patterns which have good contrast and show the details clearly, visual observation is difficult because of the very low intensity of the light and lack of contrast.

We are indebted to W. Shockley and C. Kittel for suggestions and discussions, and to J. Benford and Colin Alexander of the Bausch and Lomb Optical Company for making available to us their optical compensator so that we might explore its potentialities for work of this type.

[1] Turner, Benford, and McLean, Econ. Geol. **XL**, No. 1 (1945).
[2] L. V. Foster, J. Opt. Soc. Am. **28**, 124 (1938).
[3] Williams, Bozorth, and Shockley, Phys. Rev. **75**, 155 (1949).

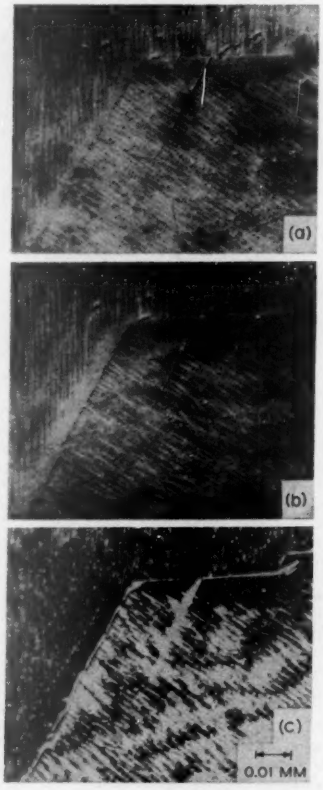

FIG. 3. Domains in polycrystalline cobalt. (a) and (b) Polarized light patterns showing change of domains in response to a magnetic field. (a) Lower field. (b) Higher field. (c) Pattern obtained with colloidal magnetite on the same region (dark field illumination).

$p-n$ Junction Rectifier and Photo-Cell

W. J. PIETENPOL
Bell Telephone Laboratories, Murray Hill, New Jersey
(Received December 21, 1950)

THIS note[1] discusses briefly the electrical characteristics of two semiconductor devices made from $p-n$ junctions in single-crystal germanium by a process described by Teal, Sparks, and Buehler.[2] The two devices are quite similar in construction but differ widely in application.

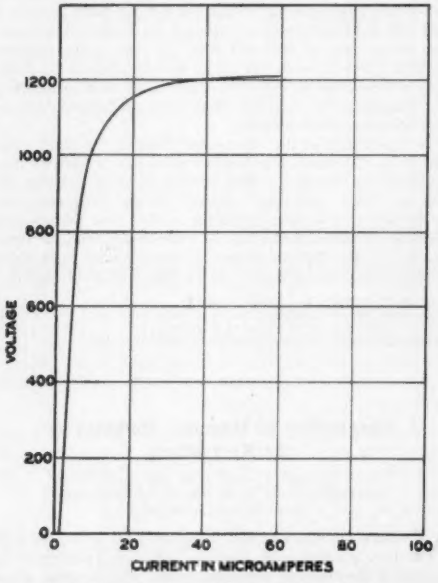

FIG. 1. $p-n$ junction rectifier reverse characteristic.

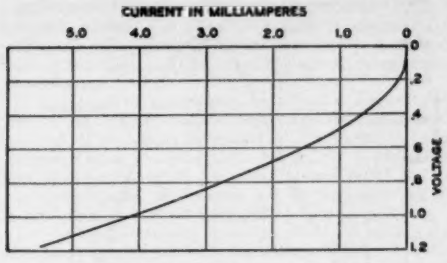

FIG. 2. $p-n$ junction rectifier forward characteristic.

The first of these is a $p-n$ junction rectifier. A typical reverse voltage-current characteristic is shown in Fig. 1, where one notes that the rectifier retains its high impedance to well over 1000 volts. From the static curve one can see that the dc resistance at 1000 volts is 117 megohms. The forward characteristic of the same unit is plotted in Fig. 2 on a much expanded scale. The curve shows the dc resistance at one volt to be 237 ohms, or an impedance ratio at 1000 volts reverse to 1 volt forward of 500,000:1. These characteristics were taken at 25°C, and the saturation current increases by about a factor of ten for an increase in temperature to 60°C. The frequency response of the rectifier makes it usable over and slightly above the audio range. Used in a rectification circuit feeding into a 50,000-ohm load in parallel with a 0.5-$\mu\mu$f condenser, the dc voltage output was down 3 db at 200 kc. The size of the unit described was roughly 0.4 cm in length with a cross section of 0.0025 cm^2. The $p-n$ junction lies perpendicular to the long dimension of the bar of germanium, and electrical contacts are made to each end. This junction differs from that reported by Dunlap[3] in method of preparation and in having higher reverse voltage.

The second device to be described here is a photo-cell which uses the photo-sensitivity of a $p-n$ junction. Figure 3 shows the characteristic curves of the cell as a function of light intensity. The $p-n$ junction responds to light of wavelengths up to $\lambda=1.9$ microns with a quantum efficiency of unity.[4] The sensitivity to a light source of 2900°K color temperature is about 0.01 ma/mlu. As can be seen, the dark impedance of the device is the order of megohms. If the junction is used with a load impedance of one megohm, a drop of 100 volts may be obtained with a hundredth of a lumen light flux. A $p-n$ junction with this flux incident on it is adequate to drive cold cathode gas triodes directly.

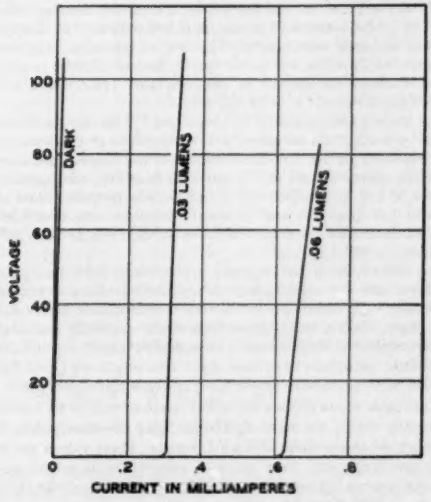

FIG. 3. $p-n$ junction photo-cell static characteristics.

The characteristics of both the $p-n$ junction rectifier and photo-cell described here are in agreement with the theory[5] of diffusion of current carriers to and from the junction discussed by Goucher *et al.*

[1] Substantially, this material was presented orally by the author at the I.R.E. conference, Ann Arbor, Michigan, June 23, 1950.
[2] Teal, Sparks, and Buehler, Phys. Rev. **81**, 637 (1951).
[3] R. N. Hall and W. C. Dunlap, Phys. Rev. **80**, 467 (1950).
[4] F. S. Goucher, Phys. Rev. **78**, 816 (1950).
[5] F. S. Goucher *et al.*, Phys. Rev. **81**, 637 (1951). W. Shockley, Bell Sys. Tech. J. **28**, 435 (1949).

Scintillation Spectrum from Cosmic Rays at 30,000 Feet*

L. REIFFEL, C. A. STONE, AND F. G. REST
Armour Research Foundation of Illinois Institute of Technology, Chicago, Illinois
(Received December 4, 1950)

THE cosmic-ray scintillation pulse distribution in anthracene has been obtained during experiments conducted in the decontaminated waist section of a B-29 circling at 30,000 feet and 50°N latitude (geomagnetic). The aircraft completed a 360° turn every five minutes, insuring that local absorption and azimuthal variations were averaged. The detector, enclosed in a housing of $\frac{1}{8}$-inch brass and $\frac{1}{16}$-inch Mumetal, was a $\frac{1}{4}\times\frac{1}{4}\times1$ inch anthracene crystal viewed by a 5819 photo-multiplier operating at 900 volts. Pulses from the detector were fed to a cathode-ray tube differential analyzer[1] set for low resolution because of the low counting rate and short time available. Space limitations prevented the use of a multiple-channel analyzer.

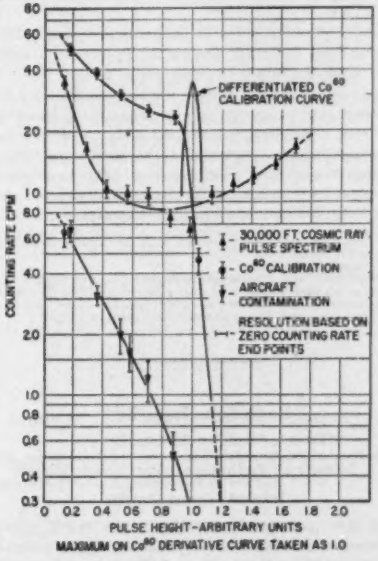

FIG. 1. Scintillation pulse distributions.

The scintillation pulse distributions from cosmic rays, from a Co^{60} source, and from the radioactive contamination of the aircraft are shown in Fig. 1. A Co^{60} calibration curve was taken after each data run; and all pulse heights are referred to the peak of the differentiated Co^{60} curve which corresponds to a Compton electron energy of ~1.0 Mev. Over a limited range, therefore, the scale for pulse height on Fig. 1 may be used as energy in Mev.

The total pulse distribution, obtained during a flight at 2000 feet, was assumed to be due to the contamination of the aircraft and was used to correct the data. This was justified on the basis of G-M tube data regarding the total cosmic-ray intensity (ionizing and gamma) at 2000 feet and introduces an error of less than 10 percent in the evaluation of the contamination.

The relatively short airborne time and low counting rate yielded a small number of counts with resultant poor statistics, as shown by the extensions of the data points in Fig. 1. These extensions are based solely on the probable error due to statistical variations.

Very brief investigation with a G-M tube guard ring around the scintillation detector indicated that pulses due to the ionizing component were in the region above 0.8 units of pulse height (0.8 Mev), whereas the region for energies below ~0.8 Mev probably consists primarily of pulses due to gamma-rays created in the atmospheric cascade process. Since the pulse distribution for a mono-energetic source (Co^{60}) rises much more slowly at small pulse heights than does the cosmic-ray distribution, it is concluded that many cosmic gamma-rays are spread over a broad energy range in the vicinity of 0.5 Mev.

The shape of the distribution above slit position 0.8 (0.8 Mev) is probably a result of nonlinear crystal response[2] in combination with an ionizing particle energy spectrum obeying an inverse power law. There is some indication that the curve has a peak in the region above 1.7 units. Most of the pulses above 0.8 Mev are due to cosmic-ray electrons which, it is estimated,[3] constitute 80 percent of the total ionizing intensity at 30,000 feet and 50° geomagnetic latitude. These electrons give up energy to the anthracene by ionization and the formation of bremsstrahlung.

Using the formula of Bloch,[4] it may be shown that electrons with energies above 5 Mev will lose about 2 Mev by ionization in 0.5 inch of anthracene. This energy loss is almost independent of the incident energy and would account for a peak in the distribution above 1.7 units.

For very high energies, the bremsstrahlung process would become increasingly important, and partial capture of the resultant radiation would contribute to pulses above 2 units. There is, of course, no reason to expect a linear relation between pulse height and incident electron energy once bremsstrahlung becomes important (even if the electron is stopped in the crystal), unless the crystal is large enough to capture all of the secondary gamma-rays.

Investigations are being continued in an effort to obtain more information about the cosmic-ray background and the various processes contributing to the scintillation spectrum.

* This work was done under contract with the United States Department of the Air Force.

[1] To be described elsewhere.

[2] The linearity of the pulse height *versus* energy curve for low energies in anthracene has been studied by J. I. Hopkins, Phys. Rev. **78**, 643 (1950).

[3] Montgomery, *Cosmic Ray Physics* (1949), p. 131.

[4] W. Heitler, *Quantum Theory of Radiation* (1944), pp. 217 ff.

Radiations from Zr^{89}

KALMAN SHURE AND MARTIN DEUTSCH
Department of Physics and the Laboratory for Nuclear Science and Engineering, Massachusetts Institute of Technology, Cambridge, Massachusetts*

(Received February 13, 1951)

THE Zr^{89}, produced by $Y(d, 2n)$ in the M.I.T. cyclotron, decays with a half-life of 79.3 hours. Figure 1 shows the momentum distribution of the particles emitted from Zr^{89} as measured with a thin lens magnetic beta-ray spectrometer. The conversion line has an energy of 910 kev, whereas the continuum of positrons has an end point of 905 kev on a conventional Fermi plot. No beta-gamma coincidences nor x-gamma coincidences have been found. No gamma-gamma coincidences except those due to annihilation radiation have been found. The conversion coefficient has been estimated as 0.5 percent.

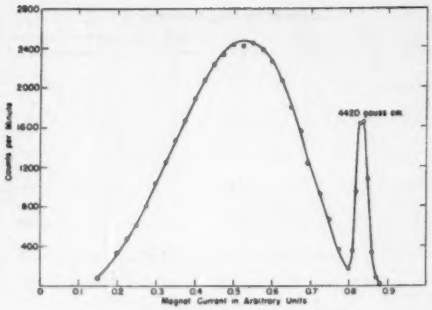

FIG. 1. Momentum spectrum of Zr^{89} particles.

From the results of this research, the level emitting the conversion electrons has a lifetime considerably greater than the resolving time of the coincidence circuit used (10^{-7} sec). This is in agreement with the high conversion coefficient found. It is not known whether the conversion takes place in Zr or Y.

* This research has been supported by a joint program of the ONR and AEC.

Cross Sections and Q-Values for the $C^{13}+D^2$ Reactions*

C. W. LI AND WARD WHALING
Kellogg Radiation Laboratory, California Institute of Technology, Pasadena, California

(Received February 9, 1951)

THE energy of the reaction products from the disintegration of C^{13} by deuterons has been analyzed with the 16″ double-focusing magnetic spectrometer. The emitted particles, identified by their mv/Ze value and pulse size in the scintillation proportional counter, correspond to the reactions (1) $C^{13}(d, \alpha)B^{11}$, (2) $C^{13}(d, p)C^{14}$, and (3) $C^{13}(d, t)C^{12}$.

The targets were prepared by depositing C^{13} on thin tantalum strips by heating the tantalum in an atmosphere of CH_3I vapor, enriched to 61 percent C^{13}. The thickness of the targets, estimated from the energy spread of the outgoing particles, was approximately 50 kev for the incident deuterons. The deuteron beam of 1006±1 kev from the van de graaff generator was controlled with an electrostatic analyzer calibrated against the $Al^{27}(p, \gamma)Si^{28}$ resonance at 993.3±1 kev.[1]

The calibration of the magnetic spectrometer with Po alpha-particles and the experimental procedure has been described previously.[2] No correction for surface contamination layers has been made, since a magnetic analysis of the elastically scattered deuterons showed these layers to be negligibly small. Appropriate relativistic corrections have been made. Our results are $Q_1=5.164\pm0.006$ Mev; $Q_2=5.940\pm0.004$ Mev; and $Q_3=1.310\pm0.003$ Mev. The probable errors include statistical errors as well as all known systematic errors, the most significant being the uncertainty in the angle of observation, 89.3±0.2 degrees. These values are in good agreement with those obtained recently by Buechner and his collaborators:[3] $Q_1=5.160\pm0.010$ Mev; $Q_2=5.948\pm0.008$ Mev; and $Q_3=1.310\pm0.006$ Mev. The agreement between independent

measurements of the $C^{13}(d,\alpha)B^{11}$ Q-value is particularly fortunate, since this reaction is of critical importance in determining the mass of the nuclei lighter than B^{11} in terms of O^{16}. A mass table based on these accurately determined Q-values is being prepared for publication.

In addition to the ground-state transitions, a group of alpha-particles was observed which we have tentatively identified with the $C^{13}(d,\alpha)^*B^{11}$, leaving B^{11} excited by 2.107 ± 0.017 Mev above the ground state. The Q-value for this reaction is 3.057 ± 0.016 Mev. The existence of this lowest excited state in B^{11} has been previously reported by Bateson[4] and by Buechner and Van Patter[5] from a study of the $B^{10}(d,p)B^{11}$ proton groups.

The method of obtaining nuclear reaction cross sections from thick target spectra has been described previously.[6] Following this procedure, we find for 0.99-Mev deuterons a differential cross section at 90 degrees of 7 millibarns/steradian for $C^{13}(d,\alpha)B^{11}$, 2 millibarns/steradian for $C^{13}(d,t)C^{12}$. The high energy protons from $C^{13}(d,p)C^{14}$ were able to pass completely through the ZnS phosphor screen of the scintillation counter, producing a non-uniform pulse height distribution and making the counter efficiency uncertain, so that we are not able to give a value for this cross section.

We wish to thank Mr. John D. Seagrave for preparing the C^{13} targets; a detailed description of his targets will appear elsewhere.

* This work was assisted by the joint program of the ONR and AEC.

[1] Herb, Snowdon, and Sala, Phys. Rev. 75, 246 (1949).
[2] Whaling and Li, Phys. Rev. 81, 150 (1951).
[3] Strait, Van Patter, Buechner, and Sperduto, Phys. Rev. 81, 747 (1951).
[4] W. O. Bateson, Phys. Rev. 80, 982 (1950).
[5] Buechner and Van Patter, Phys. Rev. 79, 240 (1950).
[6] Snyder, Rubin, Fowler, and Lauritsen, Rev. Sci. Instr. 21, 852 (1950).

The Angular Dependence of Scattering and Reaction Cross Sections

JOHN M. BLATT
University of Illinois, Urbana, Illinois
AND
LAWRENCE C. BIEDENHARN
Oak Ridge National Laboratory, Oak Ridge, Tennessee
(Received January 17, 1951)

THE general expression for the differential scattering or reaction cross sections for an unpolarized beam in terms of the scattering matrix has been given in the literature.[1] However, the practical evaluation of this expression runs into difficulties as soon as some of the particles involved have intrinsic spins. In that case, one must average over the spin directions in the incident channel and sum over the spin directions in the outgoing channel. The resulting sums over vector addition (Clebsch-Gordan) coefficients are quite tedious to evaluate directly. However, one should think that all sums over magnetic quantum numbers are essentially geometrical in character and can therefore be performed without a detailed knowledge of the particular collision process (of the elements of the scattering matrix). We wish to point out that this is indeed correct and leads to an explicit expression for the scattering or reaction cross sections free of all sums over magnetic quantum numbers. This explicit form has the additional advantage that it expresses the cross sections directly as sums of Legendre polynomials, with coefficients which are manifestly real numbers. The necessary formalism has been developed by Racah[2] in connection with the theory of complex atomic spectra.

The final result can be written most simply in terms of the quantities $Z(l_1J_1l_2J_2,sL)$ defined as follows:

$$Z(l_1J_1l_2J_2,sL)=(2l_1+1)^{\frac{1}{2}}(2J_1+1)^{\frac{1}{2}}(2l_2+1)^{\frac{1}{2}}(2J_2+1)^{\frac{1}{2}}\times W(l_1J_1l_2J_2,sL)s(l_1,l_2)_{L0}, \quad (1)$$

where W is the coefficient defined by Racah,[2] and $s(l_1,l_2)_{L0}$ is a vector addition coefficient in the notation of Wigner and Eisenbud.[1]

The differential cross section for a process leading from channel s to channel s' can then be written as follows:

$$d\sigma^{ss'}=(k_s)^{-2}\sum_{L=0}^{\infty}B_L^{ss'}P_L(\cos\theta)d\Omega_{s'}, \quad (2)$$

where $P_L(\cos\theta)$ is the Legendre polynomial defined in the usual way, and the coefficients $B_L^{ss'}$ are related to the scattering matrix $u_{sl;\,s'l'}{}^J$ of reference 1 as follows:

$$B_L^{ss'}=(-)^{j_{s'}-j_s}[4(2j_s+1)]^{-1}\sum_{J=0}^{\infty}\sum_{l=|J-j_s|}^{J+j_s}\sum_{l'=|J-j_{s'}|}^{J+j_{s'}}Z(lJlJ,j_sL)Z(l'Jl'J,j_{s'}L)\,|\delta_{ss'}\delta_{ll'}-i^{l+l'}u_{sl;\,s'l'}{}^J|^2$$
$$+(-)^{j_{s'}-j_s}[2(2j_s+1)]^{-1}\sum_{J_1}\sum_{l_1}\sum_{l_1'}\Bigg(\sum_{J_2\geq J_1}\sum_{l_2\geq|l_1-J_1|}^{l_2\leq l_1+J_1}\sum_{l_2'\geq|l_1'-J_1|}^{l_2'\leq l_1'+J_1}\Bigg)'$$
$$i^{-l_1+l_1'+l_2-l_2'}Z(l_1J_1l_2J_2,j_sL)Z(l_1'J_1l_2'J_2,j_{s'}L)$$
$$\times\text{Real Part of}\left[(\delta_{ss'}\delta_{l_1l_1'}-i^{l_1+l_1'}u_{sl_1;\,s'l_1'}{}^{J_1})^*\times(\delta_{ss'}\delta_{l_2l_2'}-i^{l_2+l_2'}u_{sl_2;\,s'l_2'}{}^{J_2})\right], \quad (3)$$

where the prime on the last three sums of the second term means that those terms are excluded for which all three inequalities become equalities, i.e., for which $J_2=J_1$, $l_2=l_1$, and $l_2'=l_1'$ simultaneously.

While one could hardly claim that (3) is a very simple expression, it is appreciably simpler than the one given in reference 1, since six sums over magnetic quantum numbers have been eliminated. Furthermore, it is satisfying that the rules about the limitations of the complexity of angular distributions[3] can be shown to follow from (3) by the use of Racah's selection rule for nonvanishing W-coefficients. All terms in (3) are manifestly real with the exception of $i^{-l_1+l_1'+l_2-l_2'}$ in the second sum of (3). This term, however, is also real because of the parity selection rule according to which l_1-l_1' and l_2-l_2' are either both even or both odd. Equation (3) simplifies considerably for a resonance reaction going through one and only one level of the compound nucleus. In that case the scattering matrix can be factored. This special case was considered already by Myers,[4] who failed to give explicit expressions for the Racah coefficients, however. The simplifications are only minor in the case of resonance scattering because of the interference between resonance and potential scattering. The formalism developed here is adequate for the description of scattering or reactions induced by neutral particles and for reactions or inelastic scattering of charged particles. In the case of elastic scattering of charged particles the series (2) contains the coulomb scattering and hence converges extremely slowly. It is possible, however, to subtract out the coulomb scattering to get a usable expression.

Further work in this connection is in progress and will be reported later in more detail. In particular, we are going to give recursion relations and tables of the Racah coefficients W and the Z-coefficients defined by (1). We would like to thank Dr. Stuart Lloyd of the University of Illinois for some valuable discussions in connection with the Racah coefficients.

[1] E. P. Wigner and L. Eisenbud, Phys. Rev. 72, 29 (1947); see Eqs. (33), (35), and (42). We shall use their notation in this letter.
[2] G. Racah, Phys. Rev. 61, 186 (1942); 62, 438 (1942).
[3] C. N. Yang, Phys. Rev. 74, 764 (1948).
[4] R. D. Myers, Phys. Rev. 54, 361 (1938).

Study of Low Energy Gamma-Radiations Emitted from Pa^{231} and U^{234}

GERTRUDE SCHARFF-GOLDHABER AND MICHAEL MCKEOWN
Brookhaven National Laboratory, Upton, Long Island, New York
(Received February 13, 1951)

MACKLIN AND KNIGHT[1] observed, with a Geiger counter, a low energy gamma-radiation from a thin source of U^{234}, an α-emitter. By absorption of this radiation in Al, they showed

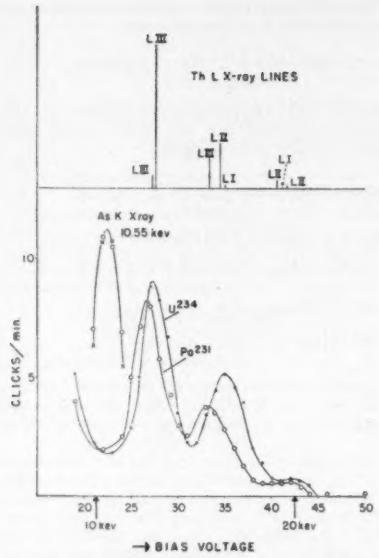

FIG. 1. L x-ray spectrum of $U^{234} \rightarrow Io^{230}$ ($Z=90$). For comparison the L x-ray spectrum of $Pa^{231} \rightarrow Ac^{227}$ ($Z=89$) is shown. In the upper part L lines from Th are given.

that its energy was comparable with that of L radiation of Th. A study of this radiation has now been carried out[2] by means of argon-filled proportional counters. After passing through a preamplifier and linear amplifier with variable gain, the pulse from the proportional counter was analyzed by a single channel pulse height discriminator and recorded by means of a scalar and mechanical counter.

A sample of about 0.4 mg U^{234} was placed above the beryllium window of the counter. The pulse height distribution found is shown in Fig. 1. An energy calibration was carried out with the As K x-ray emitted from Se^{75}, a K-capturer. In the upper part of the figure the intensities of L x-ray lines, excited in Th with external x-rays,[3] are plotted against the same energy scale. The agreement of the line groups with the measured peaks indicates

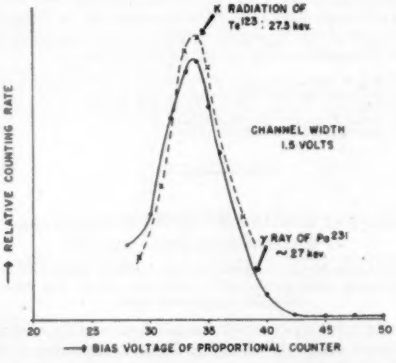

FIG. 2. 27-kev γ-ray from Pa^{231} in comparison with Te K x-ray.

FIG. 3. Oscilloscope trace of proportional counter pulse distribution. On the left are the K x-rays of Te^{125}; in the middle are the L x-rays and 27-kev γ-ray of Pa^{231} (5-sec exposure); on the right are the same (2-sec exposure).

that the radiations found by Macklin and Knight are indeed L x-rays of Th. The energy resolution obtained is illustrated by the shift of the L x-ray spectrum with decreasing Z. The curve labeled Pa^{231} shows the L x-rays of element 89 which is produced by α-decay of Pa^{231}.

Since at least one-quarter of the alpha-emissions of U^{234} were found to be followed by L x-rays, it seemed reasonable to assume that the latter are produced by conversion of low energy γ-rays in the L shell, rather than by a disturbance of the electron shell by the α-particles, as Macklin and Knight had assumed.[4] A search for these gamma-rays has so far been unsuccessful. However, J. Teillac[5] showed recently, by means of a photographic plate technique, that about every third α-particle is accompanied by a conversion electron. The energies of these electrons fall into 3 groups of ~36, 50, and 75 kev, the strongest one being at 36 kev. It therefore seems that the α-decay of U^{234} is followed, in about 30 percent of the cases, by strongly converted γ-rays of energies ranging between 50 and 90 kev.

A corresponding search for a nuclear gamma-ray responsible for most of the L x-rays from Pa^{231} yielded a peak at 27 kev, as shown

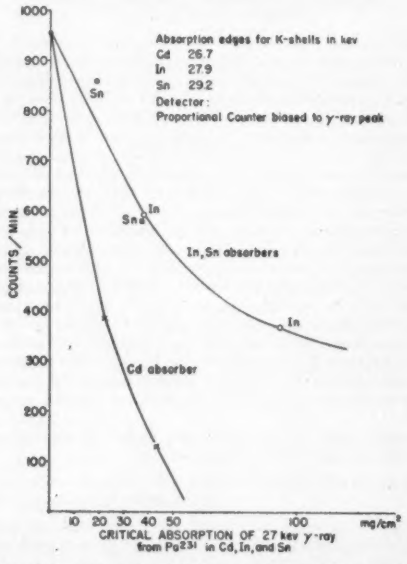

FIG. 4. Critical absorption of 27-kev γ-ray of Pa^{231} in Cd, In, and Sn.

in Fig. 2. The energy calibration was carried out by means of the K-radiation from Te. Figure 3 shows oscilloscope traces of the pulse distribution obtained from Pa^{231} in the proportional counter in comparison with the K x-rays emitted from Te^{128}. Critical absorption of the nuclear gamma-ray from Pa^{231} also showed that its energy lies between the absorption edges of Cd and In (26.7 and 27.9 kev) (Fig. 4). For this experiment, Cd, In, and Sn absorbers were placed between the sample and the beryllium window, and the discriminator voltage of the proportional counter was kept constant at the peak-value for the γ-ray. Teillac,[6] by means of a Wilson chamber technique, had observed at least 3 conversion electron groups from this isotope. The most intense group, at 24 kev, may be identified with the M-electrons from the 27-kev gamma-ray.

Low energy gamma-rays have hitherto received only scant attention. A systematic study of their occurrence is now in progress.

Our thanks are due to M. Studier of Argonne National Laboratory and G. Harbottle of this laboratory for the preparation of Pa^{231} samples, and to E. der Mateosian for valuable help.

* Research carried out under contract with AEC.

[1] R. L. Macklin and G. B. Knight, Phys. Rev. **72**, 435 (1947).
[2] Scharff-Goldhaber, der Mateosian, McKeown, and Sunyar, Phys. Rev. **78**, 325 (1950).
[3] Compton and Allison, *X-Rays in Theory and Experiment* (D. Van Nostrand Company, Inc., New York, 1934).
[4] Theory predicts only $\sim 1L$ x-ray per 10^4 α-particles for this effect. Recent experiments on polonium show that this effect is of the order of 1 per 10^2 alphas [W. Rubinson and W. Bernstein, Bull. Am. Phys. Soc. **26**, No. 1, 47 (1951)].
[5] J. Teillac, Compt. rend. **230**, 1056 (1950).
[6] J. Teillac, Compt. rend. **229**, 650 (1949).

On the Hall Effect in Ferromagnetics

N. Rostoker and Emerson M. Pugh
Department of Physics, Carnegie Institute of Technology, Pittsburgh, Pennsylvania
(Received January 18, 1951)

In a recent paper,[1] hereafter referred to as (A), Hall effect measurements for nickel were presented. The following relation was proposed to describe the Hall effect on the basis of these measurements and previous measurements made by Smith[2]

$$e_H = R_0(H + 4\pi\alpha M), \tag{1}$$

where e_H is the Hall electric field per unit current density, R_0 is the Hall constant which should depend chiefly on the numbers of electrons and holes and be substantially independent of temperature, H is the magnetizing force, M is the magnetization, and α is a field parameter which increases with temperature. (α varies from $\alpha \sim 1$ at low temperatures to $\alpha \sim 100$ in the neighborhood of the Curie point.)

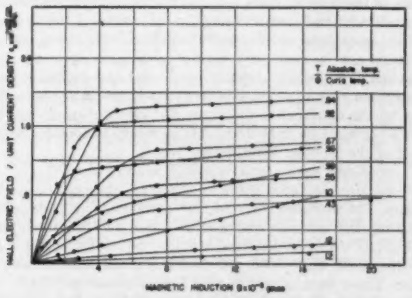

FIG. 1. Hall effect in nickel after A. W. Smith.

The experimental data of Smith are reproduced in Fig. 1. Here e_H has been plotted against B, the magnetic induction. It is clear that above technical saturation the slopes of e_H *versus* B curves are constant with increasing B and are essentially the same for different temperatures, except for the temperatures in the neighborhood of the Curie point where a sharp increase of these slopes with temperature is apparent. In (A), R_0 was computed from these data with the assumption that above technical saturation M = constant with increasing B or H, so that:

$$R_0 = \partial e_H/\partial H = \partial e_H/\partial B. \tag{2}$$

The values of R_0 thus computed from Smith's data are shown in Fig. 2, which corresponds to Fig. 3A of (A), and the "spike" in the neighborhood of the Curie point is very pronounced.

However, it has been discovered that, when the change in intrinsic magnetization with H after technical saturation is taken

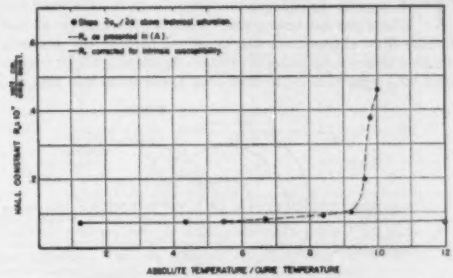

FIG. 2. Temperature dependence of the Hall constant R_0 for nickel.

into consideration, the R_0 *versus* T/θ curve is altered as shown in Fig. 2 and the anomalous behavior in the neighborhood of the Curie point disappears. The behavior of the intrinsic magnetization for high field strengths in the case of nickel has been studied by Weiss and Forrer[3] over temperatures ranging from room temperature to well above the Curie point. A susceptibility χ_i due to change in intrinsic magnetization at high field strengths can be estimated from their data:

$$\chi_i = \partial M/\partial H. \tag{3}$$

At room temperature, we find $\chi_i \sim 1.7\times 10^{-4}$, which is so small that it does not significantly alter our previously computed value of R_0. The only significant change occurs near the Curie point, where χ_i is much larger. For example, in the neighborhood of the paramagnetic Curie point θ, $\chi_i \sim 3.7\times 10^{-3}$.

From Eq. (1) $\partial e_H/\partial H = R_0(1+4\pi\alpha\chi_i)$ and, since $\partial e_H/\partial H = (1+4\pi\chi_i)\partial e_H/\partial B$,

$$R_0 = [(1+4\pi\chi_i)/(1+4\pi\alpha\chi_i)]\partial e_H/\partial B. \tag{2.1}$$

Equation (2.1) reduces to Eq. (2) when χ_i is small, which is the case in the neighborhood of the Curie point. When R_0 was computed by the more correct Eq. (2.1), using the experimental data of Weiss and Forrer, it was found that Eq. (1) is consistent with the experimental data of Smith and Schindler presented in (A), with R_0 a constant independent of both temperature and magnetic fields, and with α a parameter dependent on temperature only.

It was previously suggested[4] by one of us that Eq. (1) might be applicable to paramagnetic as well as ferromagnetic substances, but that it might be difficult to detect the contribution to the Hall effect from the magnetization in most paramagnetic substances, because the magnetization is proportional to H and very small. The above discussion indicates an observable paramagnetic contribution to the Hall effect in nickel in the neighborhood of the Curie point where the nickel is strongly paramagnetic.

By properly separating the extraordinary Hall effect due to magnetization from the ordinary Hall effect due to a uniform field (the magnetizing force H), a well-behaved Hall constant for ferromagnetics can be measured which should provide considerable information concerning the band structure of ferromagnetics.

[1] Pugh, Rostoker, and Schindler, Phys. Rev. 80, 688 (1950).
[2] A. W. Smith, Phys. Rev. 30, 1 (1910).
[3] P. Weiss and R. Forrer, Ann. phys. 5, 153 (1926).
[4] E. M. Pugh, Phys. Rev. 36, 1503 (1930).

Scattering of 20-Mev Alpha-Particles by Helium

K. B. MATHER*
*Physics Department, Birmingham University, Birmingham, England***
(Received February 9, 1951)

THE angular distribution of alphas elastically scattered from helium gas has been studied using a photographic method. Twenty-Mev alphas from the cyclotron entered the scattering chamber from a collimating slit system. Scattering angles were defined by a number of radial slots (Fig. 1) cut in an iron ring, each

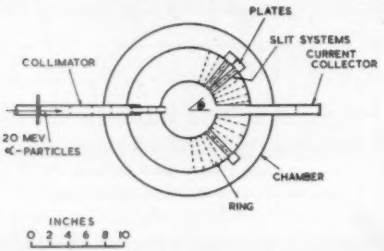

FIG. 1. Schematic of photographic scattering chamber. Angles of scattering are defined by the slits mounted in radial slots cut in the ring (dotted lines indicate positions of slit systems).

mounting a set of defining slits. Particles scattered through these slits were recorded by their tracks in photographic emulsions placed at known angles behind each slot.

The scattering cross section $\sigma(\Theta)$ at any laboratory angle Θ, could be calculated from measurements of slit dimensions, slit distances from the scattering volume, angles of tilt of the photographic plates to the horizontal, the total number of alphas traversing the chamber, and the number of tracks per unit area of plate surface. A noteworthy advantage of the chamber was its dependence predominantly on length measurements which could be made easily and accurately. The number of particles traversing the chamber was determined by collecting the total charge on a Faraday cup connected to a 1.10-μf condenser whose potential was measured with a calibrated quadrant electrometer. The helium gas pressure was obtained from an Apiezon B oil manometer.

The alpha-particle energy was ascertained by measuring the ranges in photographic emulsions of the alphas at each angle of scattering Θ; $E_0=20.0\pm0.3$ Mev.

The data reported here is preliminary only, being based on a single run and with a total track count of only ~7000. Owing to the small alpha-beams produced by the cyclotron; runs were very long, which resulted in trouble from impurity scattering, leakage corrections to the current integrator system, and relatively poor statistics. In proton scattering it is feasible to apply reliable corrections for impurity scattering (air and vapors) based on identifiably different *bona fide* and spurious track lengths. This feature is almost lost in alpha-scattering because of the less favorable mass ratio between scattered and impurity particles.

Table I lists $\sigma(\theta)$, the center-of-mass scattering cross section *versus* center-of-mass angle θ, together with probable errors based on the statistics at each angle. By comparison, other errors which affect the relative cross sections are negligible at most angles. However, absolute values of $\sigma(\theta)$ may be in error by as much as 10 percent. The starred values are very uncertain owing to impurity effects at small angles. (They probably can be taken as upper limits.) Column 4 gives the ratio of observed to Mott cross sections:

TABLE I. Center-of-mass cross sections $\sigma(\theta)$ for 20-Mev alpha-alpha scattering, and ratio to Mott cross sections.

Θ	θ	$\sigma(\theta)\times10^{28}$ cm^2 sterad^{-1}	$\sigma_{obs}/\sigma_{Mott}$
7°	14°	*14.1 ±0.7	1.53
11	22	* 7.7 0.3	4.85
15	30	3.9 0.1	7.82
16	32	3.7 0.1	9.34
21	42	2.00 0.11	12.8
25	50	1.58 0.06	17.3
30	60	1.23 0.08	21.9
35	70	0.92 0.06	22.4
40	80	1.04 0.07	30.4
45	90	—	—
50	100	0.97 0.08	28.4
55	110	1.06 0.08	25.9
60	120	1.19 0.09	21.2

$$\sigma(\theta)_{\text{Mott}}=\frac{4e^4}{E_0^2}\{\operatorname{cosec}^4\Theta+\sec^4\Theta+2\operatorname{cosec}^2\Theta\cdot\sec^2\Theta\cdot\cos(\eta\log\tan^2\Theta)\}$$

$\eta=4e^2/hv=0.282$ for 20-Mev alphas.

As expected, there was no evidence at 20 Mev of inelastic scattering. However, if the alpha-particle has excited states 10 to 20 Mev above ground, an alpha-alpha experiment at 40 Mev could (at least from energy considerations) show inelastic scattering. It is proposed to attempt this with alphas from the Birmingham 60-in. cyclotron.

* Temporarily with the University of Ceylon, Colombo, Ceylon.
** Exposures were made at Washington University, St. Louis, Missouri, in 1949, using the 45-in. cyclotron.

The Discrepancy in the Energy of Annihilation Radiation and the Possibility of Electron-Positron Mass Difference

ARNE HEDGRAN AND DAVID A. LIND*
Nobel Institute of Physics, Stockholm, Sweden
January 20, 1951

THE energies of certain gamma-radiations (Au^{198}, Co^{56}, and annihilation radiation) have been measured with good precision with a crystal spectrometer.[1] Recently, however, it became apparent from measurements on the double focusing spectrometer[2] at this laboratory that there was a discrepancy between the energy of the annihilation radiation measured in terms of the Au^{198} 411-kev line and the value calculated from the Einstein relation $E_0=m_0c^2$ using the best values of the constants.[3]

The comparison of the Au^{198} radiation with the annihilation radiation can be made very accurately because electrons ejected from the L_{III} shell in uranium by the 411-kev radiation have a momentum only 1 part in 1000 less than those ejected from the K shell by the annihilation radiation. The effect of converter thickness is the same for both lines; it is necessary to consider only the effect of the Doppler broadening.

Comparisons were carried out with sources of Au^{198}, Cu^{64}, and Co^{60} mounted in brass tubes to eliminate the continuous beta-spectra. The positrons from the Cu^{64} annihilate in copper or brass. A 0.7-mg/cm^2 uranium converter was used and the resolution set at 1.6×10^{-4}. For comparison, window curves for thorium I, L, and X lines at 1750, 2603, and 10.000 $H\rho$, respectively, were also taken. These were used to correct for the converter effects.

The shapes of the Au^{198} UL_{III} and Cu^{64} U_K lines, shown as curves A and C, respectively, in Fig. I, were obtained by a suitable

averaging of the individual curves. The Au^{198} UL_{III} line is considered the effective window since it is the response of the instrument to a mono-energetic gamma-ray. The true instrument window curve (transmission curve of the spectrometer for isotropic mono-energetic electrons) obtained from the ThL line is shown also on curve A. Curve B is the assumed electron momentum distribution arising from the Doppler broadening of the annihilation line; the points on curve C represent the form predicted by folding curves A and B together. The reference lines on curves A and C represent the true line positions when window asymmetry and converter effects have been eliminated. Each experimental curve was fitted to the average line profile and the position of the reference line was recorded on the R scale; these are the values tabulated in Table I. The potentiometer values given there are directly proportional to the momentum ($H\rho$) values of the lines.

TABLE I. Potentiometer resistance values of the various photo-lines used in this work.

Run	Au^{198} U_K	Au^{198} UL_I	Au^{198} UL_{III}	Cu^{64} U_K	Co^{60} U_K (1.33-Mev line)
1	7332.0	8709.0	8776.0	8786.0	19385.6
2	7332.7	8709.6	8775.7	8785.7	19384.4
3	7333.0	8709.4	8775.2	8784.9	19384.9
4	7330.8	8708.5	8775.4	8785.8	
5		8709.3	8774.0	8785.8	
6		8709.5			

The energy of the annihilation radiation can be calculated if the energy difference $K-L_{III}$ in uranium is known. This is just the energy of the $K\alpha_1$ line of the x-ray spectrum; its value is calculated from the wavelength given by Cauchois and Hulubei[4] to be 98.42 kev. The small momentum difference between the two lines is equivalent to 0.73±0.04 kev; hence, the difference between the Au^{198} and annihilation radiation energies will be 99.15±0.04 kev.

The directly measured energy of the Au^{198} gamma-ray is 411.2±0.1 kev.[1] We have tried to check this value in two ways.

A comparison was made between the Au^{198} UL_{III} line and the U_K line of the 1.33-Mev Co^{60} gamma-ray. In this case corrections had to be made for the effect of the converter. When one uses the crystal spectrometer value 1.3316±0.0010 Mev for the energy of the Co^{60} line, the energy of the gold gamma-ray becomes E_{Au}=411.02±0.4 kev.

Finally the energy of the 411-kev line was measured independently by measuring the U_K and UL_I lines. These data together with the energy difference between them (from the x-ray data) permit one to calculate[5] the energy of the gamma-ray to be: E_{Au}=411.52±0.4 kev. The effect of the converter was eliminated in all cases by an unfolding procedure.

If we weight these three measurements according to their assigned limits of error, the mean energy of the gold line is E_{Au}=411.22 ±0.10 kev. Then the value of the annihilation gamma-ray energy, E_A, becomes E_A=510.37±0.14 kev. The value of m_0c^2 is[3] E_0=510.96±0.02 kev. Hence the difference E_0-E_A=0.59±0.16 kev, based principally on the Au^{198} crystal value, is quite probably real.

The crystal spectrometer value of E_A is 510.68±0.1 kev;[4] this does not agree with the present determination. We were informed that this measurement is being repeated; for this reason, and because the Au^{198} crystal spectrometer measurement which we have used is the average of three separate determinations made over a period of two years with two different crystals, we prefer to keep the two results separate. In our work the effects of varying sensitivity and sloping background under the lines are insignificant. The only error which could be large enough to account for the discrepancy may be a systematic calibration error of the crystal spectrometer, but this seems unlikely.

If the effect is real, some mechanism for the disappearance of 1180 ev of energy must be found. The results of DeBenedetti,

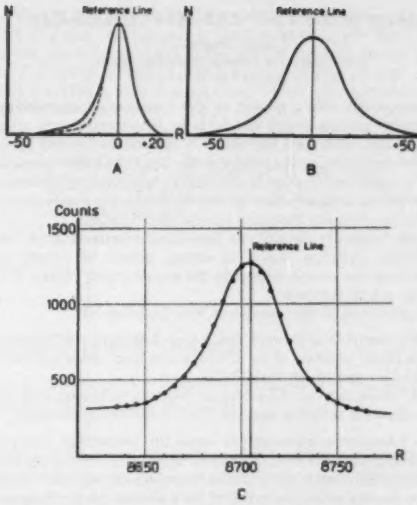

FIG. 1. Folding of Au L_{III} line with an assumed annihilation line momentum distribution to correct for Doppler broadening in the annihilation line. Curve A is the line shape of the Au L_{III} line (dashed curve is the instrument window when no converter is used). Curve B is the assumed momentum distribution of the photo-electrons. Curve C is the observed annihilation line. The dots represent the points predicted by the folding. The reference line gives in each case the true line center.

et al.,[6] indicate that the annihilation process should release the total mass energy of the positron and electron except for a small second-order effect from the Doppler broadening. If the Einstein law for the equivalence of mass and energy is incorrect, then the same law applied to moving particles which we used to determine independently the energy of the Au radiation is probably also incorrect. Unfortunately, our data on this point are not better than 1 part in 1000, but in no case have the predictions of the special relativity theory applied to atomic systems been shown to be incorrect.

The most interesting possibility is that the mass of the positron is not equal to the mass of the electron measured by other experiments. The result of our measurements indicates that, under this assumption, the positron must be lighter than the electron by 0.0023 electron masses; the crystal spectrometer annihilation energy value results in a mass difference of 0.001 electron masses. DuMond has communicated to us during the course of this work that he has been examining this question in connection with his re-evaluation of the atomic constants. A direct comparison of the e/m ratios for positron and electron is the most reliable method of answering these questions which are of extremely great theoretical significance.

The details of this investigation will be published in the *Arkiv för Fysik*.

* On leave from California Institute of Technology, Pasadena, California.

[1] J. W. M. DuMond *et al.*, Phys. Rev. **73**, 1392 (1948); **75**, 1226 (1949); **76**, 1838 (1949).

[2] Hedgran, Siegbahn, and Svartholm, Proc. Phys. Soc. (London) **63**, 960 (1950).

[3] We have used the 1947 values of the constants given by DuMond, with the exception that we use the more recent determination of e/m_0 by nuclear resonance and magnetic beam methods [Thomas, Driscoll, and Hipple, Phys. Rev. **78**, 787 (1950)] and a slightly higher value of c, the speed of light. The values used are e/m=1.75890±0.00005×10^7 emu gram^{-1} and c=2.99790×10^{10} cm sec^{-1}. The values we have used will change when the results of recent experiments are evaluated; however, these changes will have almost no effect on the conclusions of this note.

[4] Y. Cauchois and H. Hulubei, *Longueur d'Onde des Emissions X et des Discontinuités d'Absorption X* (Hermann et Cie, Paris, 1947).

[5] K. Siegbahn, Arkiv Math., Astr., och Fysik, **A30**, 20 (1944).

[6] DeBenedetti, Cowen, Konneker, and Primakoff, Phys. Rev. **77**, 205 (1950).

Energy of the ThC″ 2.62-Mev Gamma-Ray

ARNE HEDGRAN
Nobel Institute of Physics, Stockholm, Sweden
January 20, 1951

IN connection with a project in this Institute on establishing accurate gamma-energy standards for beta-spectroscopy some measurements have been performed in the double focusing spectrometer[1] to determine the energy of the ThC″ 2.62-Mev gamma-ray. The most recent value of this energy was given by Wolfson[2] who based his determination on the Au^{198} 411.2-kev gamma-ray as determined by the Pasadena crystal spectrometer.[3]

It was originally decided to base this investigation on the annihilation radiation, since its energy should be accurately derived from the atomic constants. Subsequent work[4] shows that this may not be the case.

The procedure of the experiment was the following:

(1) $H\rho$ comparison between the L and X lines of RdTh active deposits (Ellis' notation of the K-conversion lines of the 0.51- and the 2.62-Mev gamma-rays of ThC″).

(2) A comparison by the secondary electron technique between the annihilation radiation and the ThC″ 0.51-Mev gamma-ray.

This procedure enables one to make the comparison between lines having quite different $H\rho$ values under ideal conditions, and the comparison under (2) actually introduces a negligible error because the two radiations involved have almost exactly the same energy.

The source of ThC″ for the conversion line measurement was prepared by collecting RdTh active deposit on an aluminum foil 2×6 mm. Figure 1 shows how the comparison between the experimental X and L curves was made. The full curve is the L line and the open circles are the experimental points of the X line, which has been normalized to the same height and $H\rho$ scale as the L line and brought into coincidence with that curve. The fitting of the curves is very accurate at this resolution (~0.17 percent), so the error in the determination comes entirely from the field measurement. The $H\rho$ ratios between the L and X lines, which were obtained, are given in Table I. The first four runs were made about half a year earlier with less precise field measurement. (A description of the present improved field measuring system will be given elsewhere.) The assigned error in the mean value includes the estimated systematic uncertainty.

TABLE I. Measurements of the $H\rho$ ratio between the L and X lines.

Run	Ratio	Weight	Run	Ratio	Weight
1	0.26070	1	4	0.26078	1
2	0.26072	1	5	0.26070	2
3	0.26062	1	6	0.26068	2
			7	0.26064	2

Weighted mean 0.26069±0.00010

For the comparison between the ThC″ 0.51-Mev radiation and the annihilation radiation, sources of Cu^{64} and RdTh enclosed in identical brass capsules were used, and their external conversion K lines from a 2.4 mg/cm² uranium converter were alternately measured with a spectrometer resolution of 0.6 percent. The influence of the Doppler broadening of the annihilation radiation was taken into account, and the comparison between the lines was done in the same way as is described in reference 4. The results are shown in Table II. From the mean values of Tables I and II, the $H\rho$ of the ThX line becomes[5] 10.001±5.

This value is higher than Wolfson's[2], and an experiment similar to his was later performed utilizing the Au^{198} K-conversion line as a standard. The source was prepared by evaporating activated gold (~40 μg/cm²) on an aluminum foil and then collecting the RdTh active deposit on the surface. The comparison was then made between the Au^{198} K-conversion line and the ThL line.

TABLE II. Measurements of the $H\rho$ ratio between the secondary electrons from the annihilation radiation and those from the ThC″ 0.510-kev γ-ray. (U-radiator.) Calculation based on an annihilation energy of 510.96 kev.

Run	Ratio	$H\rho$ of the L line
1	1.0002±0.0002	
2	1.0002±0.0003	
	Mean 1.0002±0.0002	2607.2±0.5

Figure 2 shows the two curves compared in the same way as those in Fig. 1. The result is given in Table III and indicates a discrepancy between the Au^{198} crystal spectrometer value and the energy of the annihilation radiation obtained from the atomic constants (compare Tables II and III). The much more precise measurement described in reference 4 proves this discrepancy to be real and, for the reasons given there, the gold value is considered to be more reliable.

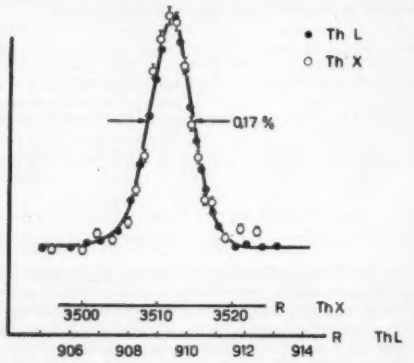

FIG. 1. The ThC″L and X lines normalized to each other and brought into coincidence for the $H\rho$ comparison.

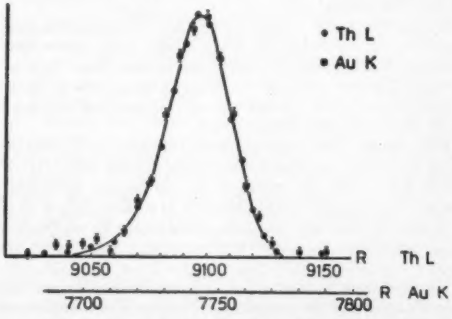

FIG. 2. The ThL and the Au^{198} K-conversion lines from the composite source. The continuous beta-spectrum subtracted and the curves compared as in Fig. 1.

TABLE III. Measurements of the $H\rho$ ratio between the ThL line and the Au^{198} K-conversion line and the $H\rho$ of the ThL line computed from a Au-energy 411.2 kev.

Run	Ratio	$H\rho$ of the L line
1	1.1731	
2	1.1732	
	Mean 1.17315±0.0002	2604.5±0.5

TABLE IV. Independent measurements of $H\rho$ of the ThL line based on the Au 411.2-kev energy.

Method	$H\rho$ of the L line
The data in Table II applied to the annihilation energy 510.37 obtained in reference 4	2604.8±0.5
Comparison between ThL and Au^{198} secondary electrons from U L_{III}	2605.0±0.5
Mean (Tables III and IV)	2604.8±0.3

Table IV gives two other determinations of the $H\rho$ for ThL based on the Au^{198} 411.2-kev value. The data are taken from the experiments described in reference 4.

These three more or less independent measurements determine the ThL line very accurately relative to the Au^{198} gamma-ray.[6] If one uses 411.2±0.1 kev as the value of the Au^{198} energy, the $H\rho$ of ThX becomes 9992±5 with the corresponding quantum energy 2.6158±0.0015. This is in good agreement with Wolfson's value 2.615±0.004.

[1] Hedgran, Siegbahn, and Svartholm, Proc. Phys. Soc. (London) **63**, 960 (1950).
[2] J. L. Wolfson, Phys. Rev. **78**, 176 (1948).
[3] DuMond, Lind, and Watson, Phys. Rev. **73**, 1392 (1948).
[4] A. Hedgran and D. A. Lind, Phys. Rev. **82**, 126 (1951).
[5] The values of the atomic constants used in this note are the same as those employed in reference 4.
[6] A precise absolute momentum measurement of the ThL line should give a valuable check on the energy value of the Au^{198} gamma-ray.

PHYSICAL REVIEW VOLUME 82, NUMBER 1 APRIL 1, 1951

Proceedings of the American Physical Society

MINUTES OF THE MEETING OF THE NEW ENGLAND SECTION AT MOUNT HOLYOKE COLLEGE, SOUTH HADLEY, MASSACHUSETTS, NOVEMBER 4, 1950

THE thirty-fifth meeting of the New England Section of the American Physical Society was held at Mount Holyoke College, South Hadley, Massachusetts, on Saturday, November 4, 1950. Approximately eighty members of the section were in attendance. The program included four invited papers and eleven contributed papers. Abstracts of the contributed papers will appear in the *Physical Review*.

At the business meeting several minor changes in the Constitution and By-Laws of the Section were enacted to bring these documents of the Section into line with the corresponding documents of the parent Society.

The following officers were elected for 1951: *Chairman*—N. C. Little, Bowdoin College; *Vice-Chairman*—Nora Mohler, Smith College; *Secretary-Treasurer*—A. G. Hill, M.I.T.; *Executive Committee*—F. W. Constant, Trinity College, and D. H. Frisch, M.I.T.

A. G. HILL, *Secretary-Treasurer*
M.I.T., Cambridge 39, Massachusetts

Invited Papers

Toxicity of Radium and Plutonium. R. D. EVANS, *M.I.T.*

Some Experiments with 300-Mev Gamma-Rays. D. H. FRISCH, *M.I.T.*

Neutron Reflection Experiments. D. J. HUGHES, *Brookhaven.*

Nuclear Magnetic Resonance Experiments. N. F. RAMSEY, *Harvard University.*

ABSTRACTS OF CONTRIBUTED PAPERS

1. Magnetically Maintained Pendulum. H. P. KNAUSS AND P. R. ZILSEL, *University of Connecticut.*—An iron bob swinging as a pendulum along the axis of a coil toward and away from its center is maintained in motion by feeding alternating current from a low resistance source into the coil forming part of a suitably tuned circuit. The iron bob may be replaced by a second coil connected in series. The transfer of energy to the pendulum is shown to be due to the phase difference between the variation in the inductance of the circuit, and the corresponding variation in the amplitude of the current with the oscillation of the pendulum. If the variation in the current amplitude lags behind the variation in inductance, the pendulum is driven, otherwise it is damped. In the limit of small amplitude of oscillation the condition for maintenance is that the circuit have predominantly inductive reactance and sufficiently high Q.

2. Impedance Function of Metals in Electrolytic Solution.* D. C. GRAHAM, *Amherst College.*—Solid metals immersed in solutions of electrolytes exhibit an impedance which is not representable as a function of frequency (at a given potential with infinitesimal test signal) by any simple combination of capacitance, resistance, and inductance. Consideration of the physical phenomena involved indicates that the concentration of hydrogen atoms at the metallic surface, y, should vary with the imposed current according to the differential equation $dy/dt = I_0 + A\sin\omega t - ky^2$. This equation does not lend itself to exact solution, but numerical solutions using reasonable values of the parameters lead to variations of concentration with time in reasonable agreement with experiment.

* A fuller account will be found in the *Monthly Notices of The Royal Astronomical Society*, Geophysical Supplement, to be published.

3. A Problem of the Temperature in an Accumulating Medium. A. E. BENFIELD, *Harvard University.*—An expression is derived for the temperature $T(x, t)$ in a semi-infinite solid accreting with constant velocity v, on whose rising surface there is impressed the temperature $T(0, t) = A + B\cos(\omega t + \theta)$, where x is depth, t is time, and A, B, ω, and θ are constants. The solution is of use in studying the temperature in an accumulating snowfield. The annual temperature wave, if accompanied by the rapid accumulation of snow, causes considerably lower temperatures than otherwise. A diffusivity which varies slowly with depth may be treated approximately as equivalent to a theoretical fictitious velocity of accumulation.

4. An Automatically-Recording Photometer for the Measurement of Light Scattered by Liquid Droplets. E. P. CLANCY, *Mount Holyoke College.*—An experimental study is being made of the scattering of light by liquid droplets whose diameters lie within the range to which the Mie theory of scattering applies.

A generator for producing artificial fogs of uniform droplet size has been built; the fog issues in a cylindrical jet. The scattering pattern is extremely dependent on the size of the droplets, and practice has shown that it is impossible to control conditions in the generator sufficiently well to prevent slow changes in diameter. Hence, measurements throughout all angles must be made within a relatively short time. An arm carrying a photo-multiplier tube is mounted on the shaft of a selsyn; the axis of this shaft coincides with the axis of the fog jet. A coupled selsyn in a light-tight box turns a disk covered with photographic paper. A lens sends light from a 2-watt concentrated-arc lamp to the mirror of a short-period suspension-type galvanometer and thence to the paper. As the photo-multiplier turns, a scattering diagram in polar coordinates of intensity *versus* scattering angle is automatically drawn. Because of the considerable range of intensities which must be recorded, a special arrangement which makes the galvanometer response logarithmic has been devised.

5. Comparison of Theories of Multiple Scattering.* W. T. SCOTT, *Smith College*.—Several recent improvements in the theory of multiple scattering will be compared. The paper of Snyder and Scott[1] provides the most extensive set of calculations, showing clearly the transition from a gaussian law at small angles to the single-scattering tail. Molière[2] discusses the theory in good detail, and provides an approximate gaussian for the central part. The tail is also accurately calculated, but ho extensive tables are provided. Butler[3] deals with the unprojected, spatial scattering and has a new method for separating the gaussian and the tail; but calculations in the intermediate region are cumbersome. Other theories will be mentioned. A gaussian expression that fits all the new theories is given: the mean square value is $\langle\eta^2\rangle_{Av}=\frac{1}{2}z(0.68+1.17\ln z)$, where η and z are angle and track-length, measured in Snyder-Scott's units.[1] This gaussian is good to 10 percent for $0<\eta<\eta_{max}$, where $\eta_{max}=(1.7+0.93\ln z)z^{\frac{1}{2}}$. The rms angle of scattering is a poor experimental criterion, and simple formulas will be given for other criteria: the mean absolute value, the median value, and the $1/e$ width of the distribution.

* Work performed at Brookhaven National Laboratory under the auspices of the AEC.
[1] H. S. Snyder and W. T. Scott, Phys. Rev. **76**, 220 (1949).
[2] G. Molière, Z. Naturforsch. **2a**, 133 (1947) and **3a**, 78 (1948).
[3] S. T. Butler, Proc. Phys. Soc. (London) **63A**, 599 (1950).

6. Inelastic Scattering of 15-Mev Neutrons by Lead, Iron, and Aluminum.* P. H. STELSON AND C. GOODMAN, *Laboratory for Nuclear Science and Engineering, M.I.T.*—A tritium-zirconium target bombarded by 1.0-Mev deuterons from the Rockefeller electrostatic generator was used as a source of high energy (~15 Mev) neutrons. This source was surrounded by lead, iron, and aluminum scatterers with dimensions of approximately one mean free path for inelastic scattering. The resulting neutron spectra were measured by means of proton recoils in photographic emulsions. An exposure without scatterer permitted an evaluation of the upper limit for the neutron background. The spectra indicate that most of the neutrons are inelastically scattered to energies below 3 Mev in the case of the lead and iron scatterers and to below 5 Mev with the aluminum scatterer. The data can be represented by a curve of the form (const $E\cdot e^{-E/kT}$) as predicted by the Weisskopf[1] statistical theory. The values obtained for the nuclear temperatures, kT, are 0.7, 0.6, and 1.1 Mev for lead, iron, and aluminum, respectively. The fact that the measured temperatures for iron and lead are approximately the same supports the hypothesis that lead nuclei are particularly stable and therefore have properties similar to much lighter nuclei.

* Supported in part by BuShips, ONR, and AEC.
[1] V. F. Weisskopf, Phys. Rev. **52**, 295 (1937).

7. Metastable States in In^{115} and Au^{197}. A. A. EBEL AND C. GOODMAN, *Laboratory for Nuclear Science and Engineering,* M.I.T.*—At the suggestion of Professor Eugene Guth an investigation has been made of the metastable states in In^{115} (4.5 hr) and Au^{197} (7.4 sec) excited by inelastic scattering of monoergic neutrons (0 to 2 Mev). The excitation curve for Au^{197} shows levels at 0.54 ± 0.02, 1.14 ± 0.03, 1.44 ± 0.03 Mev, and possibly at about 1.77 Mev. In exciting the metastable level at 0.54 Mev (spin 11/2), the neutron enters the Au^{197} nucleus (spin 3/2) with $l=3$ and parallel spin and departs with $l=0$ and antiparallel spin. From quantum excitation data the 1.14-Mev level has a spin of 7/2 or 9/2. From the properties of the isomeric transition, the level at 0.27 Mev (known from decay of Hg^{197}) has spin 5/2. All three levels have parity opposite to the ground state. The threshold for neutron activation of In^{115} is at 0.60 ± 0.04 Mev with two other levels at 0.96 ± 0.04 and 1.37 ± 0.04 Mev (which have been reported from quantum excitation). Spin assignments of 1/2 for the metastable state and 3/2 or 5/2 for the 0.60-Mev level have been made. Parity of both these levels is opposite to ground state. Existence of the beta-decay of the metastable states is confirmed.

* This research was supported by the ONR and BuShips.

8. The Low Energy Neutron Group from $Li^7(p, n)Be^7$.* H. B. WILLARD AND W. M. PRESTON, *Laboratory for Nuclear Science and Engineering,† M.I.T.*—The existence of a low energy neutron group, with about 10 percent of the total intensity, has been repeatedly confirmed by photographic plate analysis of recoils from $Li(p, n)Be^7$ neutrons at bombarding energies $E_p=2.7$ to 4.0 Mev. It arises from transitions to the first excited state in Be^7 at about 430 kev above the ground state, a level confirmed by other reactions. We have detected this neutron group at its threshold, using a thin Li target bombarded by protons and plotting the ratio of counts from a bare BF_3 counter (efficiency approximately proportional to $1/E_n^{\frac{1}{2}}$, E_n = neutron energy) to those from a uniform sensitivity "long counter." The result places the threshold at $E_p=2.378$ Mev compared with the ground-state threshold at $E_p=1.882$. The corresponding Q's are 2.081 and 1.647 Mev; their difference gives 434 kev for the excitation energy of the first state in Be^7 with a statistical and reading error of about ±1 kev.

† This work was partially supported by the ONR and BuShips.

9. Detection of Neutral Rays in Paraffin. R. D. RUSK, *Mount Holyoke College*.—In a recent paper[1] a report was made of an effect observed when paraffin was present presumably owing to production of neutral rays by penetrating cosmic rays in iron or lead. The effect was detected by using paraffin below the anticoincidence tube of a four-tube counter arrangement as described in the reference. The effect, though small, was several times the statistical error. The existence of the effect was emphasized by the fact that in the presence of paraffin there was an increase in counts, whereas the substitution of heavier materials such as iron or lead for the paraffin gave a decrease in counts. During the past year the measurements were continued and different thicknesses of paraffin were tried up to 11 cm. With increasing thicknesses the counts due to the above effect increased approximately linearly, and the increase obtained with greater thicknesses of paraffin indicates more clearly the existence of the effect.

[1] R. D. Rusk and A. Rosenbaum, Phys. Rev. **76**, 8, 1166 (1949).

10. Evidence for Magic Numbers from Some Recent Atomic Mass Measurements.* H. E. DUCKWORTH AND R. S. PRESTON,† *Wesleyan University*.—Recent mass spectrographic measurements in this laboratory lead to the mass values $Ti^{48}=47.96405\pm0.00019$, $Sr^{88}=85.933533\pm0.00043$, $Sr^{88}=87.93374\pm0.00053$, $Mo^{98}=97.93610\pm0.00040$, $Sn^{117}=116.94208\pm0.00047$, $Sn^{120}=119.94012\pm0.00072$, $Pt^{194}=194.0256$

± 0.0014, $Pr^{141} = 196.02744 \pm 0.00060$, and $Pb^{208} = 208.0422 \pm 0.0015$. These masses plus some previously reported ones may be combined with appropriate disintegration data to obtain mass values for 70 of the heavier nuclides. A packing fraction curve drawn from these data shows the unequivocal mass effect associated with the 50-neutron configuration,[1] and some mass evidence in support of the magic numbers 14, 16, 28, 32, and 40. Doubly-magic nuclides are suggested as marking major transition points in the packing fraction curve.

* Based on work done at Wesleyan University under contract with the AEC.
† Now at Yale University, New Haven, Conn.
[1] Duckworth, Woodcock, and Preston, Phys. Rev. **79**, 198 (1950).

11. Masses of Mo^{94}, Ba^{138}, Pr^{141}, Nd^{144}, and Hf^{180}. G. S. STANFORD, J. M. OLSON, AND H. E. DUCKWORTH, *Wesleyan University.**—The following packing fraction differences have been measured: $Hf^{180} - Ni^{60}$, $\partial f = 8.56 \pm 0.03$; $Hf^{180} - Zr^{90}$, $\partial f = 7.70 \pm 0.03$; $Pr^{141} - Ti^{47}$, $\partial f = 3.67 \pm 0.03$; $Ba^{138} - Zr^{96}$, $\partial f = 3.63 \pm 0.04$; $Pr^{141} - Mo^{94}$, $\partial f = 3.54 \pm 0.05$; $Nd^{144} - Mo^{96}$, $\partial f = 3.66 \pm 0.04$. These measurements when combined with previous results lead to the mass values $Mo^{94} = 93.9350 + 0.0011$, $Ba^{138} = 137.9491 \pm 0.0011$, $Pr^{141} = 140.9525 \pm 0.0016$, $Nd^{144} = 143.95666 \pm 0.00087$, and $Hf^{180} = 180.0004 \pm 0.0014$. Typical mass spectra will be shown.

* Based on work done at Wesleyan University under contract with the AEC.

MINUTES OF THE OHIO SECTION MEETING AT THE OHIO STATE UNIVERSITY, COLUMBUS, OHIO, FEBRUARY 24, 1951

THE regular mid-winter meeting of The Ohio Section of The American Physical Society was held in the newly built Physics Building of The Ohio State University, Columbus, Ohio, on Saturday, February 24, 1951. Fifty members were present. The Committee studying extension of area reported that the members were not interested in assuming the initiative for an expansion at this time. Abstracts of four papers follow; a fifth, by Professor Phillips of Marietta, was called by him "Rotary" Physics. Then followed the invited paper by Dr. Edward S. Foster, Jr., of University of Toledo, entitled "Physics of Weather."

LEON E. SMITH, Secretary,
Ohio Section,
Denison University,
Granville, Ohio.

Generation of Functions by Windup Mechanisms. R. A. HARRINGTON, *B. F. Goodrich Research Center.*—A cam driving a pen by means of a tape or string wound on it can be conveniently represented and machined as the envelope of its tangents. If the pen travel is a function F of the angle θ through which the cam shaft turns, the distance ρ between the extended tape center line and the shaft axis is given by $\rho = dF/d\theta$. The angle Φ between the tangent normal and a line fixed with respect to the cam is useful in machining the cam. If the tape after leaving the cam passes over a pulley of effective radius r, whose axis is parallel to the cam shaft axis and distant D from it, $\Phi = \theta - \text{arc}\cos[(\rho - r)/D]$. (Here r is taken as positive or negative according to whether the cam and pulley turn in the same or in opposite directions.) The correction for finite thickness of the tape or string is simple: ρ and r are altered by adding or subtracting half this thickness. In order that a function $F(\theta)$ may be generated in this way, it must be continuous and have a continuous derivative, and the sign of the quantity $\rho + d^2\rho/d\theta^2$ must not change. This quantity is approximated by $dF/d\theta + d^3F/d\theta^3$. Sometimes a function which does not satisfy this condition can be generated by a cam turning through a multiple or submultiple of θ.

The tangent envelope representation should also be useful in designing windup mechanisms in which the tape drives a second cam instead of a pen.

An Approximation to the Normal Modes and Frequencies of Extended Chain Molecules. W. EDWARD DEEDS, *The Ohio State University.*—By neglecting only the Coriolis interaction energy, it is possible to obtain a good approximation to the kinetic energy of large molecules in which characteristic groups of atoms occur by considering each characteristic group as a rigid rotator, in so far as the framework vibrations are concerned. This method has been applied to the case of an infinite, extended, zig-zag chain, such as the long chain paraffins. Rotations and out-of-plane vibrations of characteristic groups have been included, and boundary conditions have been applied to solve the problem for chains of finite length. Also, a condition on the force constants of any molecule can be obtained from the physical requirement that all of the roots of the secular equation must be real. This condition is distinct from the one that the potential function must be positive definite and can sometimes be used to put an upper limit on unknown force constants or to decide between various possible sets of force constants.

Microwave Absorption Spectrum of Hydrogen Azide.* JOHN D. ROGERS AND DUDLEY WILLIAMS, *The Ohio State University.*—Several closely spaced absorption lines in the vicinity of 23,815 mc/sec have been observed in the absorption spectrum of hydrogen azide N_3H. These lines are associated with the rotational transition $J_\tau = 0_0 \rightarrow 1_{-1}$, and the observed hyperfine structure can be explained qualitatively in terms of quadrupole interactions between the nitrogen nuclei and the molecular field. From the observed spectrum the sum of the rotational constants $B + C$ is found to be 23,813 mc/sec. The observed Stark effect is quadratic; i.e., $\Delta\nu = \beta E^2$. The Stark coefficient β was found to be 2.00 ± 0.02 mc cm^2/sec volt^2. The results obtained in the present study will be compared with those of Dailey, who has studied several isotopic species of hydrogen azide.

* The research reported has been made possible through support extended by The Geophysical Laboratories under Contract AF 19(122)-13 with the Ohio State University Research Foundation. It is published for technical information only, and does not represent recommendations or conclusions of the sponsoring agency.

Nuclear Magnetic Moment of Boron^{10}. YU TING AND DUDLEY WILLIAMS, *The Ohio State University.*—A nuclear magnetic resonance absorption peak due to B^{10} has been observed by means of super-regenerative techniques. The sample used was an aqueous solution of $Na_2B_2O_4$ containing the naturally occurring mixture of boron isotopes, in which B^{10} has an abundance of approximately 18.4 percent. The value 1.8006 nuclear magnetons obtained for the B^{10} magnetic moment will be compared with the value obtained by other methods.